RESERVOIR TEMPERATURE MODEL
AMENDED STUDY REPORT
DON PEDRO PROJECT
FERC NO. 2299



WATER & POWER
Serving Central California since 1887

MID
Modesto Irrigation District

Prepared for:
Turlock Irrigation District – Turlock, California
Modesto Irrigation District – Modesto, California

Prepared by:
HDR Engineering, Inc.

September 2017

This Page Intentionally Left Blank.

Reservoir Temperature Model
Amended Study Report

TABLE OF CONTENTS

Section No.	Description	Page No.
1.0	**Introduction**	**1-1**
1.1	Background	1-1
1.2	Relicensing Process	1-3
1.3	Study Plan	1-4
2.0	**Goals and Objectives**	**2-1**
3.0	**Study Area**	**3-1**
4.0	**Methodology**	**4-1**
4.1	Model Platform Selection	4-1
4.2	Selection of Model Time Step	4-2
4.3	Input Data, Calibration and Validation Data	4-2
4.3.1	Physical and Geomorphological	4-3
4.3.2	Inflows, Outflows, and Operations	4-3
4.3.3	Temperature Data	4-4
4.3.4	Meteorology	4-5
4.4	Model Development	4-7
4.4.1	Model Structure and Interface	4-7
4.4.2	Domain	4-8
4.4.2.1	Bathymetry	4-8
4.4.2.2	Model Mesh	4-9
4.4.3	Simulation Time	4-11
4.4.4	Module Selection	4-11
4.4.5	Hydrodynamic Module	4-12
4.4.5.1	Solution Technique	4-12
4.4.5.2	“Flood” and “Dry” Cells	4-13
4.4.5.3	Density	4-14
4.4.5.4	Eddy Viscosity	4-15
4.4.5.5	Bed Resistance	4-16
4.4.5.6	Coriolis Force	4-17
4.4.5.7	Wind Forcing	4-17
4.4.5.8	Ice Coverage	4-20
4.4.5.9	Tidal Potential	4-21

4.4.5.10 Precipitation and Evaporation 4-21
4.4.5.11 Wave Radiation 4-22
4.4.5.12 Sources 4-22
4.4.5.13 Structures 4-26
4.4.5.14 Hydrodynamic Initial Conditions 4-27
4.4.5.15 Model Boundary Conditions 4-28
4.4.6 Temperature Module 4-29
4.4.6.1 Horizontal Dispersion 4-33
4.4.6.2 Vertical Dispersion 4-34
4.4.6.3 Heat Exchange 4-35
4.4.6.4 Latent Heat Exchange 4-36
4.4.6.5 Sensible Heat Exchange 4-38
4.4.6.6 Short Wave Radiation 4-39
4.4.6.7 Long Wave Radiation 4-41
4.4.6.8 Temperature Sources 4-42
4.4.6.9 Initial Temperatures 4-43
4.4.6.10 Decoupling 4-44
4.4.7 Model Output 4-45

5.0 Model Operation and Discussion 5-1

5.1 Temperature Profile Data 5-1
5.2 Model Results – 2011 Calibration Year 5-3
5.3 Model Results – 2012 Validation Year 5-9
5.4 Comparison of Outflow Temperatures 5-21
5.5 Comparison to Observed Surface Temperature Data 5-22
5.6 QA/QC Review 5-23
5.7 Reduced Layer Version of the Model 5-24

6.0 Study Variances and Modifications 6-1

7.0 References 7-1

List of Figures

Figure No.	Description	Page No.
Figure 1.1-1.	Don Pedro Project location.	1-2
Figure 3.0-1.	Study area.	3-3
Figure 4.3-1.	Meteorological station locations	4-6
Figure 4.4-1.	MIKE3-FM master interface in “m3fm” file	4-7
Figure 4.4-2.	Model bathymetry screen.	4-8
Figure 4.4-3.	Vertical mesh option screen.	4-9
Figure 4.4-4.	Model mesh horizontal layout.	4-10

Figure 4.4-5. Example of sigma mesh reservoir longitudinal section 4-10
Figure 4.4-6. Example of combined sigma and z-level vertical mesh scheme. 4-11
Figure 4.4-7. Module selection 4-12
Figure 4.4-8. Solution technique parameters. 4-13
Figure 4.4-9. Flood and dry settings. 4-14
Figure 4.4-10. Density as a function of temperature is selected. 4-14
Figure 4.4-11. Horizontal dispersion. 4-15
Figure 4.4-12. Vertical dispersion. 4-16
Figure 4.4-13. Bed resistance. 4-16
Figure 4.4-14. Coriolis force. 4-17
Figure 4.4-15. Wind forcing. 4-18
Figure 4.4-16. Wind data collected at Don Pedro Met Station 2011. Top plot is wind speed (m/s); bottom plot is wind direction (deg). 4-19
Figure 4.4-17. Wind friction factor. 4-20
Figure 4.4-18. Ice coverage. 4-20
Figure 4.4-19. Tidal potential. 4-21
Figure 4.4-20. Precipitation and evaporation. 4-21
Figure 4.4-21. Wave Radiation. 4-22
Figure 4.4-22. Location of model inflow and outflow sources. 4-23
Figure 4.4-23. Listing of inflow and outflow sources. 4-24
Figure 4.4-24. “Tuolumne 3” source details. 4-25
Figure 4.4-25. “Tuolumne 3” inflow for 2011 in cubic-meters per second (m^3/s). 4-25
Figure 4.4-26. “Outflow at Don Pedro powerhouse” source details. 4-26
Figure 4.4-27. “Outflow at Don Pedro powerhouse” outflow for 2011 in cubic-meters per second (m^3/s). Note outflows are assigned a negative value. 4-26
Figure 4.4-28. Old Don Pedro Dam modeled as a weir. 4-27
Figure 4.4-29. Hydrodynamic initial conditions. 4-28
Figure 4.4-30. Boundary conditions: model domain showing all land boundaries. 4-29
Figure 4.4-31. Temperature module. 4-30
Figure 4.4-32. Temperature limits. 4-31
Figure 4.4-33. Solution settings. 4-32
Figure 4.4-34. Temperature dispersion main tab. 4-33
Figure 4.4-35. Temperature horizontal dispersion. 4-34
Figure 4.4-36. Temperature vertical dispersion. 4-35
Figure 4.4-37. Daltons law constants. 4-36
Figure 4.4-38. Atmospheric conditions panel. 4-37
Figure 4.4-39. Relative humidity (%) for 2011. 4-37
Figure 4.4-40. Sensible heat exchange parameters. 4-38
Figure 4.4-41. Air temperature in degree Celsius (^oC) for 2011. 4-39

Figure 4.4-42. Short wave radiation parameters. 4-40
Figure 4.4-43. Denair II solar radiation (W/m^2)..... 4-40
Figure 4.4-44. Temperature sources..... 4-42
Figure 4.4-45. Measured inflow temperature at Indian Creek Trail (^oC) for 2011. 4-43
Figure 4.4-46. Temperature initial condition. 4-44
Figure 4.4-47. Decoupling tab..... 4-45
Figure 4.4-48. Output selection screen..... 4-46
Figure 4.4-49. Geographic view of output area. 4-47
Figure 4.4-50. Output specifications. 4-48
Figure 4.4-51. Example of available output variables for 3D output..... 4-49
Figure 5.1-1. Vertical temperature profile locations. 5-2
Figure 5.2-1. January 12, 2011 calibration. (Observed = blue circles; Model = red triangles) 5-4
Figure 5.2-2. February 7, 2011 calibration. (Observed = blue circles; Model = red triangles) 5-4
Figure 5.2-3. March 22, 2011 calibration. (Observed = blue circles; Model = red triangles) 5-5
Figure 5.2-4. April 20, 2011 calibration. (Observed = blue circles; Model = red triangles) 5-5
Figure 5.2-5. May 18, 2011 calibration. (Observed = blue circles; Model = red triangles) 5-6
Figure 5.2-6. June 6, 2011 calibration. (Observed = blue circles; Model = red triangles) 5-6
Figure 5.2-7. July 11, 2011 calibration. (Observed = blue circles; Model = red triangles) 5-7
Figure 5.2-8. July 26, 2011 calibration. (Observed = blue circles; Model = red triangles) 5-7
Figure 5.2-9. Aug 30, 2011 calibration. (Observed = blue circles; Model = red triangles) 5-8
Figure 5.2-10. September 27, 2011 calibration. (Observed = blue circles; Model = red triangles) 5-8
Figure 5.2-11. Oct 13, 2011 calibration. (Observed = blue circles; Model = red triangles) 5-9
Figure 5.3-1. Jan 19, 2012 validation. (Observed = blue circles; Model = red triangles) 5-10
Figure 5.3-2. Feb 14, 2012 validation. (Observed = blue circles; Model = red triangles).... 5-11
Figure 5.3-3. Mar 14, 2012 validation. (Observed = blue circles; Model = red triangles) 5-11
Figure 5.3-4. April 23, 2012 validation. (Observed = blue circles; Model = red triangles) 5-12
Figure 5.3-5. May 8, 2012 validation. (Observed = blue circles; Model = red triangles) 5-12

Figure 5.3-6. May 17, 2012 validation. (Observed = blue circles; Model = red triangles) 5-13
Figure 5.3-7. June 13, 2012 validation. (Observed = blue circles; Model = red triangles) 5-13
Figure 5.3-8. July 3, 2012 validation. (Observed = blue circles; Model = red triangles) 5-14
Figure 5.3-9. Aug 22, 2012 validation. (Observed = blue circles; Model = red triangles) 5-14
Figure 5.3-10. Sept 19, 2012 validation. (Observed = blue circles; Model = red triangles) 5-15
Figure 5.3-11. Oct 9, 2012 validation. (Observed = blue circles; Model = red triangles) 5-15
Figure 5.3-12. Nov 19, 2012 validation. (Observed = blue circles; Model = red triangles) 5-16
Figure 5.3-13. Jan 19, 2012 validation. (CDFW data only) 5-16
Figure 5.3-14. Feb 14, 2012 validation. (CDFW data only) 5-17
Figure 5.3-15. Mar 14, 2012 validation. (CDFW data only) 5-17
Figure 5.3-16. Apr 23, 2012 validation. (CDFW data only) 5-18
Figure 5.3-17. May 8, 2012 validation. (CDFW data only) 5-18
Figure 5.3-18. June 14, 2012 validation. (CDFW data only) 5-19
Figure 5.3-19. July 10, 2012 validation. (CDFW data only) 5-19
Figure 5.3-20. Aug 10, 2012 validation. (CDFW data only) 5-20
Figure 5.3-21. Sept 12, 2012 validation. (CDFW data only) 5-20
Figure 5.3-22. Oct 25, 2012 validation. (CDFW data only) 5-21
Figure 5.4-1. Measured and modeled outflow temperatures, 2011-12. (Measured = black; Modeled = red) 5-21
Figure 5.5-1. Measured surface temperatures May 2 – June 2, 2011. 5-22
Figure 5.5-2. Modeled surface temperatures May 2, May 18 and June 2, 2011. 5-23
Figure 5.7-1. Measured and modeled vertical temperature profiles at Don Pedro Dam. 5-26
Figure 5.7-2. Don Pedro outflow temperature (2011-2012). 5-27

List of Tables

Table No.	Description	Page No.
Table 4.3-1.	MIKE3-FM model data sources.	4-4
Table 4.3-2.	Reservoir model water temperature measurement locations with period of record.	4-5

List of Attachments

Attachment A	Don Pedro Reservoir Model Recalibration 2016
Attachment B	MIKE3 FM Scientific Reference Manual 2011
Attachment C	Don Pedro Reservoir Bathymetric Study Report
Attachment D	Water Temperature and Local Meteorology Dataset (DVD available upon request)
Attachment E	Full Period of Record Meteorological Data Set
Attachment F	Full Period of Record Inflow Temperature Data Set

List of Acronyms

ac .....acres

ACEC .....Area of Critical Environmental Concern

AF .....acre-feet

ACOE.....U.S. Army Corps of Engineers

ADA .....Americans with Disabilities Act

ALJ.....Administrative Law Judge

APE .....Area of Potential Effect

ARMR.....Archaeological Resource Management Report

BA .....Biological Assessment

BDCP .....Bay-Delta Conservation Plan

BLM .....U.S. Department of the Interior, Bureau of Land Management

BLM-S .....Bureau of Land Management – Sensitive Species

BMI .....Benthic macroinvertebrates

BMP .....Best Management Practices

BO .....Biological Opinion

CalEPPC .....California Exotic Pest Plant Council

CalSPA.....California Sports Fisherman Association

CAS.....California Academy of Sciences

CCC.....Criterion Continuous Concentrations

CCIC .....Central California Information Center

CCSF .....City and County of San Francisco

CCVHJV .....California Central Valley Habitat Joint Venture

CD .....Compact Disc

CDBW.....California Department of Boating and Waterways

CDEC .....California Data Exchange Center

CDFA .....California Department of Food and Agriculture

CDFG .....California Department of Fish and Game (as of January 2013, Department of Fish and Wildlife)

CDFW .....California Department of Fish and Wildlife

CDMG.....California Division of Mines and Geology

CDOF .....California Department of Finance

CDPH.....California Department of Public Health
CDPR.....California Department of Parks and Recreation
CDSOD.....California Division of Safety of Dams
CDWR.....California Department of Water Resources
CE .....California Endangered Species
CEII.....Critical Energy Infrastructure Information
CEQA.....California Environmental Quality Act
CESA .....California Endangered Species Act
CFR.....Code of Federal Regulations
cfs.....cubic feet per second
CGS.....California Geological Survey
cm.....centimeter
CMAP .....California Monitoring and Assessment Program
CMC.....Criterion Maximum Concentrations
CNDDB.....California Natural Diversity Database
CNPS.....California Native Plant Society
CORP .....California Outdoor Recreation Plan
CPUE .....Catch Per Unit Effort
CRAM.....California Rapid Assessment Method
CRLF.....California Red-Legged Frog
CRRF .....California Rivers Restoration Fund
CSAS.....Central Sierra Audubon Society
CSBP.....California Stream Bioassessment Procedure
CT .....California Threatened Species
CTR.....California Toxics Rule
CTS .....California Tiger Salamander
CVRWQCB .....Central Valley Regional Water Quality Control Board
CWA .....Clean Water Act
CWHR.....California Wildlife Habitat Relationship
deg.....degrees
DHI .....Danish Hydraulic Institute
Districts.....Turlock Irrigation District and Modesto Irrigation District
DLA .....Draft License Application

DPRA.....Don Pedro Recreation Agency
DPS.....Distinct Population Segment
EA.....Environmental Assessment
EC.....Electrical Conductivity
EFH.....Essential Fish Habitat
EIR.....Environmental Impact Report
EIS.....Environmental Impact Statement
EPA.....U.S. Environmental Protection Agency
ESA.....Federal Endangered Species Act
ESRCD.....East Stanislaus Resource Conservation District
ESU.....Evolutionary Significant Unit
EWUA.....Effective Weighted Useable Area
FERC.....Federal Energy Regulatory Commission
FFS.....Foothills Fault System
FL.....Fork length
FM.....Flexible Mesh
FMU.....Fire Management Unit
FOT.....Friends of the Tuolumne
FPC.....Federal Power Commission
ft.....feet or foot
ft/mi.....feet per mile
FWCA.....Fish and Wildlife Coordination Act
FYLF.....Foothill Yellow-Legged Frog
g.....grams
GIS.....Geographic Information System
GLO.....General Land Office
GPS.....Global Positioning System
HCP.....Habitat Conservation Plan
HHWP.....Hetch Hetchy Water and Power
HORB.....Head of Old River Barrier
HPMP.....Historic Properties Management Plan
ILP.....Integrated Licensing Process
ISR.....Initial Study Report

ITA.....Indian Trust Assets
kV.....kilovolt
µSiemans.....microSiemans
m .....meters
m/s.....meters per second
m^3/s .....cubic meters per second
M&I.....Municipal and Industrial
MCL.....Maximum Contaminant Level
mg/kg .....milligrams/kilogram
mg/L.....milligrams per liter
mgd .....million gallons per day
mi .....miles
mi^2 .....square miles
MID.....Modesto Irrigation District
MOU .....Memorandum of Understanding
MSCS.....Multi-Species Conservation Strategy
msl.....mean sea level
MVA .....Megavolt Ampere
MW .....megawatt
MWh .....megawatt hour
mya.....million years ago
NAE .....National Academy of Engineering
NAHC .....Native American Heritage Commission
NAS.....National Academy of Sciences
NAVD 88 .....North American Vertical Datum of 1988
NAWQA .....National Water Quality Assessment
NCCP .....Natural Community Conservation Plan
NEPA .....National Environmental Policy Act
ng/g .....nanograms per gram
NGOs .....Non-Governmental Organizations
NHI .....Natural Heritage Institute
NHPA.....National Historic Preservation Act
NISC .....National Invasive Species Council

NMFS.....National Marine Fisheries Service
NOAA.....National Oceanic and Atmospheric Administration
NOI .....Notice of Intent
NPS .....U.S. Department of the Interior, National Park Service
NRCS .....National Resource Conservation Service
NRHP.....National Register of Historic Places
NRI.....Nationwide Rivers Inventory
NTU .....Nephelometric Turbidity Unit
NWI.....National Wetland Inventory
NWIS .....National Water Information System
NWR .....National Wildlife Refuge
NGVD 29.....National Geodetic Vertical Datum of 1929
O&M.....operation and maintenance
OEHHA.....Office of Environmental Health Hazard Assessment
ORV .....Outstanding Remarkable Value
PAD.....Pre-Application Document
PDO.....Pacific Decadal Oscillation
PEIR.....Program Environmental Impact Report
PGA.....Peak Ground Acceleration
PHG.....Public Health Goal
PM&E .....Protection, Mitigation and Enhancement
PMF.....Probable Maximum Flood
POAOR.....Public Opinions and Attitudes in Outdoor Recreation
ppb.....parts per billion
ppm .....parts per million
PSP.....Proposed Study Plan
PSU……Practical Salinity Units
QA.....Quality Assurance
QC.....Quality Control
RA.....Recreation Area
RBP.....Rapid Bioassessment Protocol
Reclamation .....U.S. Department of the Interior, Bureau of Reclamation
RM .....River Mile

RMP .....Resource Management Plan

RP.....Relicensing Participant

RSP .....Revised Study Plan

RST .....Rotary Screw Trap

RWF .....Resource-Specific Work Groups

RWG .....Resource Work Group

RWQCB.....Regional Water Quality Control Board

SC.....State candidate for listing under CESA

SCD.....State candidate for delisting under CESA

SCE .....State candidate for listing as endangered under CESA

SCT .....State candidate for listing as threatened under CESA

SD1 .....Scoping Document 1

SD2 .....Scoping Document 2

SE.....State Endangered Species under the CESA

SFP.....State Fully Protected Species under CESA

SFPUC .....San Francisco Public Utilities Commission

SHPO .....State Historic Preservation Office

SI.....International System

SJRA .....San Joaquin River Agreement

SJRGA .....San Joaquin River Group Authority

SJTA .....San Joaquin River Tributaries Authority

SPD .....Study Plan Determination

SRA.....State Recreation Area

SRMA .....Special Recreation Management Area or Sierra Resource Management Area (as per use)

SRMP.....Sierra Resource Management Plan

SRP .....Special Run Pools

SSC .....State species of special concern

ST.....California Threatened Species under the CESA

STORET .....Storage and Retrieval

SWAMP.....Surface Water Ambient Monitoring Program

SWE .....Snow-Water Equivalent

SWRCB.....State Water Resources Control Board

TAC.....Technical Advisory Committee
TAF .....thousand acre-feet
TCP .....Traditional Cultural Properties
TDS .....Total Dissolved Solids
TID .....Turlock Irrigation District
TMDL .....Total Maximum Daily Load
TOC.....Total Organic Carbon
TRT .....Tuolumne River Trust
TRTAC .....Tuolumne River Technical Advisory Committee
UC .....University of California
USDA.....U.S. Department of Agriculture
USDOC .....U.S. Department of Commerce
USDOI .....U.S. Department of the Interior
USFS .....U.S. Department of Agriculture, Forest Service
USFWS .....U.S. Department of the Interior, Fish and Wildlife Service
USGS .....U.S. Department of the Interior, Geological Survey
USR.....Updated Study Report
UTM.....Universal Transverse Mercator
VAMP .....Vernalis Adaptive Management Plan
VELB .....Valley Elderberry Longhorn Beetle
VRM .....Visual Resource Management
WPT .....Western Pond Turtle
WSA.....Wilderness Study Area
WSIP .....Water System Improvement Program
WWTP .....Wastewater Treatment Plant
WY .....water year
µS/cm .....microSeimens per centimeter

1.0 INTRODUCTION

1.1 Background

Turlock Irrigation District (TID) and Modesto Irrigation District (MID) (collectively, the Districts) are the co-licensees of the 168-megawatt Don Pedro Project (Project) located on the Tuolumne River in western Tuolumne County in the Central Valley region of California. The Don Pedro Dam is located at river mile (RM) 54.8 and the Don Pedro Reservoir has a normal maximum water surface elevation of 830 feet above mean sea level (ft msl; NGVD 29). At elevation 830 feet, the reservoir stores over 2,000,000 acre-feet (AF) of water and has a surface area slightly less than 13,000 acres (ac). The watershed above Don Pedro Dam is approximately 1,533 square miles (mi^2). The Project is designated by the Federal Energy Regulatory Commission (FERC) as project no. 2299.

Both TID and MID are local public agencies authorized under the laws of the State of California to provide water supply for irrigation and municipal and industrial (M&I) uses and to provide retail electric service. The Project serves many purposes including providing water storage for the beneficial use of irrigation of over 200,000 ac of prime Central Valley farmland and for the use of M&I customers in the City of Modesto (population 210,000). Consistent with the requirements of the Raker Act passed by Congress in 1913 and agreements between the Districts and City and County of San Francisco (CCSF), the Project reservoir also includes a "water bank" of up to 570,000 AF of storage. CCSF may use the water bank to more efficiently manage the water supply from its Hetch Hetchy water system while meeting the senior water rights of the Districts. The "water bank" within Don Pedro Reservoir provides significant benefits for CCSF's 2.6 million customers in the San Francisco Bay Area.

The Project also provides storage for flood management purposes in the Tuolumne and San Joaquin rivers in coordination with the U.S. Army Corps of Engineers. Other important uses supported by the Project are recreation, protection of aquatic resources in the lower Tuolumne River, and hydropower generation.

The Project Boundary extends from RM 53.2, which is one mile below the Don Pedro powerhouse, upstream to RM 80.8 at an elevation corresponding to the 845-foot contour (31 FPC 510 [1964]). The Project Boundary encompasses approximately 18,370 ac with 78 percent of the lands owned jointly by the Districts and the remaining 22 percent (approximately 4,000 ac) owned by the United States and managed as a part of the U.S. Bureau of Land Management Sierra Resource Management Area.

The primary Project facilities include the 580-foot-high Don Pedro Dam and Reservoir completed in 1971; a four-unit powerhouse situated at the base of the dam; related facilities including the Project spillway, outlet works, and switchyard; four dikes (Gasburg Creek Dike and Dikes A, B, and C); and three developed recreational facilities (Fleming Meadows, Blue Oaks, and Moccasin Point Recreation Areas). The location of the Project and its primary facilities is shown in Figure 1.1-1.

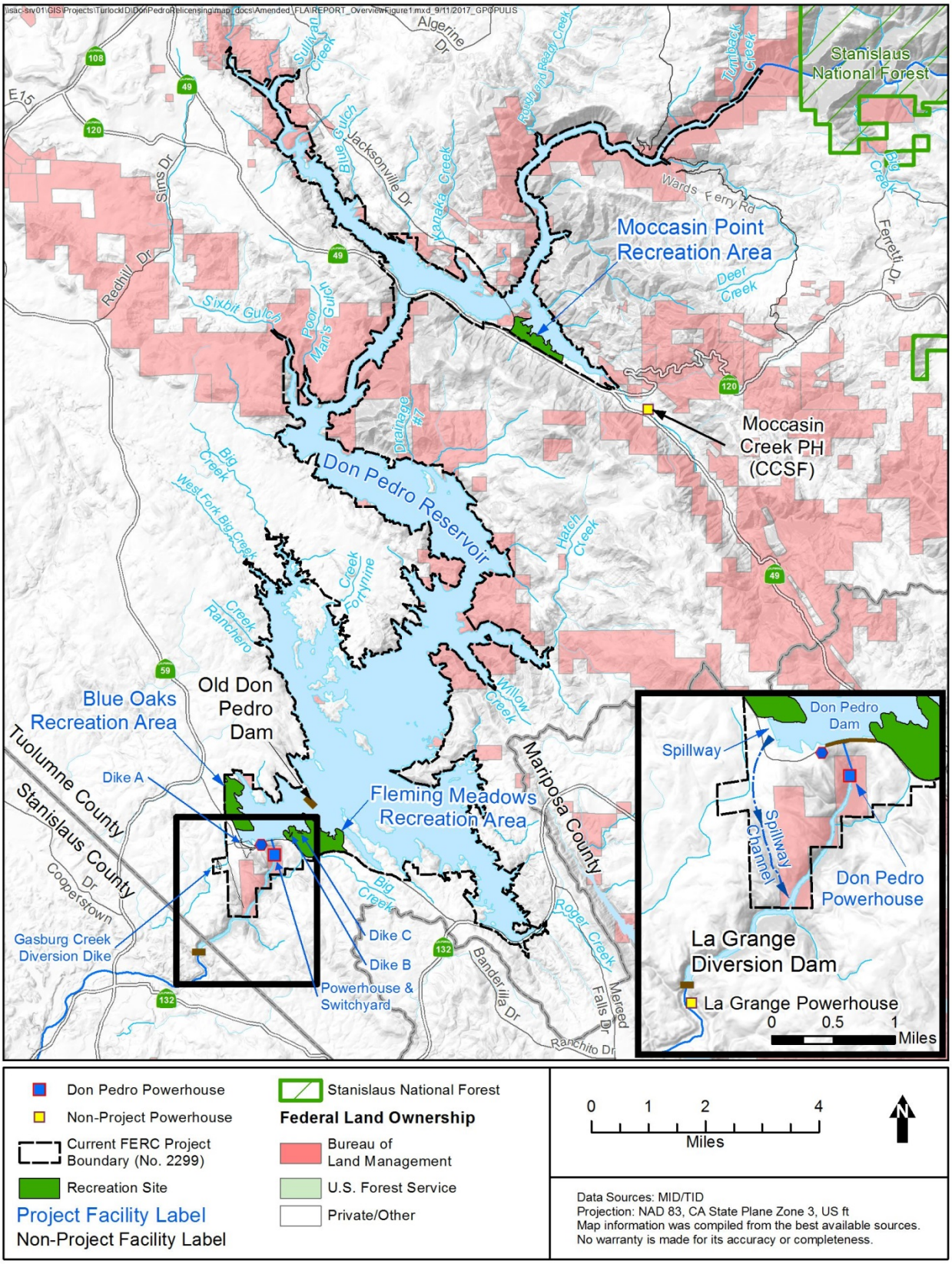

Figure 1.1-1. Don Pedro Project location.

1.2 Relicensing Process

The current FERC license for the Project expires on April 30, 2016, and the Districts will apply for a new license no later than April 30, 2014. The Districts began the relicensing process by filing a Notice of Intent and Pre-Application Document (PAD) with FERC on February 10, 2011, following the regulations governing the Integrated Licensing Process (TID/MID 2011a). The Districts' PAD included descriptions of the Project facilities, operations, license requirements, and Project lands as well as a summary of the extensive existing information available on Project area resources. The PAD also included ten draft study plans describing a subset of the Districts' proposed relicensing studies. The Districts then convened a series of Resource Work Group meetings, engaging agencies and other relicensing participants in a collaborative study plan development process culminating in the Districts' Proposed Study Plan and Revised Study Plan filings to FERC on July 25, 2011 and November 22, 2011, respectively.

On December 22, 2011, FERC issued its Study Plan Determination (SPD) for the Project, approving, or approving with modifications, 34 studies proposed in the Revised Study Plan that addressed Cultural and Historical Resources, Recreational Resources, Terrestrial Resources, and Water and Aquatic Resources. In addition, as required by the SPD, the Districts filed three new study plans (W&AR-18, W&AR-19, and W&AR-20) on February 28, 2012 and one modified study plan (W&AR-12) on April 6, 2012. Prior to filing these plans with FERC, the Districts consulted with relicensing participants on drafts of the plans. FERC approved or approved with modifications these four studies on July 25, 2012.

Following the SPD, a total of seven studies (and associated study elements) that were either not adopted in the SPD, or were adopted with modifications, formed the basis of Study Dispute proceedings. In accordance with the Integrated Licensing Process, FERC convened a Dispute Resolution Panel on April 17, 2012 and the Panel issued its findings on May 4, 2012. On May 24, 2012, the Director of FERC issued his Formal Study Dispute Determination, with additional clarifications related to the Formal Study Dispute Determination issued on August 17, 2012.

On January 17, 2013, the Districts issued the Initial Study Report (ISR) for the Project and held an ISR meeting on January 30 and 31, 2013. The draft *W&AR-03: Reservoir Temperature Model Report* was included in the ISR filing. The Districts filed a summary of the ISR meeting with FERC on February 8, 2013. Comments on the meeting summary and requests for new studies and study modifications were filed by relicensing participants on or before March 11, 2013 and the Districts filed reply comments on April 9, 2013. No requests for study modifications to W&AR-03 were made by relicensing participants. FERC issued the Determination on Requests for Study Modifications and New Studies on May 21, 2013.

This final study report includes updated graphics and clarifying edits to the draft report. This report describes the objectives, methods, and results of the Reservoir Temperature Model Study (W&AR-03) as implemented by the Districts in accordance with FERC's SPD and any subsequent study modifications and clarifications. Documents relating to the Project relicensing are publicly available on the Districts' relicensing website at www.donpedro-relicensing.com.

1.3 Study Plan

The Districts' continued operation and maintenance of the Project will affect the temperature regime of waters in the Don Pedro Reservoir. Similarly, flow releases from Don Pedro Reservoir will affect the temperature of waters downstream of Don Pedro Dam and may contribute to cumulative effects to the aquatic resources of the lower Tuolumne River.

The FERC-approved Reservoir Temperature Model Study Plan (W&AR-03) described the procedures applied to develop a three dimensional (3-D) model characterizing the thermal structure and dynamics of the Don Pedro Reservoir (TID/MID 2011b). Through this model, water temperatures in the reservoir have been simulated using historical meteorology, hydrology and water temperatures, along with current Project operations. In the relicensing process, the reservoir temperature model presented herein is a tool that will be used to evaluate the effects to the reservoir's thermal structure under potential future operating scenarios.

This study was also conducted in accordance with the Consultation Workshop protocol, a draft of which was issued to relicensing participants on March 5, 2012, reviewed during a meeting with relicensing participants on March 20, 2012 and filed with FERC as final on May 18, 2012 after a 30-day review and comment period following the March 20 meeting. No comments were received on the Workshop protocol.

The Districts conducted Workshops with relicensing participants related to the development and use of the reservoir temperature model on April 10, 2012; October 26, 2012; January 24, 2013; and June 4, 2013. Meeting materials were circulated prior to each Workshop, meeting notes were provided for review and comment, all comments were responded to, and final Workshop notes were filed with FERC.

On May 18, 2017, the Districts hosted a Modeling Tools Update Meeting with relicensing participants. At the meeting, the Districts summarized recent changes made to the MIKE3-FM model by Danish Hydraulic Institute (the model's creators) and how these changes necessitated recalibrating the Reservoir Temperature Model. The model changes and recalibration, which are summarized in Attachment A, did not result in any changes to this study report.

2.0 GOALS AND OBJECTIVES

The goal of this study is to develop a reservoir temperature model that accurately simulates and characterizes the seasonal water temperature dynamics experienced in Don Pedro Reservoir under current and potential future conditions. The model will be able to:

- reproduce observed reservoir temperatures, within acceptable calibration standards, over a range of hydrologic conditions;
- provide output that can inform other studies, analyses, and models; and
- predict potential changes in reservoir thermal conditions under alternative future operating scenarios.

The reservoir temperature model forms an integrated suite of site-specific models when combined with the Project Operations Model (Study W&AR-02) and the Lower Tuolumne River Temperature Model (Study W&AR-16) (TID/MID 2013a; TID/MID 2013b). Output from the reservoir temperature model serves as input to the river temperature model. The reservoir and river temperature models, working together, also support the Chinook and *O. mykiss* population models developed under studies W&AR-06 and W&AR-10, respectively.

3.0 STUDY AREA

The study area consists of the Don Pedro Reservoir, extending from about elevation 300 feet (ft) to about elevation 850 feet, or from the tailwater of Don Pedro powerhouse to about 20 feet above the Don Pedro Reservoir normal maximum reservoir elevation of 830 feet. The study area is shown in Figure 3.0-1.

The Don Pedro Reservoir extends upstream from the Don Pedro Dam (RM 54.8) for approximately 26 miles at the normal maximum water surface elevation of 830 feet. The surface area of the reservoir at the 830-ft elevation is approximately 12,960 ac and the gross storage capacity is 2,030,000 AF. The Don Pedro Reservoir shoreline, including the numerous islands within the reservoir, is approximately 160 miles long.

Inflows to Don Pedro Reservoir consist predominantly of flows from the main stem of the Tuolumne River. The flow in the main stem of the Tuolumne River consists of regulated releases from the Hetch Hetchy Reservoir system, located above RM 117, and unregulated flows from several significant tributaries, including the South Fork, Middle Fork, Clavey River, and the North Fork. The North Fork of the Tuolumne River joins the main stem at RM 81.5, just upstream of the Don Pedro Project Boundary.

The upper Tuolumne River watershed, defined for purposes of this report as the subbasin above about RM 80, covers approximately 1,300 mi^2 of drainage area and contains all the major tributaries of the Tuolumne River, including the North Fork, South Fork, Middle Tuolumne, Clavey River, Cherry Creek, and Eleanor Creek. The upper Tuolumne River extends from the confluence of the Dana and Lyell Forks to just below the confluence of the North Fork at approximate elevation 850 feet. The average gradient of the river is roughly 110 feet/mile, but local gradients vary greatly. Flows in the upper Tuolumne River are regulated and controlled by the CCSF's Hetch Hetchy Water and Power system, including Hetch Hetchy Reservoir, Lake Eleanor and Cherry Lake, and CCSF's extensive infrastructure of water conveyance and water power facilities.

The foothills reach of the Tuolumne River extends from RM 54 to RM 80 and is dominated by the Don Pedro Project. This portion of the watershed includes several smaller tributaries including Woods Creek, Moccasin Creek, Hatch Creek and Rogers Creek that flow into Don Pedro Reservoir. The dendritic shape of the reservoir is indicative of the topographic influence of these tributaries. The resulting bathymetry of Don Pedro Reservoir is therefore complex and tortuous in nature. Added to the complexity of the natural terrain is the presence of the Old Don Pedro Dam at RM 56.5, which was submerged in 1971 with the filling of Don Pedro Reservoir. Old Don Pedro Dam had a crest elevation of approximately 600 feet and is approximately 1,000 feet long.

Outflows from Don Pedro Reservoir are provided by the powerhouse intake tunnel with a centerline elevation of 534 feet. The maximum hydraulic capacity of the powerhouse tunnel is 6,300 cubic feet per second (cfs). Reservoir outflows can also be provided by the outlet works control gates which were installed in the original diversion tunnel used for new Don Pedro construction. The invert elevation of the intake to the outlet works is at approximate elevation

342 feet and the hydraulic capacity of the outlet works and tunnel is approximately 7500 cfs. Reservoir releases can also be provided at the gated and ungated spillways located to the north of the main dam.

The primary purpose of the Don Pedro Reservoir is to provide water storage to meet the needs of the Districts' irrigation and M&I water supply customers, flood control, and a "water bank" for the City and County of San Francisco to supplement its Hetch Hetchy water system. As a storage reservoir, Don Pedro can experience significant variations in water levels in a given year. Historically, the highest water level reached was approximately 831 feet (1997) and the lowest level was approximately 598 feet (1977). The minimum power pool for Don Pedro Reservoir is 600 feet.

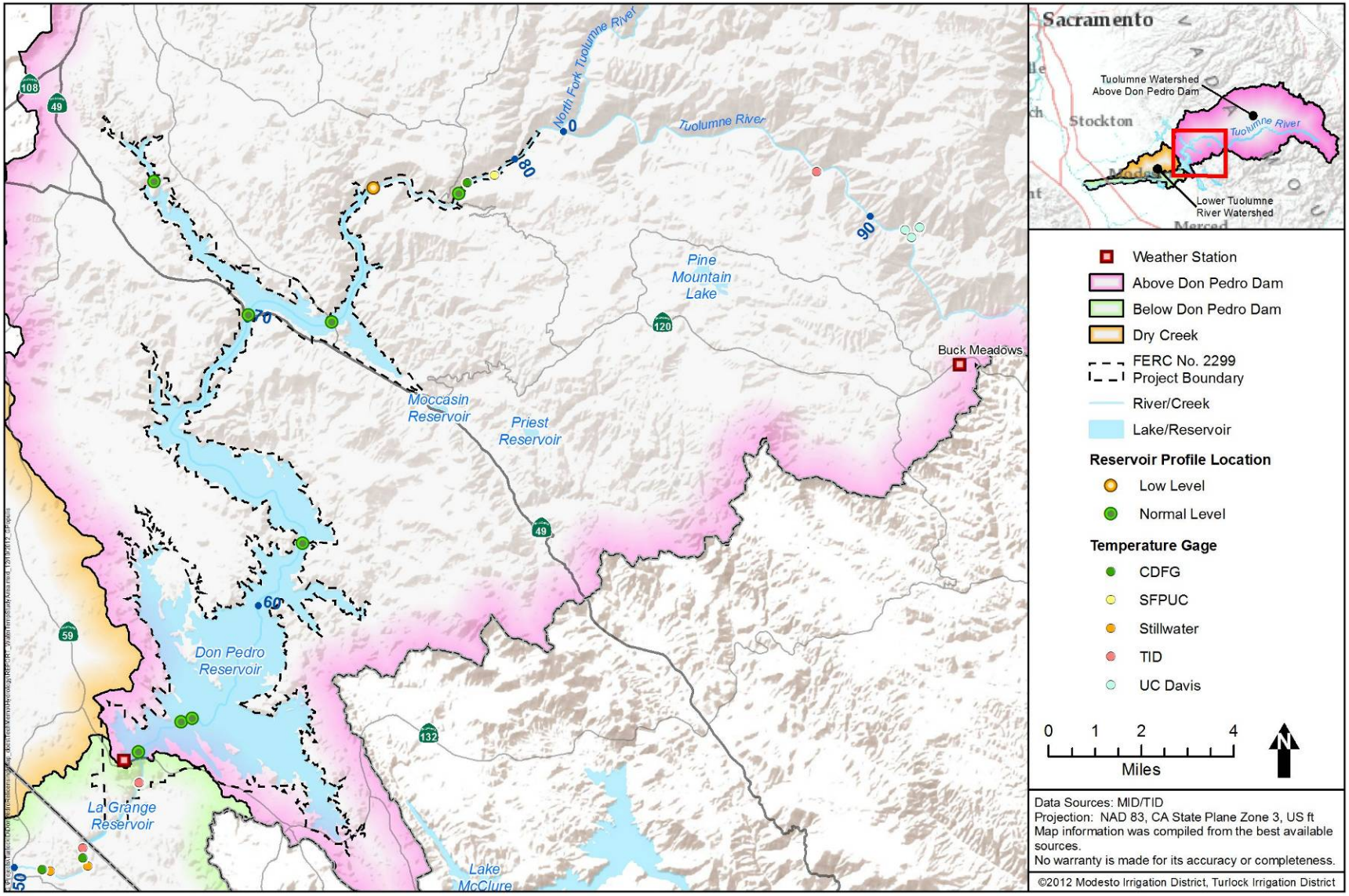

Figure 3.0-1. Study area.

4.0 METHODOLOGY

4.1 Model Platform Selection

To select the appropriate reservoir temperature model, the Districts developed a list of required water temperature model capabilities necessary to meet the study goals and objectives. The primary model requirements are to:

- simulate water temperatures on an appropriate time-step to capture water temperature variability on a temporal scale which is biologically meaningful;
- simulate water temperatures over a range of historical hydrology and meteorology experienced in the Project area;
- account for the effect of major physical in-reservoir complexities on reservoir temperatures, including the old Don Pedro Dam and the reservoir's geometry; and
- simulate the effects of changes in storage, climatological factors, inflow temperatures and discharge elevation on the temperature of Don Pedro releases.

The following water temperature model platforms were originally considered for use[1]:

- HEC-5Q, one-dimensional (1-D), longitudinally- and laterally-averaged (AD Consultants et. al. 2009)
- CE-QUAL-W2, two-dimensional (2-D), laterally averaged (Cole and Wells 2003)
- RMA-10, three-dimensional (3-D) (King 1993)
- MIKE3-FM, three-dimensional (3-D) (DHI 2009a)

The 1-D model, HEC-5Q, has been widely used across many relicensing and water resource processes[2] and has been found to provide consistent and reliable results where appropriately applied. HEC-5Q is empirical in design and reservoir behavior is estimated by equations and algorithms developed from long and narrow (highly longitudinal) or short and wide (highly transverse) reservoirs. The one dimensional (1-D) structure of the model does not determine the horizontal variation in temperatures that would be observed in the 24 mile long, highly dendritic Don Pedro Reservoir, nor does it have the ability to adequately model the effects on reservoir temperature variability of the now submerged Old Don Pedro Dam, especially at lower reservoir levels. Temperature data obtained from actual vertical profiles in the reservoir and upstream and downstream temperature data describe a more complex temperature regime. Hence, model results from the 1-D model would be of limited value.

The 2-D model, CE-QUAL-W2, has been widely used and is recognized as a reliable model. However, like the HEC-5Q model, CE-QUAL assumes complete lateral mixing and averages

[1] For additional detail, see W&AR-03 Reservoir Temperature Model Study Plan (TID/MID 2011b).

[2] The San Joaquin River Basin Water Temperature Model (SJR5Q) is an application of the HEC-5Q modeling platform that represents the Don Pedro Reservoir as a one-dimensional vertically-segmented reservoir (AD Consultants 2009).

lateral temperatures. The CE-QUAL-W2 model would require multiple branches to accurately represent the complex geometry of the Don Pedro Reservoir and result in the loss of detail where branches overlap. Segment widths in the middle, south and north Bays of the 2-D model would exceed two miles at certain locations; the 2-D model assumes uniform parameters (i.e., velocity, temperature) throughout the width of the segment. Hence, the model results would also be of somewhat limited value.

Two 3-D model platforms were considered, the RMA-10 and MIKE3 models. Both models account for environmental variability, providing results that are more biologically relevant, and provide greater flexibility when evaluating outflow temperature dynamics than the 1-D or 2-D models. However, the MIKE3 documentation, graphical user interface, and technical support were considered to be more suitable for purposes of relicensing where relicensing participants need to fully understand and potentially use the model. Hence, based on review of the two 3-D modeling platforms, MIKE3-FM was selected for the temperature modeling of the Don Pedro Reservoir.

The selected modeling approach allows the Districts to develop a model that meets the full needs of the relicensing process. MIKE3 was developed by the Danish Hydraulic Institute (DHI) as a professional engineering software package for 3-D free-surface flows (DHI 2009a, 2009b, 2009c). MIKE3 is fully integrated with geographic information systems enabling the user to efficiently set up model geometry given geo-referenced bathymetric data. The Graphical User Interface enables the modeler to efficiently prepare input and graphically present output. The flexible mesh version of the model (MIKE3-FM) (DHI 2011) allows variable-spacing of computational grid points to obtain high spatial resolution in areas of prime interest while saving on model run time through a coarse mesh in other areas. It simulates unsteady three-dimensional flows taking into account density variations, bathymetry, and external forcing such as meteorology, water levels, currents and other hydrographic conditions.

4.2 Selection of Model Time Step

The reservoir temperature model interfaces with the Project Operations Model (Study W&AR-02) and the lower Tuolumne River temperature model (Study W&AR-16) (TID/MID, 2013a; TID/MID 2013b). Output from the reservoir temperature model serves as input to the river temperature model. Flow releases from Don Pedro and reservoir levels are provided by the Operations Model on a mean daily basis. Therefore, a daily time step was chosen for the reservoir model.

4.3 Input Data, Calibration and Validation Data

The two broad categories of data required by the model are (1) input data on reservoir characteristics and (2) data used for model calibration/verification. Input data pertain to the detailed physical characteristics of the reservoir being modeled, including bathymetry and boundary conditions. The boundary conditions include inflows, withdrawals/releases, temperature of inflows, and local meteorological data (air temperature, wind speed and direction, relative humidity). Mechanistic response parameters such as heat exchange coefficients were also input along with reservoir operation rules to create the outflow data set that served as an

input to this model (see Project Operations Model, W&AR-02). Data for model calibration/verification are primarily measurements of the metrics that are calculated by the model, which in this case are temperature measurements in the reservoir (i.e., vertical profiles). The specific data required for the MIKE3-FM model are listed in Table 4.3-1 under four headings: (1) physical and geomorphological, (2) flow and operation parameters (3) inflow temperatures, and (4) meteorology. Additional detail regarding each type of data is presented in the sections below.

4.3.1 Physical and Geomorphological

Construction of the reservoir's topographic surface for modeling is documented in the Districts' Don Pedro Reservoir Bathymetric Study Report provided as Attachment C. In brief, the reservoir ground surface below the full pool elevation of 830 feet was determined by two techniques: underwater surfaces were surveyed using field measurements collected from May 1 to June 5, 2011, and dry surfaces topography was obtained using radar technology collected in August 2004. Data obtained by the two techniques were then synthesized into one surface using geographic information systems software. The data above elevation 760 feet and below 792 feet overlapped; topographic measurements in the overlapping interval showed a good correlation. The Bathymetric Report was submitted to relicensing participants for review October 18, 2012 and was discussed at the Workshop held on October 26, 2012.

4.3.2 Inflows, Outflows, and Operations

Daily flows developed as part of the Tuolumne River Operations Model (W&AR-02) (TID/MID 2013a) were used as input to the reservoir temperature model calibration and verification procedures. The combined total inflow to the reservoir was calculated by using a mass balance equation that derives inflow from the record of reservoir releases, change in storage and estimated reservoir losses. This computed value is then disaggregated between regulated and unregulated components by recognizing the unregulated component of inflow which has been separately computed as the difference between the estimated unimpaired flow at the U.S. Geological Survey's La Grange gage less the estimated unimpaired flow at the Hetch Hetchy system. The unimpaired flow record was developed within a series of Workshops with relicensing participants held as part of the W&AR-02: Operations Modeling Study, culminating in a consensus approach finalized in Workshop No. 4 on March 27, 2013.[3]

The main stem of the Tuolumne River provides the overwhelming majority of reservoir inflows. There are several local tributaries to the reservoir as well (e.g., Moccasin, Sullivan, Woods Creeks). These are small, low elevation tributaries, all of which are intermittent streams except for Moccasin Creek which has a minimum flow provided by CCSF's upstream facilities of about 20 cfs. These small tributaries account for about 1 percent of total reservoir inflows.

[3] The method of developing the unimpaired flow is described in Attachment 2 of the Districts April 9, 2013 filing with FERC entitled "*Response to Relicensing Participants Comments on Initial Study Report*."

Table 4.3-1. MIKE3-FM model data sources.

Required Data	Source		
Physical and Geomorphological—Don Pedro Reservoir and Dam			
Bathymetry	Field survey	Attachment C	
Normal maximum water level	Design drawings	830 ft	
Minimum power pool	Design drawings	600 ft	
Dam spillway, ungated (elevation)	Design drawings	830 ft	
Dam spillway, ungated (length, type)	Design drawings	995 ft long; ogee crest	
Powerhouse intake (invert elevation)	Design drawings	525 ft	
Powerhouse intake (lat/long)	Design drawings	37.70342	120.419095
Diversion Tunnel/Outlet works (invert elevation)	Design drawings	342 ft	
Diversion Tunnel Intake/Outlet works (lat/long)	Design drawings	37.70402	120.420002
Physical and Geomorphological—Old Don Pedro Dam			
Old Don Pedro Dam (lat/long above/below)	TID and MID 2011	729134 E	4177175 N
		728741 E	4177044 N
Old Don Pedro normal maximum water level	Design drawings	600 ft	
Old Don Pedro Dam top of gates elevation	Design drawings; TID and MID 2011	605.5 ft (NGVD 29)	
Old Don Pedro Dam crest (length, type)	Design drawings	1000 ft	
Old Don Pedro outlets (elevations, arrangement)	TID	multiple[1]	
Flow and Operations			
Tuolumne River upstream of reservoir (regulated)	CCSF, TID[2]	See W&AR-02 Project Operations Model (TID/MID 2013a)	
Tuolumne River upstream of reservoir (total flow)	TID		
Storage (daily)	TID		
Releases through powerhouse and outlets (daily)	TID		
Temperature			
Tuolumne River upstream of reservoir (Tuolumne River at Indian Creek Trail, Tuolumne River at Ward's Ferry, and other upstream locations)[2]	Districts CCSF CDFW	See Attachment D	
Tributaries: Rough & Ready, Moccasin, Sullivan and Woods Creeks	Districts		
Reservoir Profiles	Districts CDFW		
Tuolumne River downstream of reservoir (below Don Pedro Powerhouse)	Districts		
Meteorology			
Air temperature, wind speed/direction relative humidity	Don Pedro Weather Station	See Attachment D	

[1] The Old Don Pedro Dam had 12 gated outlets arranged in two rows of six gates. Each outlet was 52-inches in diameter; the lower row of six have a centerline at elevation 421 ft and the upper row of six has a centerline of elevation 511 ft. All of these gates were left in the open position when Old Don Pedro Dam was inundated by the new Don Pedro Dam. There are also three 5-ft diameter sluiceway gates, each with a centerline at 355 ft; these gates are believed to be closed.

[2] CCSF's site, TR-8, and California Department of Fish and Game's site, TRWARDS, are located within the reservoir at approximately 785 msl and 763 msl, respectively. The Districts' site Tuolumne River at Indian Creek Trail is upstream of the reservoir's influence.

4.3.3 Temperature Data

Temperature data have been collected at a number of locations in the Tuolumne River watershed and the Don Pedro Reservoir (Table 4.3-2; Figure 3.0-1; also see Attachment D). Obtaining a complete inflow temperature data set was particularly challenging, as CCSF's data collection site TR-8, and CDFW's site TRWARDS, are located within the reservoir's drawdown zone at approximate elevation 785 feet and 763 feet, respectively, and as such may alternate between

being within a reservoir environment or a river environment. When a station is located within the reservoir it cannot be used as an inflow input to the reservoir model. The Districts' temperature station Tuolumne River at Indian Creek Trail, installed in October 2010, was located above the influence of the Don Pedro Reservoir at elevation 1,080 feet. Located near the North Fork Tuolumne River confluence, this temperature gage was used to estimate inflow temperatures in the model.

CDFW has collected monthly temperature profiles at six stations in Don Pedro Reservoir since 2004. This data set has been augmented by the Districts since 2010. Since October 2010, the Districts have collected temperature profiles at CDFW's six established stations plus stations above and below the Old Don Pedro dam. Monthly profiles were collected using a Hydrolab MS5 multi-parameter water quality sonde (temperature sensor +/- 0.2°C).

The reservoir outflow water temperature, measured just below the powerhouse release, has been recorded since October 2010. This is a point measurement, not a profile.

Table 4.3-2. Reservoir model water temperature measurement locations with period of record.

Site Location	Approximate River Mile	Latitude	Longitude	Period of Record
Tuolumne River at Indian Creek Trail	83.0	37.88383	-120.15361	10/2010 - 11/2012
Near New Don Pedro Dam	55.1	37.702638	-120.421722	8/2004 – 11/2012
Below Old Don Pedro Dam	56.3	37.712083	-120.405	7/2011 – 11/2012
Above Old Don Pedro Dam	56.4	37.71316	-120.4005	7/2011 – 11/2012
At Middle Bay	62.0	37.76794	-120.357	8/2004 – 11/2012
At Highway 49 Bridge	70.1	37.83955	-120.378305	8/2004 – 11/2012
At Woods Creek Arm	--	37.88127	-120.415361	8/2004 – 11/2012
At Jacksonville Bridge	72.3	37.83733	-120.34525	8/2004 – 11/2012
At Ward's Ferry	78.4	37.87744	-120.295	8/2004 – 11/2012
Tuolumne River below Don Pedro Powerhouse (reservoir outflow temp – not a profile)	54.3	37.6929	-120.421616	10/2010 - 11/2012

4.3.4 Meteorology

Air temperature, wind speed and direction, and relative humidity are required inputs for the model. To provide data on local weather conditions, the Districts installed a weather station near the Blue Oaks area of the reservoir on November 30, 2010 (see Figure 3.0-1; the data are available in Attachment D). For comparison purposes, data from other local meteorological stations were also compiled (Figure 4.3-1). Data collected from these stations were used for calibration and validation of the model herein. Development of the meteorological data set for the full period of record, Water Year 1971 through 2012, is described in Attachment E.

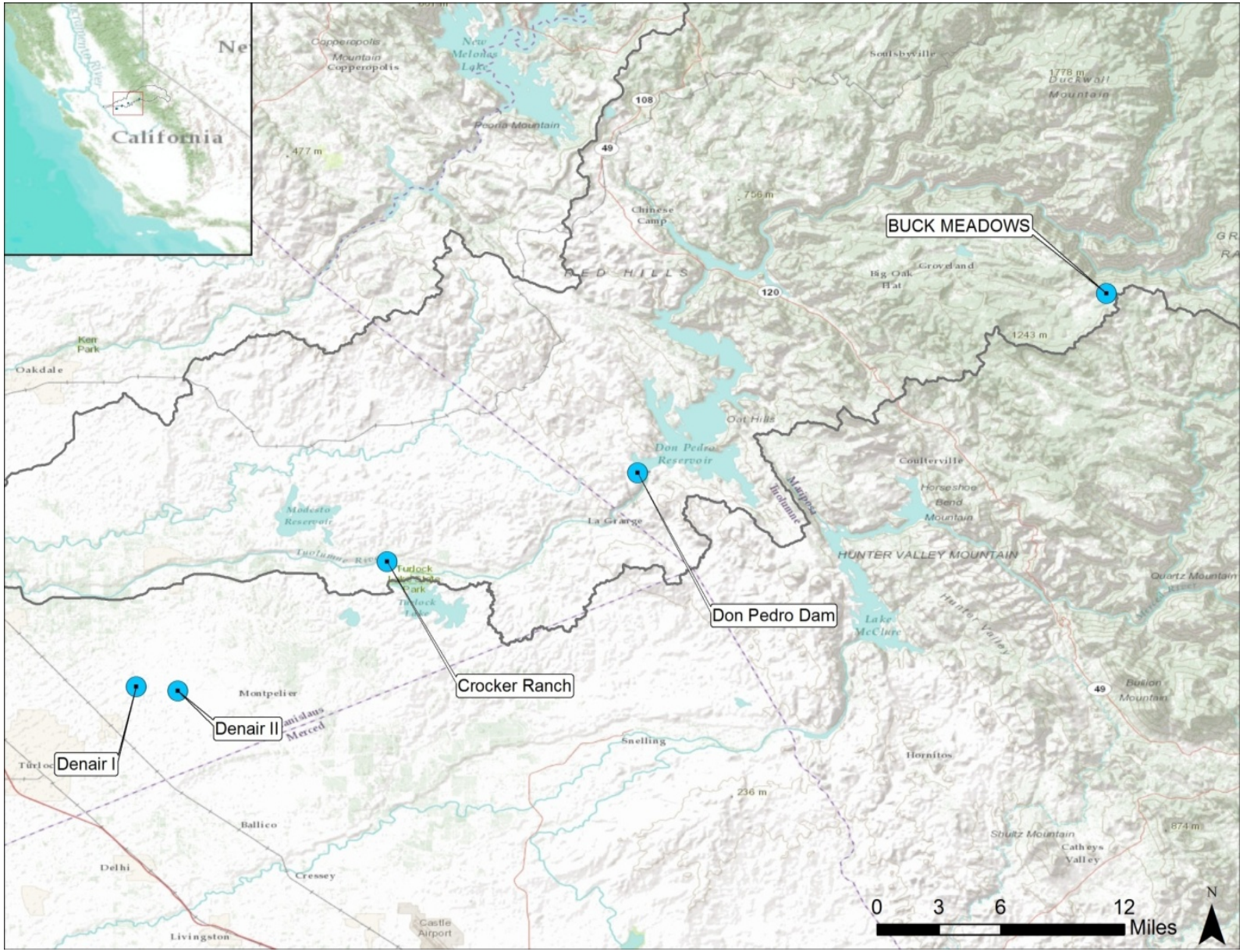

Figure 4.3-1. Meteorological station locations

4.4 Model Development

4.4.1 Model Structure and Interface

The MIKE3-FM model uses a master file called an "m3fm" file that controls all aspects of the simulation. The "*m3*" refers to the *m*odel *3* dimensional, and the "*fm*" refers to the *f*lexible *m*esh (FM) version that is being used for the Don Pedro Reservoir temperature model.

As shown in Figure 4.4-1, the "m3fm" file uses a graphical interface and a folder format that is similar to Windows Explorer[4] . The Don Pedro MIKE3-FM model and its components are best described by following the structure of the "m3fm" file itself (Figure 4.4-1). The main sections include:

- Domain (Section 4.4.2)
- Time (Section 4.4.3)
- Module Selection (Section 4.4.4)
- Hydrodynamic Module (Section 4.4.5)
- Temperature Module (Section 4.4.6)
- Output (Section 4.4.7)

Figure 4.4-1. MIKE3-FM master interface in "m3fm" file.

[4] By clicking on the "+" icon the underlying directories can be expanded and similarly collapsed using the "-" icon.

The bulk of the Don Pedro Reservoir temperature model is contained within the Hydrodynamic Module. Figure 4.4-1 shows the Hydrodynamic Module expanded. This module consists of 18 parts. Each of the components, and associated parts, is discussed below. The latest release of the DHI MIKE software in 2012 allows the use of either SI or English units. However the Don Pedro model was originally developed prior to the 2012 release, when only SI units were supported, thus they are used throughout the model.

4.4.2 Domain

The model domain details are described individually in this section.

4.4.2.1 Bathymetry

The first tab under the Domain folder will show the model bathymetry (Figure 4.4-2). As mentioned above, the bathymetry data are detailed in a separate report, provided herein as Attachment C. The model bathymetry data were measured as elevations above mean sea level; elevations are converted to meters for use in the model.

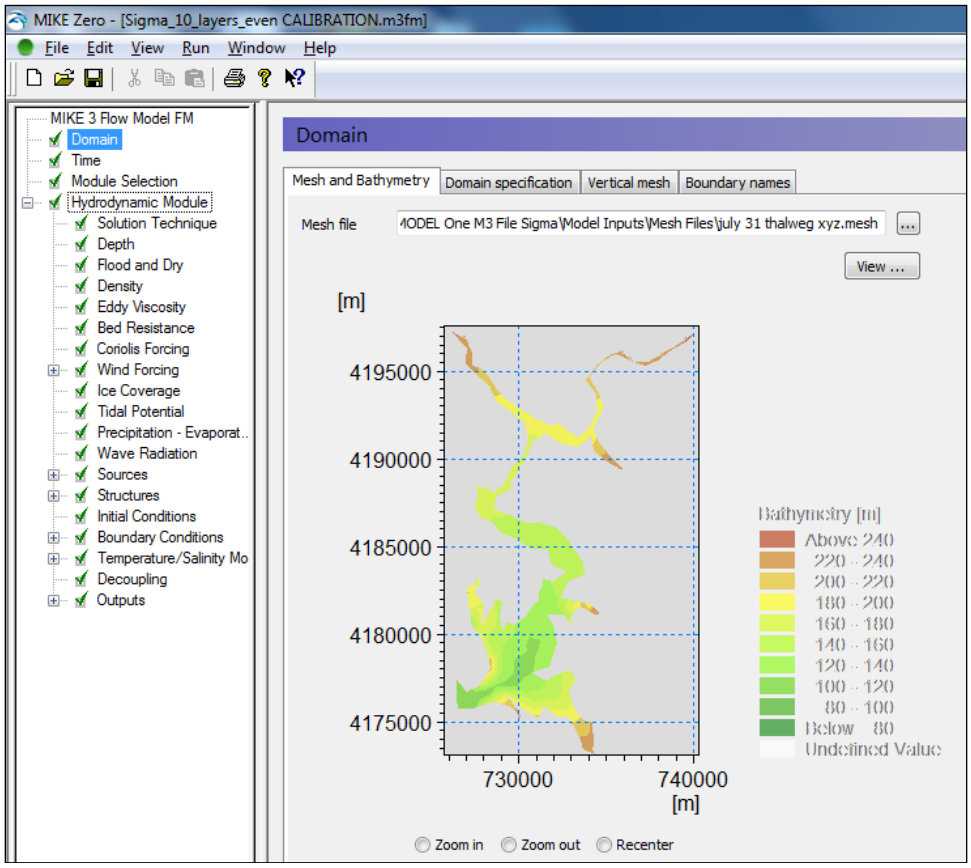

Figure 4.4-2. Model bathymetry screen.

4.4.2.2 Model Mesh

The second tab under the Domain folder displays mesh information and is not shown. The third tab will show the model vertical mesh options (Figure 4.4-3). The horizontal model mesh is created using DHI mesh creation tools and then imported into the "m3fm" run file. For the horizontal plane, the mesh uses unstructured triangular elements (Figure 4.4-4). For the vertical structure, the model has two options and within each option there are refinement choices (Figures 4.4-5 through 4.4-7). The options for the vertical structure are:

- Sigma Level. Under this option, a sigma level only grid is used. A sigma level grid uses a terrain following coordinate system. The model vertical mesh expands and contracts as the water depth changes, but keeps the number of vertical layers the same. An example of a sigma scheme transect along Don Pedro Reservoir is shown in Figure 4.4-5.
- Sigma and Z-level Combination (Combined Scheme). The sigma and z-level combined option allows the use of a fixed depth grid in deep water (z-level), with the sigma grid used in shallower water. A schematic of this option is shown in Figure 4.4-6.

Both schemes work well for the Don Pedro Reservoir. The type of scheme can be selected at the beginning of a model run. The number of vertical layers can also be set at the start of a model run. The combined scheme has the advantage of faster run times over the sigma scheme. The limitation of the combined scheme is that the water level must remain above the level where the fixed z-level grid begins. For this project, if the combined scheme was used, the z-level base elevation was set just above the Old Don Pedro Dam. Any run that will draw the reservoir level to, or below the Old Pedro Dam would use a sigma vertical scheme.

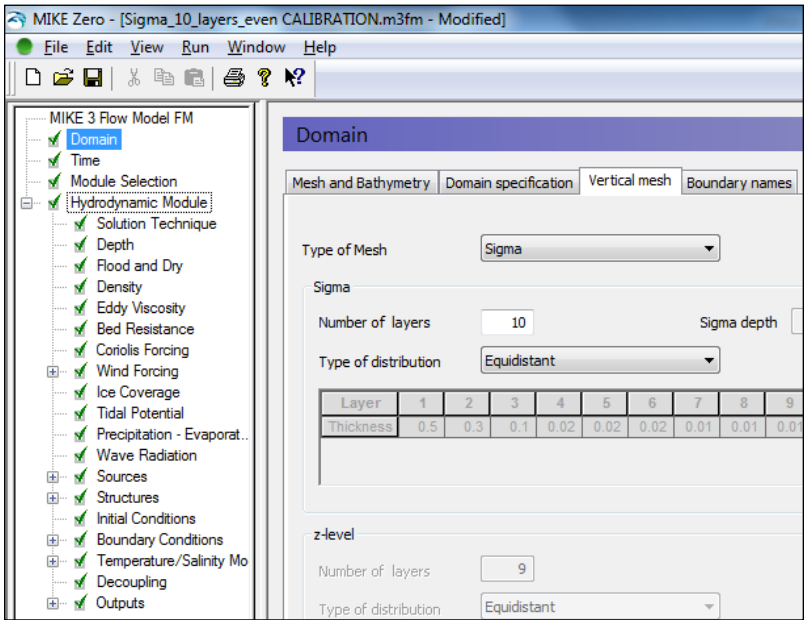

Figure 4.4-3. Vertical mesh option screen.

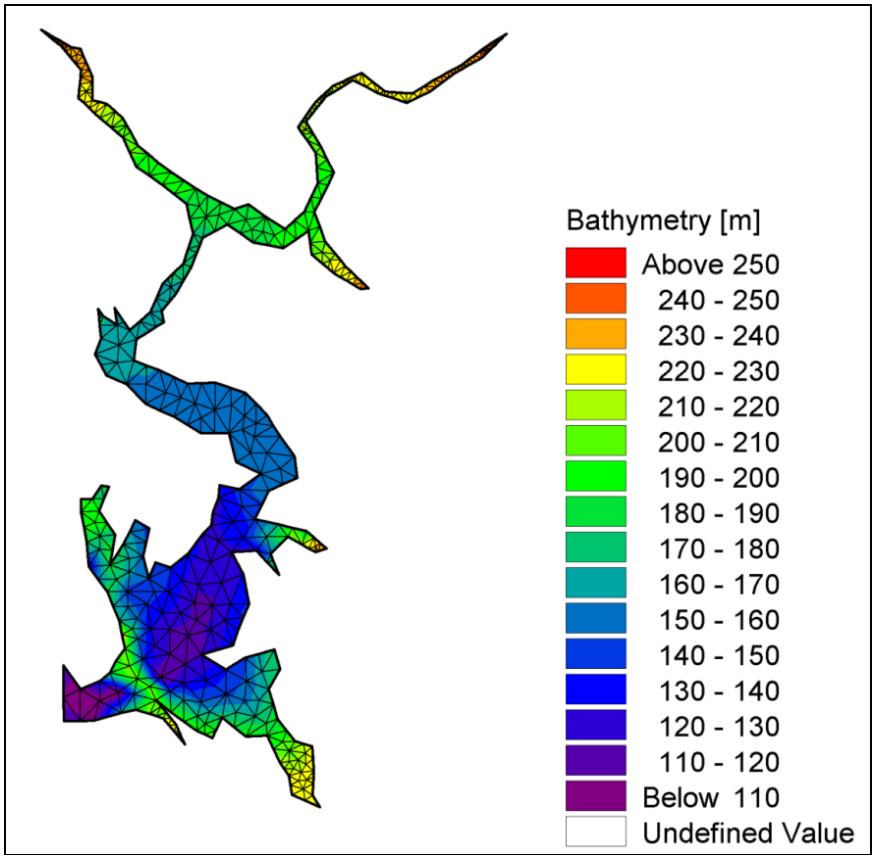

Figure 4.4-4. Model mesh horizontal layout.

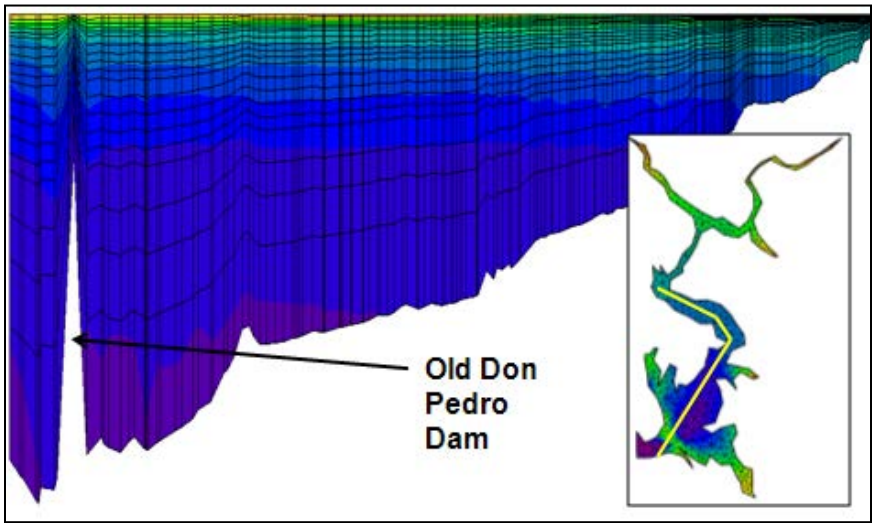

Figure 4.4-5. Example of sigma mesh reservoir longitudinal section

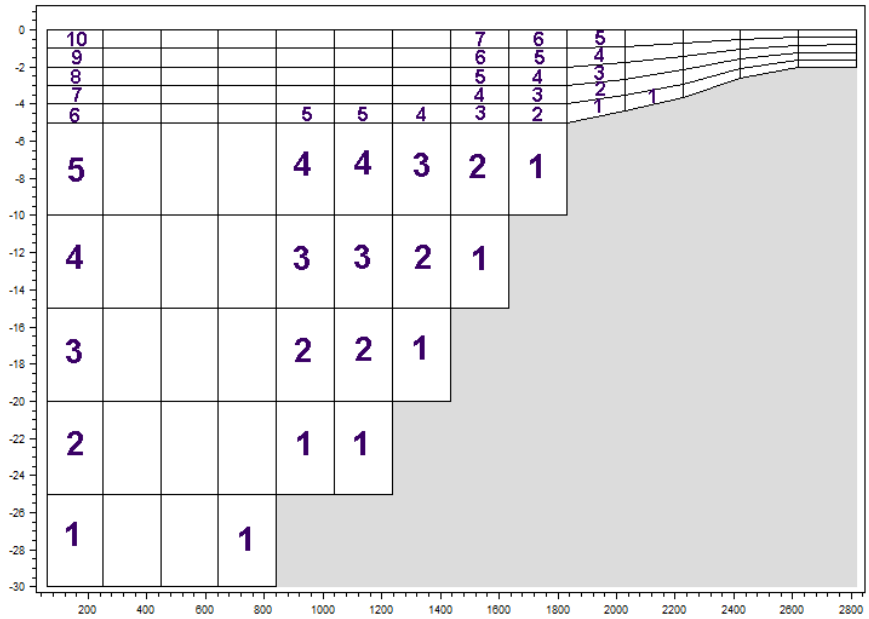

Figure 4.4-6. Example of combined sigma and z-level vertical mesh scheme.

4.4.3 Simulation Time

The model's time step is detailed in this section. The period-of-record for a model run is set using the "Time" tab, as shown in Figure 4.4-1. The user specifies the start date, the time step interval, and the number of time steps. The model will then compute the end date. The time step interval is only of relevance for the output of results, as results cannot be saved at less than the time step interval. For example, if the time step interval is set to 86,400 seconds, i.e. one day, then only daily output can be specified on the Output tab (see Section 4.4.7). For Don Pedro Reservoir the time step is almost always kept at one hour. The actual computational time step used by the model is calculated internally and continually varies, usually limited by computational stability considerations.

4.4.4 Module Selection

The temperature calculations, the focus of this study, are contained within the Hydrodynamic Module (Figure 4.4-7), which is the base module and is by default always included (Section 4.4.5).

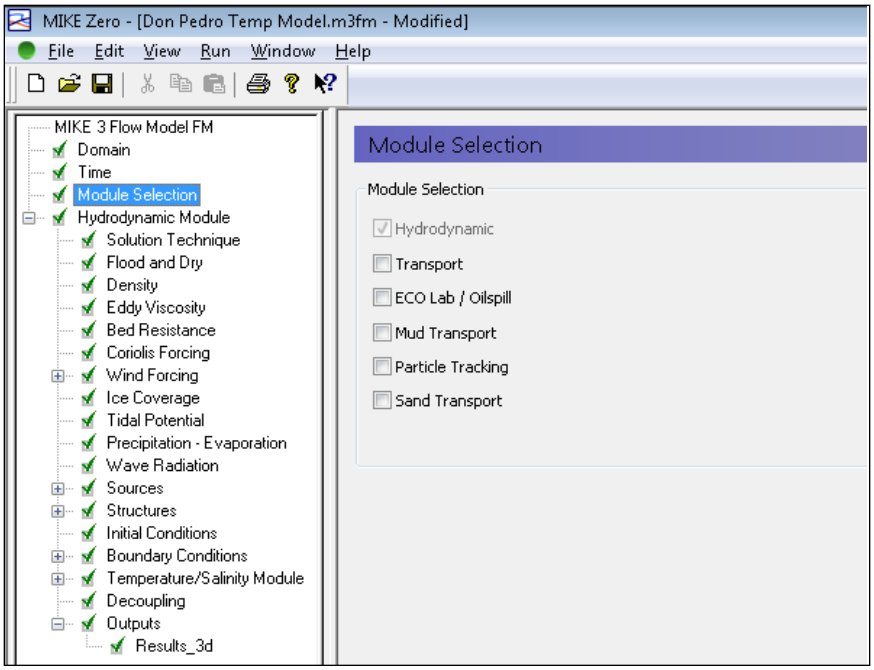

Figure 4.4-7. Module selection

4.4.5 Hydrodynamic Module

The model's hydrodynamic module details are contained in this section. As is shown above in Figure 4.4-7, only the hydrodynamic module is selected for the Don Pedro Reservoir temperature model. Each of the 18 components of the Hydrodynamic Module are discussed below.

4.4.5.1 Solution Technique

The first tab shows the solution technique parameters (Figure 4.4-8 below). In general the default values for these tend to produce good results. Most of the parameters here address the constraints around the internal time step calculation.

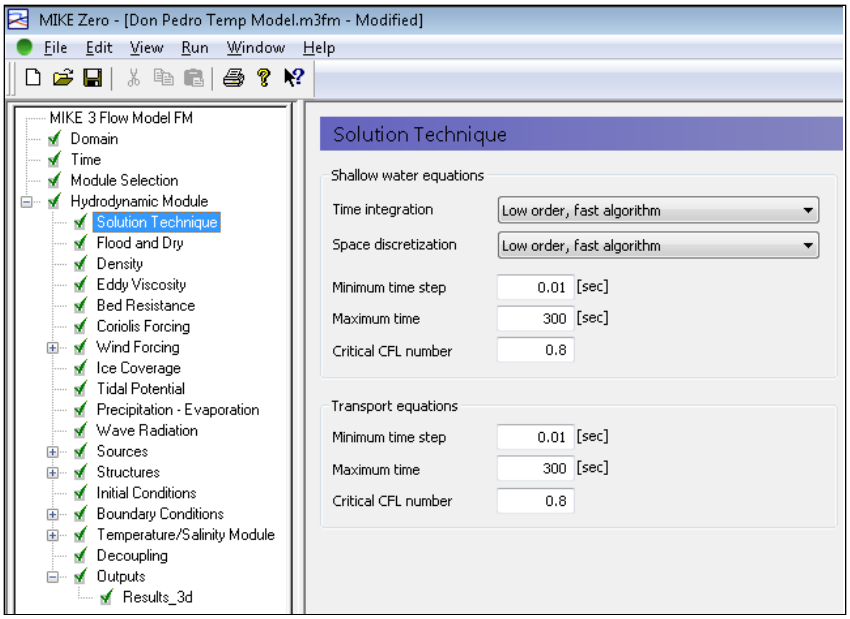

Figure 4.4-8. Solution technique parameters.

4.4.5.2 "Flood" and "Dry" Cells

The MIKE3 model has the option to allow model cells to go dry if the water level decreases or fill ("flood") if the water level rises. This feature is important for a system like Don Pedro where reservoir level variations are significant. This "flood" and "dry" mechanism allows the same model mesh to be used for all current and future operating scenarios. When the water level decreases the model will stop including dry cells in the hydrodynamic calculation. As shown in Figure 4.4-9, three parameters determine when a model cell is removed from the calculation (i.e. "dry"), when it is re-entered into the calculation ("wet"), or when the hydrodynamic solution is adapted because of a very shallow water depth ("flooding depth").

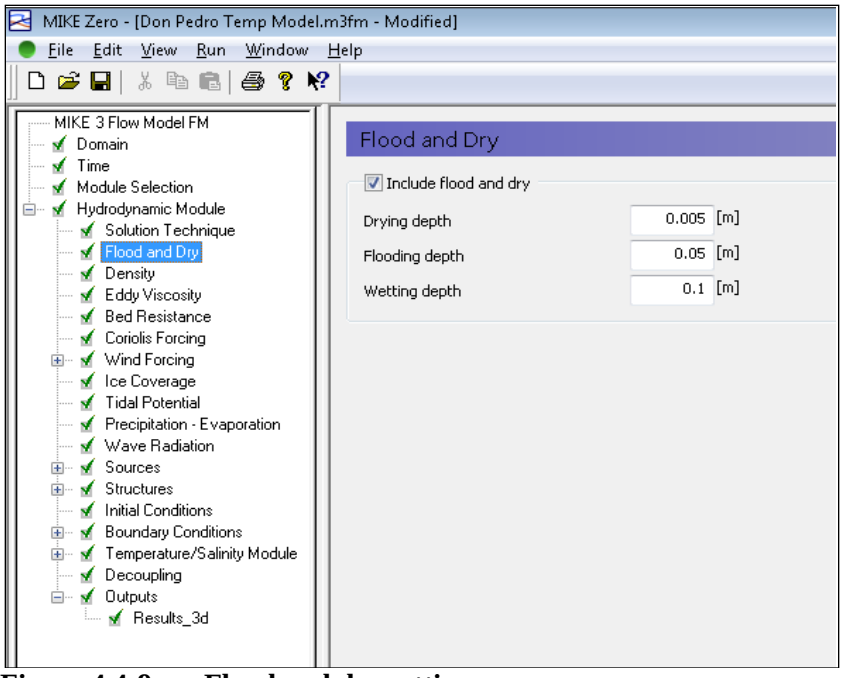

Figure 4.4-9. Flood and dry settings.

4.4.5.3 Density

As shown in Figure 4.4-10, the density of the water at any point is modeled as a function of temperature. Selecting this option turns on the temperature module. A reference temperature could be used if adjustments to the basic density-temperature relationship of water are needed. No adjustment is used in the Don Pedro Reservoir model.

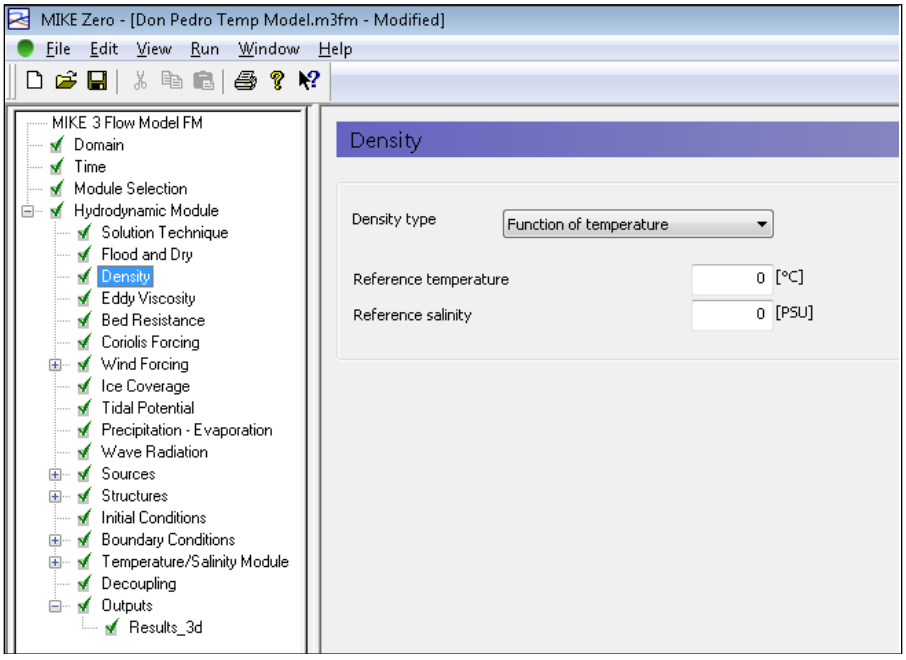

Figure 4.4-10. Density as a function of temperature is selected.

4.4.5.4 Eddy Viscosity

The eddy viscosity panel describes how the model will set the horizontal and vertical dispersion.

Horizontal Dispersion

Figure 4.4-11 shows that the option used for the Don Pedro Reservoir temperature model's horizontal dispersion is the Smagorinksy Formulation (Smagorinky 1963). There are two other options in the horizontal: (a) no dispersion or (b) constant dispersion. It was found that the Smagorinksy Formulation worked well, although the model results for Don Pedro Reservoir were found to be relatively insensitive to horizontal dispersion.

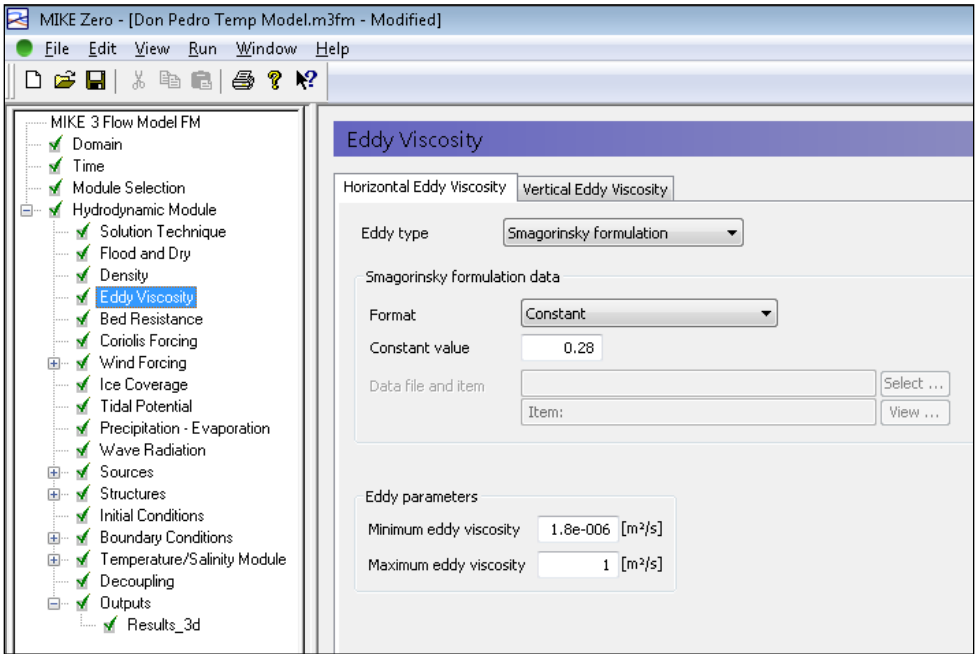

Figure 4.4-11. Horizontal dispersion.

Vertical Dispersion

Vertical dispersion is a key parameter in stratified systems such as Don Pedro Reservoir. There are four options available (Rodi 1984):

- no dispersion;
- constant dispersion;
- log law; or
- k – epsilon.

Figure 4.4-12 shows that the option used for the Don Pedro Reservoir temperature model's vertical dispersion is the log law. Using both log law and k-epsilon resulted in the modeled temperatures matching favorably with the calibration and verification year measurements. However, the log law option was preferred as the run times are shorter. There is a further option

to include damping terms but this did not improve the results and increased run times, so it was not incorporated into the model.

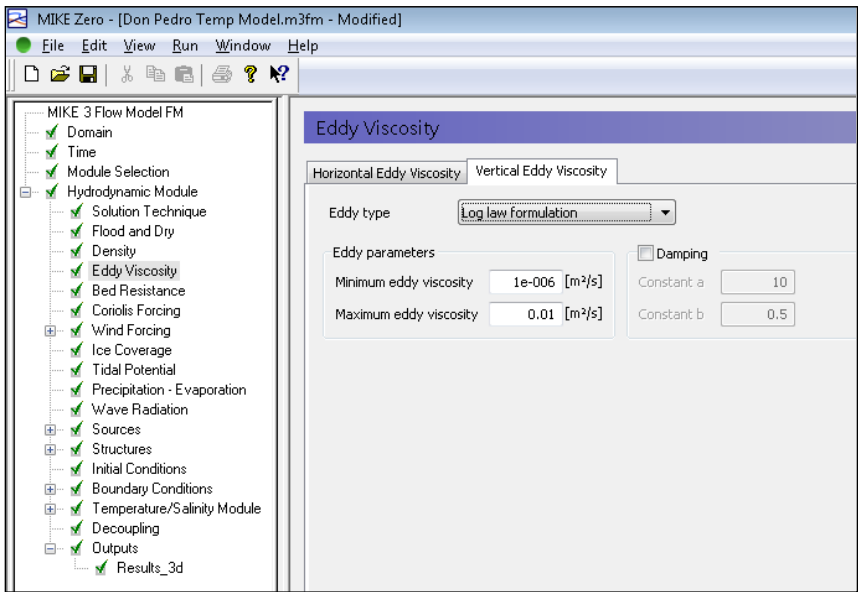

Figure 4.4-12. Vertical dispersion.

4.4.5.5 Bed Resistance

As water flows over a solid surface, like the bed of the reservoir or river, there are friction losses that occur. The rougher the surface, the greater the losses. In the bed resistance tab the height of the surface indentations is specified (Figure 4.4-13). In a slow moving system like a reservoir, the calculation is very insensitive to this parameter. A value of 5 centimeters (0.05 meter) was used.

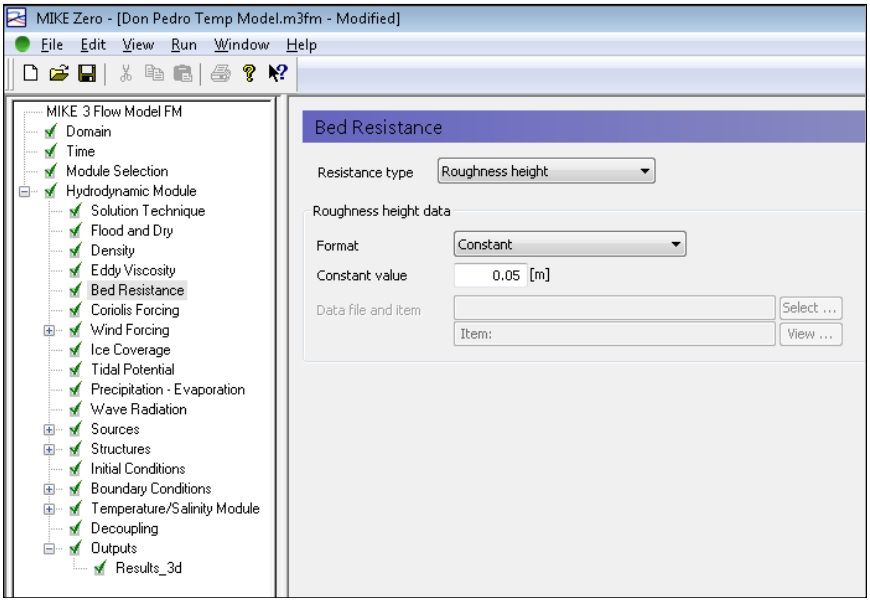

Figure 4.4-13. Bed resistance.

4.4.5.6 Coriolis Force

In large water masses the rotation of the earth can affect the circulation pattern and the MIKE3 model accounts for this (Figure 4.4-14). For the Don Pedro Reservoir temperature model, no noticeable change in calibration or verification results occurred when the model was tested for sensitivity to this parameter. Hence, because model computation time could be decreased without it, the Don Pedro Reservoir model does not include Coriolis force.

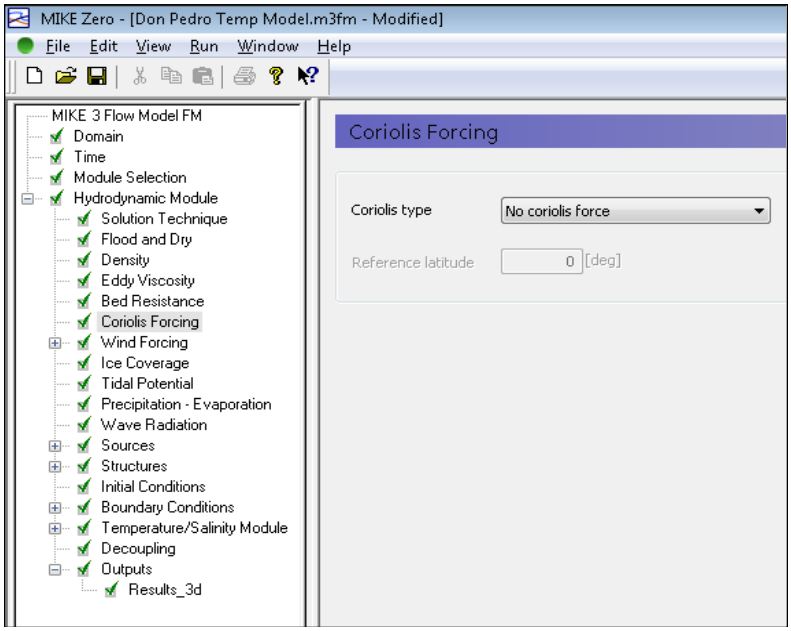

Figure 4.4-14. Coriolis force.

4.4.5.7 Wind Forcing

In lakes and reservoirs the circulation can be effected by wind (Figure 4.4-15) and this effect was included in the Don Pedro Reservoir model. The wind data reside in a data file that is called by the "m3fm" file. The wind speed and direction data was collected by the Districts' meteorological station located at Don Pedro Reservoir (See Section 4.3.3).

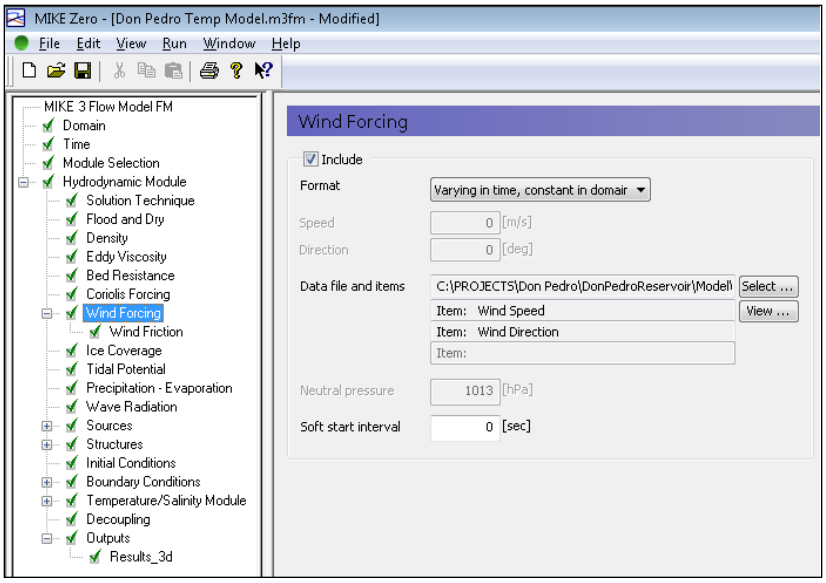

Figure 4.4-15. Wind forcing.

By selecting the "View" button on the tab the wind speed and direction can be viewed. Figure 4.4-16 shows the data for 2011, where wind speed is provided in meters per second (m/s) and direction is provided in degrees (deg). Also specified in the wind forcing folder is the wind friction constant. This is the conversion factor that relates the wind speed to the force that will drag on the water surface. For Don Pedro Reservoir the default value was used (Figure 4.4-17) (DHI 2011).

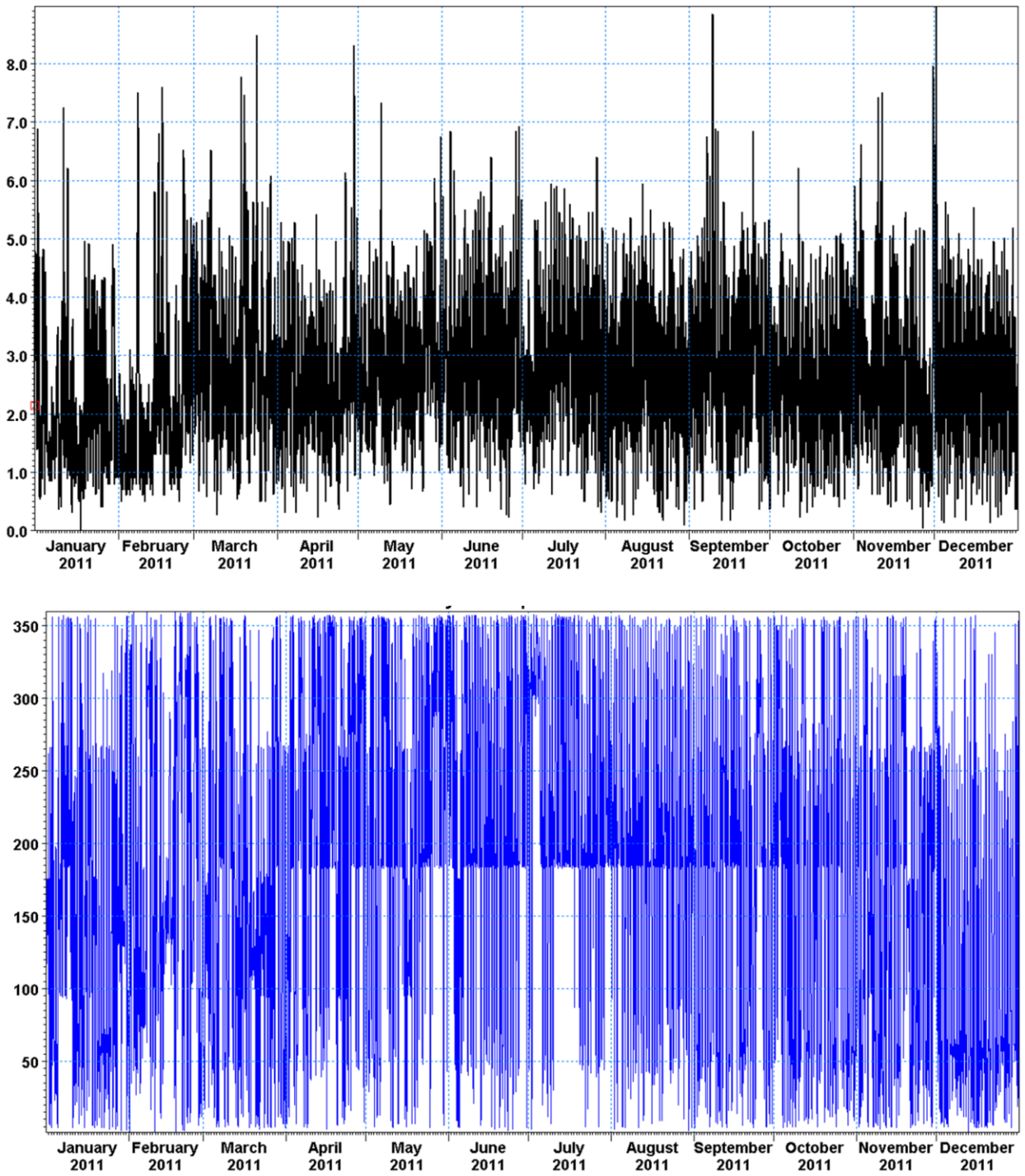

Figure 4.4-16. Wind data collected at Don Pedro Met Station 2011. Top plot is wind speed (m/s); bottom plot is wind direction (deg).

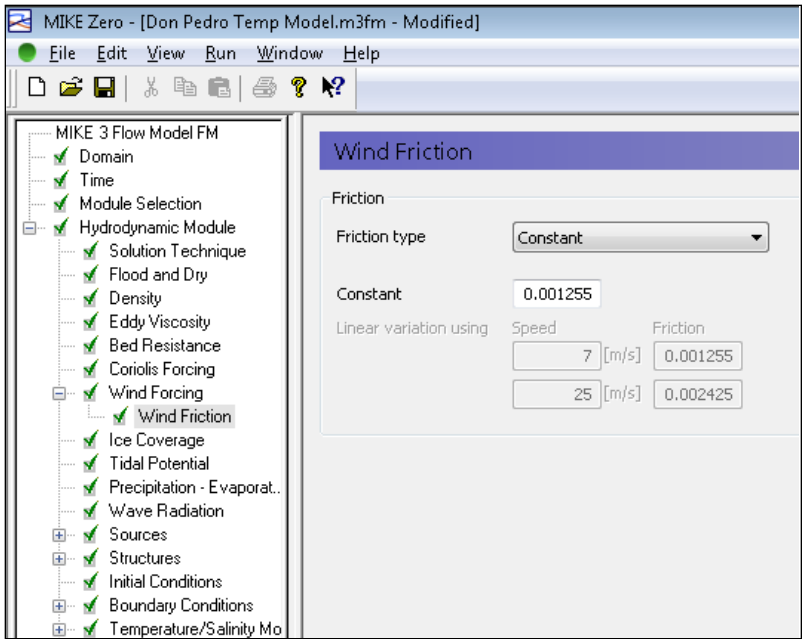

Figure 4.4-17. Wind friction factor.

4.4.5.8 Ice Coverage

Located in a Mediterranean climate, ice coverage is not applicable to the Don Pedro Reservoir and was not included (Figure 4.4-18).

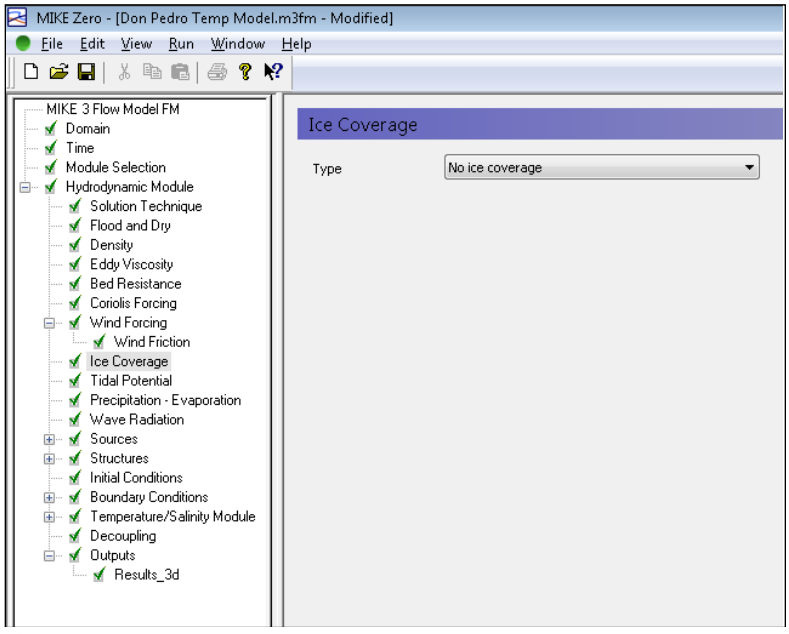

Figure 4.4-18. Ice coverage.

4.4.5.9 Tidal Potential

Located in California's Central Valley, upstream of the Sacramento-San Joaquin Delta, tidal influence is not applicable to the Don Pedro Reservoir and was not included (Figure 4.4-19).

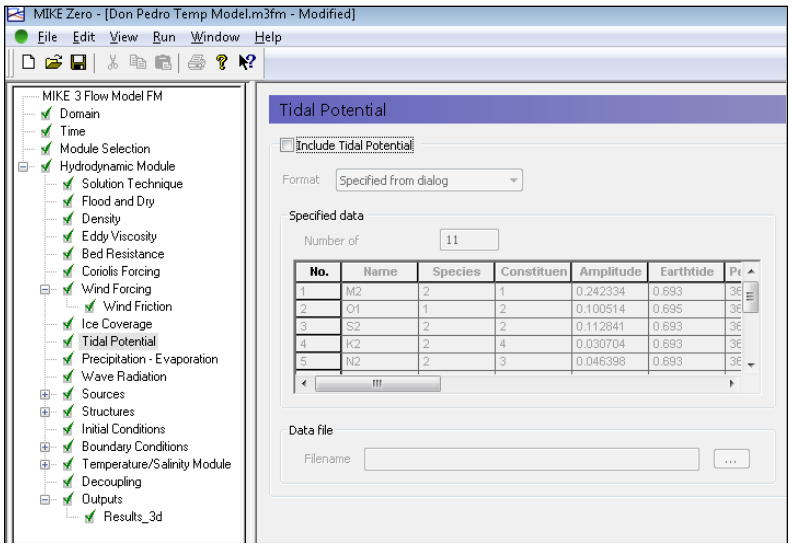

Figure 4.4-19. Tidal potential.

4.4.5.10 Precipitation and Evaporation

Precipitation and evaporation values were monthly averages excerpted from the hydrology appendix of Tuolumne River Operations Model (W&AR-02), which accounted for precipitation directly on the reservoir surface and evaporation (TID/MID 2013a).

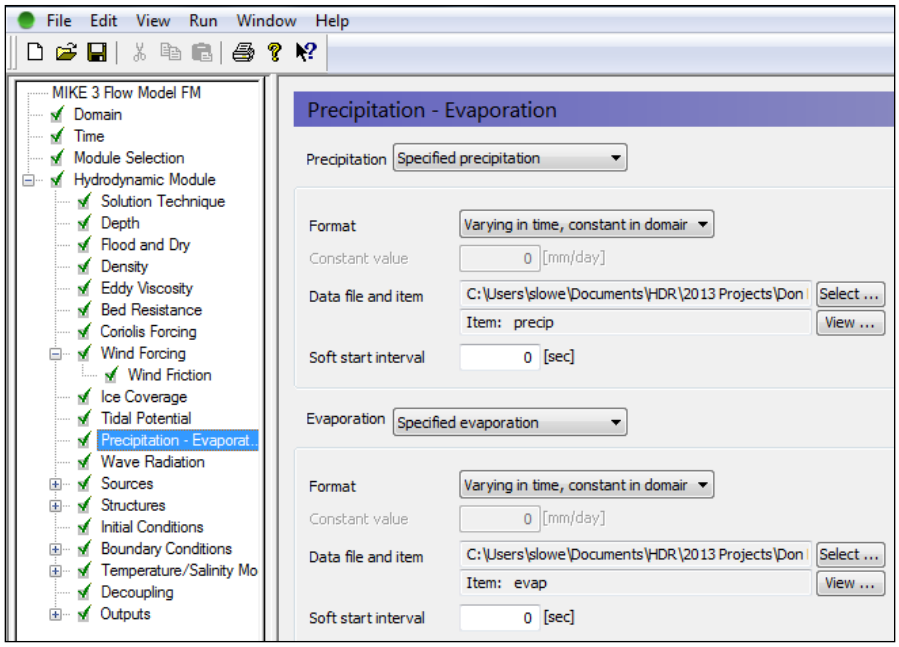

Figure 4.4-20. Precipitation and evaporation.

4.4.5.11 Wave Radiation

The effect of breaking shoreline waves is not an issue in Don Pedro Reservoir and is not included (Figure 4.4-21).

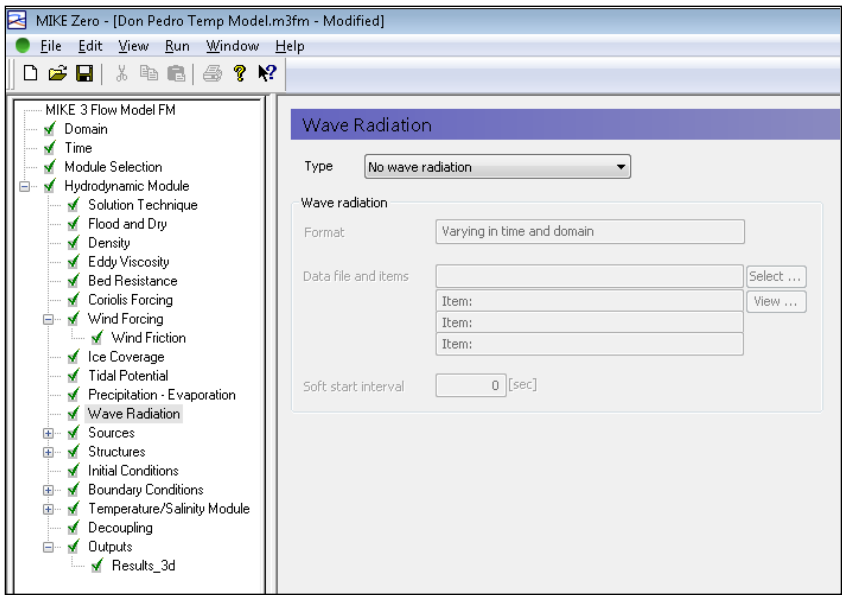

Figure 4.4-21. Wave Radiation.

4.4.5.12 Sources

Reservoir model inflows and outflows are specified by placing "sources" in the model through the hydrodynamic module. For the purpose of modeling, outflows are specified as a source with negative flow values.

The main inflow into the model is the flow in the Tuolumne River and the outflow is the release at Don Pedro Dam either through the powerhouse units 1 through 4, the powerhouse hollow jet valve, the outlet works, or the spillway. To ensure consistency between study findings, inflows to and outflows from the Don Pedro Reservoir were taken from the hydrology data set provided in the Tuolumne River Daily Operations Model (W&AR-02) (TID/MID 2013a). Inflows and outflows are provided as mean daily flows.

For model stability, it is desirable to spread the total reservoir inflow over more than one source point. This prevents placing all the flow into one model cell which may cause stability problems in the model. Additionally there are a number of smaller tributaries that contribute flow to the reservoir, and although their flows are not directly measured, they are accounted for in the hydrology data set. Hence, the total inflow from the Operations Model was split into 10 source points, each contributing 10 percent of the total inflow. The locations of these inflow points, and the single outflow point at Don Pedro Dam, are shown in Figure 4.4-22, which shows the "geographic view" tab under "sources," while the list of source points is shown in Figure 4.4-23. The names of the various sources are listed by selecting the "list view" tab, as shown in Figure 4.4-23. The sources considered are:

(a) Tuolumne River

(b) Woods Creek

(c) Hatch Creek

(d) North Bay

(e) Rogers Creek

(f) Moccasin Creek

(g) Unknown creek at Six-bit and Poor Mans Gulch

Note that the two larger tributaries, the Tuolumne River and Woods Creek have multiple source points, with the overwhelming majority of the inflow coming from the main stem Tuolumne River.

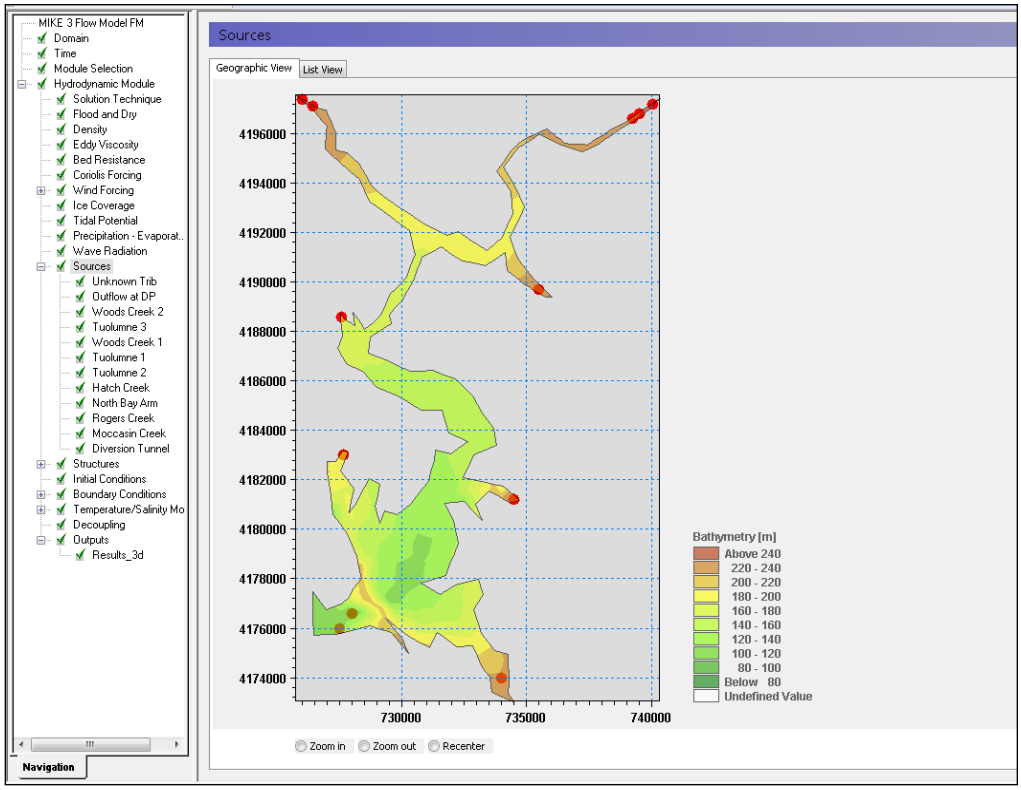

Figure 4.4-22. Location of model inflow and outflow sources.

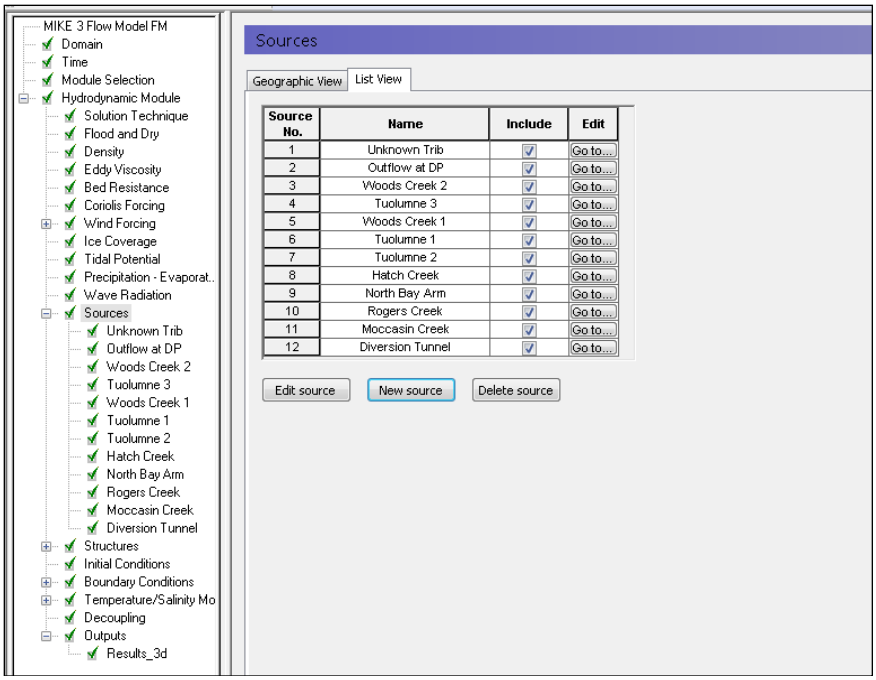

Figure 4.4-23. Listing of inflow and outflow sources.

When in the list view, the details of an individual source can be shown by using the "go to" button. The details for the source "Tuolumne 3", one of three sources located near the head of the Tuolumne River inlet to the reservoir, are shown in Figure 4.4-24. This includes the Easting and Northing in Universal Transverse Mercator coordinates and the model layer where the flow, provided as cubic meters per second (m^3/s) is input. The data file that contains the time-variable flows is also specified; by selecting the "view" button this data can be displayed, as shown in Figure 4.4-25.

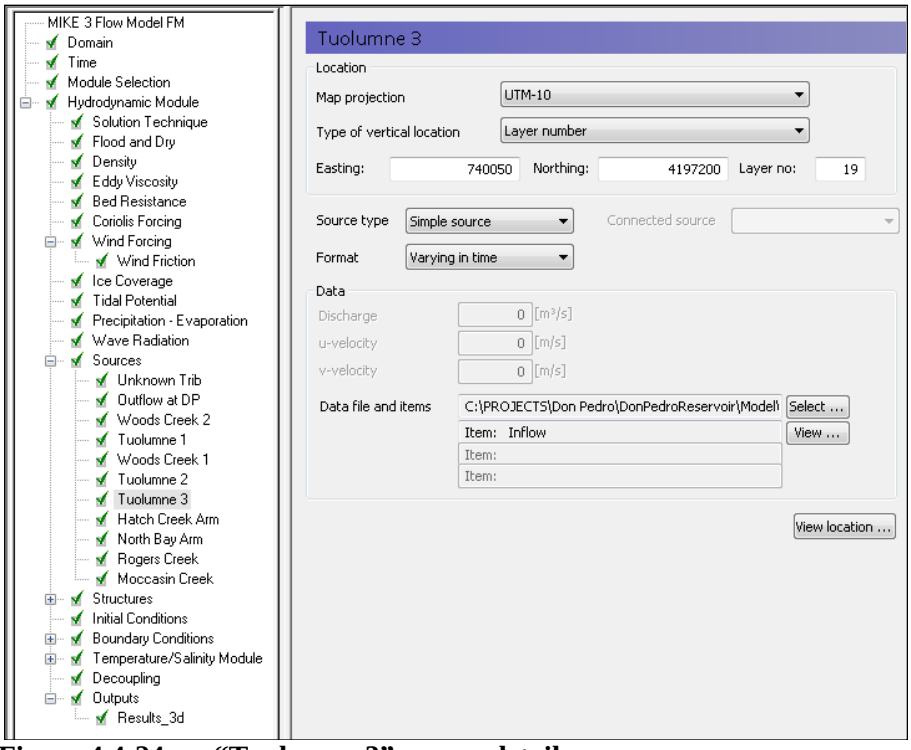

Figure 4.4-24. "Tuolumne 3" source details.

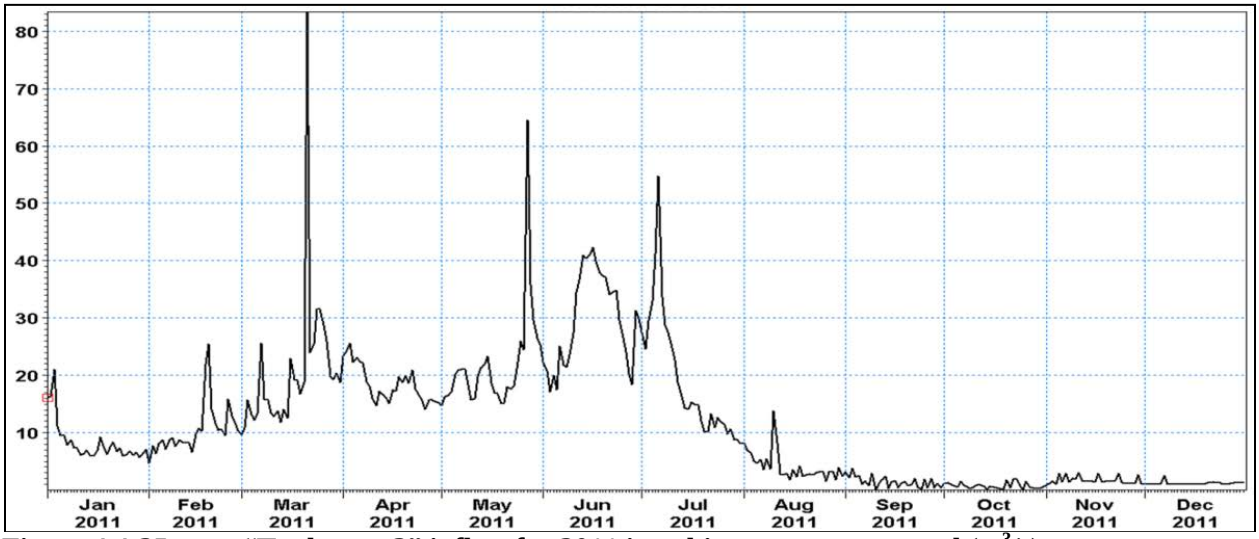

Figure 4.4-25. "Tuolumne 3" inflow for 2011 in cubic-meters per second (m^3/s).

Likewise, the details of the outflow at the Don Pedro powerhouse are shown in Figure 4.4-26. In this case, the source point's specific elevation of 535 feet or 163 m is specified in Figure 4.4-26, while the outflow data for 2011 is shown in Figure 4.4-27. When outflow exceeds the hydraulic capacity of the four units plus the hollow jet valve (6,300 cfs; 178.4 m^3/s), the excess flow exits via the diversion tunnel at elevation 345 feet (105.2 meters). In 2011 the flow did exceed 6300 cfs, as shown by the flat portions of Figure 4.4-27. The flow never exceeded the hydraulic capacity of the combined powerhouse and diversion tunnels and the reservoir did not spill in

2011. In 2012 the flow never exceeded 6300 cfs; therefore, all flow passed through the powerhouse tunnel.

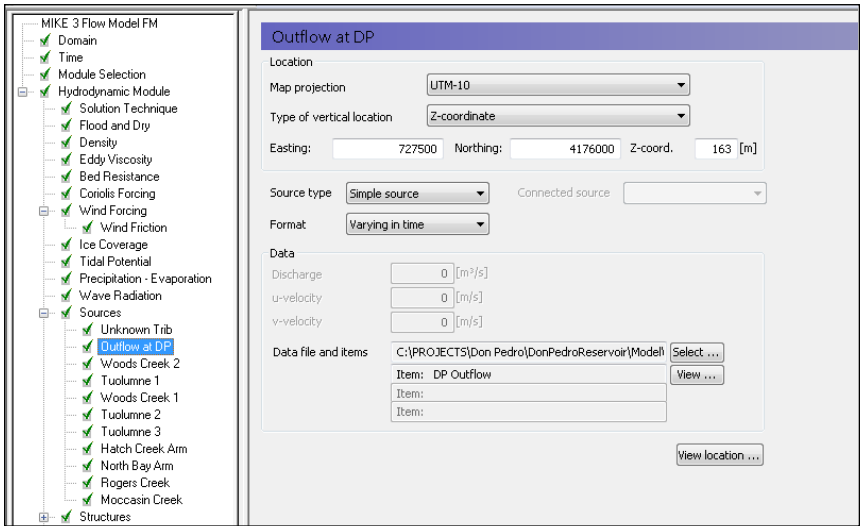

Figure 4.4-26. "Outflow at Don Pedro powerhouse" source details.

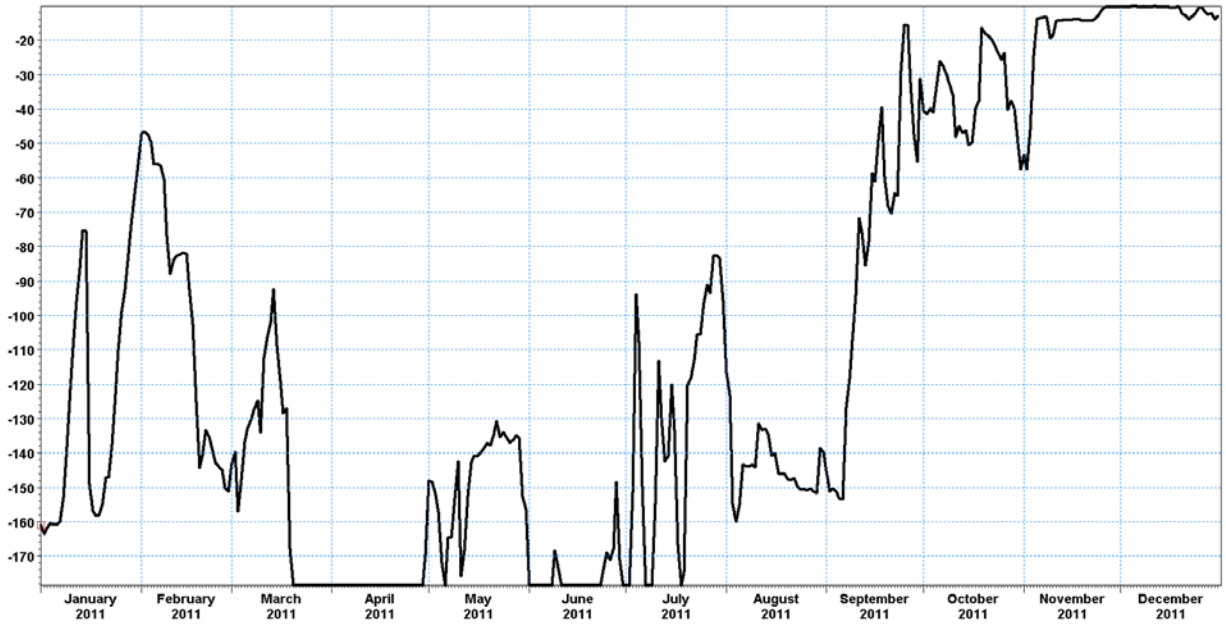

Figure 4.4-27. "Outflow at Don Pedro powerhouse" outflow for 2011 in cubic-meters per second (m^3/s). Note outflows are assigned a negative value.

4.4.5.13 Structures

The model allows certain structures to be defined, as listed in Figure 4.4-28 (weirs, culverts, gates, etc.). Within the Don Pedro Reservoir, the only significant structure is the Old Don Pedro Dam. The Old Don Pedro dam was modeled as an internal weir with a weir crest height of 187 meters (top of parapet at 613.5 feet) and a length of 304.8 meters (1,000 feet). At normal operating levels the submerged dam will act as a deep bathymetric feature. As the water level approaches 613.5 feet the dam will act as a weir. As water levels continue to drop, the twelve

open sluice gates (see below) pass water from the old Don Pedro Reservoir to the space between the two dams.

Old Don Pedro Dam contains 12 circular gates, each 52” diameter, that were left open during the filling of the new Don Pedro Dam. These are modeled using the Culvert option under the structures menu. The gates are arranged in two levels at 511.5 feet and 421.5 feet (centerline elevations), each with six gates. The total length through the dam of the upper sluiceways is 60 feet and the length of the lower sluiceways is 110 feet.

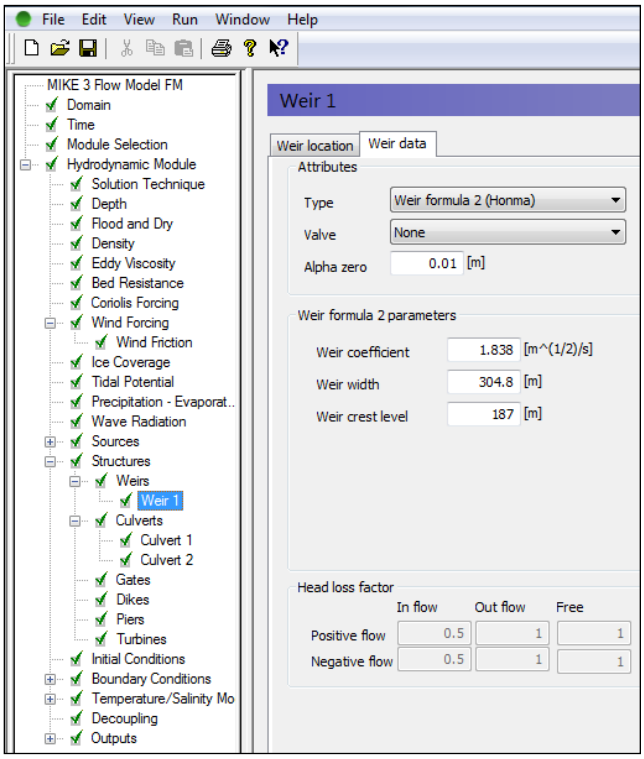

Figure 4.4-28. Old Don Pedro Dam modeled as a weir.

4.4.5.14 Hydrodynamic Initial Conditions

The initial condition option used in the Don Pedro Reservoir model is to specify the observed water surface elevation on the start date of the model run, in this case January 10, 2011. This is shown in Figure 4.4-29. Other options include specifying initial velocities and varying surface elevations, where these are usually generated from previous model runs. The initial conditions referred to here do not include the initial temperatures, which are listed below in Section 4.4.6.

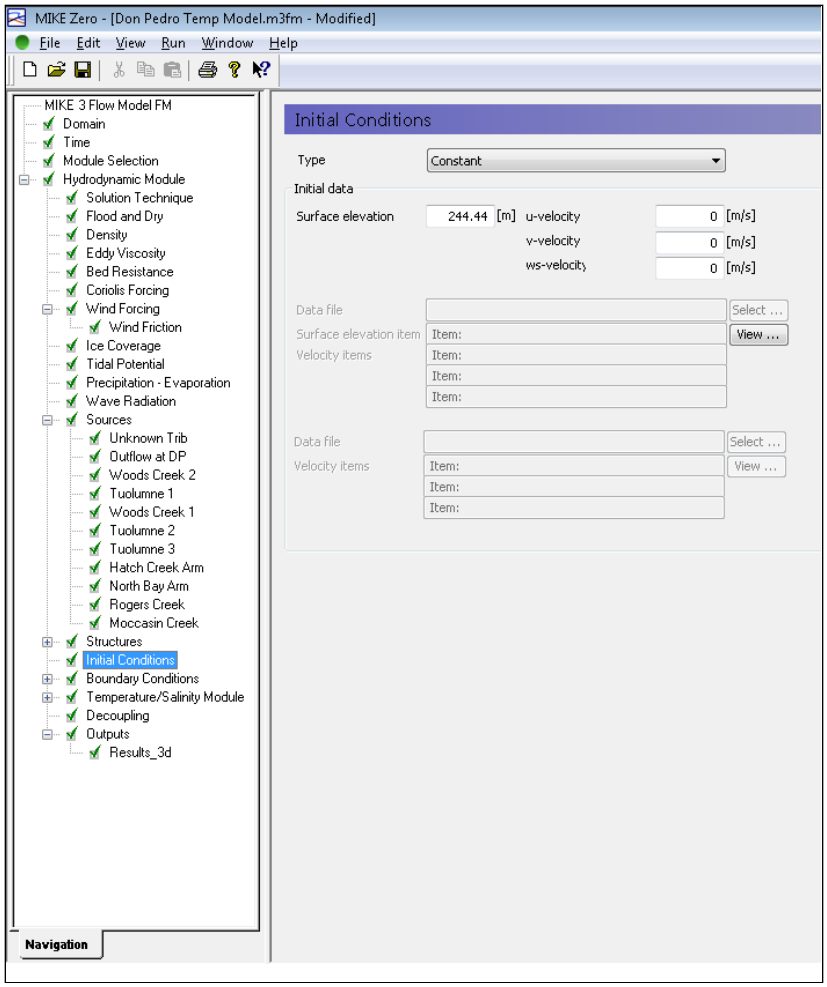

Figure 4.4-29. Hydrodynamic initial conditions.

4.4.5.15 Model Boundary Conditions

In the Don Pedro Reservoir model the inflow and outflow are specified using sources. There are no open water boundaries, so the model domain looks like a closed system with land boundaries on all sides (Figure 4.4-30). There are no additional boundary conditions.

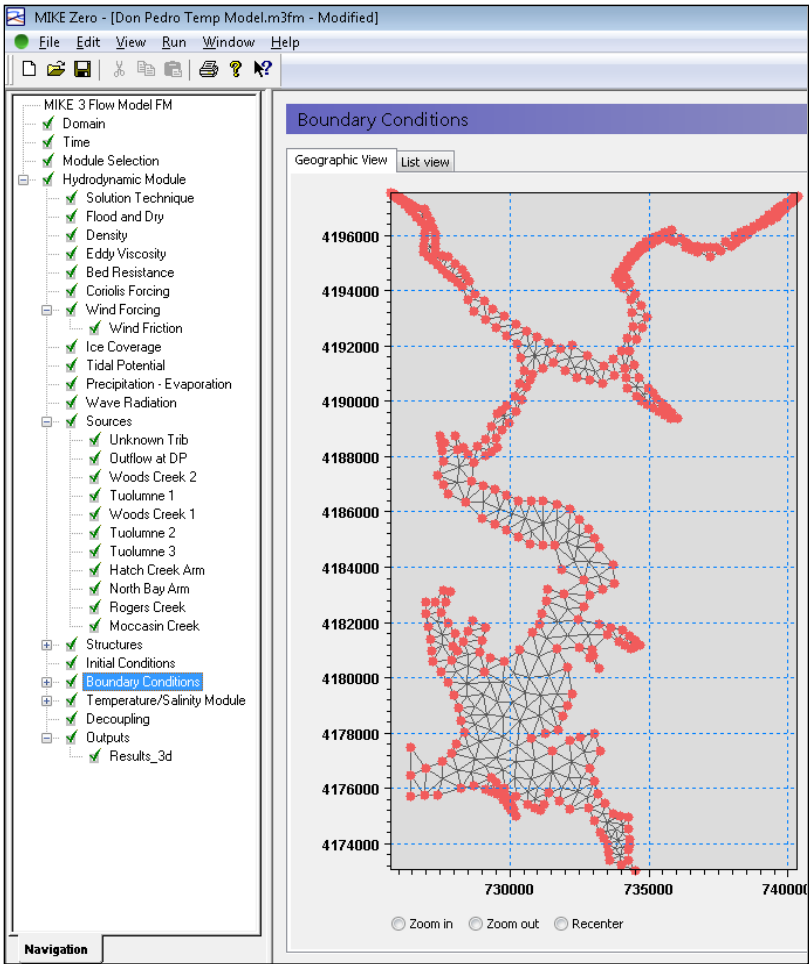

Figure 4.4-30. Boundary conditions: model domain showing all land boundaries.

4.4.6 Temperature Module

When density is set as a function of temperature in the density tab, as shown earlier (Section 4.4.5.3), then the temperature module is turned on. Figure 4.4-31 shows the temperature module's main tab.

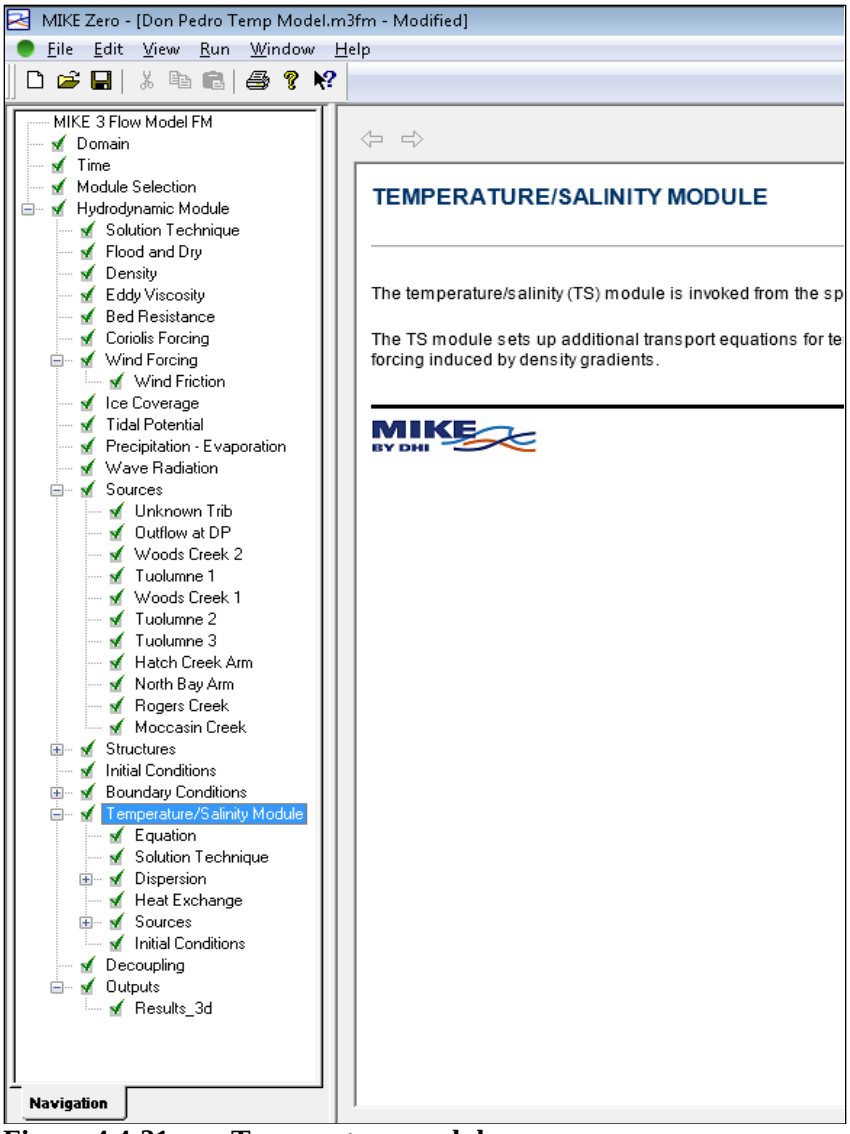

Figure 4.4-31. Temperature module.

It is possible to require the model to operate within a specified temperature range. Any temperatures above or below the limits set by the user will be automatically capped at these values. As this was not a desired feature for the Don Pedro Reservoir model the limits were set beyond the range of any expected temperatures, i.e. -5^{o} C minimum and 40^{o} C maximum, as shown in Figure 4.4-32.

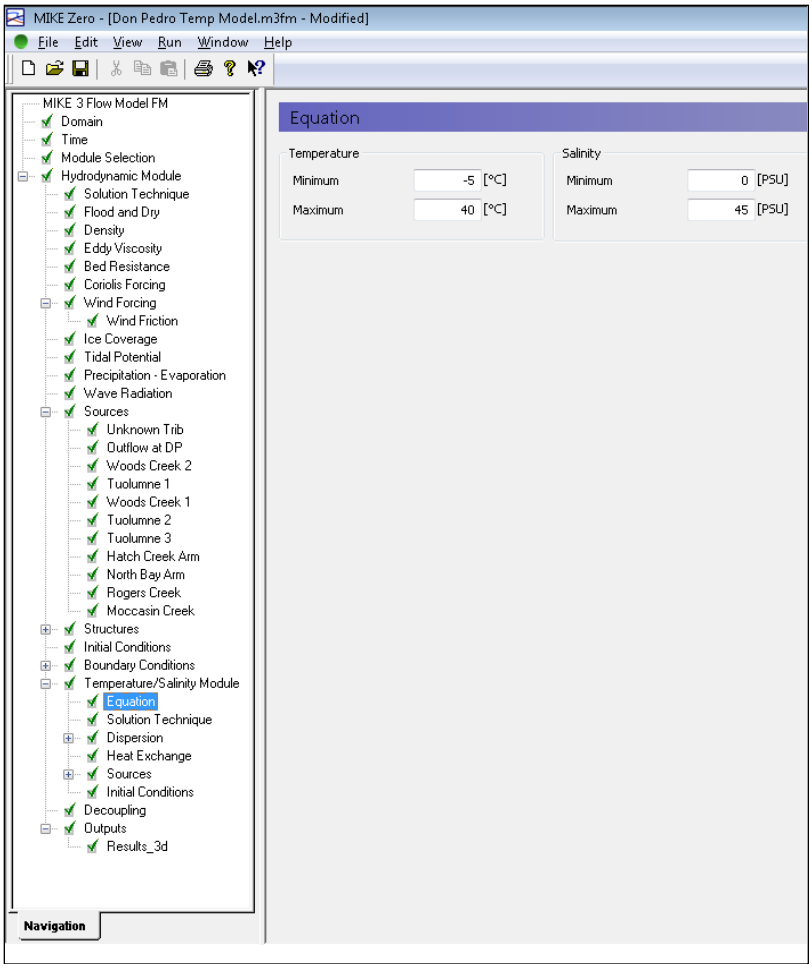

Figure 4.4-32. Temperature limits.

Internal control of the solution for the temperature equations can be set by the user for the purpose of using model run times effectively and efficiently (Figure 4.4-33). There are two options available to the user for both time integration and space discretization: Low Order and High Order. Generally High Order solutions are only used if the Low Order solutions fail, as they increase model run times.

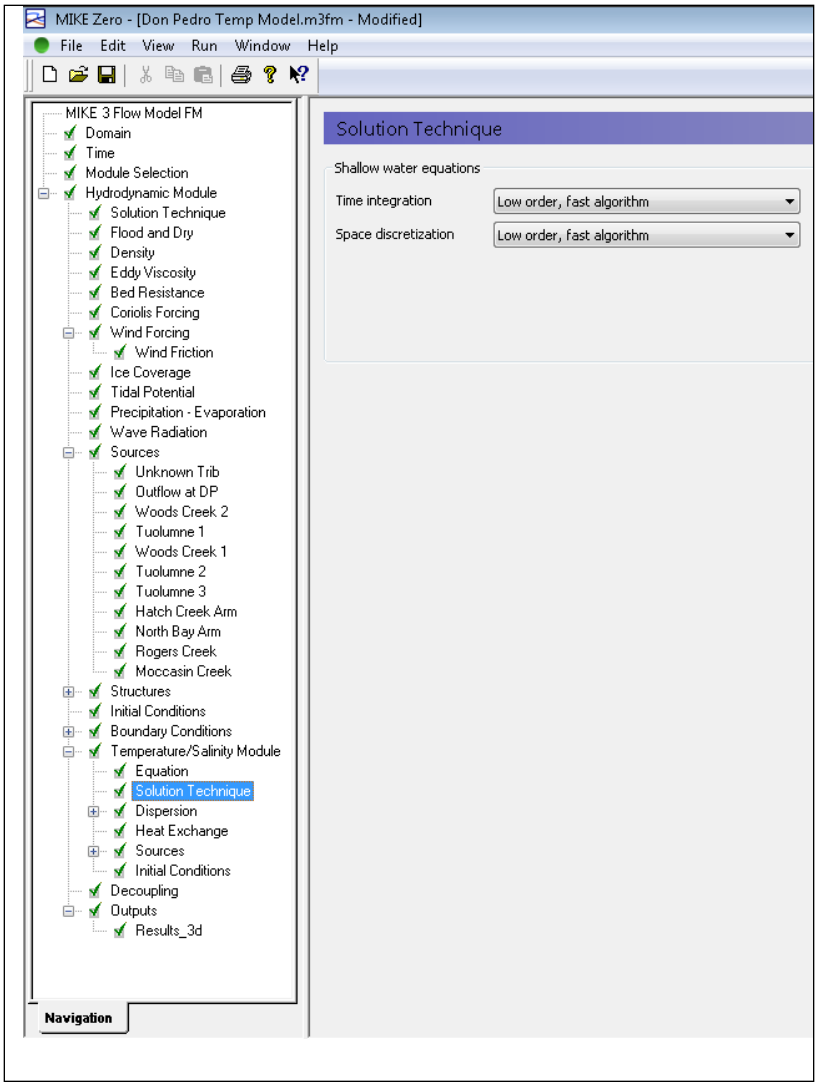

Figure 4.4-33. Solution settings.

Similar to the hydrodynamic dispersion, the user can specify the horizontal and vertical temperature dispersion through the dispersion tab, as shown in Figure 4.4-34.

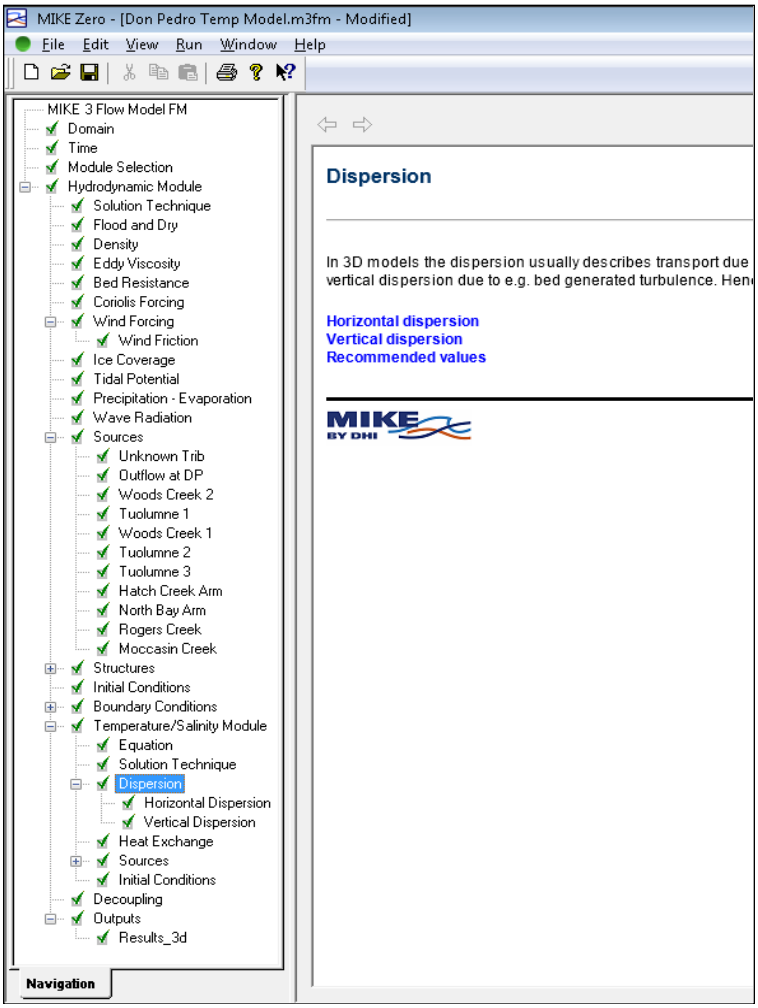

Figure 4.4-34. Temperature dispersion main tab.

4.4.6.1 Horizontal Dispersion

There are three options available for the horizontal temperature dispersion: (1) no dispersion; (2) scaled eddy viscosity and (3) a constant dispersion. For the Don Pedro Reservoir temperature model, a constant horizontal dispersion of 1 m^2/s was used (Figure 4.4-35). This is a typical value used for reservoirs (e.g., Maiss et al. 1994).

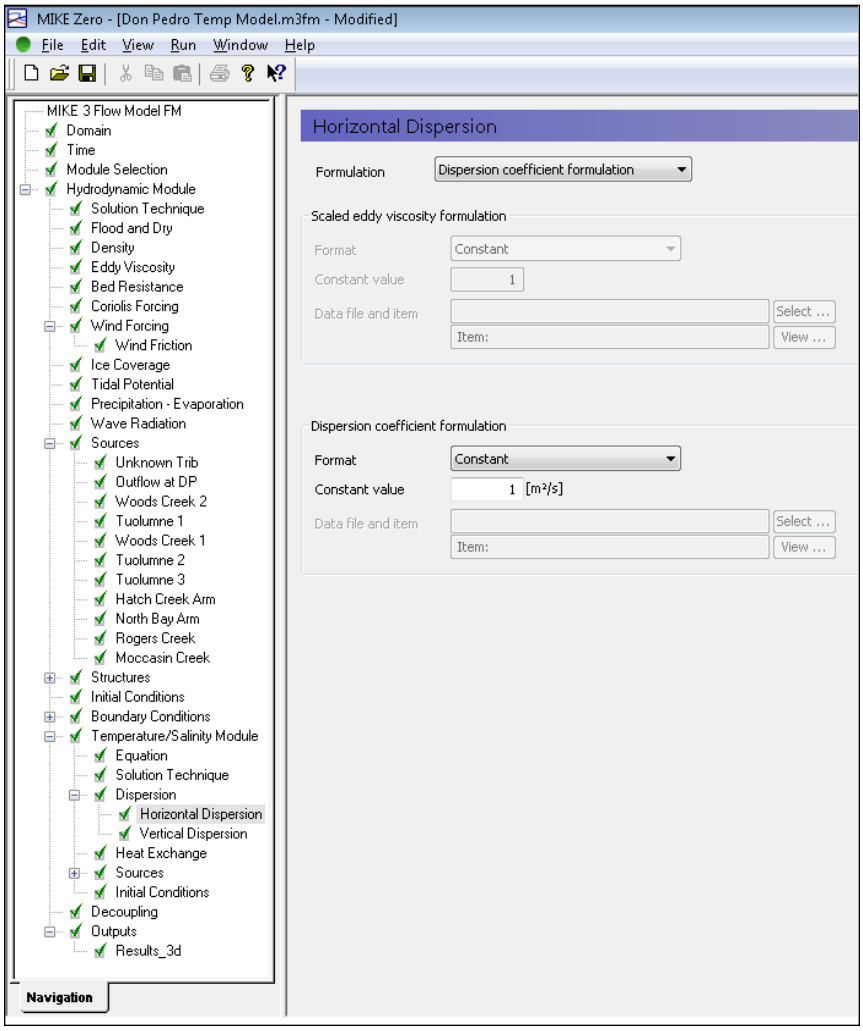

Figure 4.4-35. Temperature horizontal dispersion.

4.4.6.2 Vertical Dispersion

The same three vertical temperature dispersion options are available as for the horizontal dispersion discussed above. Again constant dispersion was used, with a value of 1×10^{-6} m^2/s (Figure 4.4-36). This value is typical of those used in deep, stratified systems (e.g., Fischer, 1979; Bonnet et al. 2000).

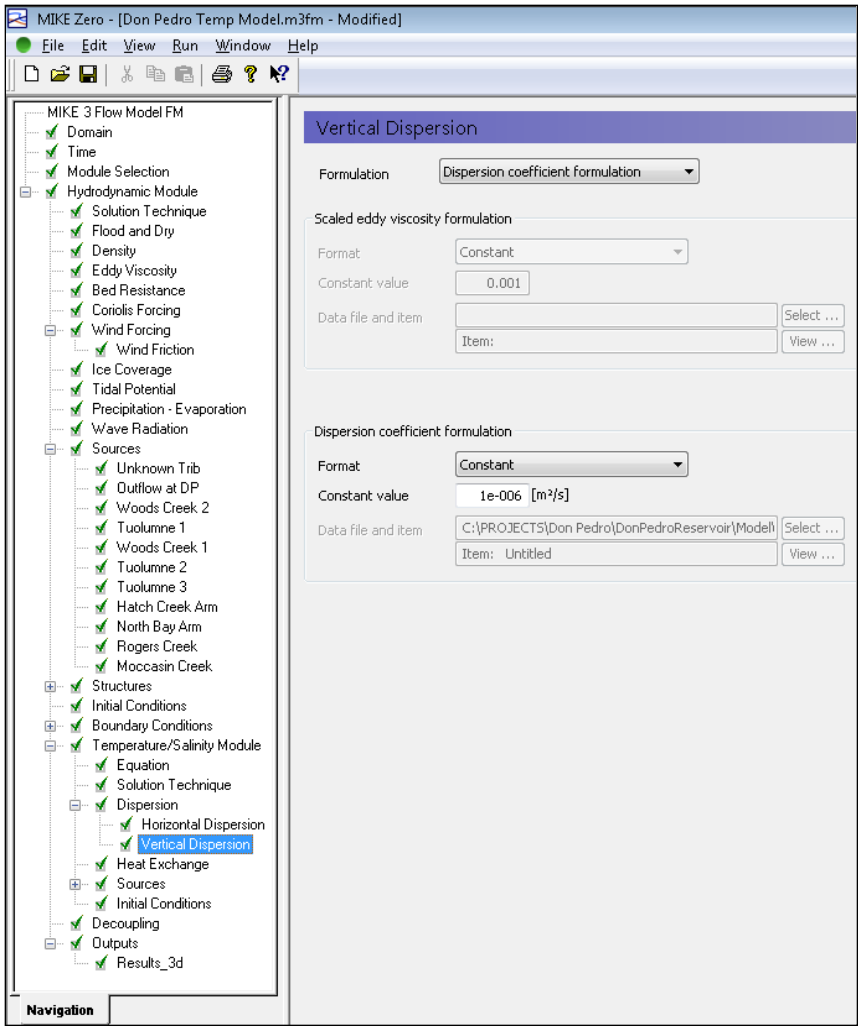

Figure 4.4-36. Temperature vertical dispersion.

4.4.6.3 Heat Exchange

The model computes a heat balance in the water based on the four physical controlling processes:

- heat loss due to vaporization (also called latent heat flux);
- heat transfer between the air and water due to temperature differences (also called sensible heat exchange);
- short wave radiation; and
- long wave radiation.

These processes and how they are formulated in the MIKE model are described in detail in the "MIKE 21 and MIKE 3, FLOW MODULE FM, Hydrodynamic and Transport Module, Scientific Documentation" (DHI 2009a). The discussion is condensed here to the final equations and how they relate to the parameters shown in the various heat exchange tabs.

4.4.6.4 Latent Heat Exchange

The heat loss due to vaporization (evaporation) is computed in the model using a form of Dalton's Law (circa 1801):

$$q_v = LC_e(a_1 + b_1 W_{2m})(Q_{water} - Q_{air})$$

where:

q_v	heat loss	(W/m^2)
L	latent heat constant	(J/kg)
C_e	moisture transfer coefficient	(unitless)
W_{2m}	wind speed 2 meters above the water surface	(m/s)
Q_{water}	vapor pressure of water	(Pa)
Q_{air}	vapor pressure in atmosphere	(Pa)

a_1 and b_1 are user specified constants as shown in Figure 4.4-37, below. The values used for a_1 and b_1 are typically seasonally adjusted. For March – October the values used were 0.5 and 0.1, and over winter they were 2 for both constants. The critical wind speed is the lowest wind speed used in the calculation. DHI recommends using 2 m/s as the minimum wind speed.

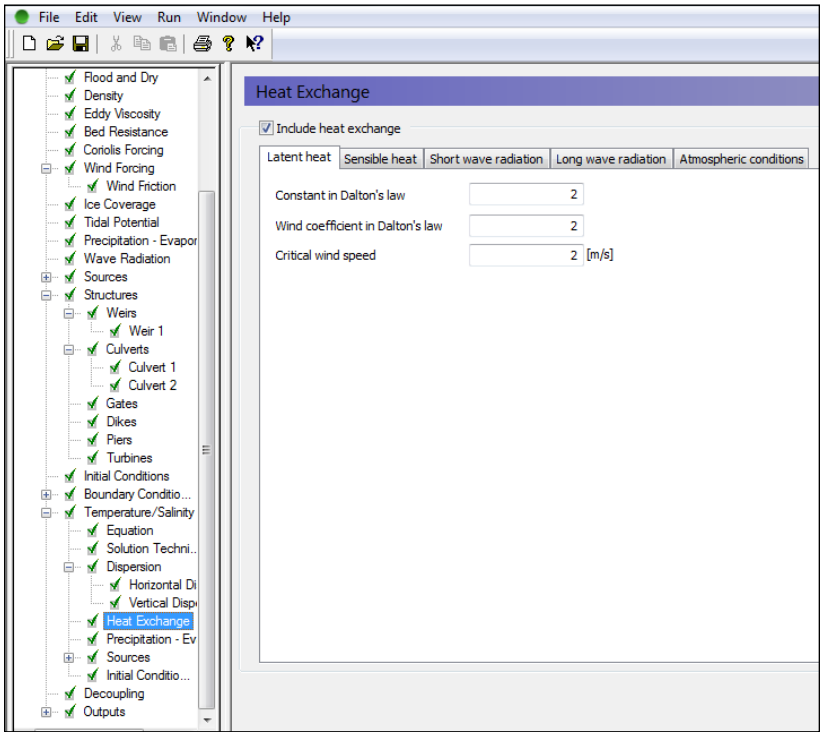

Figure 4.4-37. Daltons law constants.

The vapor pressure in the atmosphere, Q_{air}, is a function of the humidity. Humidity data were collected by the Districts' station at Don Pedro Dam (Figure 3.0-1; Section 4.3.4). The data file

can be viewed by selecting the "view" button of the Atmospheric Conditions panel (shown below in Figure 4.4-38). The humidity for 2011 is shown in Figure 4.4-39.

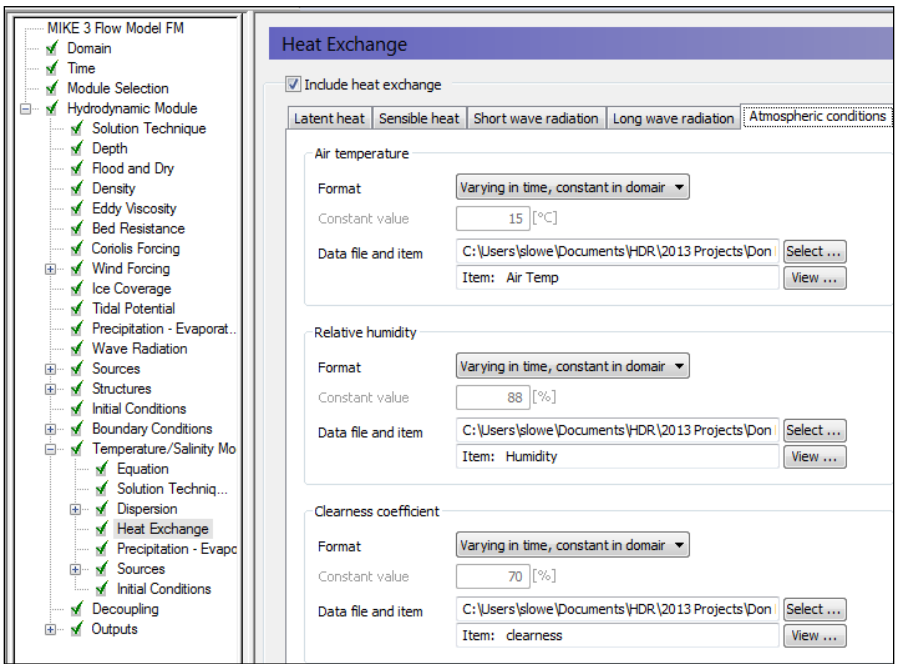

Figure 4.4-38. Atmospheric conditions panel.

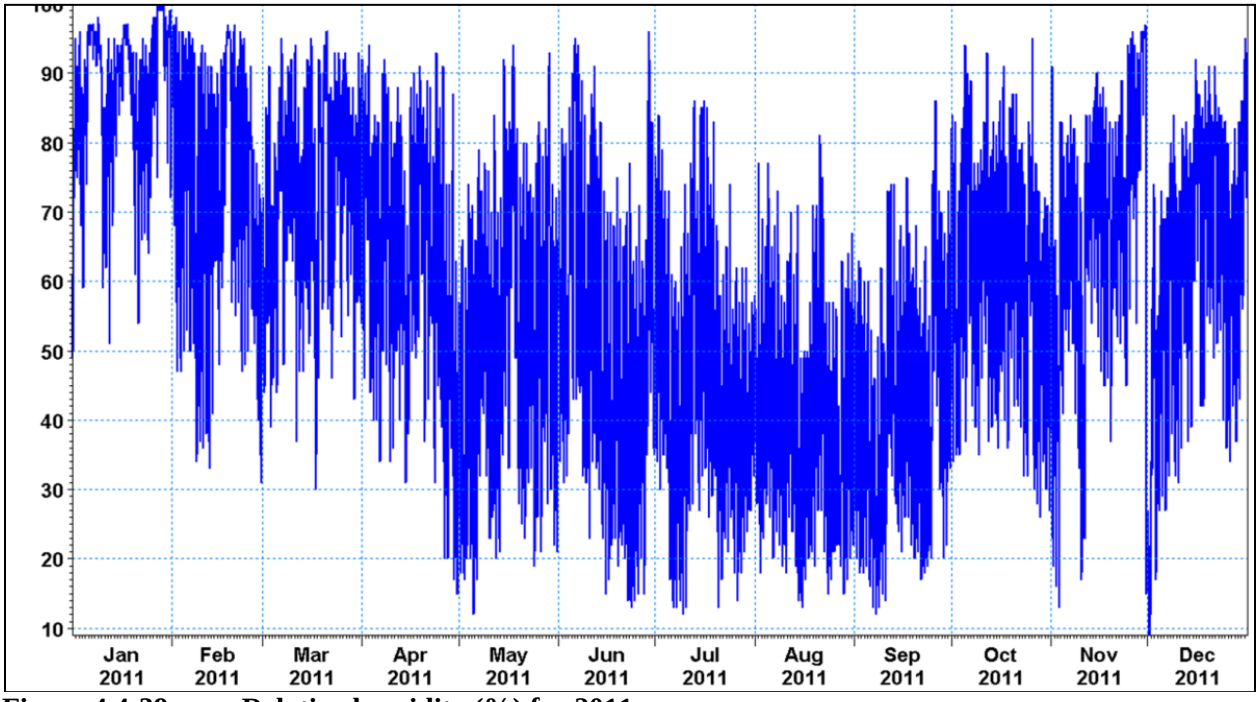

Figure 4.4-39. Relative humidity (%) for 2011.

4.4.6.5 Sensible Heat Exchange

Heat exchange due to temperature differences between the air and water surface are called sensible heat exchange. These can result in either a heat gain or loss to the water. They are described as:

$$q_c = \begin{cases} \rho_{air} c_{air} c_{heating} W_{10} (T_{air} - T_{water}) & T_{air} \geq T \\ \rho_{air} c_{air} c_{cooling} W_{10} (T_{air} - T_{water}) & T_{air} < T \end{cases}$$

where:

q_v	heat loss or gain	(W/m^2)
ρ_{air}	air density	(kg/m^3)
c_{air}	specific heat of air	($J/kg/^oC$)
$c_{heating}$	heat transfer constant	(unitless)
$c_{cooling}$	heat transfer constant	(unitless)
q_c	heat loss or gain	(W/m^2)
ρ_{air}	air density	(kg/m^3)
W_{10}	wind speed 10 meters above the water surface	(m/s)
T_{air}	air temperature	(^oC)
T_{water}	water temperature	(^oC)

Many of the above parameters are known physical constants (e.g. the specific heat of air and water) and so do not appear in the sensible heat exchange panel (Figure 4.4-40). The two constants that can be set are the heat transfer coefficients for heating and cooling. These were set at 0.0011 (Kantha and Clayson, 2000).

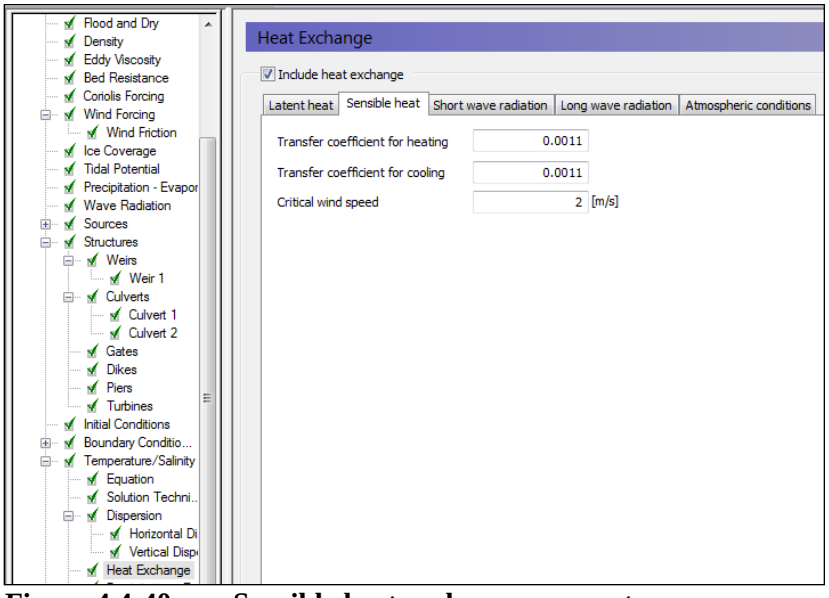

Figure 4.4-40. Sensible heat exchange parameters.

The air temperatures (T_{air} in the above formula) are based on data collected at the Districts' station at Don Pedro Dam. By selecting the "view" button on the Atmospheric Conditions panel, shown previously, the data file can be accessed. The air temperature for 2011 is shown in Figure 4.4-41.

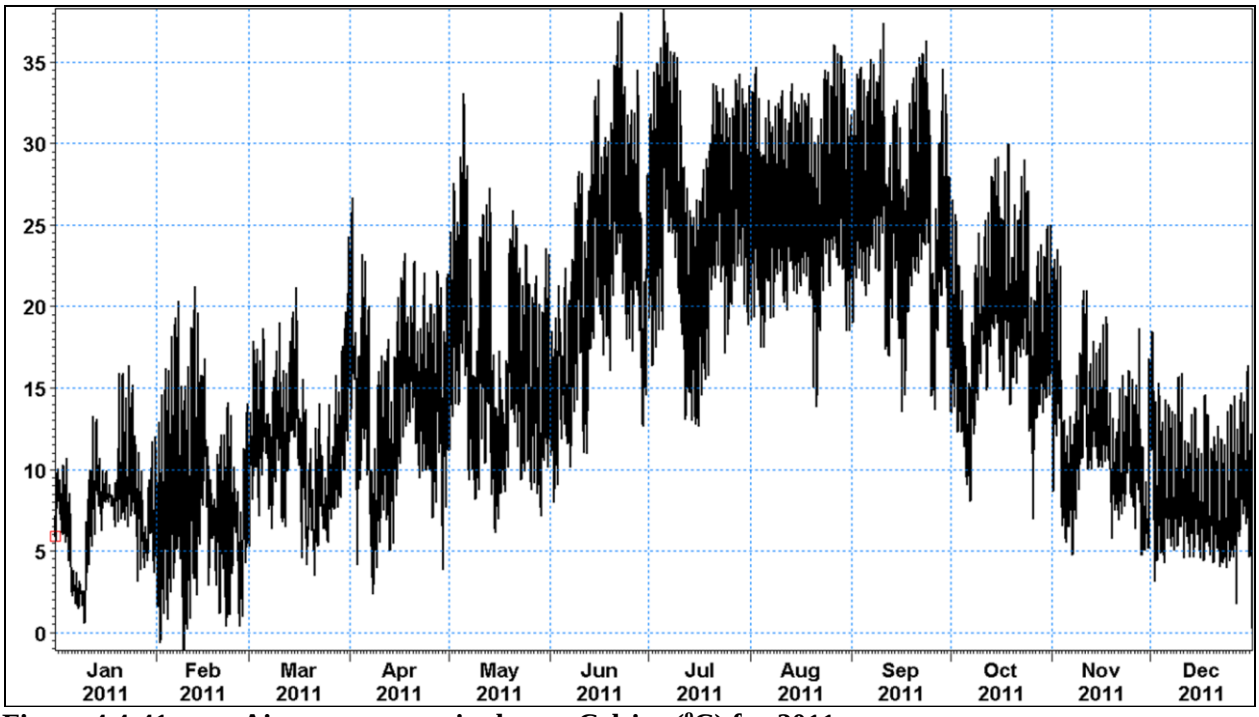

Figure 4.4-41. Air temperature in degree Celsius (^{o}C) for 2011.

4.4.6.6 Short Wave Radiation

The short wave radiation panel is shown below in Figure 4.4-42. Short wave radiation was based on measurements taken at the Denair II station in Turlock. Solar radiation data was collected at Don Pedro Dam but this data was found to have problems associated with a build up of dust on the collector panel. The Denair data is shown in Figure 4.4-43.

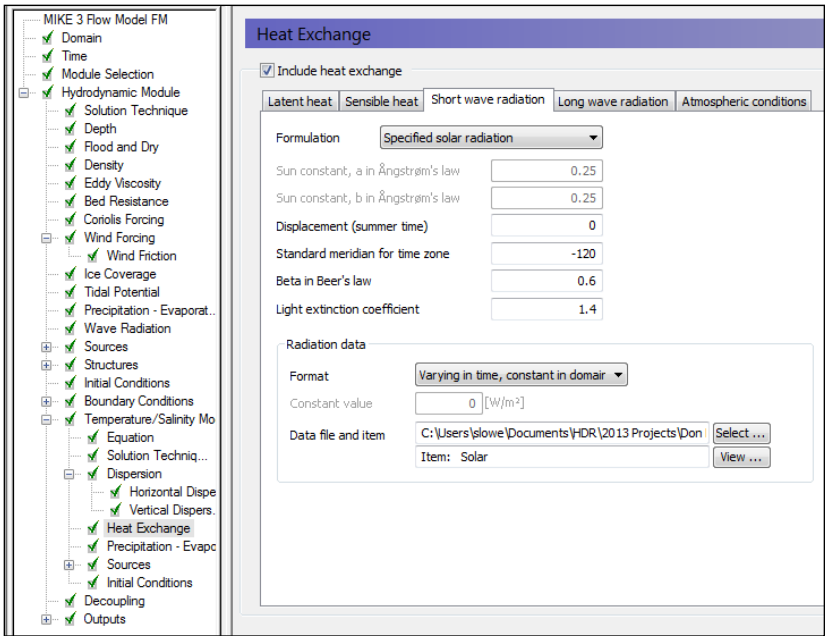

Figure 4.4-42. Short wave radiation parameters.

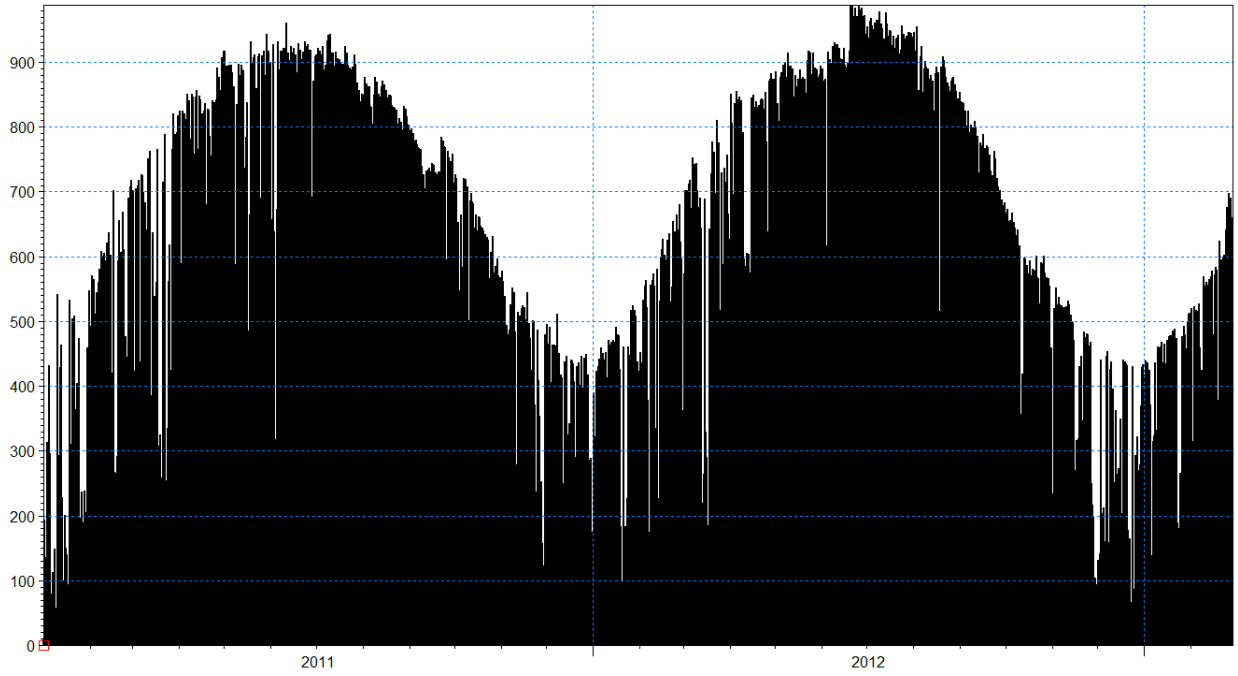

Figure 4.4-43. Denair II solar radiation (W/m^2).

The displacement and standard meridian time zone parameters in the panel are not used when the short wave radiation is specified directly. Also the clearness coefficient, which appears in the Atmospheric Conditions tab, is not used when measured short wave radiation is used.

The measured short wave radiation basically describes the amount of radiation present at the water surface. Some of the short wave radiation in the visible spectrum (i.e. light) has the ability

to penetrate the surface of the water. This radiation is rapidly absorbed by the water, warming it. The rate of light absorption, or attentuation, is described by Beer's Law (circa 1852):

$$I(d) = (1 - \beta) I_0 e^{- \lambda d}$$

where:

I(d)	short wave radiation intensity, I, at depth, d, below the surface	(W/m^2)
β	amount of radiation absorbed at the surface	fraction
I_o	light intensity just below the surface	(W/m^2)
λ	first order light absorption rate	(m^{-1})
d	depth	(m)

The constants β and λ (also known as the light extinction coefficient) are typically seasonally adjusted. For March – October they were: $\beta = 0.1$ and $\lambda = 10$; and over winter they were: $\beta = 0.6$ and $\lambda = 1.4$. For numerical models these constants are typically calibration parameters and are strongly dependent on the vertical layer structure of the model.

4.4.6.7 Long Wave Radiation

Long wave radiation is heat that escapes from the water in the infrared range. The two options available to the user are:

(1) Let the model compute (calculation shown below).

(2) Input the measured long wave radiation.

As measured long wave radiation was not available the model calculation option was used.

The model uses Brunts equation (circa 1932):

$$q_{lr,net} = -\sigma_{sb}(T_{air} + T_K)^4 \left(a - b\sqrt{e_d}\right)\left(c + d\frac{n}{n_d}\right)$$

where:

$q_{lr,net}$	heat loss; outgoing long wave radation	(W/m^2)
σ_{sb}	Stefan-Boltzman constant	($W/m^2/^oC^4$)
T_{air}	surface air temperature	(^oC)
T_k	equilibrium temperature	(^oC)
e_d	vapor pressure of air	(Pa)
n	number of sunshine hours	(hrs)
n_d	max number of sunshine hours	(hrs)

a, b, c, d are well known coefficients and are not variable by the user.

4.4.6.8 Temperature Sources

Water inflows and outflows were previously defined in terms of flow rate. In this section they are assigned time variable temperatures through the source temperature tab (Figure 4.4-44). The format is similar to the source tab described previously, except that now a variable temperature time series will be read from a data file. In the Don Pedro Reservoir model the inflow temperature is taken from measured data from the Tuolumne River at Indian Creek Trail (See Figure 3.0-1 Study Area). The Indian Creek Trail data for 2011 are shown in Figure 4.4-45. In the absence of other measured tributary temperatures, these values are assigned to all the sources. The outflow temperature is computed by the model.

In order to run the reservoir model over a longer historical time frame a long term inflow temperature data set has been developed. The development of the long term data set is described in Attachment F: *Full Period of Record Inflow Temperature Data Set.*

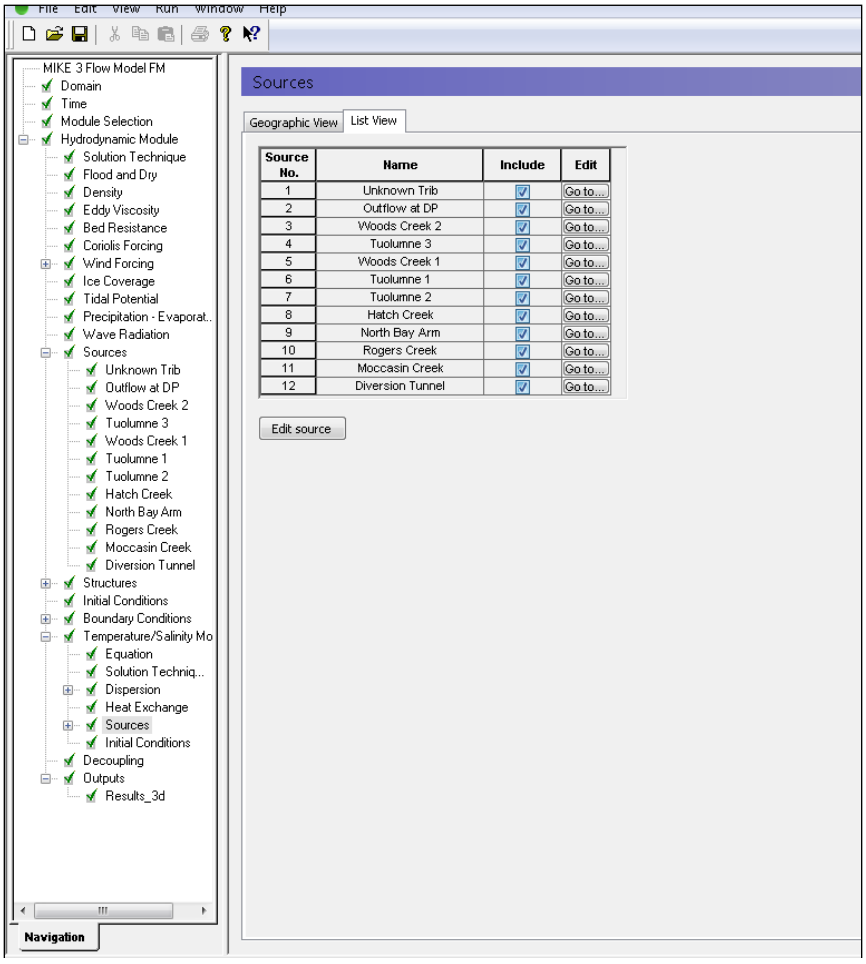

Figure 4.4-44. Temperature sources.

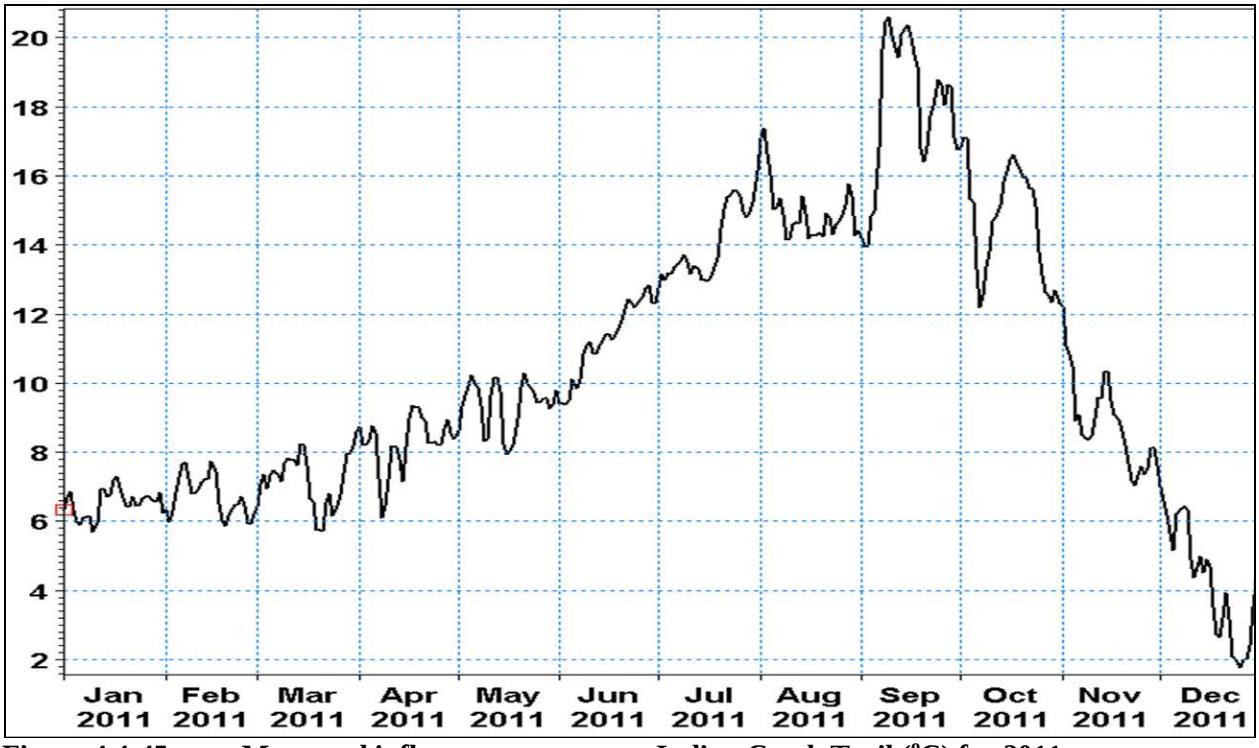

Figure 4.4-45. Measured inflow temperature at Indian Creek Trail (^{o}C) for 2011.

4.4.6.9 Initial Temperatures

Initial reservoir temperatures can either be specified as constant, as shown in Figure 4.4-46, or varying throughout the model. For Don Pedro Reservoir an initial value of 10^{o} C everywhere in the reservoir was used. This value is representative of the reservoir's wintertime, non-stratified, equilibrium temperature.

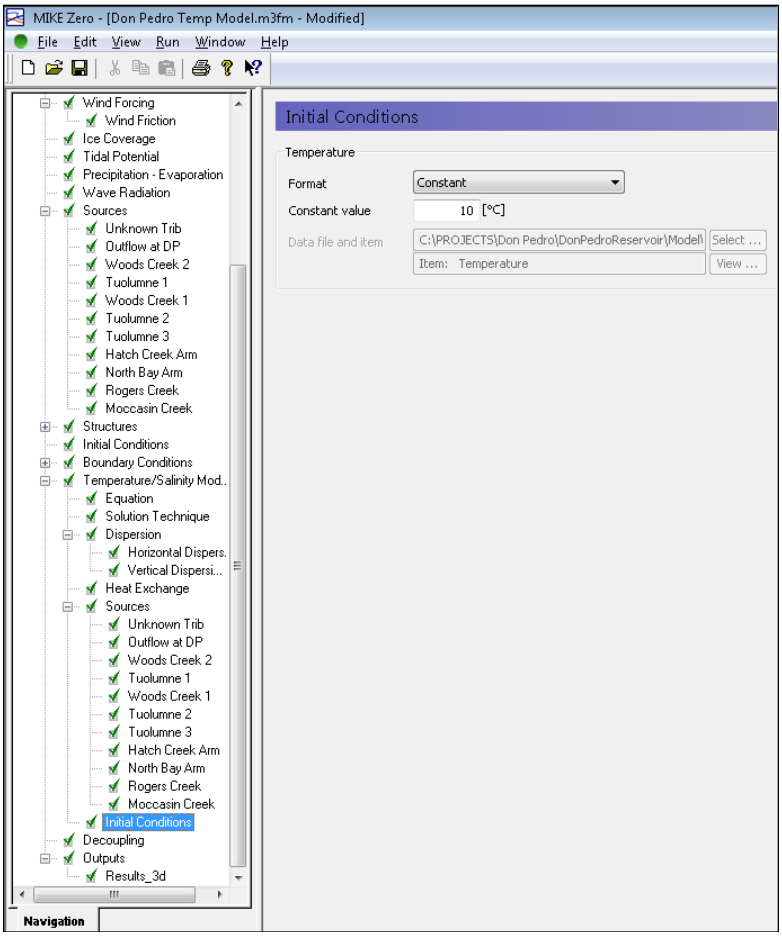

Figure 4.4-46. Temperature initial condition.

4.4.6.10 Decoupling

In some cases where water quality is being simulated, the water quality calculation does not need to be updated every hydrodynamic time step. This is aimed at increasing run times. It is not relevant in this case. The input tab is shown below in Figure 4.4-47.

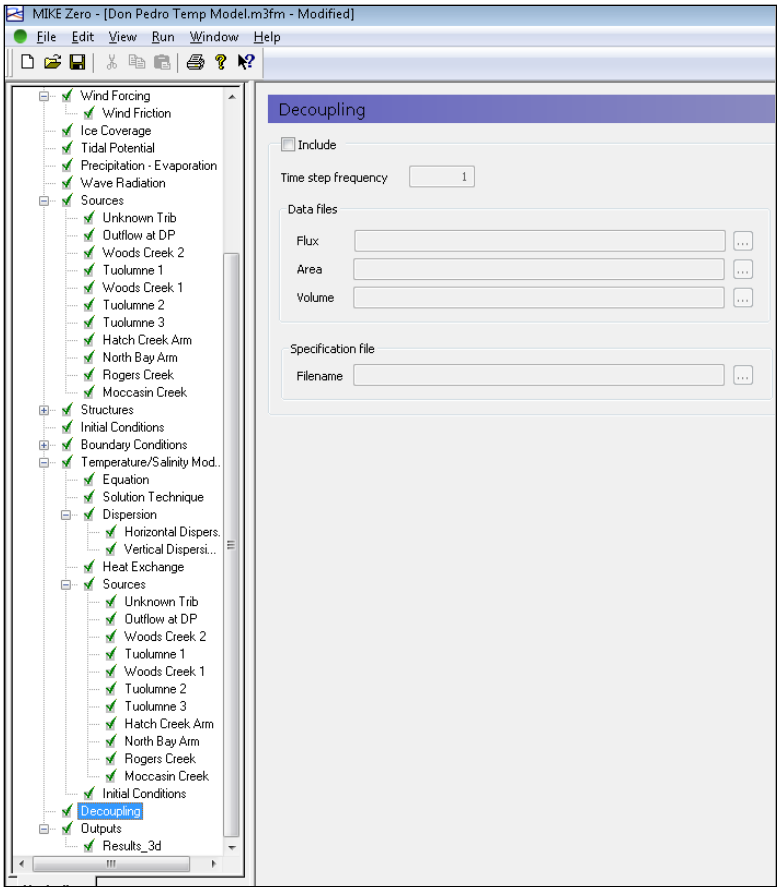

Figure 4.4-47. Decoupling tab.

4.4.7 Model Output

The model allows results to be written to data files with many options. The main output tab displays the various data files the user has set up, as shown in Figure 4.4-48. The files can also be deselected, so not every file needs to be written for every model run.

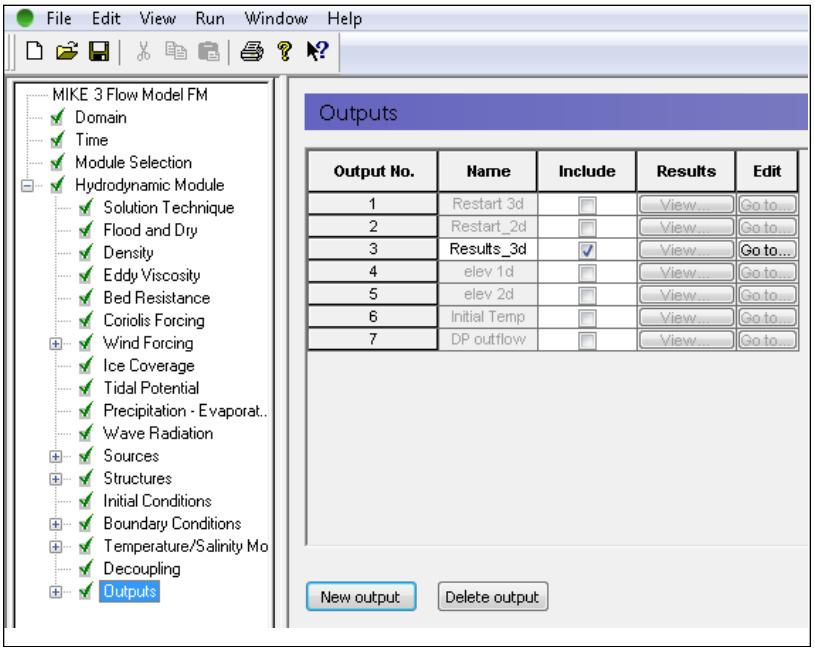

Figure 4.4-48. Output selection screen.

The model output folder (Figure 4.4-49) contains three tabs:

- geographic view
- output specification
- output Items

The geographic view displays the extent of where data will be output, as described in the output specification tab. As shown in Figure 4.4-49, the entire Don Pedro Reservoir model domain is selected.

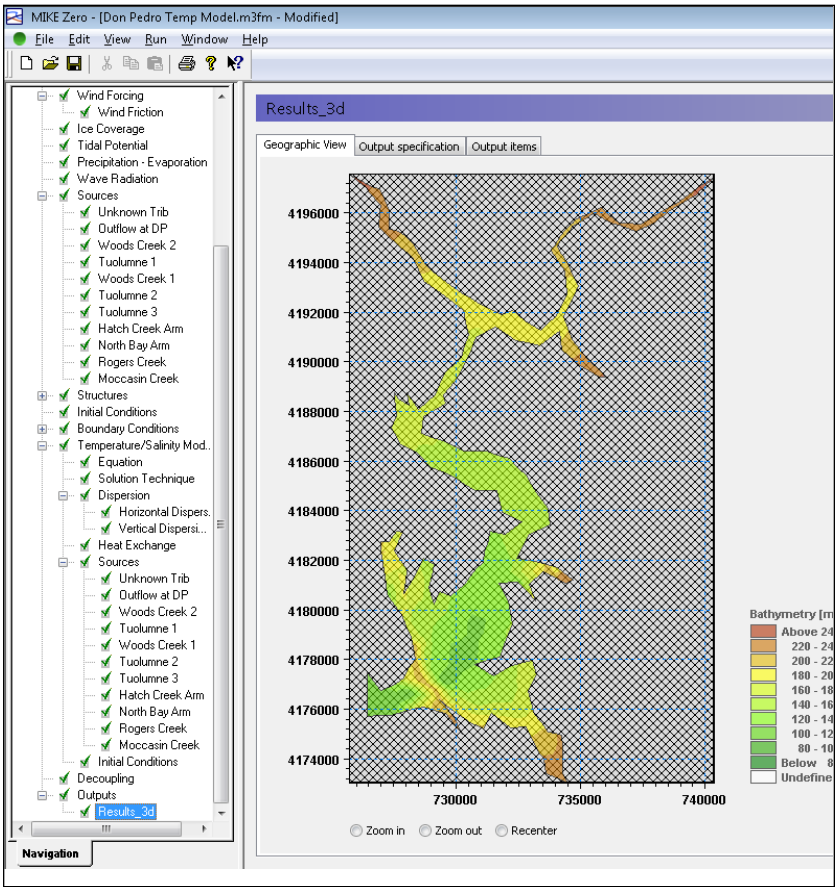

Figure 4.4-49. Geographic view of output area.

In the output specification tab there are options to select the geographic extent of the data; whether the output will contain 1D, 2D or 3D data; the time steps that will be output; and which vertical layers in the model will be output. The path and filename of the output file is specified. These are shown in Figure 4.4-50.

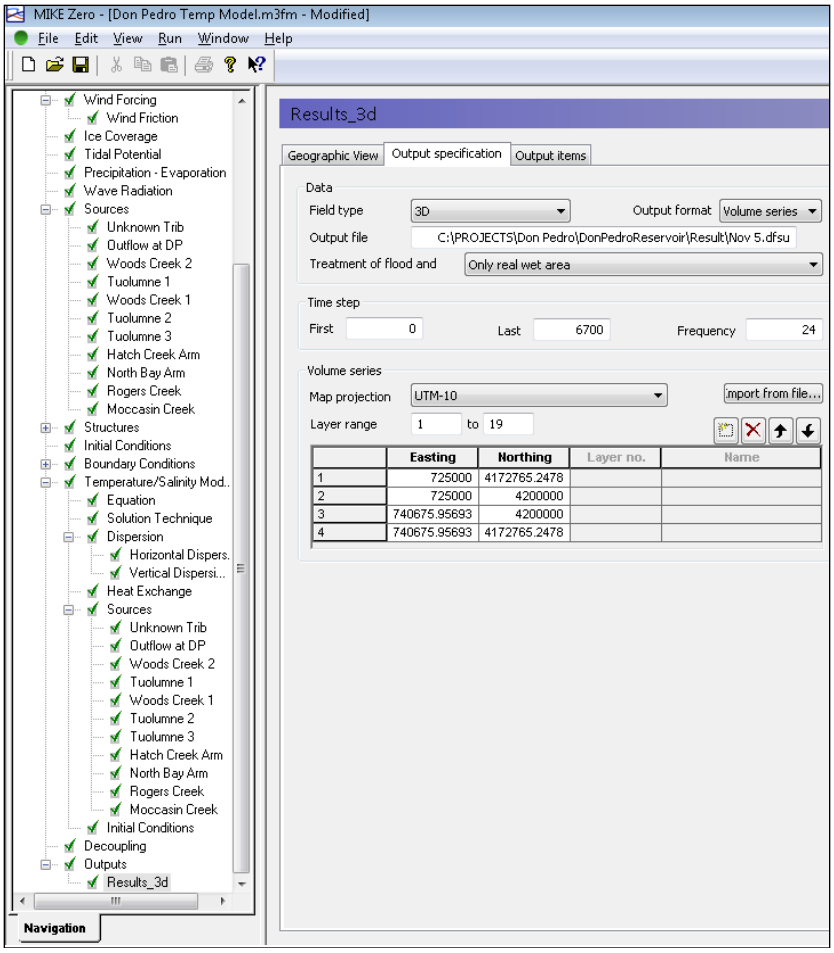

Figure 4.4-50. Output specifications.

The final output tab contains the variables that can be selected for output. Different file types have different variable options. For example “surface elevation” is available for a 2D horizontal output file but not for a 3D file, as shown below in Figure 4.4-51.

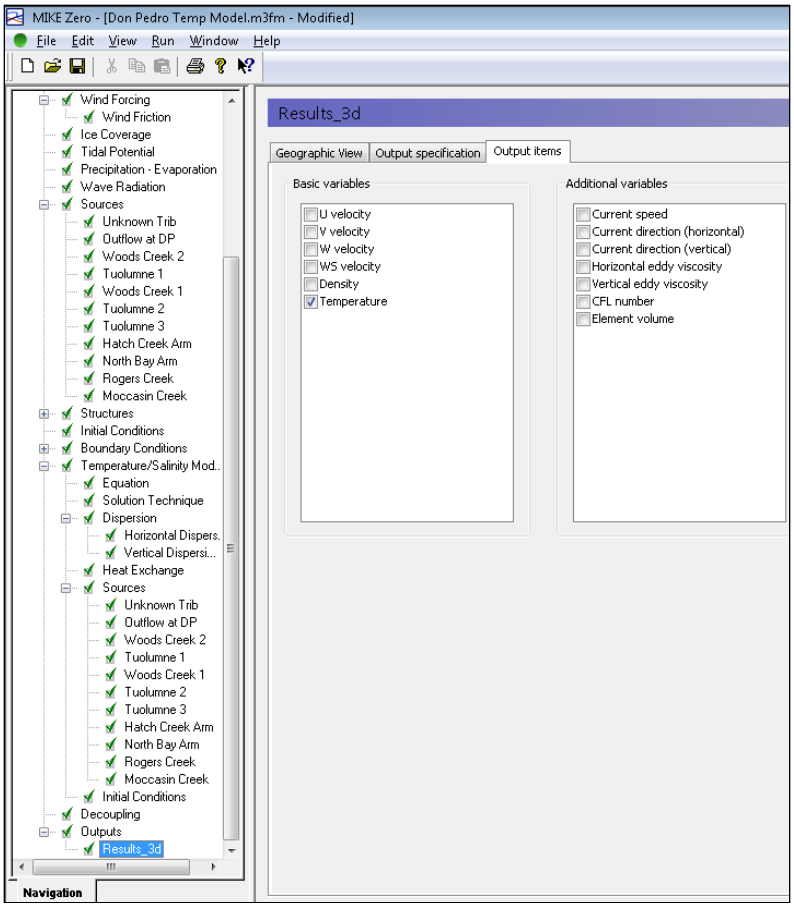

Figure 4.4-51. Example of available output variables for 3D output.

5.0 MODEL OPERATION AND DISCUSSION

The FERC-approved Study Plan lists the following requirements:

- the model will be calibrated and verified using field data that cover continuously the periods of stratification (April through October) and de-stratification (November through March) of the Don Pedro Reservoir; the data used for the calibration are discussed in Section 5.1;
- model-computed temperatures will be compared to monthly temperature profiles (see Sections 5.2 and 5.3 below);
- model–computed temperature of the Don Pedro releases will be compared to the temperature data collected at the powerhouse; temperature measurements at the powerhouse (1978 through 1988, 2010 through present) will also be used for the model calibration/verification (see Section 5.4 below);
- surface water temperature recorded concurrently with the bathymetric data in May and June 2011 will also be used in the model calibration; and
- a QA/QC review of the modeling following the calibration and verification.

5.1 Temperature Profile Data

Vertical temperature profiles collected in the Don Pedro impoundment were used to calibrate and validate the reservoir model. The calibration year is 2011 and the validation year is 2012. As discussed previously these years were chosen as they were the years with complete data sets. Reservoir temperature profiles are obtained approximately monthly for most of the year, typically February through October/November. The profile data are collected by both CDFW and the Districts. The profile locations are listed above in Table 4.3-2 and are shown on Figure 5.1-1. The locations of the temperature profiles are:

- Highway 49 Bridge (CDFW and Districts)
- Above Old Don Pedro Dam (Districts)
- Below Old Don Pedro Dam (Districts)
- Don Pedro Dam (CDFW and Districts)
- Jacksonville Bridge (CDFW and Districts)
- Middle Bay (CDFW and Districts)
- Woods Creek (CDFW and Districts)
- Ward's Ferry (CDFW and Districts)

Plots of reservoir profiles are provided in Attachment D. The vertical temperature profiles show that in the early portion of the year, January through March, the reservoir is not stratified and equilibrium temperatures are around 10^{o} C. In April the data indicate significant warming at the surface with temperatures around 18^{o} C observed, and initial reservoir stratification beginning to occur. The data for May and June look similar to April, but with the surface heat penetrating to

some depth. By July the surface temperatures have risen above 25° C and the reservoir temperature stratification is well-defined. The profiles show a decrease in temperature with depth that extends some 200 feet until the temperature stabilizes around 10-12° C. The temperature stratification remains strong through July, August, and September. At the end of September the reservoir is still strongly stratified, but surface temperatures have dropped by a couple of degrees and are usually just below 25° C. When the last profiles were measured in 2011 on October 13 the reservoir remained stratified. Surface temperatures continued to drop and were around 20° C.

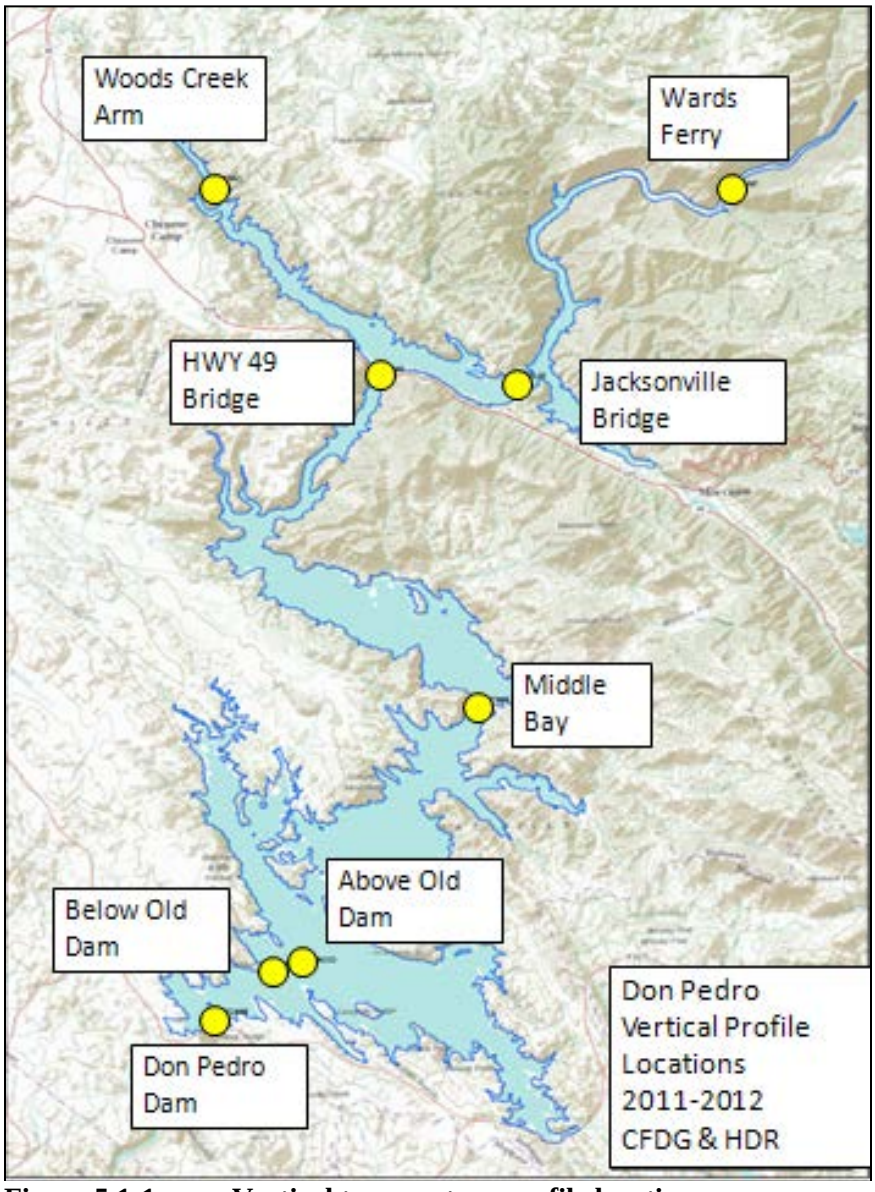

Figure 5.1-1. Vertical temperature profile locations.

5.2 Model Results – 2011 Calibration Year

Figures 5.2-1 through 5.2-11 show the calibration results for 2011. Vertical temperature profiles for 2011 were measured on the following days (Attachment D):

January 12	July 11
February 7	July 26
March 22	August 30
April 20	September 27
May 18	October 13
June 6	--

As mentioned in Section 1, the current version of the model works in SI units; therefore, the temperatures are in Celsius and depth is in meters. The y-axis represents depth as measured from an elevation of 260 meters (853 feet). This benchmark elevation was chosen as water will never be above this height so no data would ever be excluded from the plots. For reference the normal maximum pool elevation of 830 feet and the minimum power pool of 600 feet are also shown. As noted on the plot captions, the observed data are shown by open blue circles with model results given by open red triangles.

The model temperature was initially set at 10^{o} C when the model run started on January 10, and it takes until April to see the heat transferring through the deeper model surface layers. The model profiles in January, February and March show the slow progression of temperature from the surface. The shallower areas of the reservoir respond quicker and so the model profiles in Ward's Ferry and Woods Creek show a better fit in the early months.

From April the reservoir begins to show noticeable stratification and this remains through October when the last profiles were measured for 2011. The model reproduces the strong reservoir stratification and is a good fit in to the measured data throughout the year at the various stations.

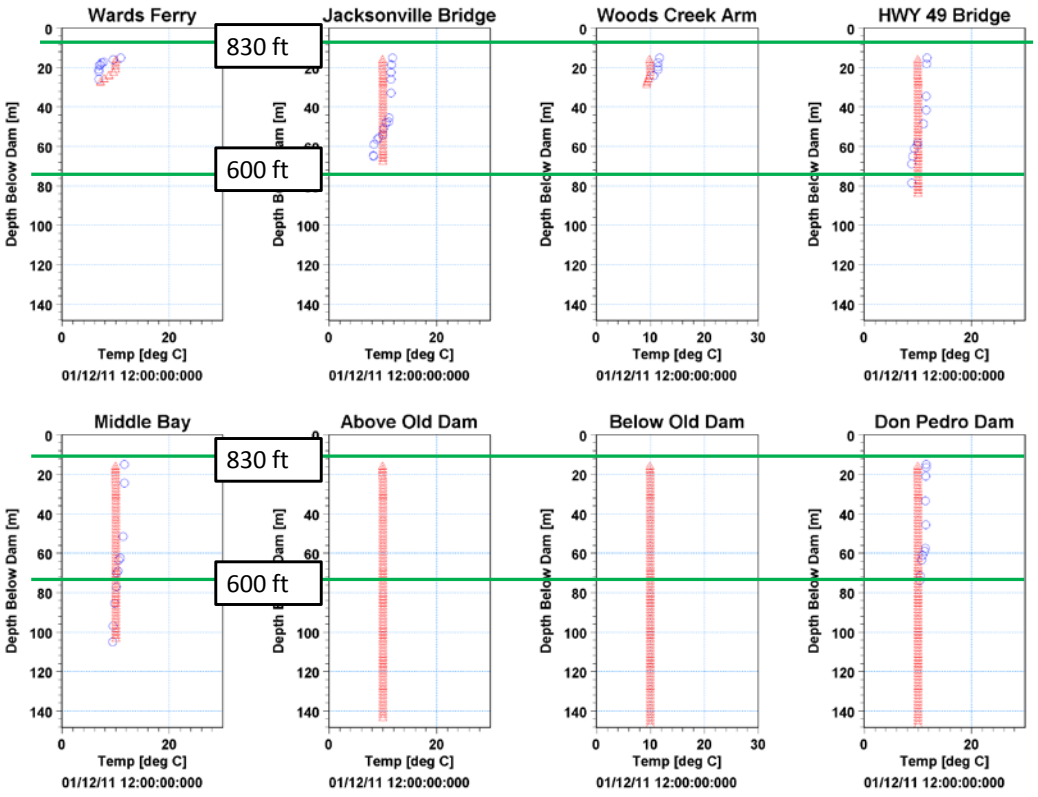

Figure 5.2-1. January 12, 2011 calibration. (Observed = blue circles; Model = red triangles)

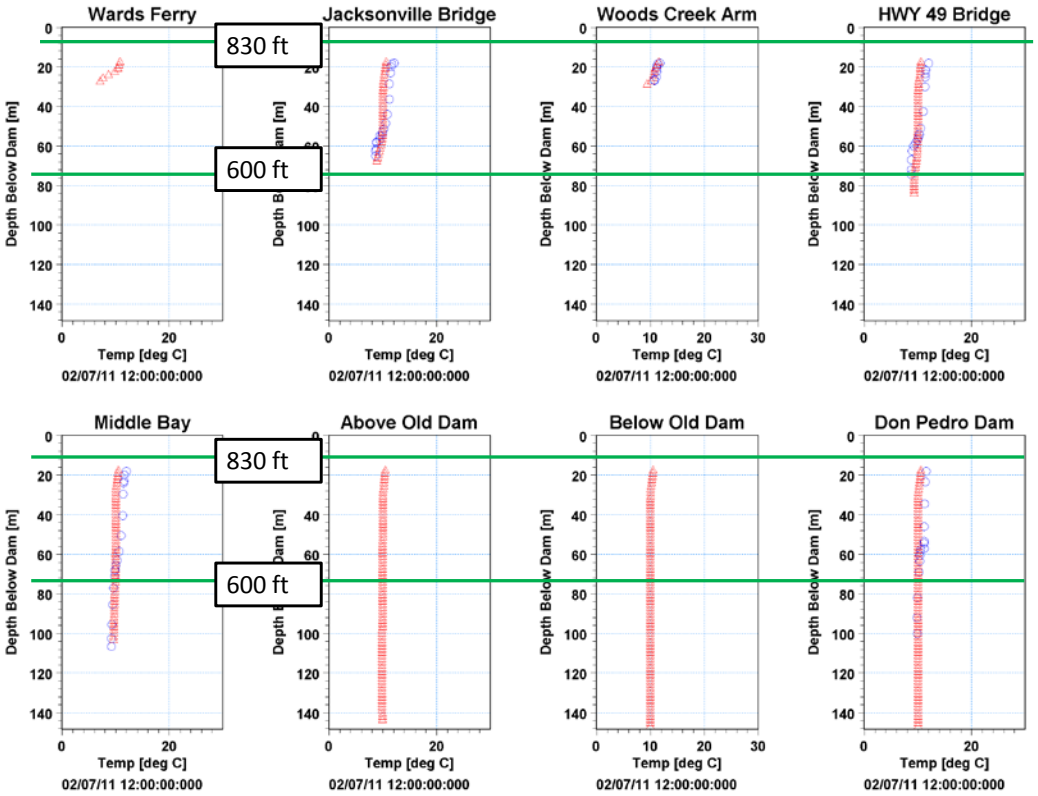

Figure 5.2-2. February 7, 2011 calibration. (Observed = blue circles; Model = red triangles)

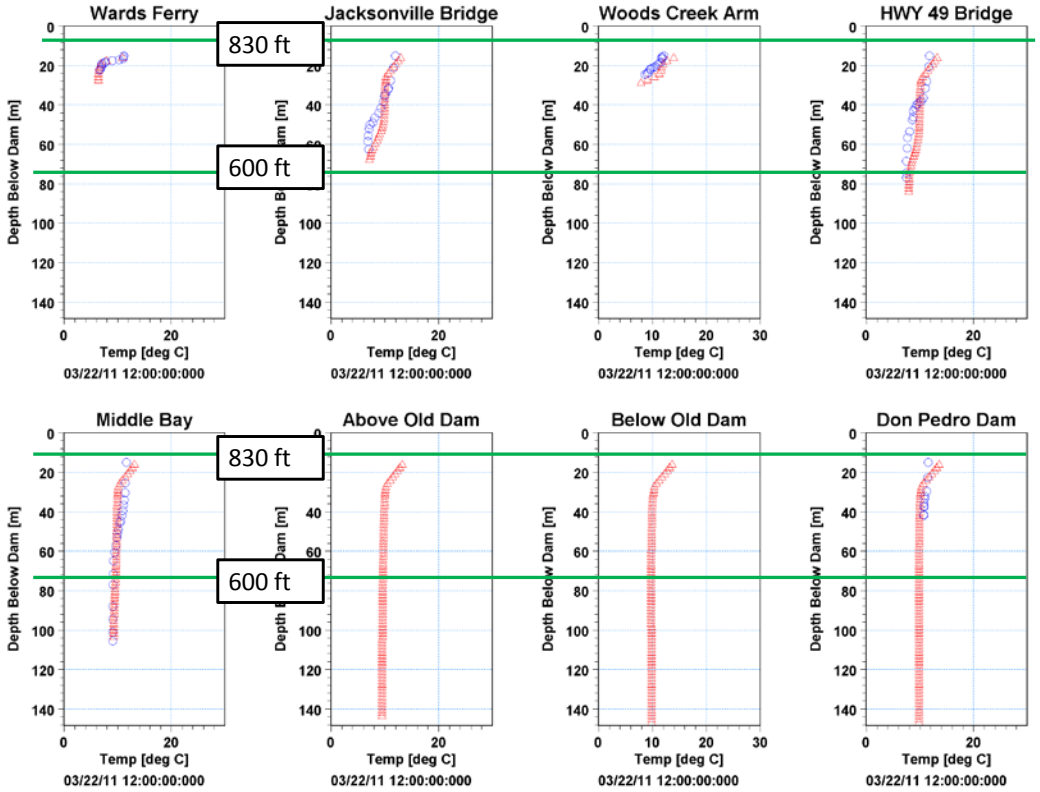

Figure 5.2-3. March 22, 2011 calibration. (Observed = blue circles; Model = red triangles)

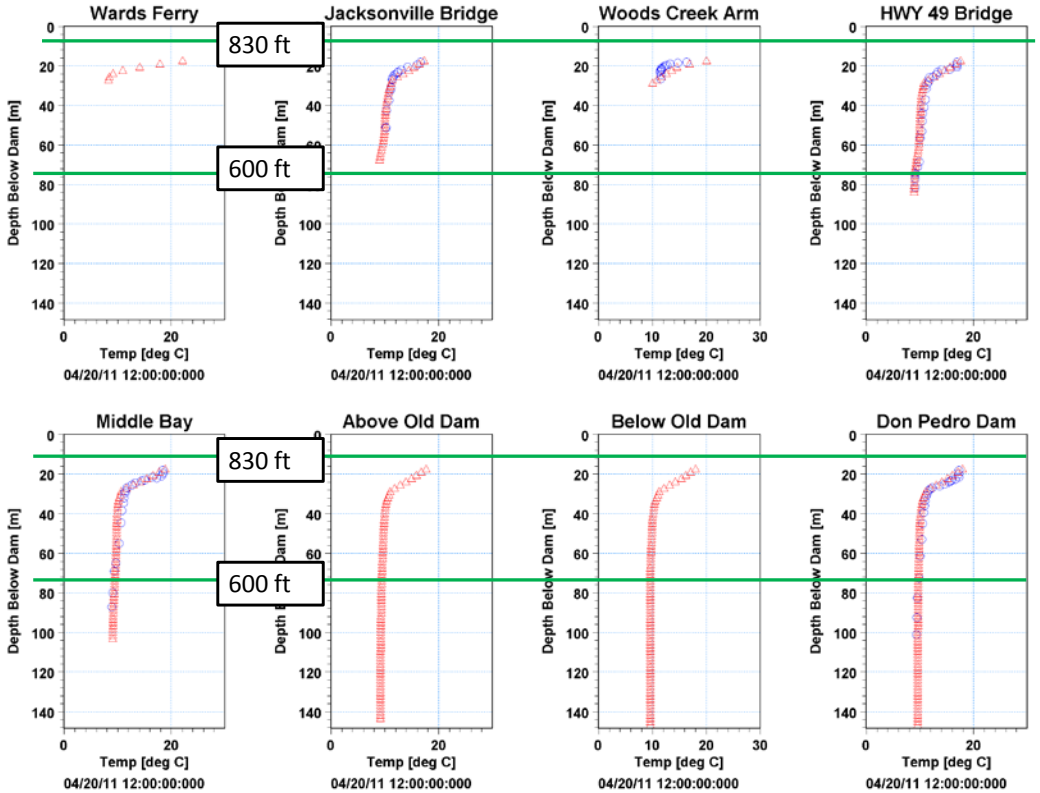

Figure 5.2-4. April 20, 2011 calibration. (Observed = blue circles; Model = red triangles)

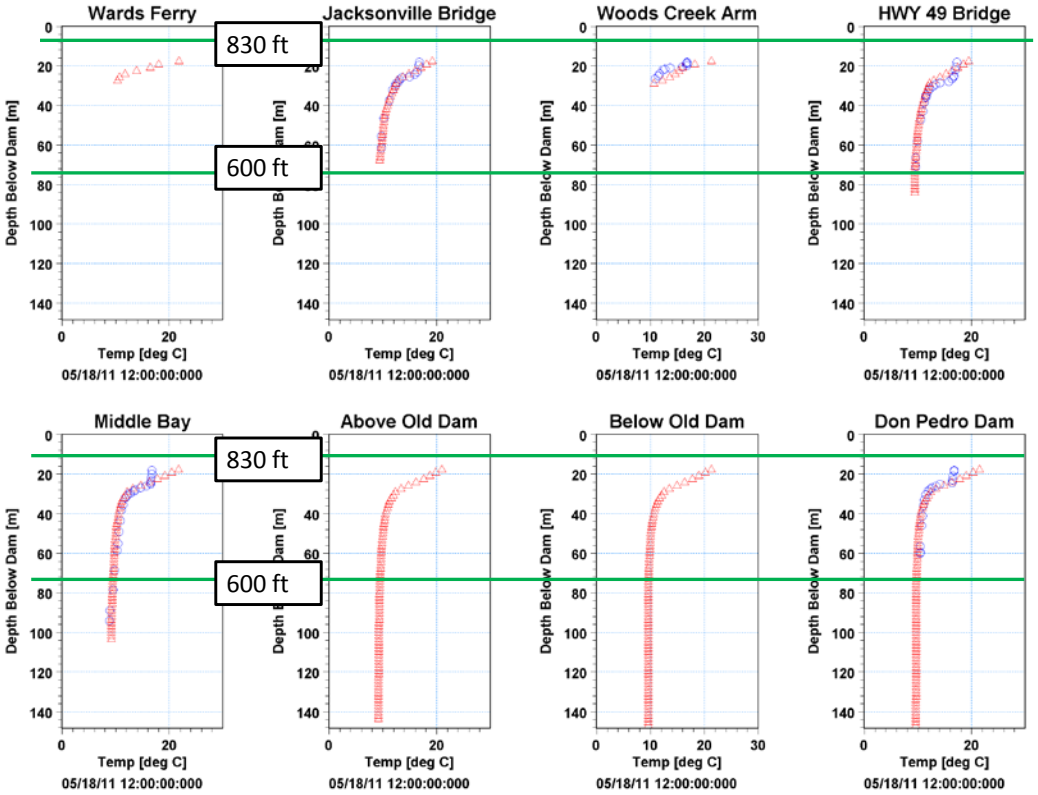

Figure 5.2-5. May 18, 2011 calibration. (Observed = blue circles; Model = red triangles)

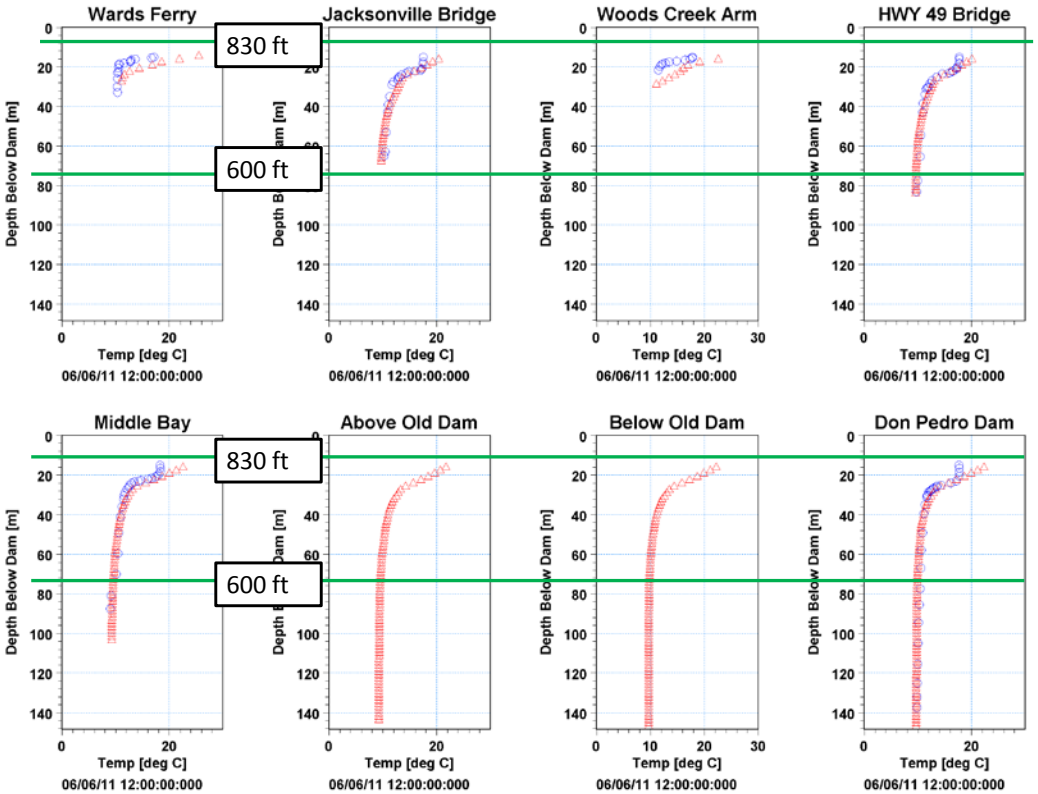

Figure 5.2-6. June 6, 2011 calibration. (Observed = blue circles; Model = red triangles)

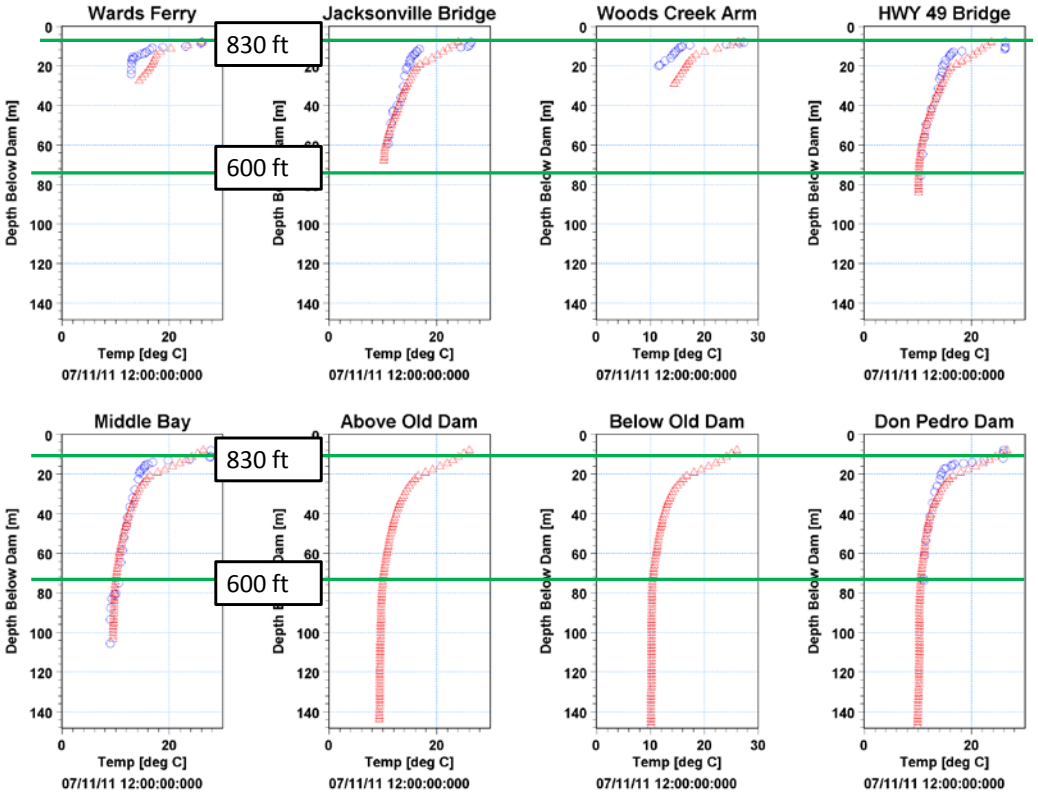

Figure 5.2-7. July 11, 2011 calibration. (Observed = blue circles; Model = red triangles)

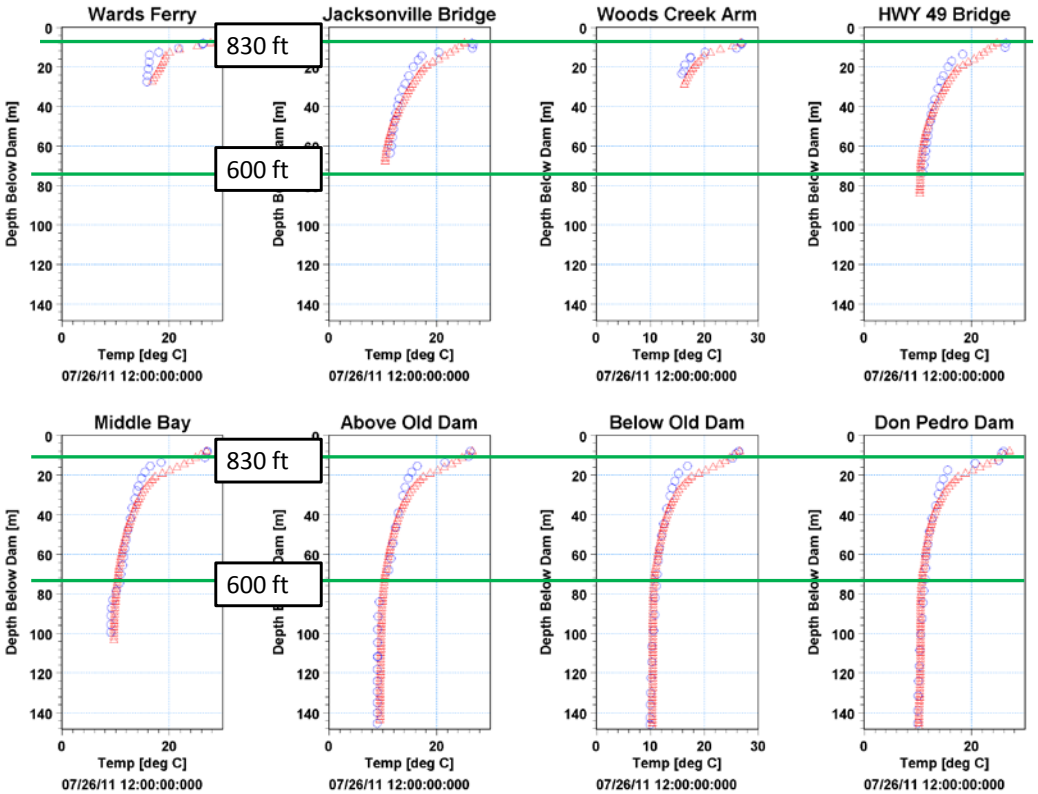

Figure 5.2-8. July 26, 2011 calibration. (Observed = blue circles; Model = red triangles)

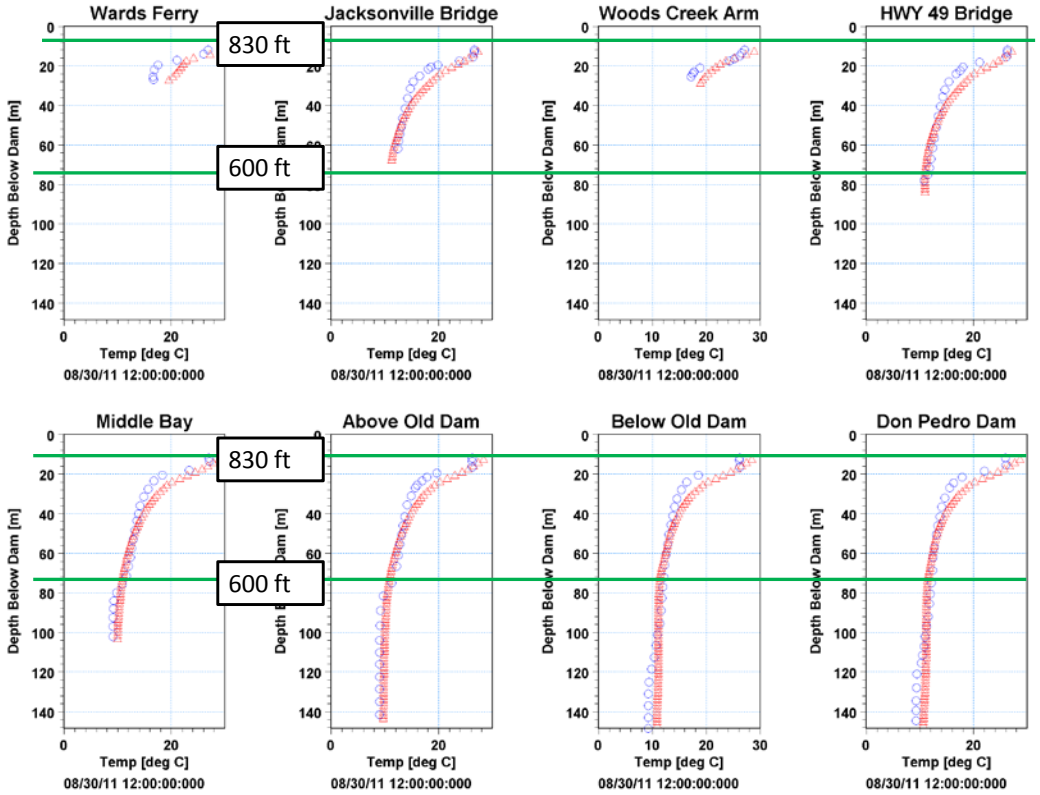

Figure 5.2-9. Aug 30, 2011 calibration. (Observed = blue circles; Model = red triangles)

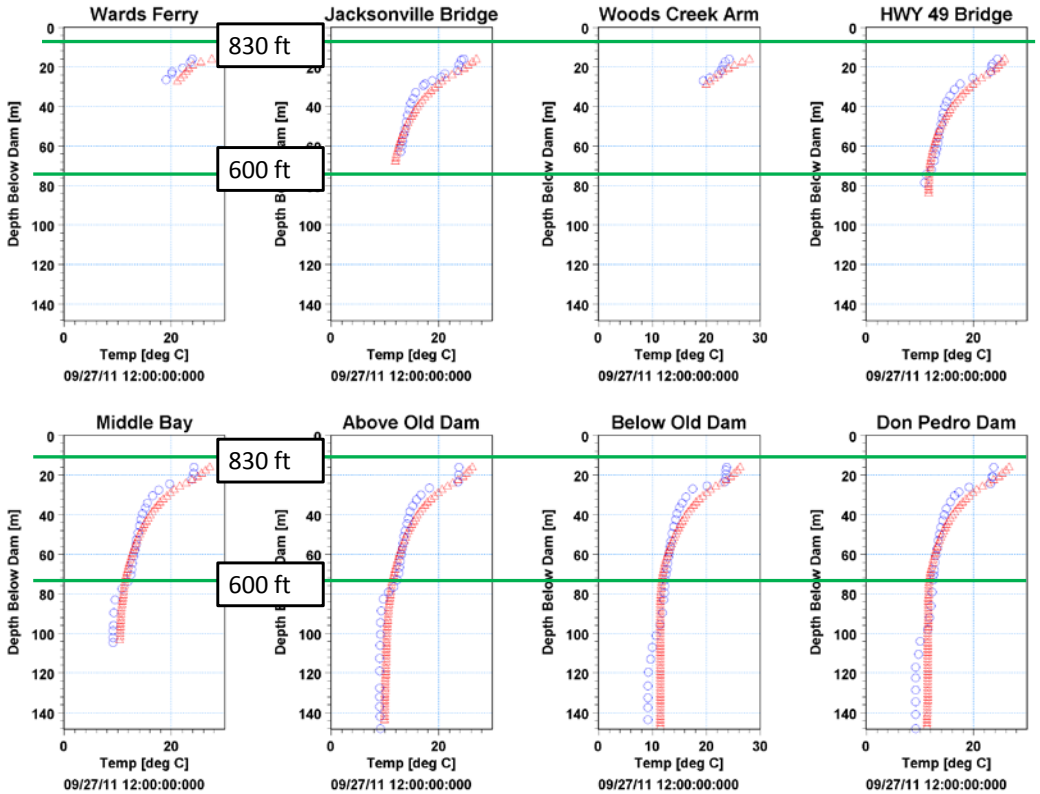

Figure 5.2-10. September 27, 2011 calibration. (Observed = blue circles; Model = red triangles)

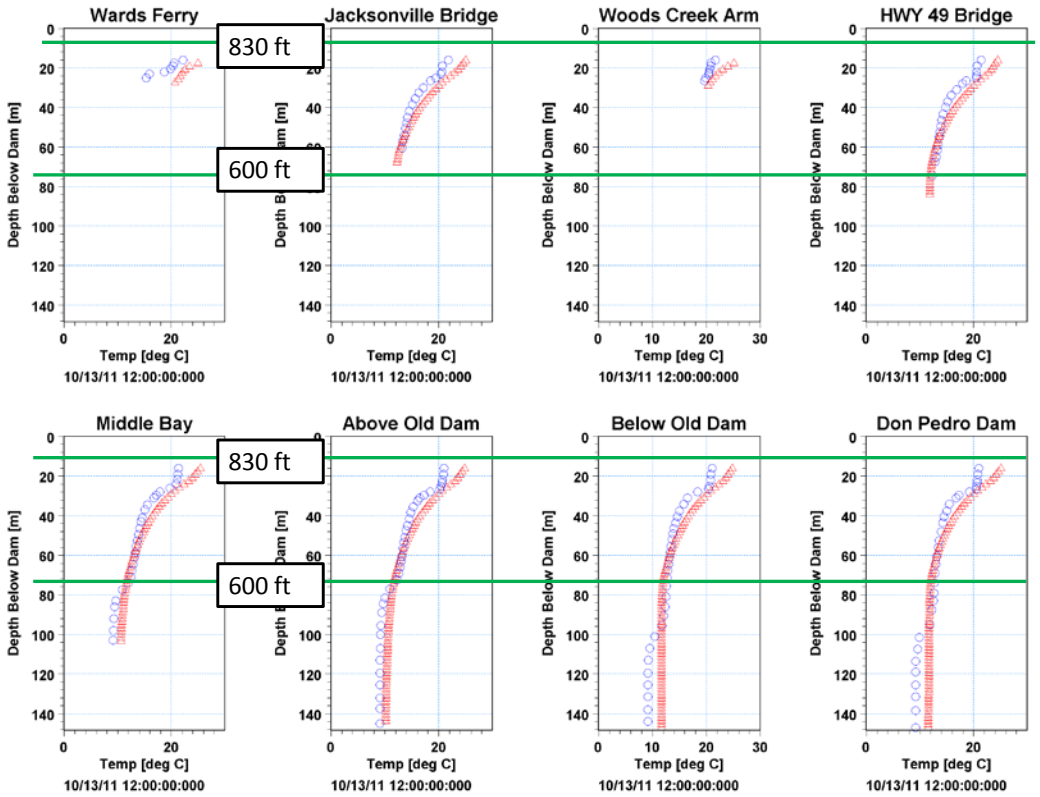

Figure 5.2-11. Oct 13, 2011 calibration. (Observed = blue circles; Model = red triangles)

5.3 Model Results – 2012 Validation Year

Figures 5.3-1 through 5.3-12 show the validation results for 2012 using data collected by the Districts. Vertical temperature profiles for 2012 were measured on the following days:

January 19	June 13
February 14	July 3
March 14	August 22
April 23	September 19
May 8	October 9
May 17	November 19

The model was run continuously from January 10, 2011 to December 5, 2012, when the available data ended. The figures show that the model compares well with the measured data throughout 2012. The measured data for 2012 are very similar to 2011 with the same trends in the timing, and amount of stratification occurring.

In March 2013 the CDFW data set was provided to the Districts. Figures 5.3-13 through 5.3-22 show the comparison to this data set. The plots are virtually identical to the previous plots using data collected by the Districts, as the two measured datasets are in excellent agreement. The days that CDFW collected vertical temperature profiles in 2012 were:

January 19	July 10
February 14	August 10
March 14	September 12
April 23	October 25
May 8	December 26
June 14	

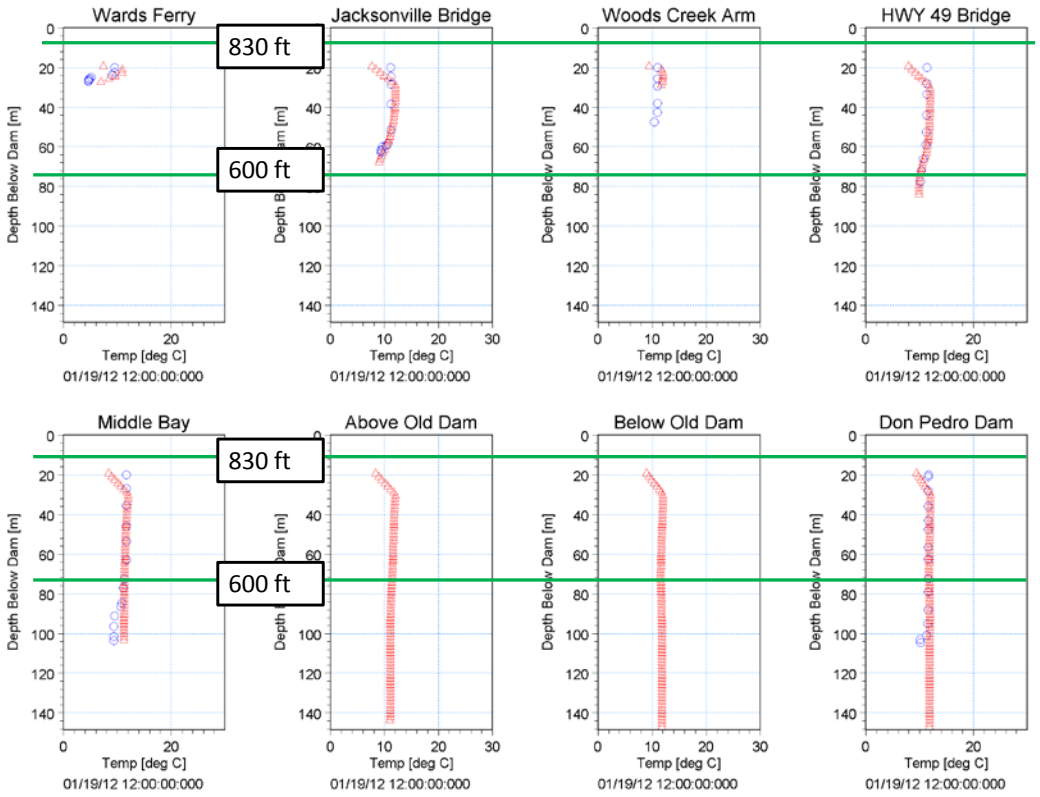

Figure 5.3-1. Jan 19, 2012 validation. (Observed = blue circles; Model = red triangles)

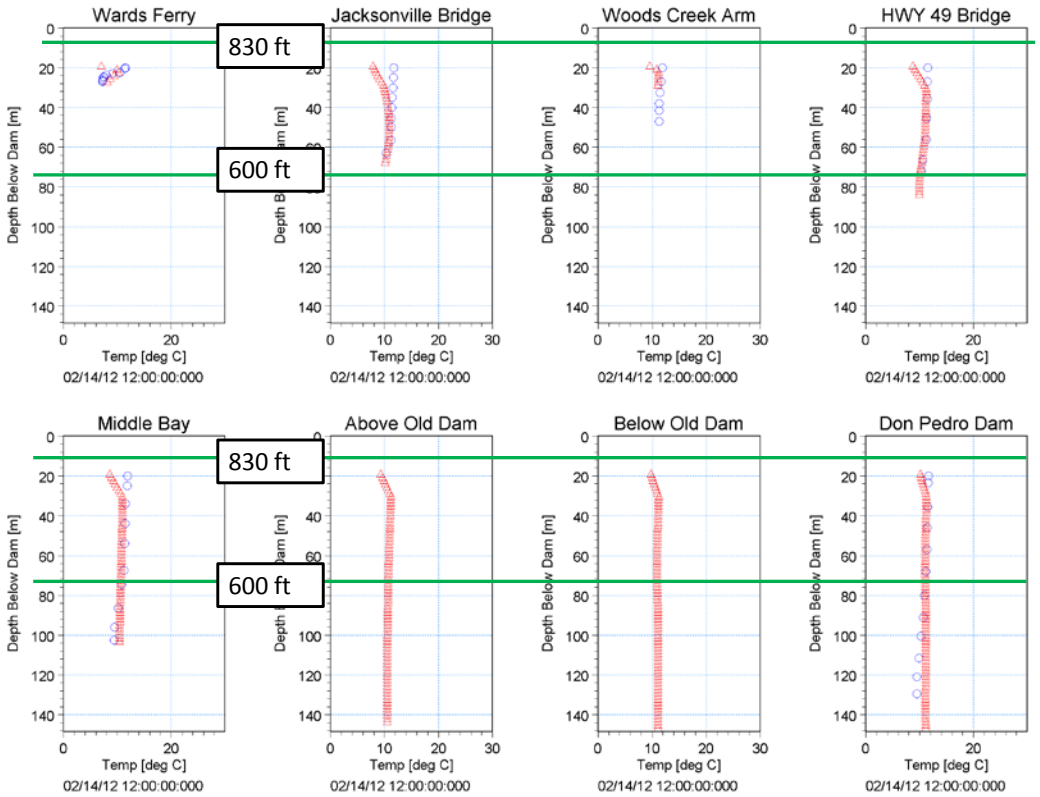

Figure 5.3-2. Feb 14, 2012 validation. (Observed = blue circles; Model = red triangles)

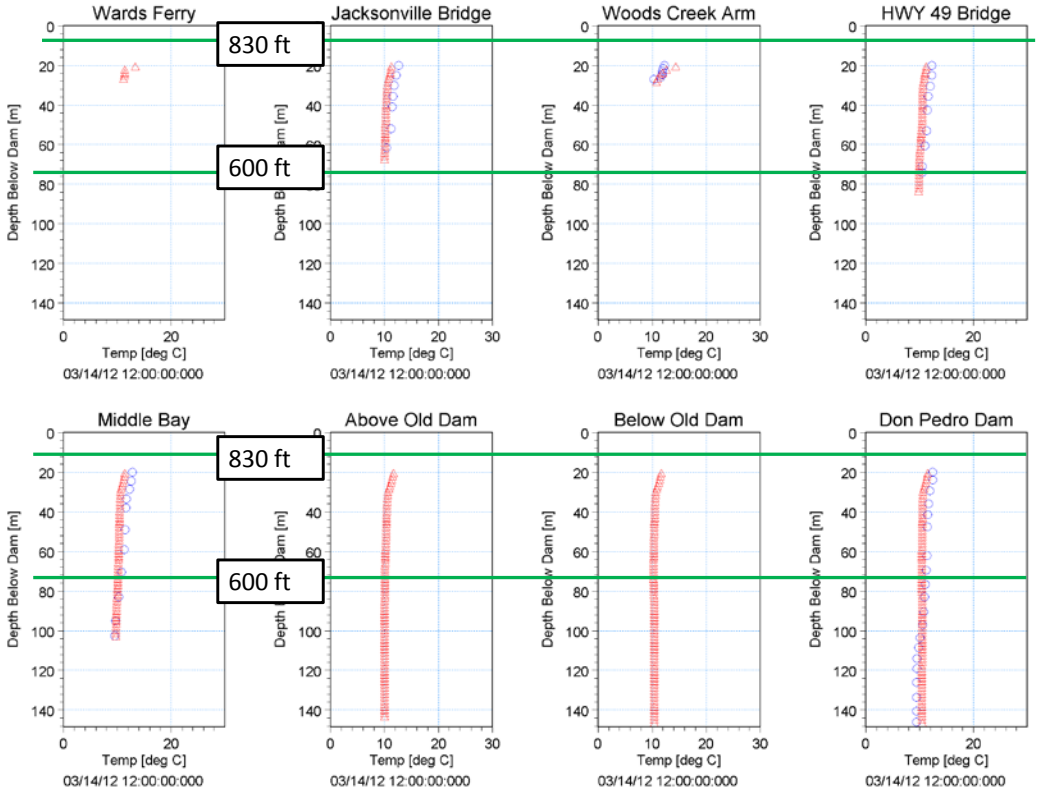

Figure 5.3-3. Mar 14, 2012 validation. (Observed = blue circles; Model = red triangles)

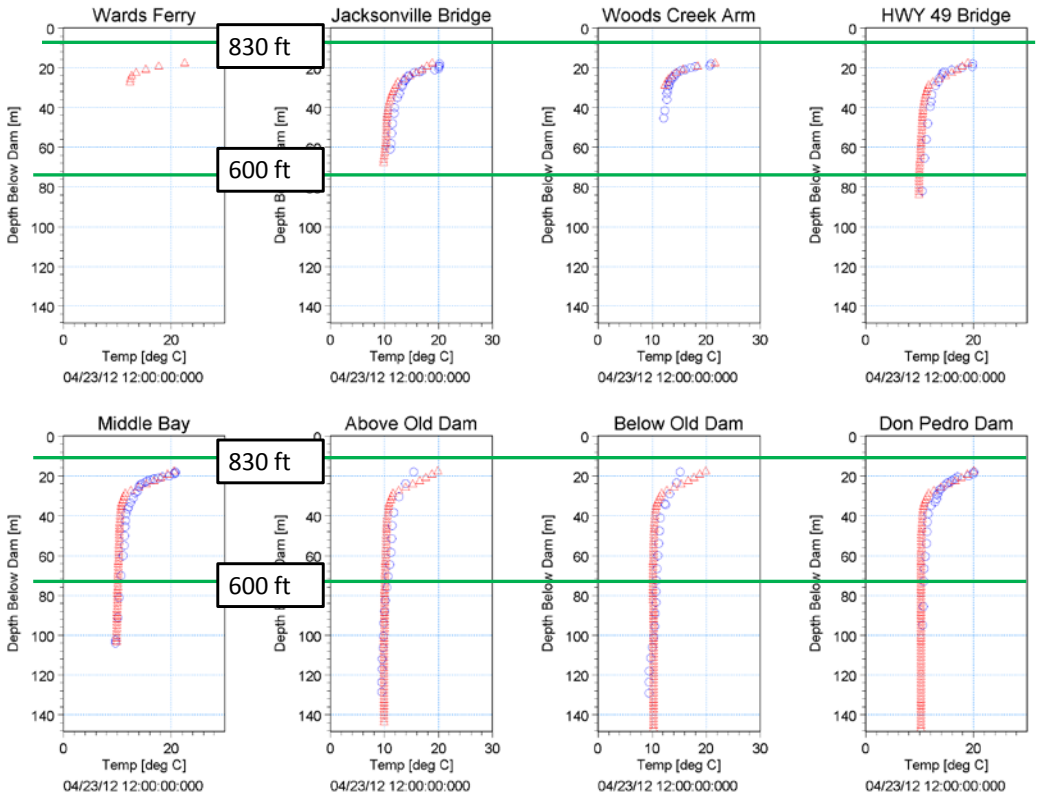

Figure 5.3-4. April 23, 2012 validation. (Observed = blue circles; Model = red triangles)

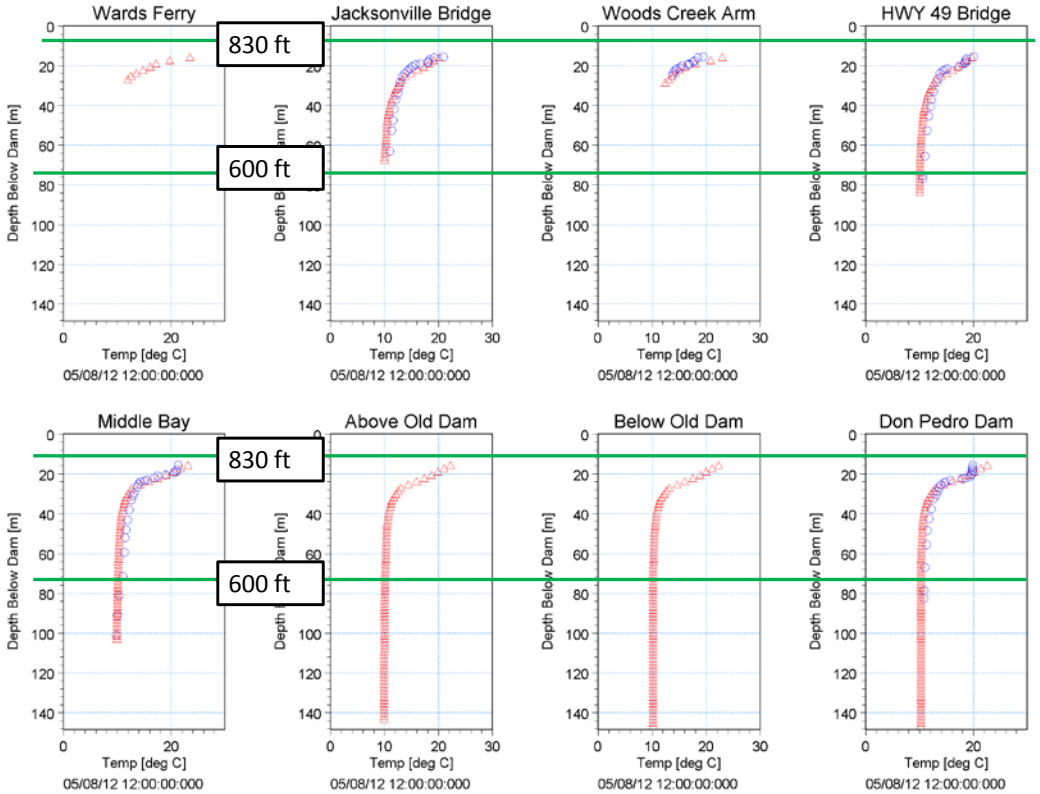

Figure 5.3-5. May 8, 2012 validation. (Observed = blue circles; Model = red triangles)

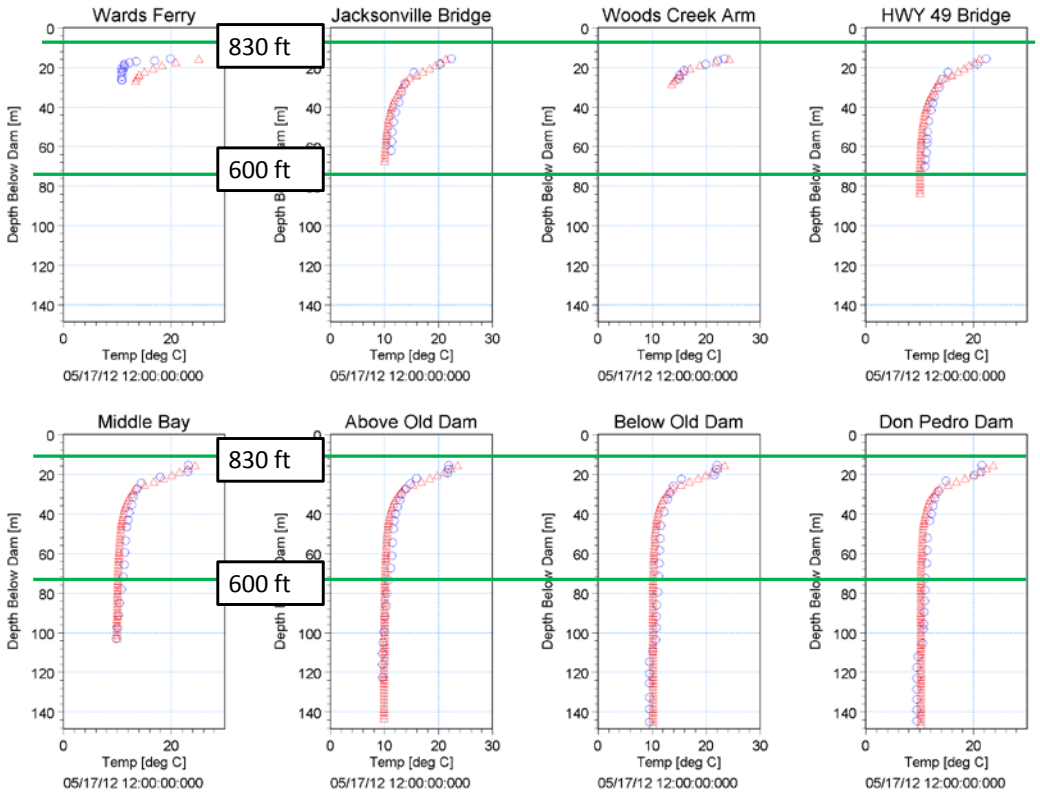

Figure 5.3-6. May 17, 2012 validation. (Observed = blue circles; Model = red triangles)

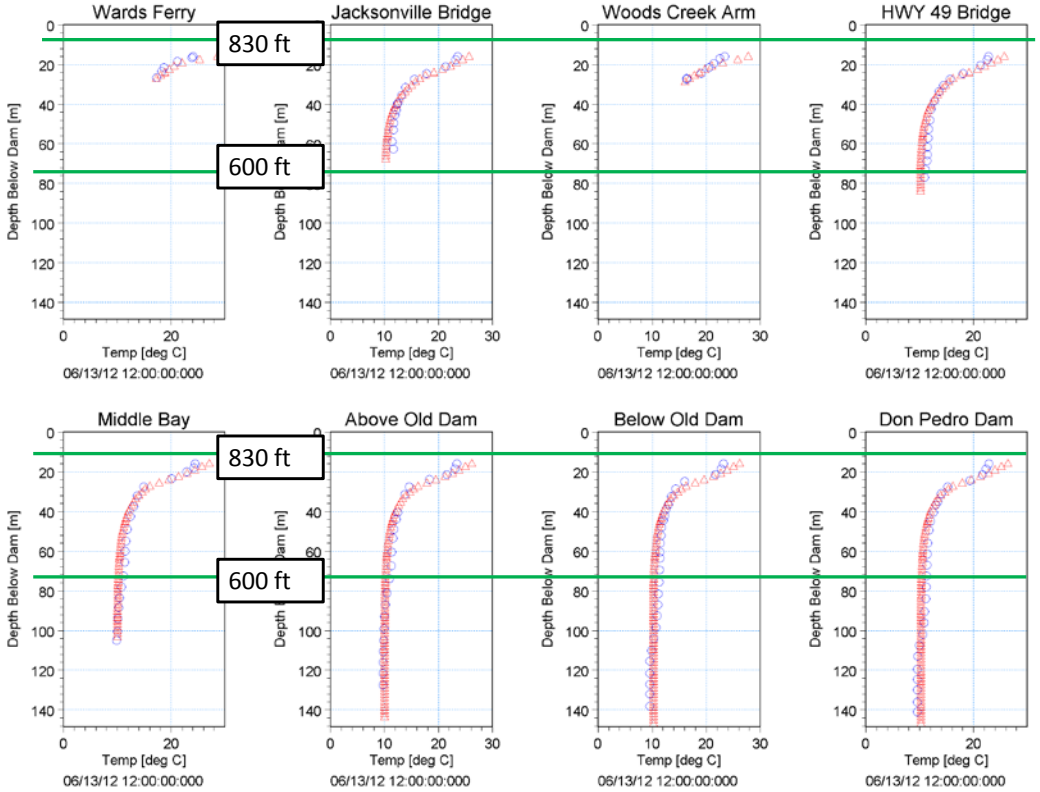

Figure 5.3-7. June 13, 2012 validation. (Observed = blue circles; Model = red triangles)

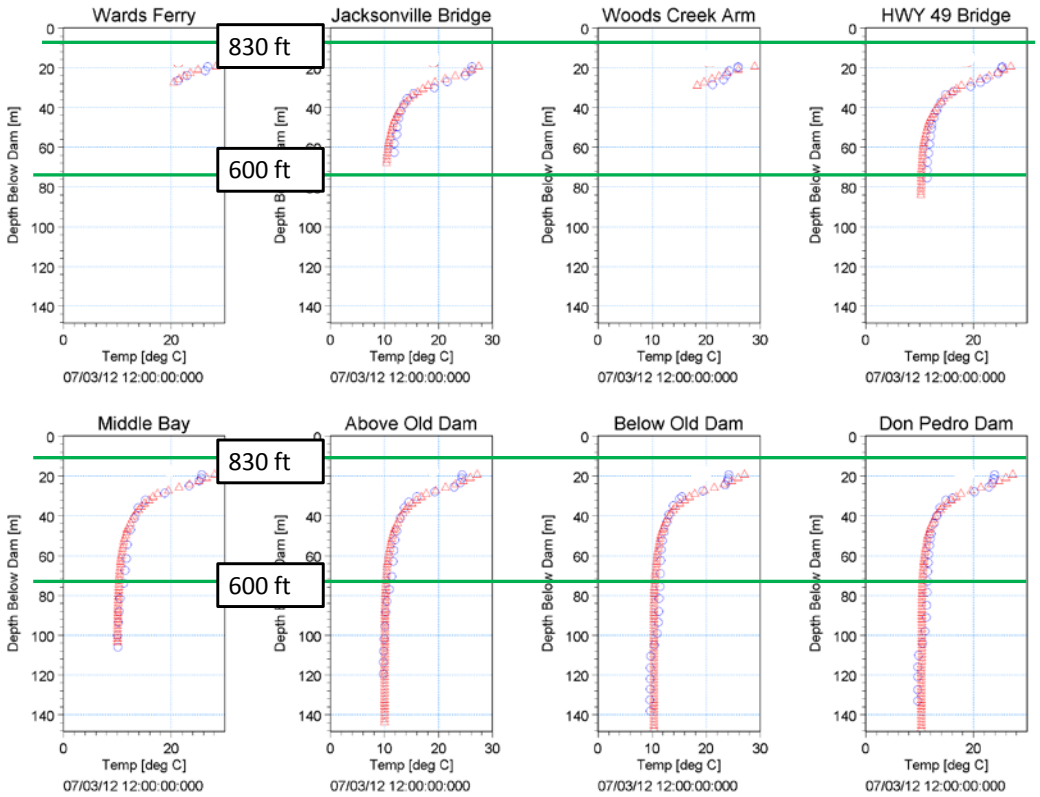

Figure 5.3-8. July 3, 2012 validation. (Observed = blue circles; Model = red triangles)

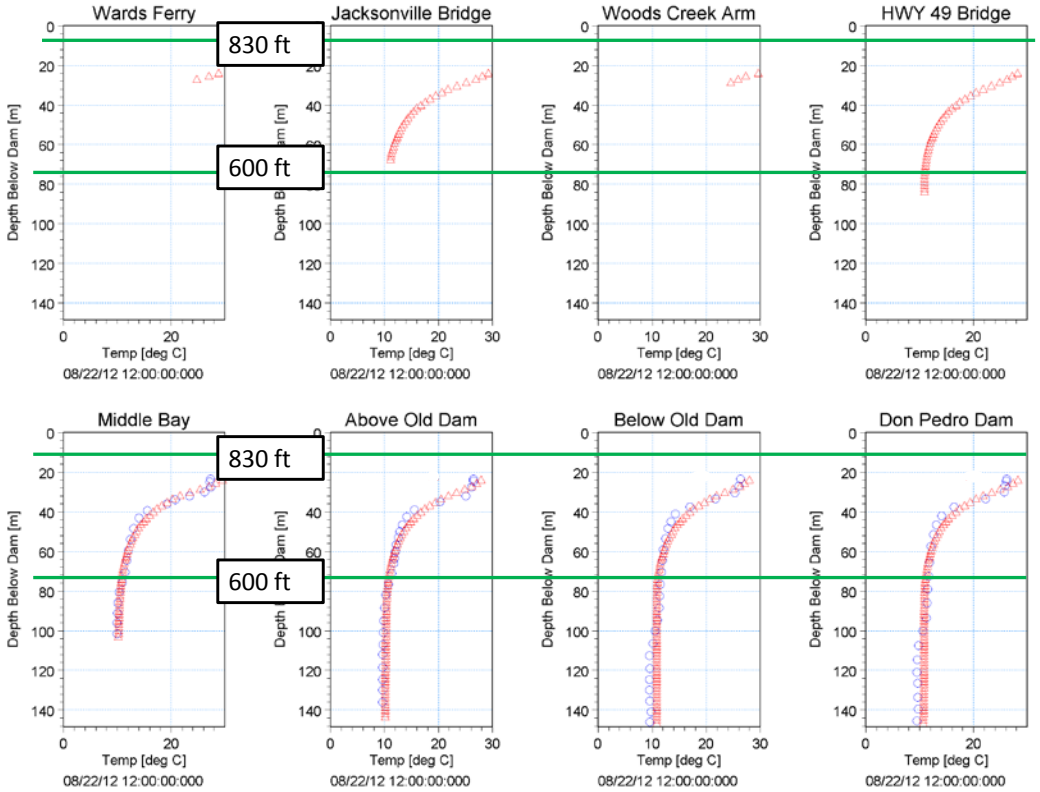

Figure 5.3-9. Aug 22, 2012 validation. (Observed = blue circles; Model = red triangles)

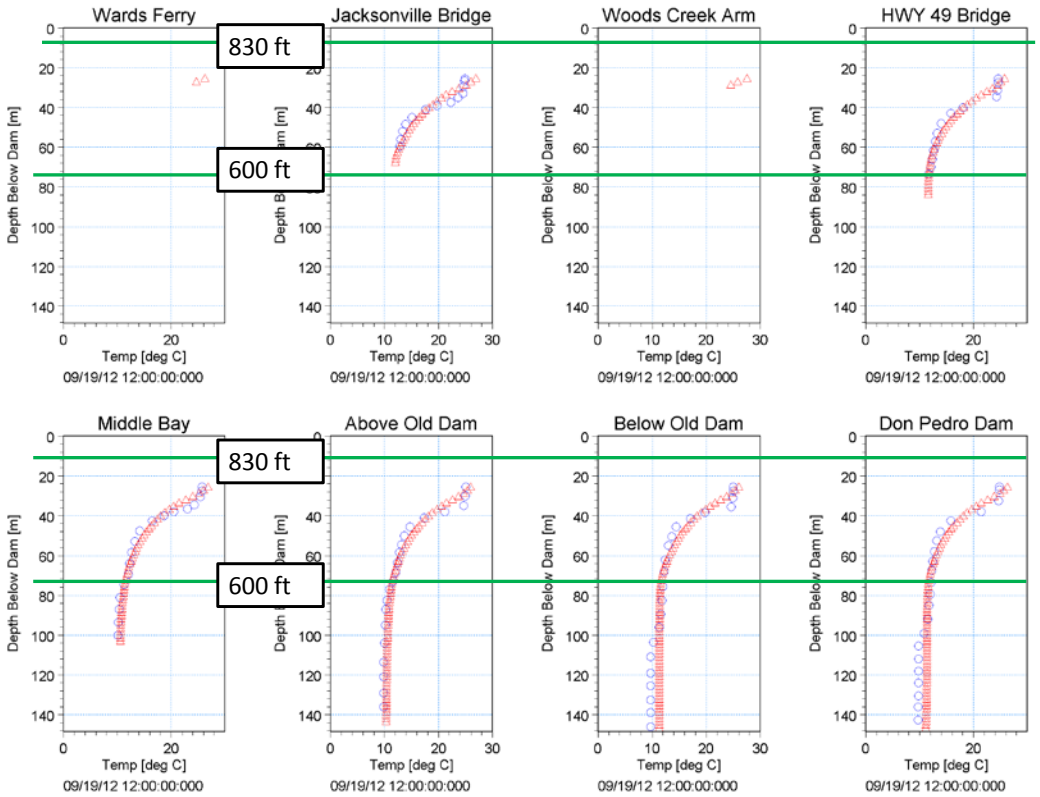

Figure 5.3-10. Sept 19, 2012 validation. (Observed = blue circles; Model = red triangles)

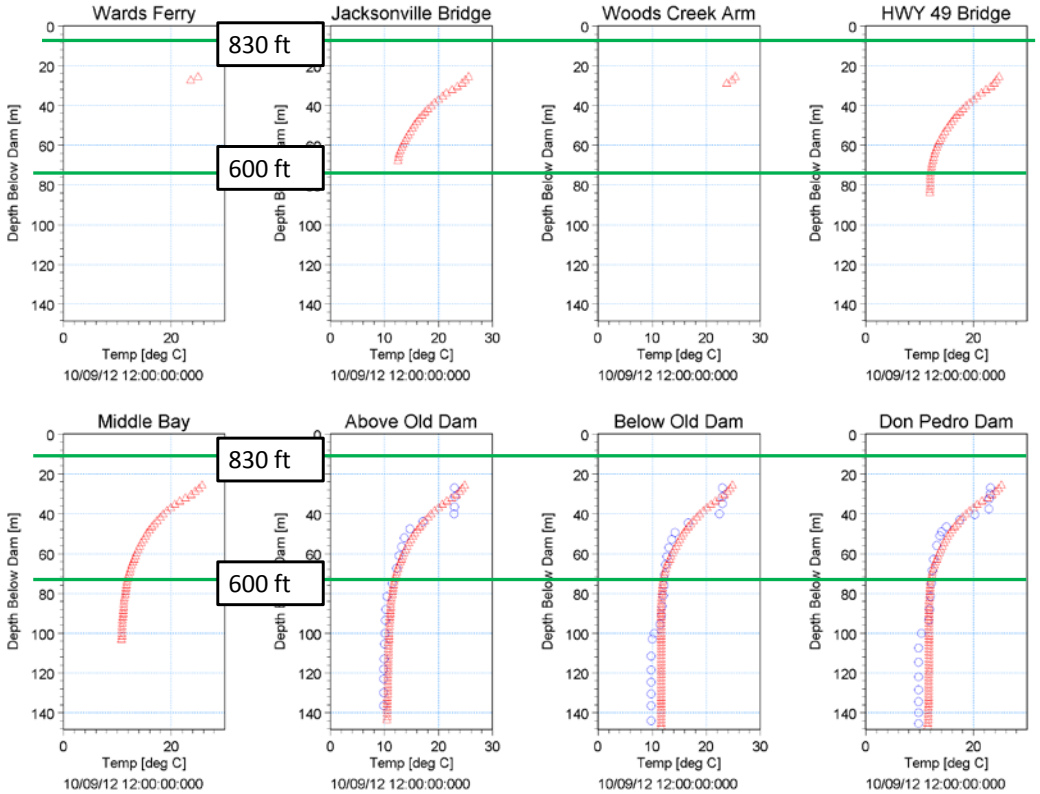

Figure 5.3-11. Oct 9, 2012 validation. (Observed = blue circles; Model = red triangles)

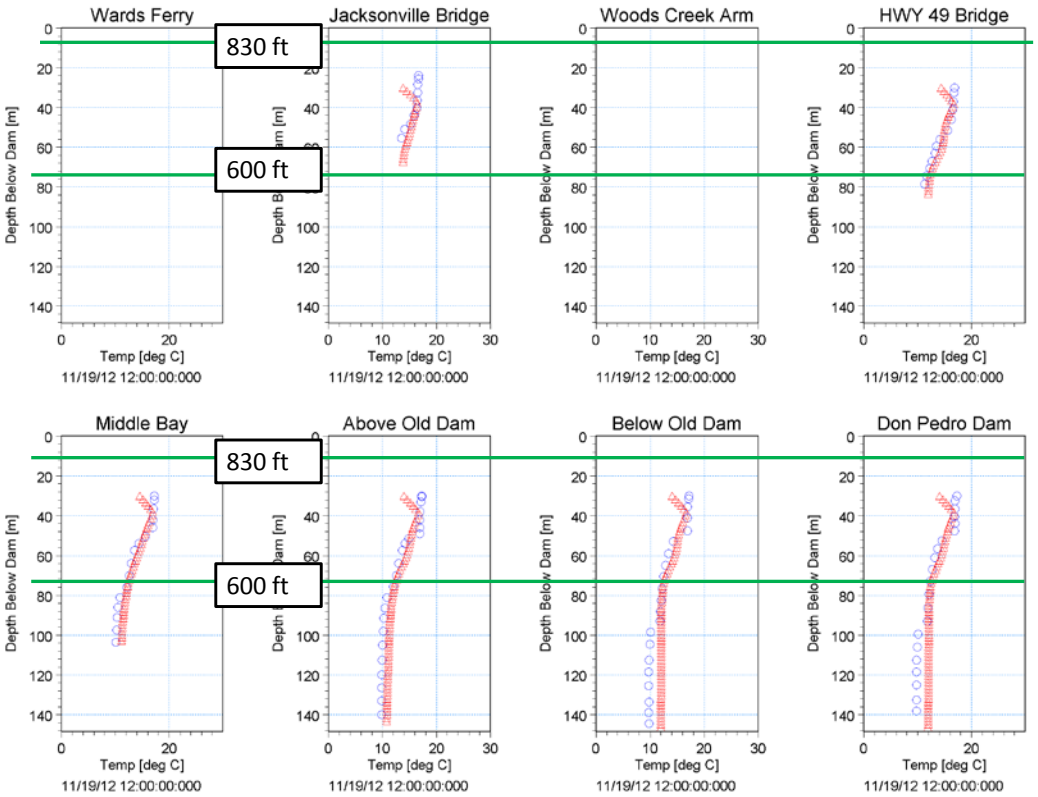

Figure 5.3-12. Nov 19, 2012 validation. (Observed = blue circles; Model = red triangles)

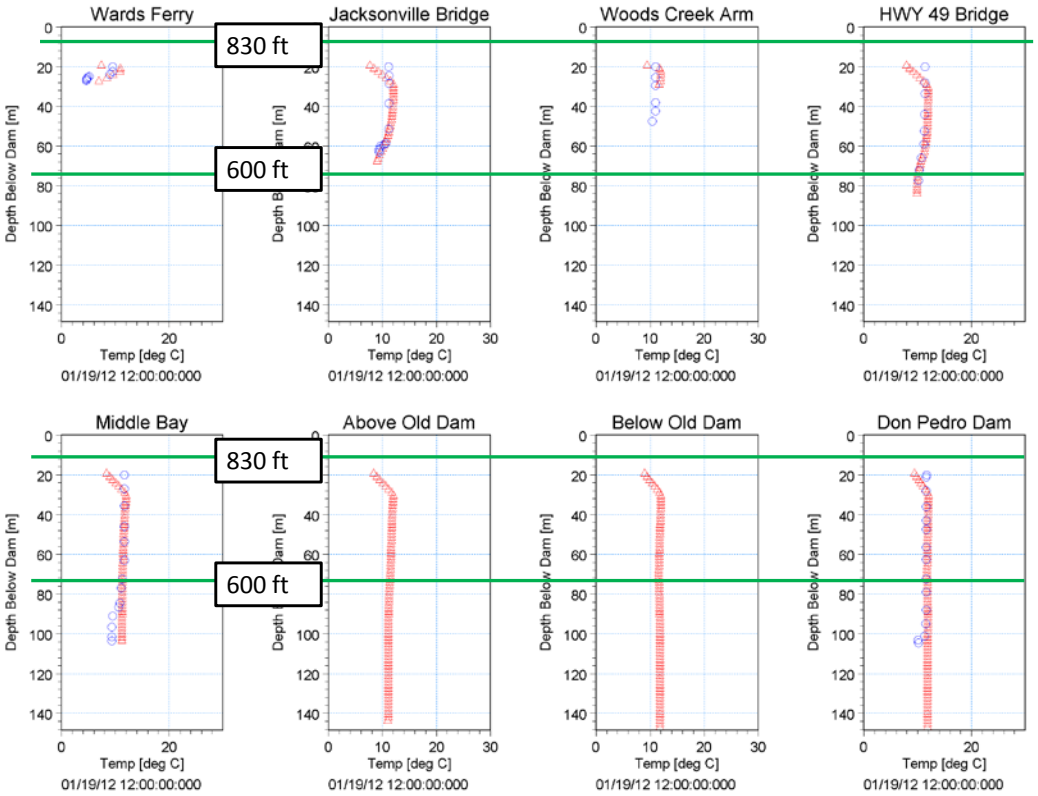

Figure 5.3-13. Jan 19, 2012 validation. (CDFW data only)

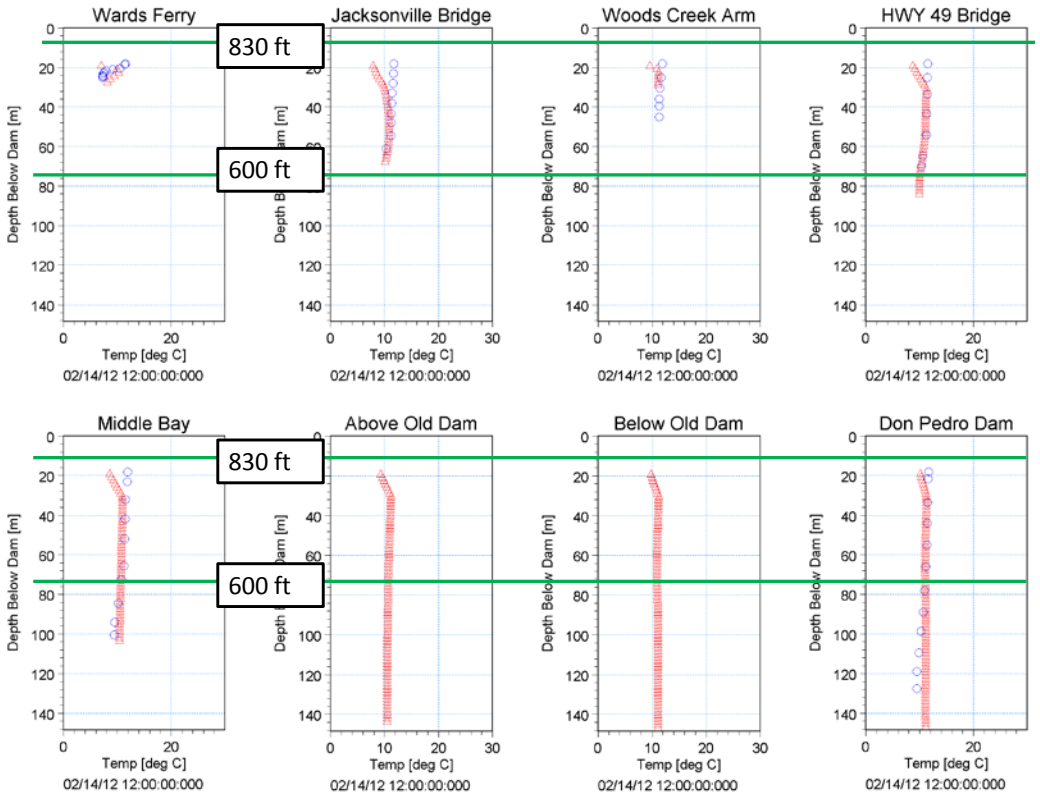

Figure 5.3-14. Feb 14, 2012 validation. (CDFW data only)

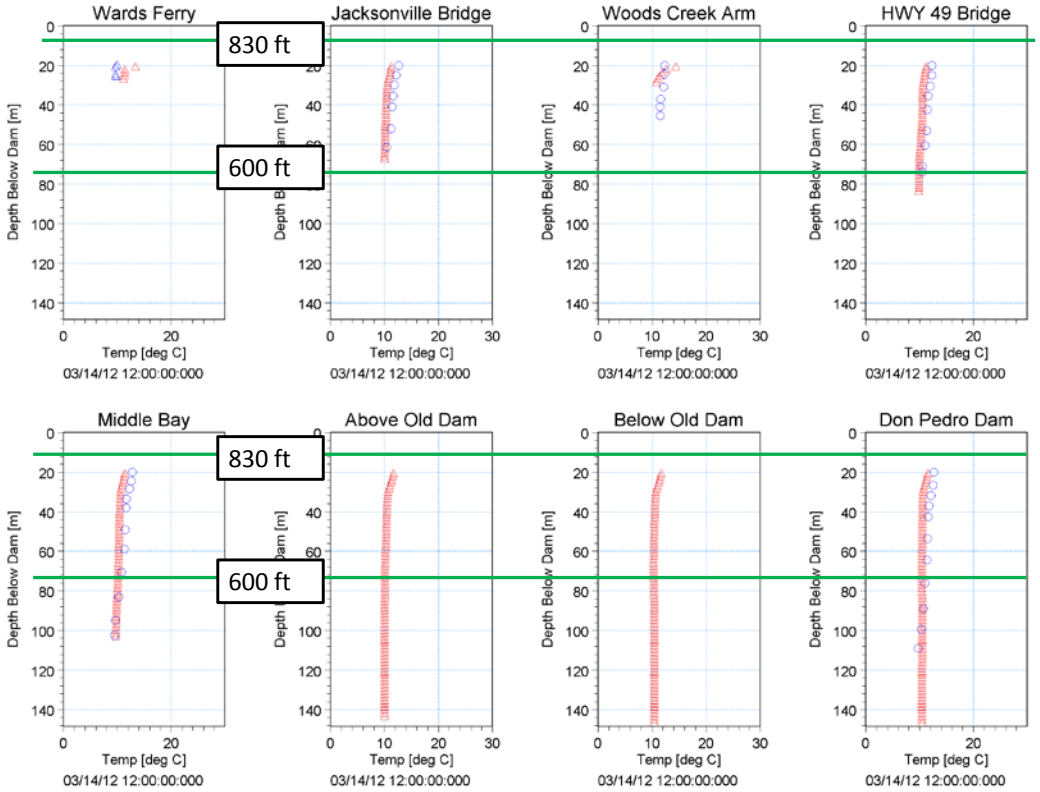

Figure 5.3-15. Mar 14, 2012 validation. (CDFW data only)

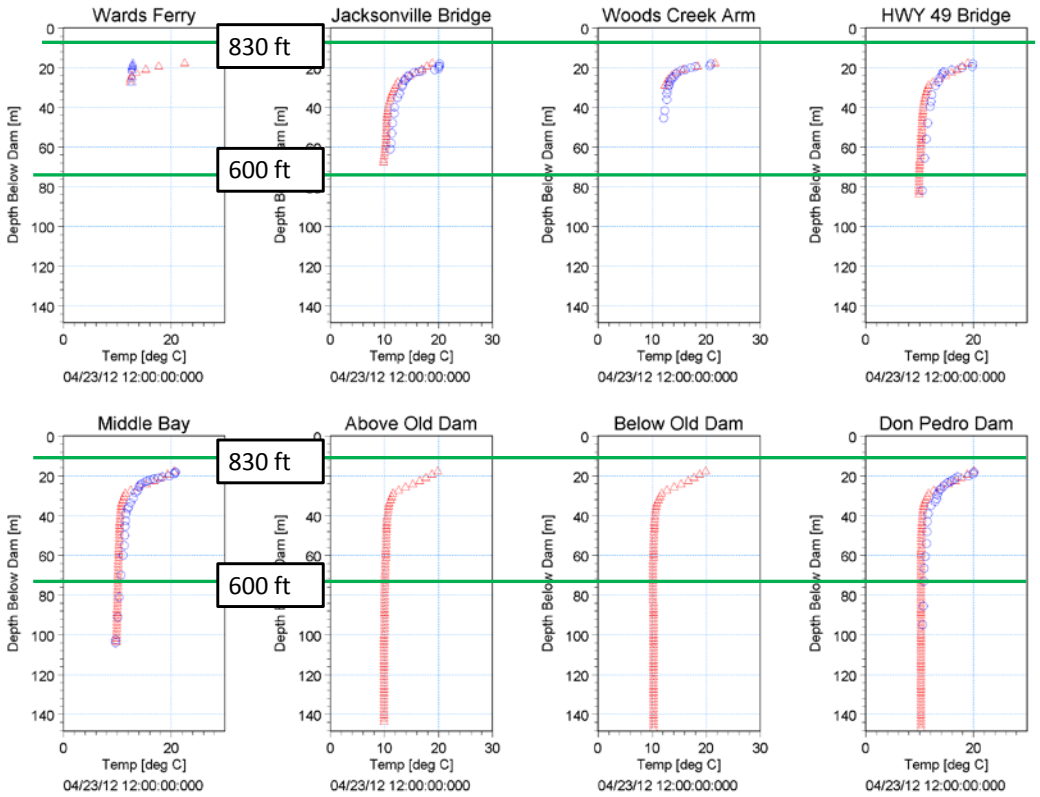

Figure 5.3-16. Apr 23, 2012 validation. (CDFW data only)

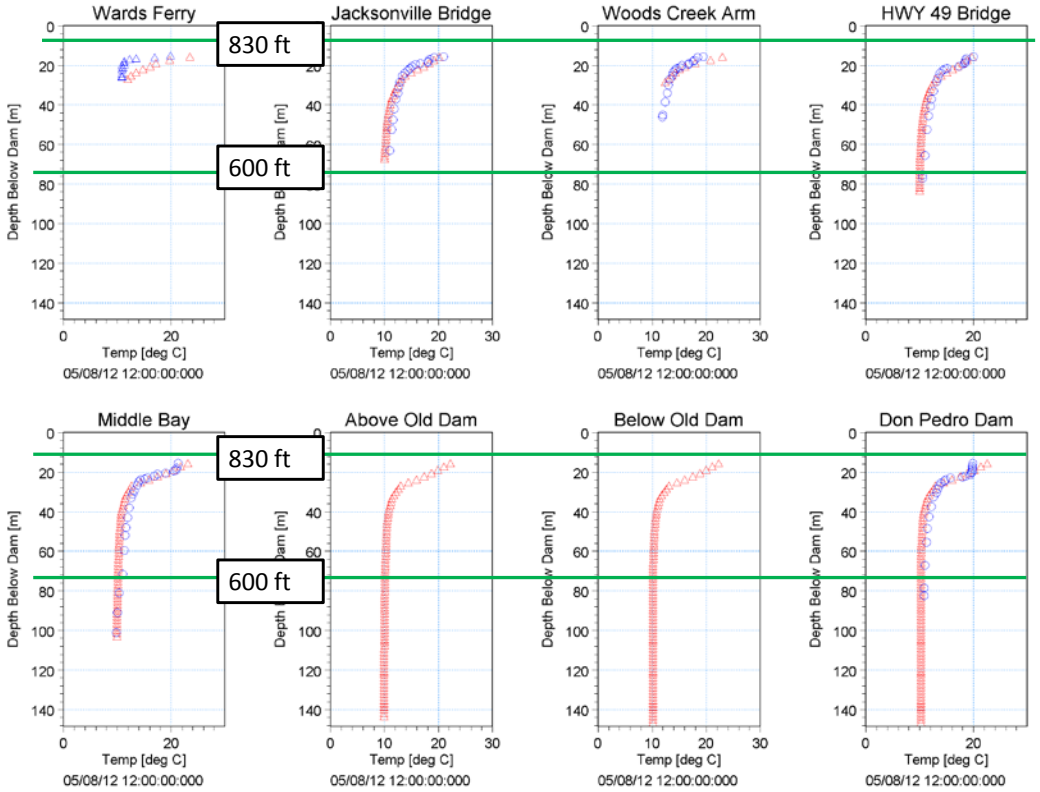

Figure 5.3-17. May 8, 2012 validation. (CDFW data only)

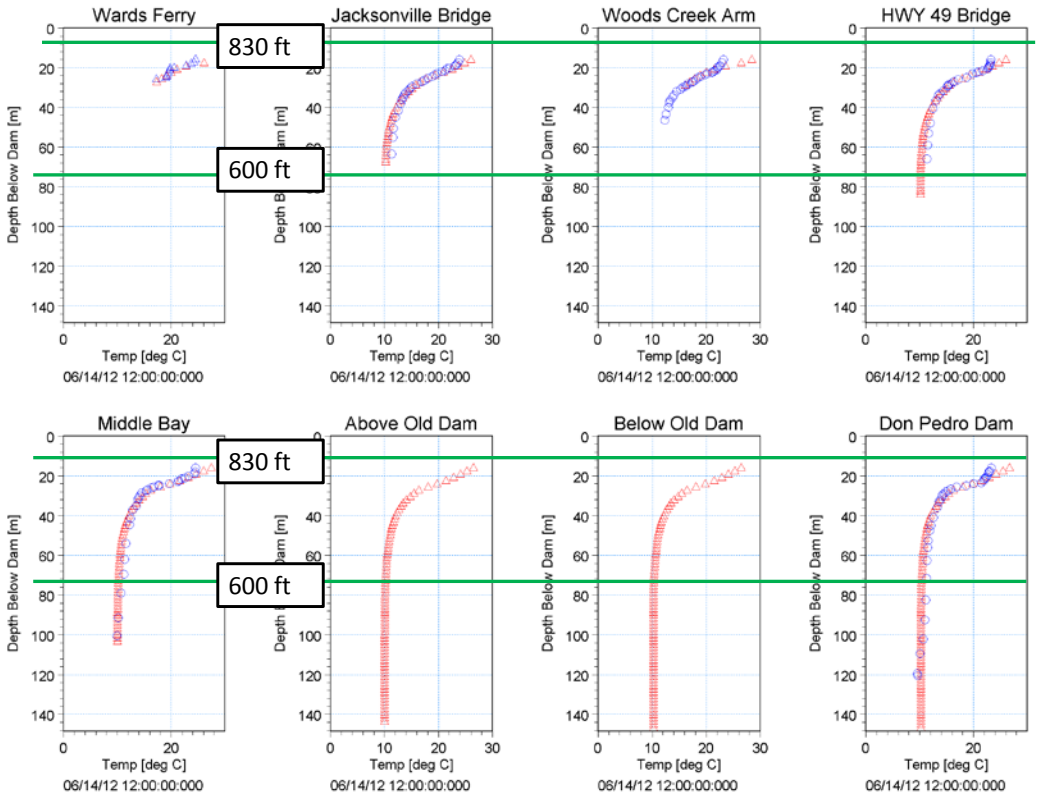

Figure 5.3-18. June 14, 2012 validation. (CDFW data only)

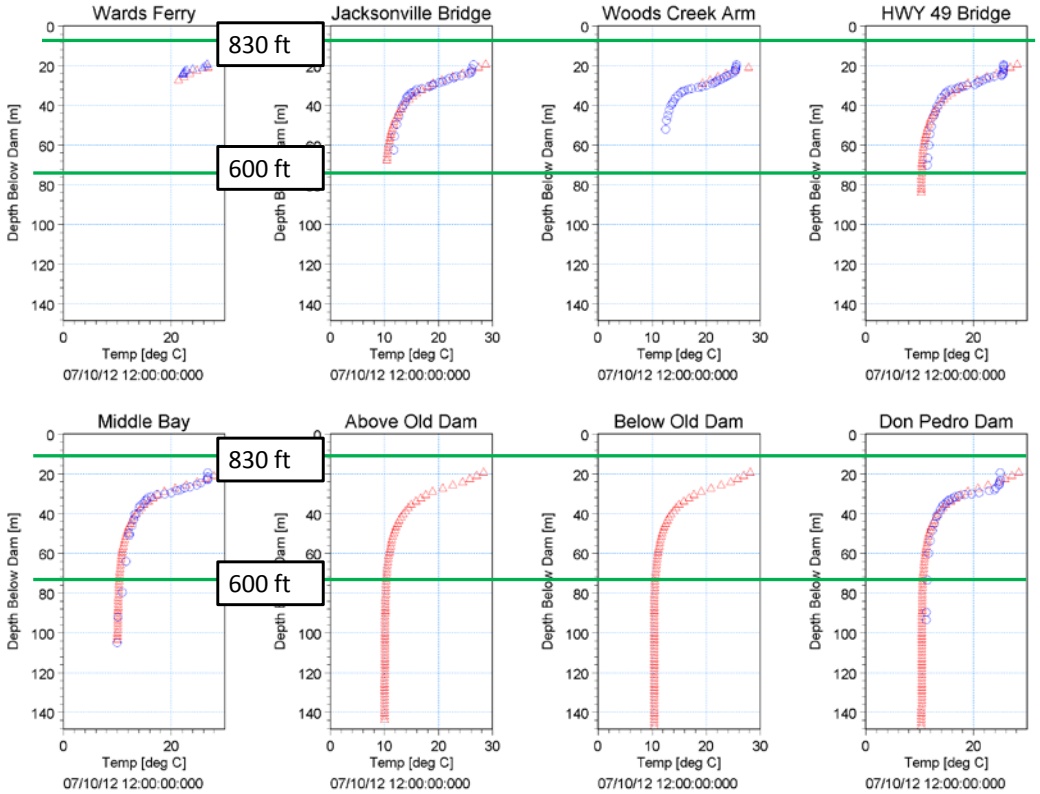

Figure 5.3-19. July 10, 2012 validation. (CDFW data only)

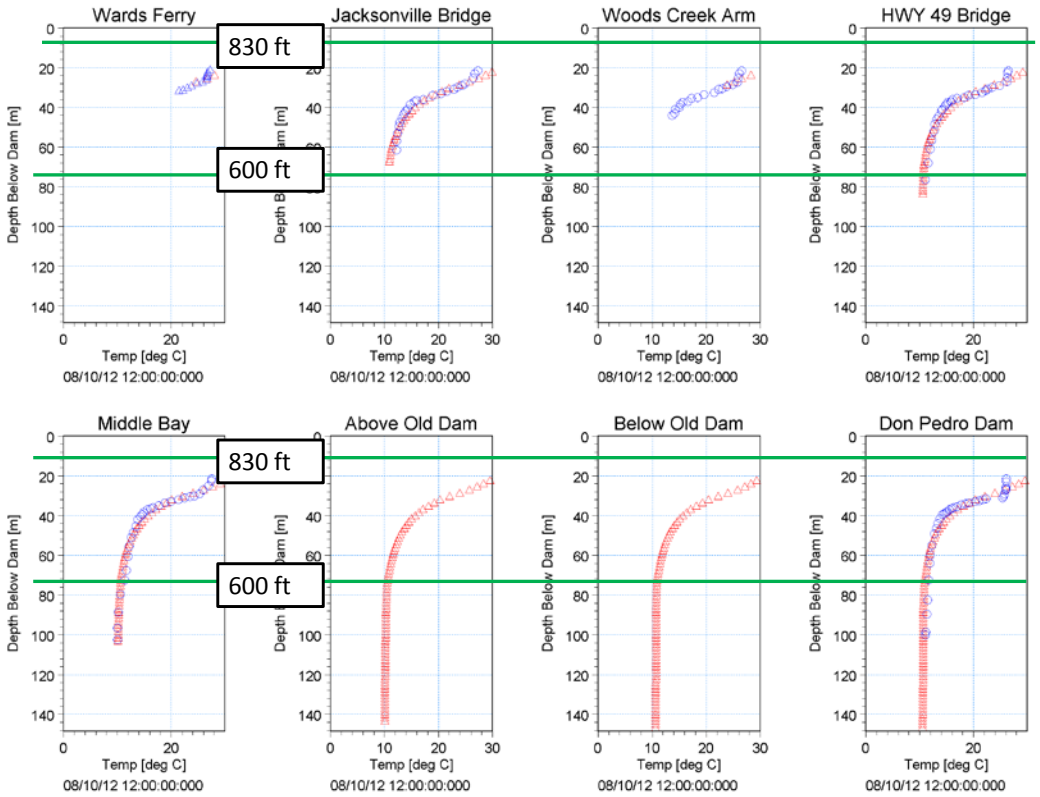

Figure 5.3-20. Aug 10, 2012 validation. (CDFW data only)

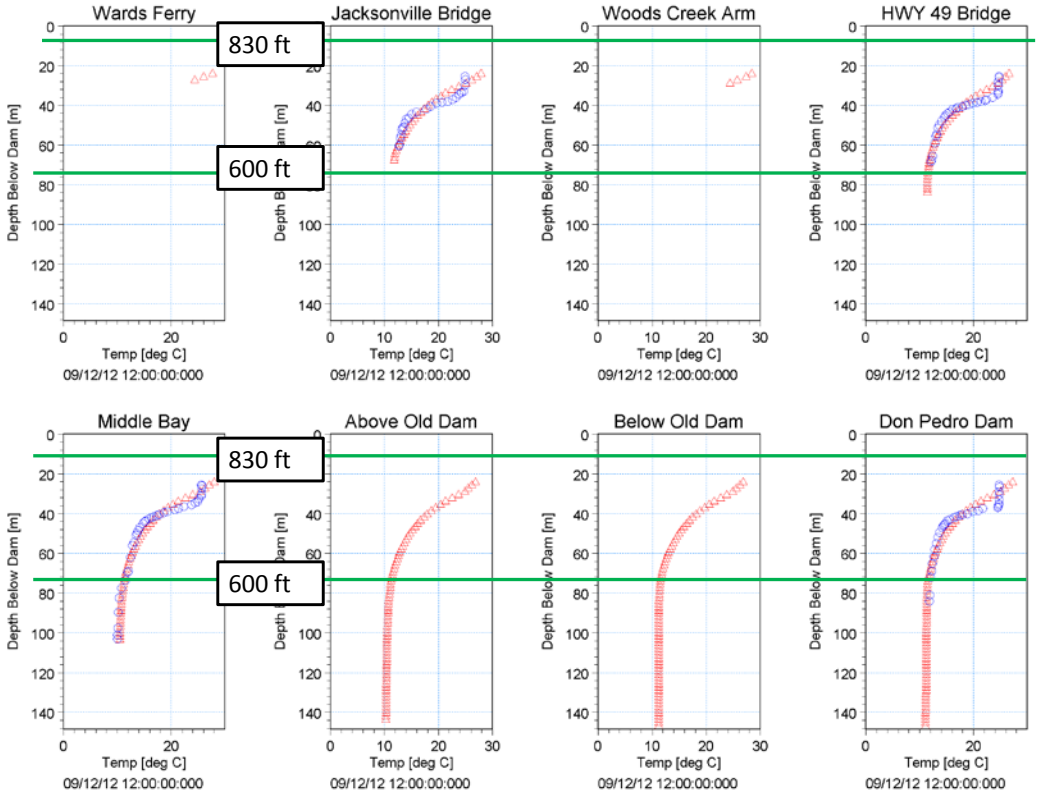

Figure 5.3-21. Sept 12, 2012 validation. (CDFW data only)

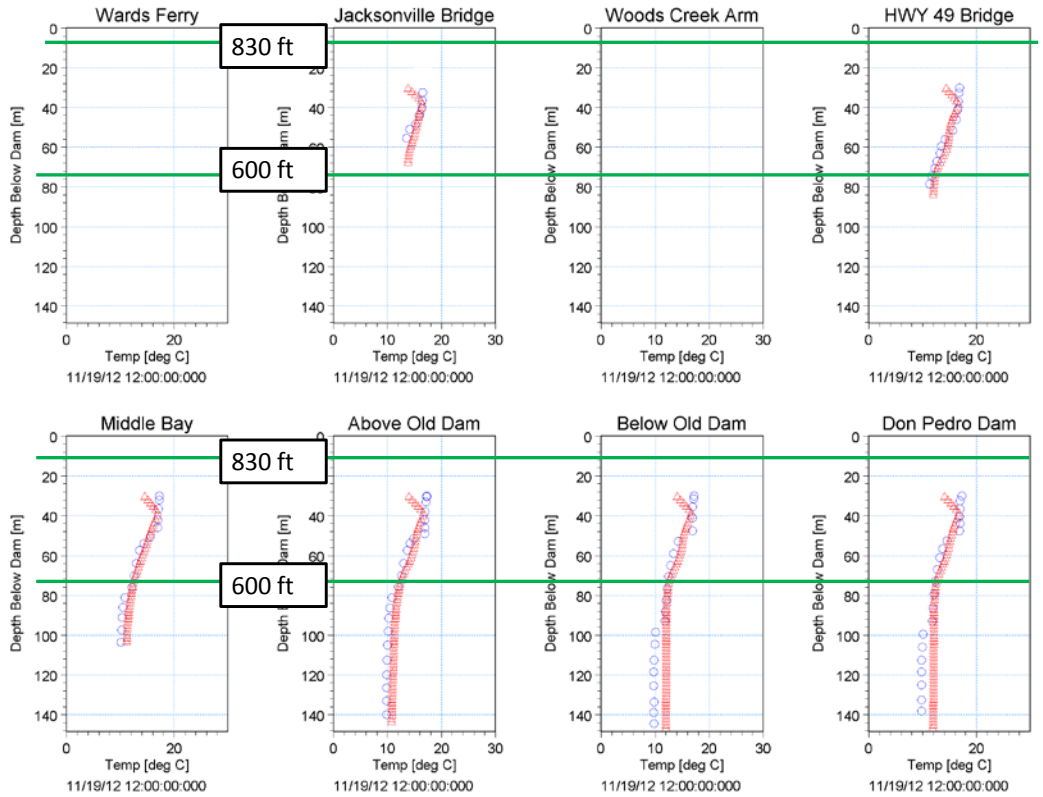

Figure 5.3-22. Oct 25, 2012 validation. (CDFW data only)

5.4 Comparison of Outflow Temperatures

The model was run continuously from January 10, 2011 to December 6, 2012. The computed and measured outflow temperatures over this period are shown in Figure 5.4-1. The model shows good agreement with the measured data, except for a brief period in November 2011 when the powerhouse experienced a forced outage and the outlet gates were used to release flows. The release from the outlet works appeared to be about 2 to 3 degrees Celsius cooler than the power tunnel at this time.

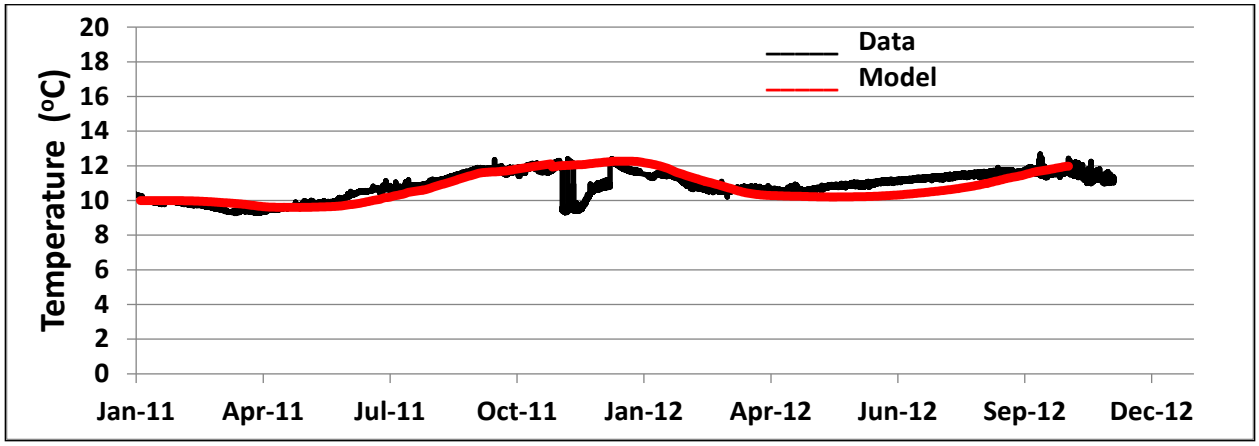

Figure 5.4-1. Measured and modeled outflow temperatures, 2011-12. (Measured = black; Modeled = red)

5.5 Comparison to Observed Surface Temperature Data

During the bathymetric surveys conducted in May and June 2011, surface temperature was recorded. This is shown in Figure 5.5-1. The data is hard to compare directly to the model output as it was collected piecemeal over a five week period (May 2 to June 2), i.e. Figure 5.5-1 represents a composite surface temperature. The model surface temperatures are shown at the beginning, middle and end of the survey time span – May 2, May 18 and June 2, 2011 (Figure 5.5-2). The figures show the model is predicting temperatures that are in the same range as those measured over the same period.

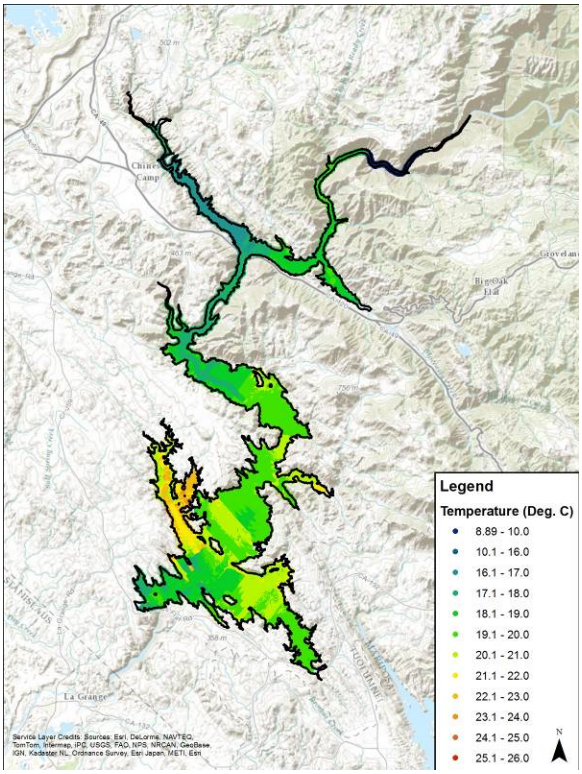

Figure 5.5-1. Measured surface temperatures May 2 – June 2, 2011.

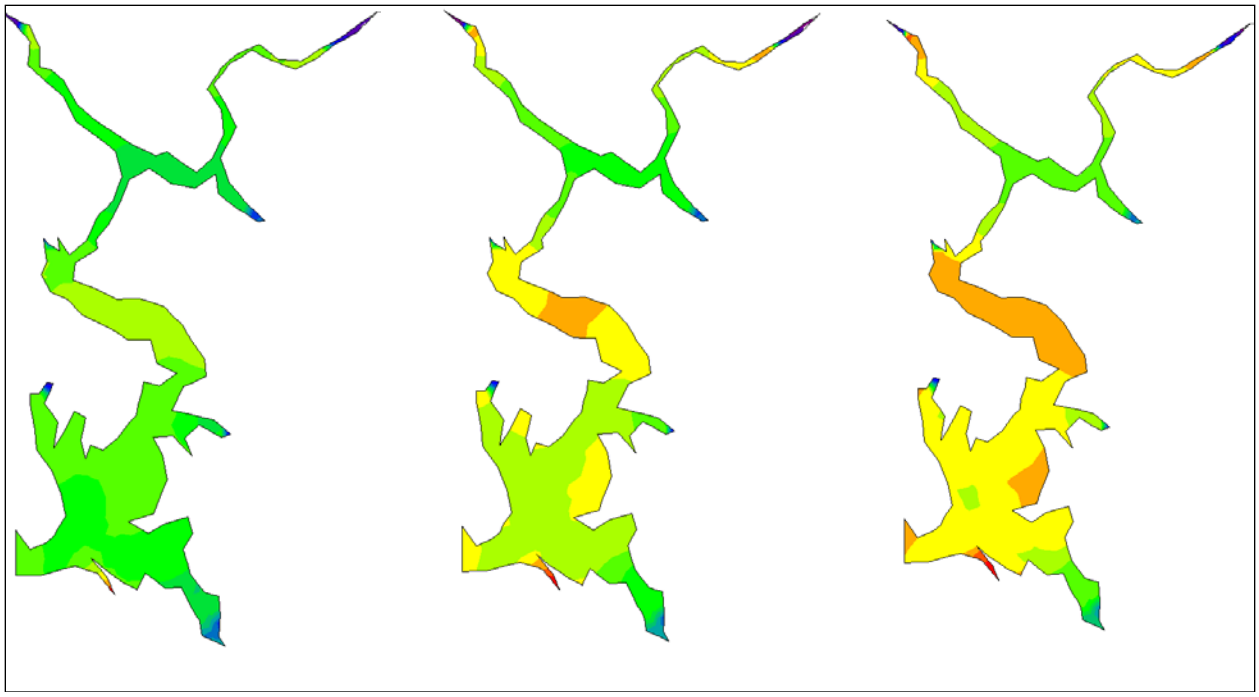

Figure 5.5-2. Modeled surface temperatures May 2, May 18 and June 2, 2011.

5.6 QA/QC Review

A review of all the model input data was performed by an engineer who had not worked on the project and was not involved in the development of the reservoir model, but who is familiar with the DHI MIKE3-FM platform. Each model input time series was compared to the original data that resided in an excel file. These were:

- Inflow
- Reservoir releases
- Inflow temperatures
- Air temperature
- Relative humidity
- Evaporation rates
- Precipitation
- Wind speed
- Wind direction

The model bathymetry was compared to the bathymetric survey data. The model parameters that are included in the master run file for the model, the m3fm file, were also checked for consistency with the values reported here. As an inherent check the parameter ranges in the MIKE model are constrained to within reasonable limits set by DHI, and will result in an error if a value outside the range is entered.

5.7 Reduced Layer Version of the Model

The model discussed above used 19 vertical layers in a combined vertical scheme. The base elevation of the ten sigma layers was 185 meters. Below this there were nine z-level layers each 10 meters deep. The model used four parameters (a_1 and b_1 in Daltons Law, β and λ in Beers Law) that varied seasonally, one set for March – October and another from November-February. Although the model gave good results there were concerns about (1) the length of run times for 40+ year scenarios (e.g. 1970 – 2012); (2) the amount of m3fm master run files that would be needed for these runs (2 per year) and (3) potential for operational scenarios that would result in drawing the reservoir down below 185 meters (~600 feet) and would require switching to a sigma only vertical mesh scheme.

To address these concerns a version of the model was made that used ten sigma layers and one set of year round parameters. This model would run faster than the 19 layer model; could run over any period of time using one m3fm file; and could run any drawdown scenario. The previously seasonal parameters were set as follows and not altered seasonally:

(1) Daltons Law (a_1 and b_1) = 2 and 2

(2) Beers Law (β and λ) = 0.6 and 1.4

The results of the ten layer, non-seasonal model are shown in Figure 5.7-1. A representative location, at Don Pedro Dam, was chosen for the vertical profile comparison. As the system now has layers approximately 14 meters thick, the surface layer reflects an average value over this depth. The results show the model still matches the measured profiles. The model surface temperatures do begin cooling earlier in the year in 2012 than the measured data indicate, with actual reservoir surface temperatures remaining very warm through October in 2012. This is a compromise associated with non-seasonal parameters.

The focus of the project, however, is the release temperatures through the powerhouse intake, located at elevation 535 feet (163 meters). The results of the model outflow temperatures are shown in Figure 5.7-2. The results show that the 10 layer model is very consistent with the results obtained from the previous 19 layer mixed vertical mesh scheme model, including seasonal parameters. Both models are able to successfully reproduce the observed reservoir outflow temperatures.

Based on the advantages of the ten layer model mentioned above, this model is preferred for running long term scenarios and deep draw down conditions.

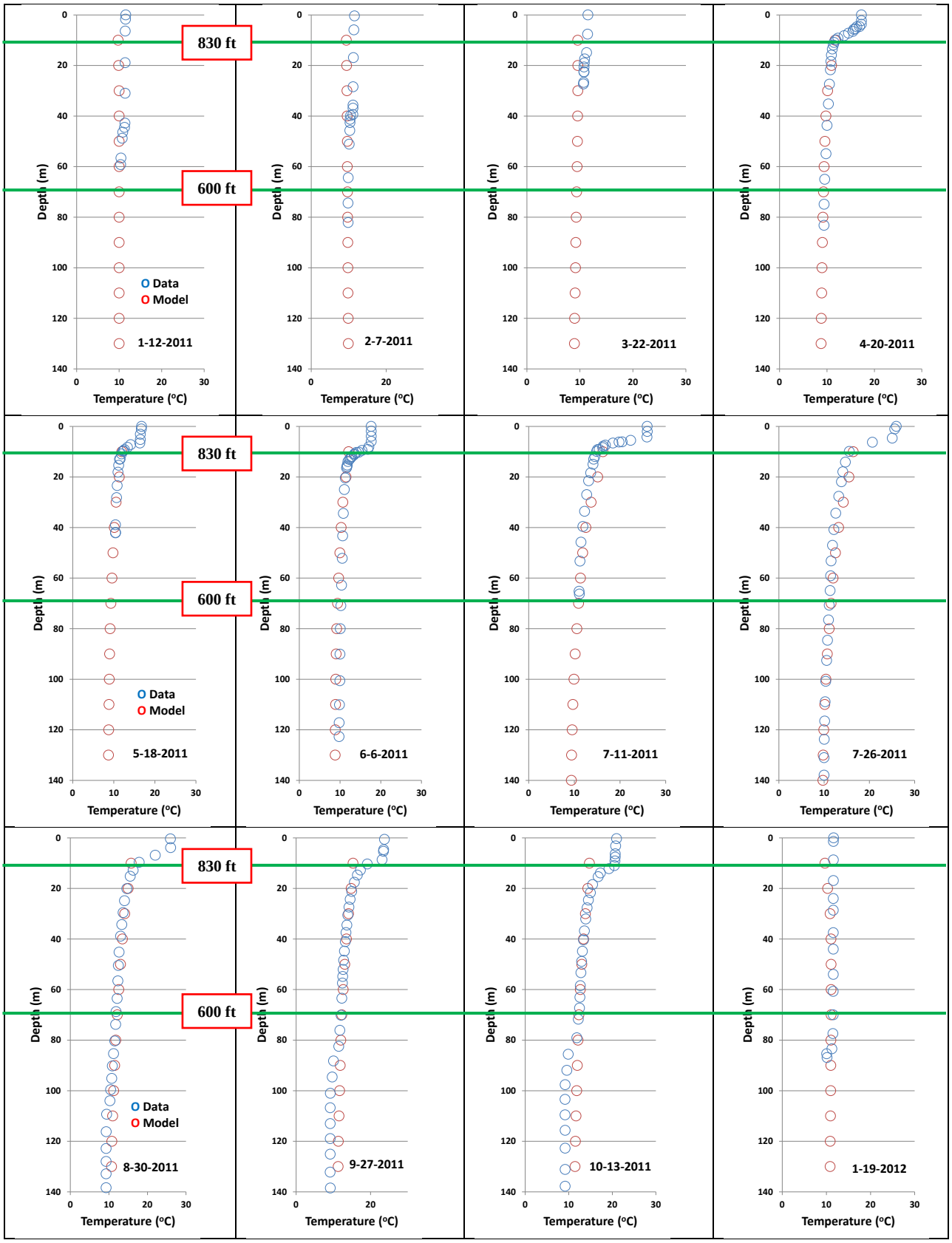
830 ft
600 ft
Depth (m)
Temperature (°C)
O Data
O Model
1-12-2011
2-7-2011
3-22-2011
4-20-2011
5-18-2011
6-6-2011
7-11-2011
7-26-2011
8-30-2011
9-27-2011
10-13-2011
1-19-2012

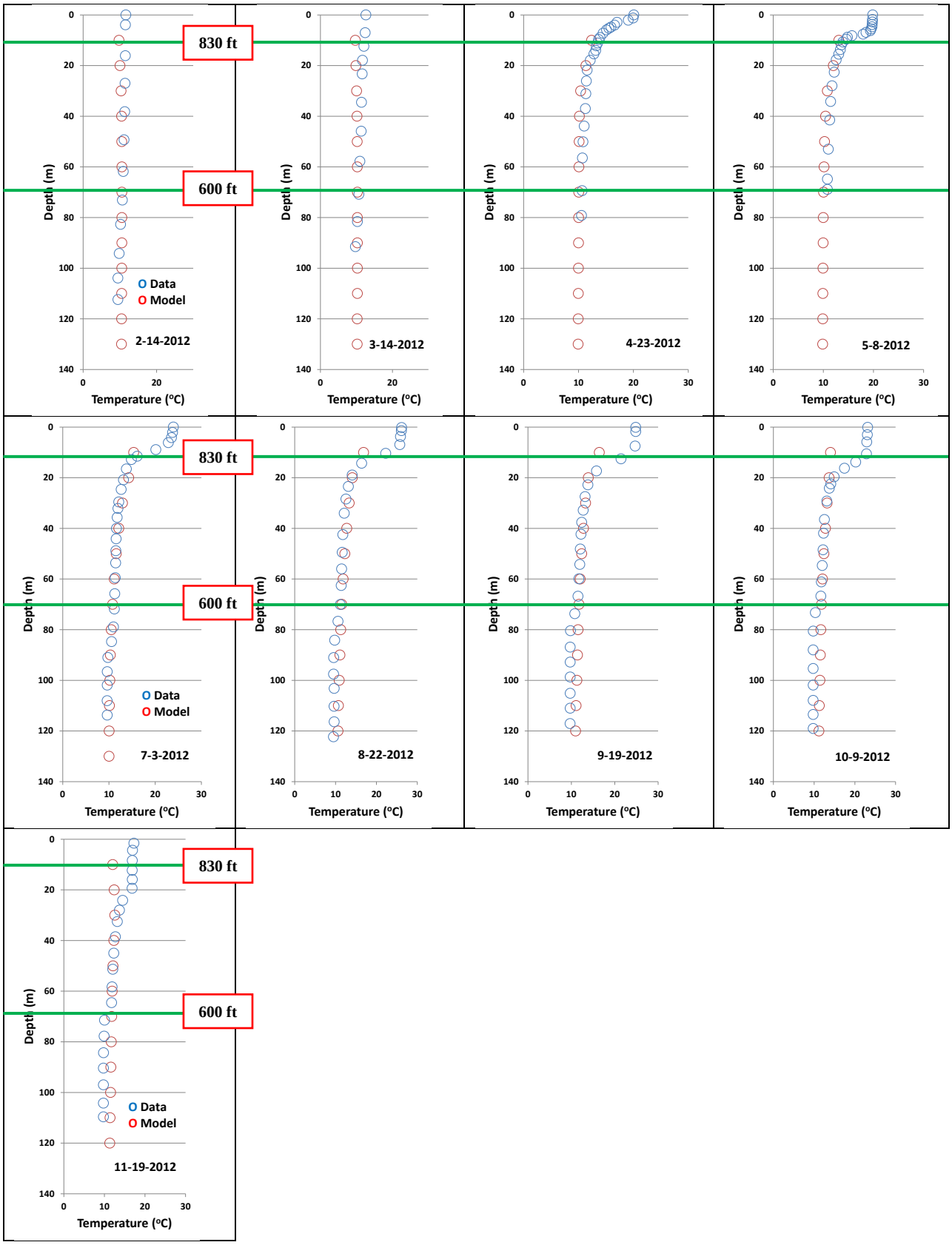

Figure 5.7-1. Measured and modeled vertical temperature profiles at Don Pedro Dam.

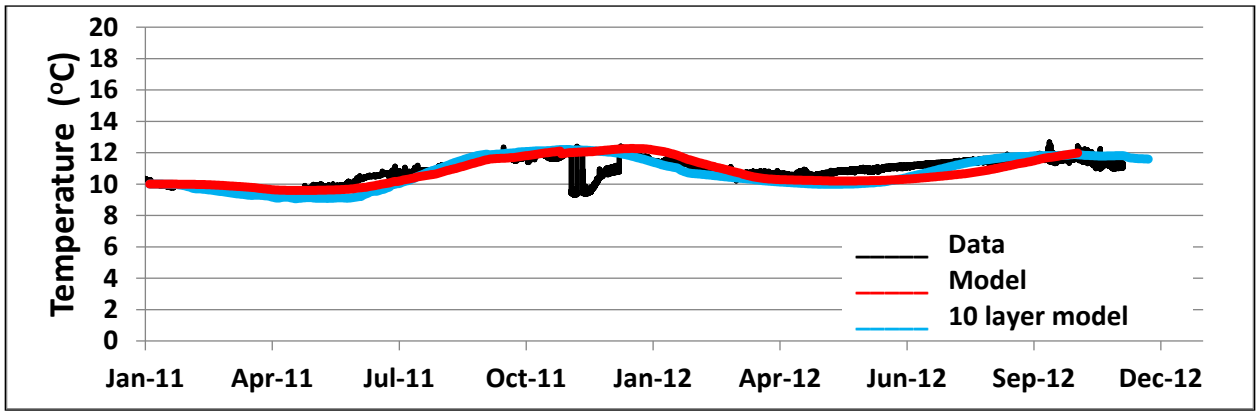

Figure 5.7-2. Don Pedro outflow temperature (2011-2012).

6.0 STUDY VARIANCES AND MODIFICATIONS

This study was conducted following the methods described in Study Plan W&AR-03 included in the Districts' Revised Study Plan filed with FERC on November 11, 2011, and approved by FERC in its Study Plan Determination on December 22, 2011. The study was performed in accordance with the FERC-approved study with three exceptions.

The FERC-approved study states that "….January to December 2008 is proposed as one of the model calibration periods." Instead of using 2008 for the calibration period, the Districts used 2011 because the modeling data set for 2008 required synthesizing several input parameters that the Districts were able to directly measure in 2011 and 2012. Hence, the Districts determined that having direct measurements during 2011and 2012 was superior to using estimated values for purposes of model calibration/validation.

The FERC-approved study calls for including the four tributary creeks where water temperature has been measured by the Districts since late April 2011 (Rough and Ready, Woods, Moccasin and Sullivan Creeks; data provided in Attachment D). Both temperature and flow information are required to incorporate the tributaries. During several monitoring periods, all three of these streams were dry. In addition, because hydrology information for the Don Pedro Reservoir Temperature Model was adopted from Tuolumne River Operations Model, (W&AR-02) tributaries could not be directly inserted into the model. The water balance approach developed for the Operations Model accounted for all flow into/out of reservoir, but did not distinguish between the main stem Tuolumne and local tributaries. Adding in the tributary sources would have resulted in double counting. In recognition that not all of the flow into the reservoir enters via the Tuolumne River, the model includes sources that correspond to some of the major tributaries. As observed, these streams contribute only minor amounts of flow, and for many periods no flow, to the reservoir.

The FERC-approved study states that "….a final report will be produced by November 30, 2012" and "the model will be available by December 2012 to evaluate alternative future reservoir operation scenarios." The selection of 2012 as the validation year impacted this schedule, as the final hydrology data set, reservoir profiles, and input temperature data were not all available until the end of February 2013. To stay reasonably on schedule, the Districts conducted an initial training session for relicensing participants in the structure, function, and use of the model on January 24, 2013. Additional training sessions were held in June 2013, and web-based access to the updated model was provided to relicensing participants at that time.

7.0 REFERENCES

AD Consultants, Resources Management Associates, Inc., and Watercourse Engineering, Inc. 2009. San Joaquin River Basin Water Temperature Modeling and Analysis, Prepared for CALFED ERP-06D-S20, October 2009

Bonnet, M.P., M Poulin and J Devaux. 2000. Numerical modeling of thermal stratification in a lake reservoir. Aquatic Sciences. Vol 62. pp 105-124.

Cole, Thomas M., and Wells S.A. 2003. CE-QUAL-W2: A Two-Dimensional, Laterally Average, Hydrodynamic and Water Quality Model, Version 3.2, User Manual. U.S. Army Corps of Engineers, Department of the Army, Washington, D.C.

Danish Hydraulic Institute (DHI). 2011. MIKE 21 and MIKE 3 Flow Model FM, Hydrodynamic and Transport Module, Scientific Documentation.

_____. 2009a. MIKE21 & MIKE3 Flow Model FM, Hydrodynamic and Flow Transport Model, Scientific Documentation, January 2009

_____. 2009b. MIKE21 & MIKE3 Flow Model FM, Hydrodynamic and Flow Transport Model, Step by step training guide, January 2009

_____. 2009c. MIKE3 Flow Model FM, Hydrodynamic Model, User's Guide, January 2009

Fischer, H. B. 1979. *Mixing in inland and coastal waters*. Academic Pr.

Kantha, L.H. and Clayson, C.A. 2000. Small Scale Processes in Geophysical Fluid Flows. International Geophysics Series. Vol 67. Academic Press.

King, I.P. 1993. RMA-10, A Finite Element Model for Three-Dimensional Density Stratified Flow. Report prepared in co-operation with Australian Water and Coastal Studies for Sydney Deepwater Outfalls Environmental Monitoring Program Post.

Maiss, M., Ilmberger, A.Z. and Munnich, K.O. 1994. A SF_6 tracer study of horizontal mixing in Lake Constance. Aquatic Sciences. Vol 56. No. 4.

Rodi W. 1984 Turbulence models and their applications in hydraulics. IAHR, Delft, The Netherlands

Smagorinky, J. 1963. General Circulation Experiments with the Primitive Equation. Monthly Weather Review Vol. 91, pp 99-164

Turlock Irrigation District and Modesto Irrigation District (TID/MID). 2011a. Pre-Application Document. Don Pedro Project. FERC No. 2299. February 2011.

_____. 2011b. Reservoir Temperature Model Study Plan (W&AR-03). Attachment to Don Pedro Hydroelectric Project Revised Study Plan. November 2011.

_____. 2011c. Bathymetry Study Plan. Attachment to Reservoir Temperature Model Study Plan (W&AR-03). Don Pedro Hydroelectric Project Revised Study Plan. November 2011.

_____. 2013a. Project Operations/Water Balance Model Study Report (W&AR-02). Attachment to Don Pedro Hydroelectric Project Initial Study Report. January 2013.

_____. 2013b. Lower Tuolumne River Temperature Progress Report (W&AR-16). Attachment to Don Pedro Hydroelectric Project Initial Study Report. January 2013.

_____. 2013c. Tuolumne River Chinook Salmon Population Model Progress Report (W&AR-06), Section 2.4.6 of the Don Pedro Hydroelectric Project Initial Study Report. January 2013.

_____. 2013d. *Oncorhynchus mykiss* Population Study Progress Report (W&AR-10), Section 2.4.10 of the Don Pedro Hydroelectric Project Initial Study Report. January 2013.

_____. 2013e. Water Quality Assessment Study Report (W&AR-01). Attachment to Don Pedro Hydroelectric Project Initial Study Report. January 2013.

STUDY REPORT W&AR-03
RESERVOIR TEMPERATURE MODEL

ATTACHMENT A

DON PEDRO RESERVOIR MODEL RECALIBRATION 2016

This Page Intentionally Left Blank

Don Pedro Reservoir Model Recalibration 2016

The Don Pedro Reservoir Model (DPRM) is a three dimensional hydrodynamic model of the reservoir based on the Danish Hydraulic Institute (DHI) MIKE platform. MIKE3 was developed by DHI as a professional engineering software package for 3-D free-surface flows (DHI 2017, available as Appendix A). The original model was developed in 2012. In 2016, the model was used by the Districts to run various reservoir operation scenarios. In the four-year interim period, DHI made an adjustment to the temperature module.

The adjustment made by DHI removed the need for the user to specify the incoming long wave radiation that is used in the temperature calculation. This is now computed internally based on the physical location of the project. Once the model input files were adjusted to the new format, the calibration period was rerun. It was found that the calibration results had changed from the original model.

Minor adjustments were made to some of the temperature constants in the model to bring the calibration back to where it was before. The resulting new calibration is shown below in Figure 1. The previous calibration is shown in Figure 2.

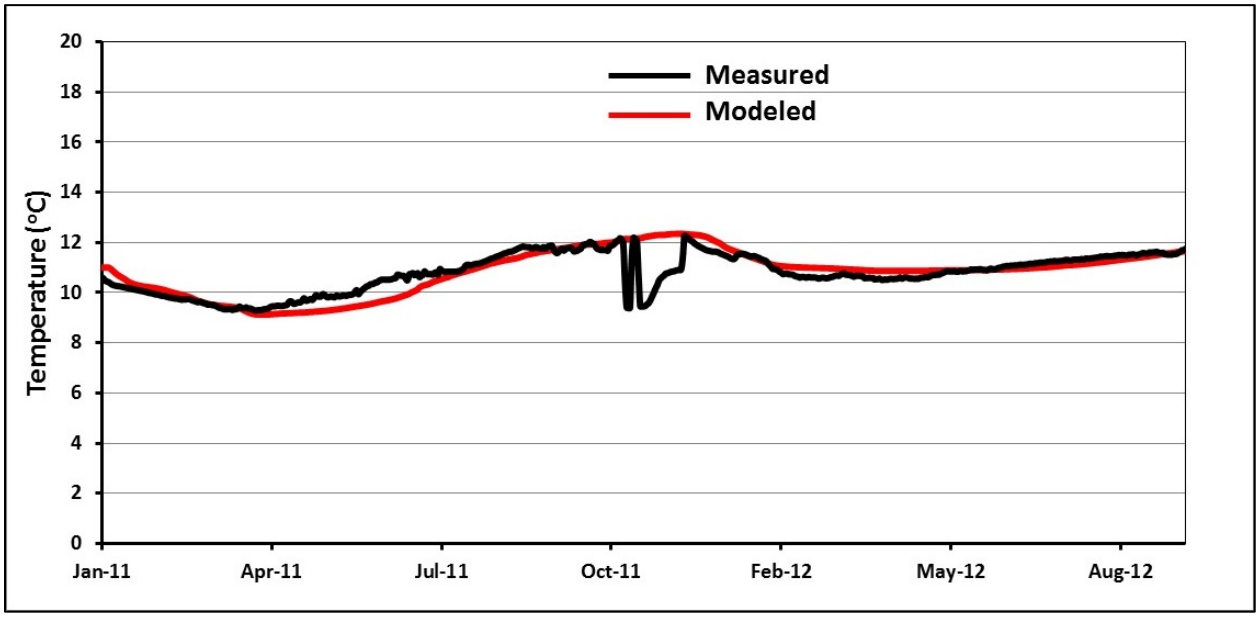

Figure 1. July 2016 Recalibration – outflow temperature at Don Pedro powerhouse.

Figure 2. Original calibration of Don Pedro powerhouse outflow temperature.

STUDY REPORT W&AR-03
RESERVOIR TEMPERATURE MODEL

APPENDIX A

MIKE3 FM SCIENTIFIC REFERENCE MANUAL 2017

This Page Intentionally Left Blank.

MIKE
Powered by DHI

MIKE 21 & MIKE 3 Flow Model FM

Hydrodynamic and Transport Module

Scientific Documentation

DHI headquarters
Agern Allé 5
DK-2970 Hørsholm
Denmark

+45 4516 9200 Telephone
+45 4516 9333 Support
+45 4516 9292 Telefax

mike@dhigroup.com
www.mikepoweredbydhi.com

MIKE
Powered by DHI

PLEASE NOTE

MIKE
Powered by DHI

CONTENTS

MIKE 21 & MIKE 3 Flow Model FM
Hydrodynamic and Transport Module
Scientific Documentation

1 Introduction 1

2 Governing Equations 2
2.1 3D Governing Equations in Cartesian Coordinates 2
2.1.1 Shallow water equations 2
2.1.2 Transport equations for salt and temperature 4
2.1.3 Transport equation for a scalar quantity 5
2.1.4 Turbulence model 5
2.1.5 Governing equations in Cartesian and sigma coordinates 8
2.2 3D Governing Equations in Spherical and Sigma Coordinates 10
2.3 2D Governing Equations in Cartesian Coordinates 12
2.3.1 Shallow water equations 12
2.3.2 Transport equations for salt and temperature 12
2.3.3 Transport equations for a scalar quantity 13
2.4 2D Governing Equations in Spherical Coordinates 13
2.5 Bottom Stress 14
2.6 Wind Stress 15
2.7 Ice Coverage 16
2.8 Tidal Potential 17
2.9 Wave Radiation 18
2.10 Heat Exchange 18
2.10.1 Vaporisation 19
2.10.2 Convection 21
2.10.3 Short wave radiation 21
2.10.4 Long wave radiation 24

3 Numerical Solution 26
3.1 Spatial Discretization 26
3.1.1 Vertical Mesh 28
3.1.2 Shallow water equations 31
3.1.3 Transport equations 34
3.2 Time Integration 35
3.3 Boundary Conditions 36
3.3.1 Closed boundaries 36
3.3.2 Open boundaries 37
3.3.3 Flooding and drying 37

4 Infiltration and Leakage 39
4.1 Net Infiltration Rates 39
4.2 Constant Infiltration with Capacity 40

5 Validation 42
5.1 Dam-break Flow through Sharp Bend 42

5.1.1 Physical experiments 42
5.1.2 Numerical experiments 43
5.1.3 Results 44

6 References 47

1 Introduction

This document presents the scientific background for the new MIKE 21 & MIKE 3 Flow Model FM[1] modelling system developed by DHI Water & Environment. The objective is to provide the user with a detailed description of the flow and transport model equations, numerical discretization and solution methods. Also model validation is discussed in this document.

The MIKE 21 & MIKE 3 Flow Model FM is based on a flexible mesh approach and it has been developed for applications within oceanographic, coastal and estuarine environments. The modelling system may also be applied for studies of overland flooding.

The system is based on the numerical solution of the two/three-dimensional incompressible Reynolds averaged Navier-Stokes equations invoking the assumptions of Boussinesq and of hydrostatic pressure. Thus, the model consists of continuity, momentum, temperature, salinity and density equations and it is closed by a turbulent closure scheme. For the 3D model the free surface is taken into account using a sigma coordinate transformation approach.

The spatial discretization of the primitive equations is performed using a cell-centred finite volume method. The spatial domain is discretized by subdivision of the continuum into non-overlapping elements/cells. In the horizontal plane an unstructured grid is used while in the vertical domain in the 3D model a structured mesh is used. In the 2D model the elements can be triangles or quadrilateral elements. In the 3D model the elements can be prisms or bricks whose horizontal faces are triangles and quadrilateral elements, respectively.

[1] Including the MIKE 21 Flow Model FM (two-dimensional flow) and MIKE 3 Flow Model FM (three-dimensional flow)

2 Governing Equations

2.1 3D Governing Equations in Cartesian Coordinates

2.1.1 Shallow water equations

The model is based on the solution of the three-dimensional incompressible Reynolds averaged Navier-Stokes equations, subject to the assumptions of Boussinesq and of hydrostatic pressure.

The local continuity equation is written as

$$\frac{\partial u}{\partial x}+\frac{\partial v}{\partial y}+\frac{\partial w}{\partial z}=S \tag{2.1}$$

and the two horizontal momentum equations for the x- and y-component, respectively

$$\frac{\partial u}{\partial t}+\frac{\partial u^2}{\partial x}+\frac{\partial vu}{\partial y}+\frac{\partial wu}{\partial z}=fv-g\frac{\partial \eta}{\partial x}-\frac{1}{\rho_0}\frac{\partial p_a}{\partial x}-\frac{g}{\rho_0}\int_z^\eta \frac{\partial \rho}{\partial x}dz-\frac{1}{\rho_0 h}\left(\frac{\partial s_{xx}}{\partial x}+\frac{\partial s_{xy}}{\partial y}\right)+F_u+\frac{\partial}{\partial z}\left(\nu_t\frac{\partial u}{\partial z}\right)+u_sS \tag{2.2}$$

$$\frac{\partial v}{\partial t}+\frac{\partial v^2}{\partial y}+\frac{\partial uv}{\partial x}+\frac{\partial wv}{\partial z}=-fu-g\frac{\partial \eta}{\partial y}-\frac{1}{\rho_0}\frac{\partial p_a}{\partial y}-\frac{g}{\rho_0}\int_z^\eta \frac{\partial \rho}{\partial y}dz-\frac{1}{\rho_0 h}\left(\frac{\partial s_{yx}}{\partial x}+\frac{\partial s_{yy}}{\partial y}\right)+F_v+\frac{\partial}{\partial z}\left(\nu_t\frac{\partial v}{\partial z}\right)+v_sS \tag{2.3}$$

where t is the time; x, y and z are the Cartesian coordinates; η is the surface elevation; d is the still water depth; $h=\eta+d$ is the total water depth; u, v and w are the velocity components in the x, y and z direction; $f=2\Omega\sin\phi$ is the Coriolis parameter (Ω is the angular rate of revolution and ϕ the geographic latitude); g is the gravitational acceleration; ρ is the density of water; s_{xx}, s_{xy}, s_{yx} and s_{yy} are components of the radiation stress tensor; ν_t is the vertical turbulent (or eddy) viscosity; p_a is the atmospheric pressure; ρ_o is the reference density of water. S is the magnitude of the discharge due to point sources and (u_s, v_s) is the velocity by which the water is discharged into the ambient water. The horizontal stress terms are described using a gradient-stress relation, which is simplified to

$$F_u=\frac{\partial}{\partial x}\left(2A\frac{\partial u}{\partial x}\right)+\frac{\partial}{\partial y}\left(A\left(\frac{\partial u}{\partial y}+\frac{\partial v}{\partial x}\right)\right) \tag{2.4}$$

$$F_v = \frac{\partial}{\partial x}\left(A\left(\frac{\partial u}{\partial y} + \frac{\partial v}{\partial x}\right)\right) + \frac{\partial}{\partial y}\left(2A\frac{\partial v}{\partial y}\right) \tag{2.5}$$

where A is the horizontal eddy viscosity.

The surface and bottom boundary condition for u, v and w are

At $z = \eta$:

$$\frac{\partial \eta}{\partial t} + u\frac{\partial \eta}{\partial x} + v\frac{\partial \eta}{\partial y} - w = 0, \quad \left(\frac{\partial u}{\partial z}, \frac{\partial v}{\partial z}\right) = \frac{1}{\rho_0 \nu_t}\left(\tau_{sx}, \tau_{sy}\right) \tag{2.6}$$

At $z = -d$:

$$u\frac{\partial d}{\partial x} + v\frac{\partial d}{\partial y} + w = 0, \quad \left(\frac{\partial u}{\partial z}, \frac{\partial v}{\partial z}\right) = \frac{1}{\rho_0 \nu_t}\left(\tau_{bx}, \tau_{by}\right) \tag{2.7}$$

where $\left(\tau_{sx}, \tau_{sy}\right)$ and $\left(\tau_{bx}, \tau_{by}\right)$ are the x and y components of the surface wind and bottom stresses.

The total water depth, h, can be obtained from the kinematic boundary condition at the surface, once the velocity field is known from the momentum and continuity equations. However, a more robust equation is obtained by vertical integration of the local continuity equation

$$\frac{\partial h}{\partial t} + \frac{\partial h\bar{u}}{\partial x} + \frac{\partial h\bar{v}}{\partial y} = hS + \hat{P} - \hat{E} \tag{2.8}$$

where $\hat{P}$ and $\hat{E}$ are precipitation and evaporation rates, respectively, and $\bar{u}$ and $\bar{v}$ are the depth-averaged velocities

$$h\bar{u} = \int_{-d}^{\eta} u\,dz, \quad h\bar{v} = \int_{-d}^{\eta} v\,dz \tag{2.9}$$

The fluid is assumed to be incompressible. Hence, the density, ρ, does not depend on the pressure, but only on the temperature, T, and the salinity, s, via the equation of state

$$\rho = \rho(T, s) \tag{2.10}$$

Here the UNESCO equation of state is used (see UNESCO, 1981).

2.1.2 Transport equations for salt and temperature

The transports of temperature, *T*, and salinity, *s*, follow the general transport-diffusion equations as

$$\frac{\partial T}{\partial t}+\frac{\partial uT}{\partial x}+\frac{\partial vT}{\partial y}+\frac{\partial wT}{\partial z}=F_T+\frac{\partial}{\partial z}\left(D_v\frac{\partial T}{\partial z}\right)+\hat{H}+T_sS \tag{2.11}$$

$$\frac{\partial s}{\partial t}+\frac{\partial us}{\partial x}+\frac{\partial vs}{\partial y}+\frac{\partial ws}{\partial z}=F_s+\frac{\partial}{\partial z}\left(D_v\frac{\partial s}{\partial z}\right)+s_sS \tag{2.12}$$

where D_v is the vertical turbulent (eddy) diffusion coefficient. $\hat{H}$ is a source term due to heat exchange with the atmosphere. T_s and s_s are the temperature and the salinity of the source. *F* are the horizontal diffusion terms defined by

$$(F_T,F_s)=\left[\frac{\partial}{\partial x}\left(D_h\frac{\partial}{\partial x}\right)+\frac{\partial}{\partial y}\left(D_h\frac{\partial}{\partial y}\right)\right](T,s) \tag{2.13}$$

where D_h is the horizontal diffusion coefficient. The diffusion coefficients can be related to the eddy viscosity

$$D_h=\frac{A}{\sigma_T}\quad\text{and}\quad D_v=\frac{\nu_t}{\sigma_T} \tag{2.14}$$

where σ_T is the Prandtl number. In many applications a constant Prandtl number can be used (see Rodi (1984)).

The surface and bottom boundary conditions for the temperature are

At $z=\eta$:

$$D_h\frac{\partial T}{\partial z}=\frac{Q_n}{\rho_0c_p}+T_p\hat{P}-T_e\hat{E} \tag{2.15}$$

At $z=-d$:

$$\frac{\partial T}{\partial z}=0 \tag{2.16}$$

where Q_n is the surface net heat flux and $c_p=4217\ J/(kg\cdot°K)$ is the specific heat of the water. A detailed description for determination of $\hat{H}$ and Q_n is given in Section 2.10.

The surface and bottom boundary conditions for the salinity are

At $z = \eta$:

$$\frac{\partial s}{\partial z} = 0 \tag{2.17}$$

At $z = -d$:

$$\frac{\partial s}{\partial z} = 0 \tag{2.18}$$

When heat exchange from the atmosphere is included, the evaporation is defined as

$$\hat{E} = \begin{cases} \dfrac{q_v}{\rho_0 l_v} & q_v > 0 \\ 0 & q_v \le 0 \end{cases} \tag{2.19}$$

where q_v is the latent heat flux and $l_v = 2.5 \cdot 10^6$ is the latent heat of vaporisation of water.

2.1.3 Transport equation for a scalar quantity

The conservation equation for a scalar quantity is given by

$$\frac{\partial C}{\partial t} + \frac{\partial uC}{\partial x} + \frac{\partial vC}{\partial y} + \frac{\partial wC}{\partial z} = F_C + \frac{\partial}{\partial z}\left(D_v \frac{\partial C}{\partial z}\right) - k_p C + C_s S \tag{2.20}$$

where C is the concentration of the scalar quantity, k_p is the linear decay rate of the scalar quantity, C_s is the concentration of the scalar quantity at the source and D_v is the vertical diffusion coefficient. F_C is the horizontal diffusion term defined by

$$F_C = \left[\frac{\partial}{\partial x}\left(D_h \frac{\partial}{\partial x}\right) + \frac{\partial}{\partial y}\left(D_h \frac{\partial}{\partial y}\right)\right] C \tag{2.21}$$

where D_h is the horizontal diffusion coefficient.

2.1.4 Turbulence model

The turbulence is modelled using an eddy viscosity concept. The eddy viscosity is often described separately for the vertical and the horizontal transport. Here several turbulence models can be applied: a constant viscosity, a vertically parabolic viscosity and a standard k-ε model (Rodi, 1984). In many numerical simulations the small-scale turbulence cannot be resolved with the chosen spatial resolution. This kind of turbulence can be approximated using sub-grid scale models.

Vertical eddy viscosity

The eddy viscosity derived from the log-law is calculated by

$$\nu_t = U_\tau h\left(c_1\frac{z+d}{h}+c_2\left(\frac{z+d}{h}\right)^2\right) \tag{2.22}$$

where $U_\tau = \max(U_{\tau s}, U_{\tau b})$ and c_1 and c_2 are two constants. $U_{\tau s}$ and $U_{\tau b}$ are the friction velocities associated with the surface and bottom stresses, $c_1 = 0.41$ and $c_2 = -0.41$ give the standard parabolic profile.

In applications with stratification the effects of buoyancy can be included explicitly. This is done through the introduction of a Richardson number dependent damping of the eddy viscosity coefficient, when a stable stratification occurs. The damping is a generalisation of the Munk-Anderson formulation (Munk and Anderson, 1948)

$$\nu_t = \nu_t^*(1+aRi)^{-b} \tag{2.23}$$

where ν_t^* is the undamped eddy viscosity and *Ri* is the local gradient Richardson number

$$Ri = -\frac{g}{\rho_0}\frac{\partial\rho}{\partial z}\left(\left(\frac{\partial u}{\partial z}\right)^2+\left(\frac{\partial v}{\partial z}\right)^2\right)^{-1} \tag{2.24}$$

$a = 10$ and $b = 0.5$ are empirical constants.

In the k-ε model the eddy-viscosity is derived from turbulence parameters *k* and ε as

$$\nu_t = c_\mu\frac{k^2}{\varepsilon} \tag{2.25}$$

where *k* is the turbulent kinetic energy per unit mass (TKE), ε is the dissipation of TKE and c_μ is an empirical constant.

The turbulent kinetic energy, *k*, and the dissipation of TKE, ε, are obtained from the following transport equations

$$\frac{\partial k}{\partial t}+\frac{\partial uk}{\partial x}+\frac{\partial vk}{\partial y}+\frac{\partial wk}{\partial z} = F_k+\frac{\partial}{\partial z}\left(\frac{\nu_t}{\sigma_k}\frac{\partial k}{\partial z}\right)+P+B-\varepsilon \tag{2.26}$$

$$\frac{\partial\varepsilon}{\partial t}+\frac{\partial u\varepsilon}{\partial x}+\frac{\partial v\varepsilon}{\partial y}+\frac{\partial w\varepsilon}{\partial z} = F_\varepsilon+\frac{\partial}{\partial z}\left(\frac{\nu_t}{\sigma_\varepsilon}\frac{\partial\varepsilon}{\partial z}\right)+\frac{\varepsilon}{k}\left(c_{1\varepsilon}P+c_{3\varepsilon}B-c_{2\varepsilon}\varepsilon\right) \tag{2.27}$$

where the shear production, *P*, and the buoyancy production, *B*, are given as

$$P = \frac{\tau_{xz}}{\rho_0}\frac{\partial u}{\partial z} + \frac{\tau_{yz}}{\rho_0}\frac{\partial v}{\partial z} \approx \nu_t\left(\left(\frac{\partial u}{\partial z}\right)^2 + \left(\frac{\partial v}{\partial z}\right)^2\right) \tag{2.28}$$

$$B = -\frac{\nu_t}{\sigma_t}N^2 \tag{2.29}$$

with the Brunt-Väisälä frequency, *N*, defined by

$$N^2 = -\frac{g}{\rho_0}\frac{\partial \rho}{\partial z} \tag{2.30}$$

σ_t is the turbulent Prandtl number and σ_k, σ_ε, $c_{1\varepsilon}$, $c_{2\varepsilon}$ and $c_{3\varepsilon}$ are empirical constants. *F* are the horizontal diffusion terms defined by

$$(F_k, F_\varepsilon) = \left[\frac{\partial}{\partial x}\left(D_h\frac{\partial}{\partial x}\right) + \frac{\partial}{\partial y}\left(D_h\frac{\partial}{\partial y}\right)\right](k, \varepsilon) \tag{2.31}$$

The horizontal diffusion coefficients are given by $D_h = A/\sigma_k$ and $D_h = A/\sigma_\varepsilon$, respectively.

Several carefully calibrated empirical coefficients enter the k-e turbulence model. The empirical constants are listed in (2.47) (see Rodi, 1984).

Table 2.1 Empirical constants in the k-ε model.

c_μ	$c_{1\varepsilon}$	$c_{2\varepsilon}$	$c_{3\varepsilon}$	σ_t	σ_k	σ_ε
0.09	1.44	1.92	0	0.9	1.0	1.3

At the surface the boundary conditions for the turbulent kinetic energy and its rate of dissipation depend on the wind shear, $U_{\tau s}$

At $z = \eta$:

$$k = \frac{1}{\sqrt{c_\mu}}U_{\tau s}^2 \tag{2.32}$$

$$\varepsilon = \frac{U_{\tau s}^3}{\kappa \Delta z_b} \qquad \text{for} \quad U_{\tau s} > 0$$

$$\frac{\partial k}{\partial z} = 0 \qquad \varepsilon = \frac{\left(k\sqrt{c_\mu}\right)^{3/2}}{a\kappa h} \qquad \text{for} \quad U_{\tau s} = 0 \tag{2.33}$$

where κ =0.4 is the von Kármán constant, $a = 0.07$ is and empirical constant and Δz_s is the distance from the surface where the boundary condition is imposed. At the seabed the boundary conditions are

At $z = -d$:

$$k = \frac{1}{\sqrt{c_\mu}} U_{\tau b}^2 \qquad \varepsilon = \frac{U_{\tau b}^3}{\kappa \Delta z_b} \tag{2.34}$$

where Δz_b is the distance from the bottom where the boundary condition is imposed.

Horizontal eddy viscosity

In many applications a constant eddy viscosity can be used for the horizontal eddy viscosity. Alternatively, Smagorinsky (1963) proposed to express sub-grid scale transports by an effective eddy viscosity related to a characteristic length scale. The subgrid scale eddy viscosity is given by

$$A = c_s^2 l^2 \sqrt{2 S_{ij} S_{ij}} \tag{2.35}$$

where c_s is a constant, l is a characteristic length and the deformation rate is given by

$$S_{ij} = \frac{1}{2}\left(\frac{\partial u_i}{\partial x_j} + \frac{\partial u_j}{\partial x_i} \right) \quad (i, j = 1,2) \tag{2.36}$$

2.1.5 Governing equations in Cartesian and sigma coordinates

The equations are solved using a vertical σ-transformation

$$\sigma = \frac{z - z_b}{h}, \quad x' = x, \quad y' = y \tag{2.37}$$

where σ varies between 0 at the bottom and 1 at the surface. The coordinate transformation implies relations such as

$$\frac{\partial}{\partial z} = \frac{1}{h}\frac{\partial}{\partial \sigma} \tag{2.38}$$

$$\left(\frac{\partial}{\partial x}, \frac{\partial}{\partial y} \right) = \left(\frac{\partial}{\partial x'} - \frac{1}{h}\left(-\frac{\partial d}{\partial x} + \sigma \frac{\partial h}{\partial x} \right) \frac{\partial}{\partial \sigma}, \frac{\partial}{\partial y'} - \frac{1}{h}\left(-\frac{\partial d}{\partial y} + \sigma \frac{\partial h}{\partial y} \right) \frac{\partial}{\partial \sigma} \right) \tag{2.39}$$

In this new coordinate system the governing equations are given as

$$\frac{\partial h}{\partial t} + \frac{\partial hu}{\partial x'} + \frac{\partial hv}{\partial y'} + \frac{\partial h\omega}{\partial \sigma} = hS \tag{2.40}$$

$$\frac{\partial hu}{\partial t}+\frac{\partial hu^2}{\partial x'}+\frac{\partial hvu}{\partial y'}+\frac{\partial h\omega u}{\partial \sigma}=fvh-gh\frac{\partial \eta}{\partial x'}-\frac{h}{\rho_0}\frac{\partial p_a}{\partial x'}-\frac{hg}{\rho_0}\int_z^\eta \frac{\partial \rho}{\partial x}dz-\frac{1}{\rho_0}\left(\frac{\partial s_{xx}}{\partial x}+\frac{\partial s_{xy}}{\partial y}\right)+hF_u+\frac{\partial}{\partial \sigma}\left(\frac{\nu_v}{h}\frac{\partial u}{\partial \sigma}\right)+hu_sS \tag{2.41}$$

$$\frac{\partial hv}{\partial t}+\frac{\partial huv}{\partial x'}+\frac{\partial hv^2}{\partial y'}+\frac{\partial h\omega v}{\partial \sigma}=-fuh-gh\frac{\partial \eta}{\partial y'}-\frac{h}{\rho_0}\frac{\partial p_a}{\partial y'}-\frac{hg}{\rho_0}\int_z^\eta \frac{\partial \rho}{\partial y}dz-\frac{1}{\rho_0}\left(\frac{\partial s_{yx}}{\partial x}+\frac{\partial s_{yy}}{\partial y}\right)+hF_v+\frac{\partial}{\partial \sigma}\left(\frac{\nu_v}{h}\frac{\partial v}{\partial \sigma}\right)+hv_sS \tag{2.42}$$

$$\frac{\partial hT}{\partial t}+\frac{\partial huT}{\partial x'}+\frac{\partial hvT}{\partial y'}+\frac{\partial h\omega T}{\partial \sigma}=hF_T+\frac{\partial}{\partial \sigma}\left(\frac{D_v}{h}\frac{\partial T}{\partial \sigma}\right)+h\hat{H}+hT_sS \tag{2.43}$$

$$\frac{\partial hs}{\partial t}+\frac{\partial hus}{\partial x'}+\frac{\partial hvs}{\partial y'}+\frac{\partial h\omega s}{\partial \sigma}=hF_s+\frac{\partial}{\partial \sigma}\left(\frac{D_v}{h}\frac{\partial s}{\partial \sigma}\right)+hs_sS \tag{2.44}$$

$$\frac{\partial hk}{\partial t}+\frac{\partial huk}{\partial x'}+\frac{\partial hvk}{\partial y'}+\frac{\partial h\omega k}{\partial \sigma}=hF_k+\frac{1}{h}\frac{\partial}{\partial \sigma}\left(\frac{\nu_t}{\sigma_k}\frac{\partial k}{\partial \sigma}\right)+h(P+B-\varepsilon) \tag{2.45}$$

$$\frac{\partial h\varepsilon}{\partial t}+\frac{\partial hu\varepsilon}{\partial x'}+\frac{\partial hv\varepsilon}{\partial y'}+\frac{\partial h\omega\varepsilon}{\partial \sigma}=hF_\varepsilon+\frac{1}{h}\frac{\partial}{\partial \sigma}\left(\frac{\nu_t}{\sigma_\varepsilon}\frac{\partial \varepsilon}{\partial \sigma}\right)+h\frac{\varepsilon}{k}\left(c_{1\varepsilon}P+c_{3\varepsilon}B-c_{2\varepsilon}\varepsilon\right) \tag{2.46}$$

$$\frac{\partial hC}{\partial t}+\frac{\partial huC}{\partial x'}+\frac{\partial hvC}{\partial y'}+\frac{\partial h\omega C}{\partial \sigma}=hF_C+\frac{\partial}{\partial \sigma}\left(\frac{D_v}{h}\frac{\partial C}{\partial \sigma}\right)-hk_pC+hC_sS \tag{2.47}$$

The modified vertical velocity is defined by

$$\omega=\frac{1}{h}\left[w+u\frac{\partial d}{\partial x'}+v\frac{\partial d}{\partial y'}-\sigma\left(\frac{\partial h}{\partial t}+u\frac{\partial h}{\partial x'}+v\frac{\partial h}{\partial y'}\right)\right] \tag{2.48}$$

The modified vertical velocity is the velocity across a level of constant σ. The horizontal diffusion terms are defined as

$$hF_u\approx\frac{\partial}{\partial x}\left(2hA\frac{\partial u}{\partial x}\right)+\frac{\partial}{\partial y}\left(hA\left(\frac{\partial u}{\partial y}+\frac{\partial v}{\partial x}\right)\right) \tag{2.49}$$

$$hF_v\approx\frac{\partial}{\partial x}\left(hA\left(\frac{\partial u}{\partial y}+\frac{\partial v}{\partial x}\right)\right)+\frac{\partial}{\partial y}\left(2hA\frac{\partial v}{\partial y}\right) \tag{2.50}$$

$$h(F_T,F_s,F_k,F_\varepsilon,F_c) \approx \left[\frac{\partial}{\partial x}\left(hD_h\frac{\partial}{\partial x}\right)+\frac{\partial}{\partial y}\left(hD_h\frac{\partial}{\partial y}\right)\right](T,s,k,\varepsilon,C) \tag{2.51}$$

The boundary condition at the free surface and at the bottom are given as follows

At σ=1:

$$\omega = 0, \quad \left(\frac{\partial u}{\partial \sigma},\frac{\partial v}{\partial \sigma}\right)=\frac{h}{\rho_0 \nu_t}\left(\tau_{sx},\tau_{sy}\right) \tag{2.52}$$

At σ=0:

$$\omega = 0, \quad \left(\frac{\partial u}{\partial \sigma},\frac{\partial v}{\partial \sigma}\right)=\frac{h}{\rho_0 \nu_t}\left(\tau_{bx},\tau_{by}\right) \tag{2.53}$$

The equation for determination of the water depth is not changed by the coordinate transformation. Hence, it is identical to Eq. (2.6).

2.2 3D Governing Equations in Spherical and Sigma Coordinates

In spherical coordinates the independent variables are the longitude, λ , and the latitude, ϕ . The horizontal velocity field (u,v) is defined by

$$u = R\cos\phi\frac{d\lambda}{dt} \qquad v = R\frac{d\phi}{dt} \tag{2.54}$$

where R is the radius of the earth.

In this coordinate system the governing equations are given as (all superscripts indicating the horizontal coordinate in the new coordinate system are dropped in the following for notational convenience)

$$\frac{\partial h}{\partial t}+\frac{1}{R\cos\phi}\left(\frac{\partial hu}{\partial \lambda}+\frac{\partial hv\cos\phi}{\partial \phi}\right)+\frac{\partial h\omega}{\partial \sigma}=hS \tag{2.55}$$

$$\begin{aligned}\frac{\partial hu}{\partial t}+\frac{1}{R\cos\phi}\left(\frac{\partial hu^2}{\partial \lambda}+\frac{\partial hvu\cos\phi}{\partial \phi}\right)+\frac{\partial h\omega u}{\partial \sigma}&=\left(f+\frac{u}{R}\tan\phi\right)vh-\\ \frac{1}{R\cos\phi}\left(gh\frac{\partial \eta}{\partial \lambda}+\frac{1}{\rho_0}\frac{\partial p_a}{\partial \lambda}+\frac{g}{\rho_0}\int_z^\eta\frac{\partial \rho}{\partial \lambda}dz+\frac{1}{\rho_0}\left(\frac{\partial s_{xx}}{\partial \lambda}+\cos\phi\frac{\partial s_{xy}}{\partial \phi}\right)\right)+&\\ hF_u+\frac{\partial}{\partial \sigma}\left(\frac{\nu_v}{h}\frac{\partial u}{\partial \sigma}\right)+hu_sS&\end{aligned} \tag{2.56}$$

$$\frac{\partial hv}{\partial t}+\frac{1}{R\cos\phi}\left(\frac{\partial huv}{\partial\lambda}+\frac{\partial hv^2\cos\phi}{\partial\phi}\right)+\frac{\partial h\omega v}{\partial\sigma}=-\left(f+\frac{u}{R}\tan\phi\right)uh-$$
$$\frac{1}{R}\left(gh\frac{\partial\eta}{\partial\phi}+\frac{1}{\rho_0}\frac{\partial p_a}{\partial\phi}+\frac{g}{\rho_0}\int_z^\eta\frac{\partial\rho}{\partial\phi}dz+\frac{1}{\rho_0}\left(\frac{1}{\cos\phi}\frac{\partial s_{yx}}{\partial\lambda}+\frac{\partial s_{yy}}{\partial\phi}\right)\right)+ \quad (2.57)$$
$$hF_v+\frac{\partial}{\partial\sigma}\left(\frac{\nu_v}{h}\frac{\partial v}{\partial\sigma}\right)+hv_sS$$

$$\frac{\partial hT}{\partial t}+\frac{1}{R\cos\phi}\left(\frac{\partial huT}{\partial\lambda}+\frac{\partial hvT\cos\phi}{\partial\phi}\right)+\frac{\partial h\omega T}{\partial\sigma}= \quad (2.58)$$
$$hF_T+\frac{\partial}{\partial\sigma}\left(\frac{D_v}{h}\frac{\partial T}{\partial\sigma}\right)+h\bar{H}+hT_sS$$

$$\frac{\partial hs}{\partial t}+\frac{1}{R\cos\phi}\left(\frac{\partial hus}{\partial\lambda}+\frac{\partial hvs\cos\phi}{\partial\phi}\right)+\frac{\partial h\omega s}{\partial\sigma}= \quad (2.59)$$
$$hF_s+\frac{\partial}{\partial\sigma}\left(\frac{D_v}{h}\frac{\partial s}{\partial\sigma}\right)+hs_sS$$

$$\frac{\partial hk}{\partial t}+\frac{1}{R\cos\phi}\left(\frac{\partial huk}{\partial\lambda}+\frac{\partial hvk\cos\phi}{\partial\phi}\right)+\frac{\partial h\omega k}{\partial\sigma}= \quad (2.60)$$
$$hF_k+\frac{1}{h}\frac{\partial}{\partial\sigma}\left(\frac{\nu_t}{\sigma_k}\frac{\partial k}{\partial\sigma}\right)+h(P+B-\varepsilon)$$

$$\frac{\partial h\varepsilon}{\partial t}+\frac{1}{R\cos\phi}\left(\frac{\partial hu\varepsilon}{\partial\lambda}+\frac{\partial hv\varepsilon\cos\phi}{\partial\phi}\right)+\frac{\partial h\omega\varepsilon}{\partial\sigma}= \quad (2.61)$$
$$hF_\varepsilon+\frac{1}{h}\frac{\partial}{\partial\sigma}\left(\frac{\nu_t}{\sigma_\varepsilon}\frac{\partial\varepsilon}{\partial\sigma}\right)+h\frac{\varepsilon}{k}\left(c_{1\varepsilon}P+c_{3\varepsilon}B-c_{2\varepsilon}\varepsilon\right)$$

$$\frac{\partial hC}{\partial t}+\frac{1}{R\cos\phi}\left(\frac{\partial huC}{\partial\lambda}+\frac{\partial hvC\cos\phi}{\partial\phi}\right)+\frac{\partial h\omega C}{\partial\sigma}= \quad (2.62)$$
$$hF_C+\frac{\partial}{\partial\sigma}\left(\frac{D_v}{h}\frac{\partial C}{\partial\sigma}\right)-hk_pC+hC_sS$$

The modified vertical velocity in spherical coordinates is defined by

$$\omega=\frac{1}{h}\left[w+\frac{u}{R\cos\phi}\frac{\partial d}{\partial\lambda}+\frac{v}{R}\frac{\partial d}{\partial y}-\sigma\left(\frac{\partial h}{\partial t}+\frac{u}{R\cos\phi}\frac{\partial h}{\partial\lambda}+\frac{v}{R}\frac{\partial h}{\partial\phi}\right)\right] \quad (2.63)$$

The equation determining the water depth in spherical coordinates is given as

$$\frac{\partial h}{\partial t}+\frac{1}{R\cos\phi}\left(\frac{\partial h\bar{u}}{\partial\lambda}+\frac{\partial h\bar{v}\cos\phi}{\partial\phi}\right)=hS \quad (2.64)$$

2.3 2D Governing Equations in Cartesian Coordinates

2.3.1 Shallow water equations

Integration of the horizontal momentum equations and the continuity equation over depth $h = \eta + d$ the following two-dimensional shallow water equations are obtained

$$\frac{\partial h}{\partial t} + \frac{\partial h\bar{u}}{\partial x} + \frac{\partial h\bar{v}}{\partial y} = hS \tag{2.65}$$

$$\begin{aligned}\frac{\partial h\bar{u}}{\partial t} + \frac{\partial h\bar{u}^2}{\partial x} + \frac{\partial h\overline{vu}}{\partial y} = f\bar{v}h - gh\frac{\partial \eta}{\partial x} - \frac{h}{\rho_0}\frac{\partial p_a}{\partial x} - \\ \frac{gh^2}{2\rho_0}\frac{\partial \rho}{\partial x} + \frac{\tau_{sx}}{\rho_0} - \frac{\tau_{bx}}{\rho_0} - \frac{1}{\rho_0}\left(\frac{\partial s_{xx}}{\partial x} + \frac{\partial s_{xy}}{\partial y}\right) + \\ \frac{\partial}{\partial x}\left(hT_{xx}\right) + \frac{\partial}{\partial y}\left(hT_{xy}\right) + hu_sS\end{aligned} \tag{2.66}$$

$$\begin{aligned}\frac{\partial h\bar{v}}{\partial t} + \frac{\partial h\overline{uv}}{\partial x} + \frac{\partial h\bar{v}^2}{\partial y} = -f\bar{u}h - gh\frac{\partial \eta}{\partial y} - \frac{h}{\rho_0}\frac{\partial p_a}{\partial y} - \\ \frac{gh^2}{2\rho_0}\frac{\partial \rho}{\partial y} + \frac{\tau_{sy}}{\rho_0} - \frac{\tau_{by}}{\rho_0} - \frac{1}{\rho_0}\left(\frac{\partial s_{yx}}{\partial x} + \frac{\partial s_{yy}}{\partial y}\right) + \\ \frac{\partial}{\partial x}\left(hT_{xy}\right) + \frac{\partial}{\partial y}\left(hT_{yy}\right) + hv_sS\end{aligned} \tag{2.67}$$

The overbar indicates a depth average value. For example, $\bar{u}$ and $\bar{v}$ are the depth-averaged velocities defined by

$$h\bar{u} = \int_{-d}^{\eta} u\,dz, \quad h\bar{v} = \int_{-d}^{\eta} v\,dz \tag{2.68}$$

The lateral stresses T_{ij} include viscous friction, turbulent friction and differential advection. They are estimated using an eddy viscosity formulation based on of the depth average velocity gradients

$$T_{xx} = 2A\frac{\partial \bar{u}}{\partial x}, \quad T_{xy} = A\left(\frac{\partial \bar{u}}{\partial y} + \frac{\partial \bar{v}}{\partial x}\right), \quad T_{yy} = 2A\frac{\partial \bar{v}}{\partial y} \tag{2.69}$$

2.3.2 Transport equations for salt and temperature

Integrating the transport equations for salt and temperature over depth the following two-dimensional transport equations are obtained

$$\frac{\partial h\bar{T}}{\partial t} + \frac{\partial h\bar{u}\bar{T}}{\partial x} + \frac{\partial h\bar{v}\bar{T}}{\partial y} = hF_T + h\tilde{H} + hT_sS \tag{2.70}$$

$$\frac{\partial h\overline{s}}{\partial t}+\frac{\partial h\overline{u}\overline{s}}{\partial x}+\frac{\partial h\overline{v}\overline{s}}{\partial y}=hF_s+hs_sS \tag{2.71}$$

where $\overline{T}$ and $\overline{s}$ is the depth average temperature and salinity.

2.3.3 Transport equations for a scalar quantity

Integrating the transport equations for a scalar quantity over depth the following two-dimensional transport equations are obtained

$$\frac{\partial h\overline{C}}{\partial t}+\frac{\partial h\overline{u}\overline{C}}{\partial x}+\frac{\partial h\overline{v}\overline{C}}{\partial y}=hF_C-hk_p\overline{C}+hC_sS \tag{2.72}$$

where $\overline{C}$ is the depth average scalar quantity.

2.4 2D Governing Equations in Spherical Coordinates

In spherical coordinates the independent variables are the longitude, λ ,and the latitude, ϕ . The horizontal velocity field (u,v) is defined by

$$\overline{u}=R\cos\phi\frac{d\lambda}{dt}\qquad\overline{v}=R\frac{d\phi}{dt} \tag{2.73}$$

where R is the radius of the earth.

In spherical coordinates the governing equation can be written

$$\frac{\partial h}{\partial t}+\frac{1}{R\cos\phi}\left(\frac{\partial h\overline{u}}{\partial\lambda}+\frac{\partial h\overline{v}\cos\phi}{\partial\phi}\right)=0 \tag{2.74}$$

$$\begin{aligned}&\frac{\partial h\overline{u}}{\partial t}+\frac{1}{R\cos\phi}\left(\frac{\partial h\overline{u}^2}{\partial\lambda}+\frac{\partial h\overline{v}\overline{u}\cos\phi}{\partial\phi}\right)=\left(f+\frac{\overline{u}}{R}\tan\phi\right)\overline{v}h\\&-\frac{1}{R\cos\phi}\left(gh\frac{\partial\eta}{\partial\lambda}-\frac{h}{\rho_0}\frac{\partial p_a}{\partial\lambda}+\frac{gh^2}{2\rho_0}\frac{\partial\rho}{\partial\lambda}+\frac{1}{\rho_0}\left(\frac{\partial s_{xx}}{\partial\lambda}+\cos\phi\frac{\partial s_{xy}}{\partial\phi}\right)\right)+\\&\frac{\tau_{sx}}{\rho_0}-\frac{\tau_{bx}}{\rho_0}+\frac{\partial}{\partial x}\left(hT_{xx}\right)+\frac{\partial}{\partial y}\left(hT_{xy}\right)+hu_sS\end{aligned} \tag{2.75}$$

$$\begin{aligned}&\frac{\partial h\overline{v}}{\partial t}+\frac{1}{R\cos\phi}\left(\frac{\partial h\overline{u}\overline{v}}{\partial\lambda}+\frac{\partial h\overline{v}^2\cos\varphi}{\partial\iota}\right)=-\left(f+\frac{\overline{u}}{R}\tan\phi\right)\overline{u}h\\&-\frac{1}{R}\left(gh\frac{\partial\eta}{\partial\phi}-\frac{h}{\rho_0}\frac{\partial p_a}{\partial\phi}+\frac{gh^2}{2\rho_0}\frac{\partial\rho}{\partial\phi}+\frac{1}{\rho_0}\left(\frac{1}{\cos\phi}\frac{\partial s_{yx}}{\partial\lambda}+\frac{\partial s_{yy}}{\partial\phi}\right)\right)+\\&\frac{\tau_{sy}}{\rho_0}-\frac{\tau_{by}}{\rho_0}+\frac{\partial}{\partial x}\left(hT_{xy}\right)+\frac{\partial}{\partial y}\left(hT_{yy}\right)+hv_sS\end{aligned} \tag{2.76}$$

$$\frac{\partial h\overline{T}}{\partial t}+\frac{1}{R\cos\phi}\left(\frac{\partial h\overline{u}\overline{T}}{\partial\lambda}+\frac{\partial h\overline{v}\overline{T}\cos\phi}{\partial\phi}\right)=hF_T+h\hat{H}+hT_sS \tag{2.77}$$

$$\frac{\partial h\overline{s}}{\partial t}+\frac{1}{R\cos\phi}\left(\frac{\partial h\overline{u}\overline{s}}{\partial\lambda}+\frac{\partial h\overline{v}\overline{s}\cos\phi}{\partial\phi}\right)=hF_s+hs_sS \tag{2.78}$$

$$\frac{\partial h\overline{C}}{\partial t}+\frac{1}{R\cos\phi}\left(\frac{\partial h\overline{u}\overline{C}}{\partial\lambda}+\frac{\partial h\overline{v}\overline{C}\cos\phi}{\partial\phi}\right)=hF_C-hk_p\overline{C}+hC_sS \tag{2.79}$$

2.5 Bottom Stress

The bottom stress, $\vec{\tau}_b=(\tau_{bx},\tau_{by})$, is determined by a quadratic friction law

$$\frac{\vec{\tau}_b}{\rho_0}=c_f\vec{u}_b|\vec{u}_b| \tag{2.80}$$

where c_f is the drag coefficient and $\vec{u}_b=(u_b,v_b)$ is the flow velocity above the bottom. The friction velocity associated with the bottom stress is given by

$$U_{\tau b}=\sqrt{c_f|u_b|^2} \tag{2.81}$$

For two-dimensional calculations $\vec{u}_b$ is the depth-average velocity and the drag coefficient can be determined from the Chezy number, C, or the Manning number, M

$$c_f=\frac{g}{C^2} \tag{2.82}$$

$$c_f=\frac{g}{\left(Mh^{1/6}\right)^2} \tag{2.83}$$

For three-dimensional calculations $\vec{u}_b$ is the velocity at a distance Δz_b above the sea bed and the drag coefficient is determined by assuming a logarithmic profile between the seabed and a point Δz_b above the seabed

$$c_f=\frac{1}{\left(\frac{1}{\kappa}\ln\left(\frac{\Delta z_b}{z_0}\right)\right)^2} \tag{2.84}$$

where κ =0.4 is the von Kármán constant and z_0 is the bed roughness length scale. When the boundary surface is rough, z_0, depends on the roughness height, k_s

$$z_0=mk_s \tag{2.85}$$

where m is approximately 1/30.

Note, that the Manning number can be estimated from the bed roughness length using the following

$$M = \frac{25.4}{k_s^{1/6}} \tag{2.86}$$

The wave induced bed resistance can be determined from

$$c_f = \left(\frac{u_{fc}}{u_b} \right)^2 \tag{2.87}$$

where U_{fc} is the friction velocity calculated by considering the conditions in the wave boundary layer. For a detailed description of the wave induced bed resistance, see Fredsøe (1984) and Jones et.al. (2014).

2.6 Wind Stress

In areas not covered by ice the surface stress, $\vec{\tau}_s = (\tau_{sx}, \tau_{sy})$, is determined by the winds above the surface. The stress is given by the following empirical relation

$$\vec{\tau}_s = \rho_a c_d |u_w| \vec{u}_w \tag{2.88}$$

where ρ_a is the density of air, c_d is the drag coefficient of air, and $\vec{u}_w = (u_w, v_w)$ is the wind speed 10 m above the sea surface. The friction velocity associated with the surface stress is given by

$$U_\tau = \sqrt{\frac{\rho_a c_f |\vec{u}_w|^2}{\rho_0}} \tag{2.89}$$

The drag coefficient can either be a constant value or depend on the wind speed. The empirical formula proposed by Wu (1980, 1994) is used for the parameterisation of the drag coefficient.

$$c_f = \begin{cases} c_a & w_{10} < w_a \\ c_a + \dfrac{c_b - c_a}{w_b - w_a}(w_{10} - w_a) & w_a \le w_{10} < w_b \\ c_b & w_{10} \ge w_b \end{cases} \tag{2.90}$$

where c_a, c_b, w_a and w_b are empirical factors and w_{10} is the wind velocity 10 m above the sea surface. The default values for the empirical factors are $c_a = 1.255 \cdot 10^{-3}$, $c_b = 2.425 \cdot 10^{-3}$, $w_a = 7$ m/s and $w_b = 25$ m/s. These give generally good results for open sea applications. Field measurements of the drag coefficient collected over lakes indicate that the drag coefficient is larger than open ocean data. For a detailed description of the drag coefficient see Geernaert and Plant (1990).

2.7 Ice Coverage

It is possible to take into account the effects of ice coverage on the flow field.

In areas where the sea is covered by ice the wind stress is excluded. Instead, the surface stress is caused by the ice roughness. The surface stress, $\vec{\tau}_s = (\tau_{sx}, \tau_{sy})$, is determined by a quadratic friction law

$$\frac{\vec{\tau}_s}{\rho_0} = c_f \vec{u}_s |\vec{u}_s| \tag{2.91}$$

where c_f is the drag coefficient and $\vec{u}_s = (u_s, v_s)$ is the flow velocity below the surface. The friction velocity associated with the surface stress is given by

$$U_{\tau s} = \sqrt{c_f |u_s|^2} \tag{2.92}$$

For two-dimensional calculations $\vec{u}_s$ is the depth-average velocity and the drag coefficient can be determined from the Manning number, M

$$c_f = \frac{g}{\left(Mh^{1/6}\right)^2} \tag{2.93}$$

The Manning number is estimated from the bed roughness length using the following

$$M = \frac{25.4}{k_s^{1/6}} \tag{2.94}$$

For three-dimensional calculations $\vec{u}_s$ is the velocity at a distance Δz_s below the surface and the drag coefficient is determined by assuming a logarithmic profile between the surface and a point Δz_b below the surface

$$c_f = \frac{1}{\left(\frac{1}{\kappa}\ln\left(\frac{\Delta z_s}{z_0}\right)\right)^2} \tag{2.95}$$

where κ =0.4 is the von Kármán constant and z_0 is the bed roughness length scale. When the boundary surface is rough, z_0, depends on the roughness height, k_s

$$z_0 = mk_s \tag{2.96}$$

where m is approximately 1/30.

If ice thickness is specified, the water level is supressed by ρ_{ice} / ρ_{water} of the ice thickness, where ρ_{ice} = 971 kg/m^3 and ρ_{water} is the actual density of the water.

2.8 Tidal Potential

The tidal potential is a force, generated by the variations in gravity due to the relative motion of the earth, the moon and the sun that act throughout the computational domain. The forcing is expanded in frequency space and the potential considered as the sum of a number of terms each representing different tidal constituents. The forcing is implemented as a so-called equilibrium tide, which can be seen as the elevation that theoretically would occur, provided the earth was covered with water. The forcing enters the momentum equations (e.g. (2.66) or (2.75)) as an additional term representing the gradient of the equilibrium tidal elevations, such that the elevation η can be seen as the sum of the actual elevation and the equilibrium tidal potential.

$$\eta = \eta_{ACTUAL} + \eta_T \tag{2.97}$$

The equilibrium tidal potential η_T is given as

$$\eta_T = \sum_i e_i H_i f_i L_i \cos(2\pi \frac{t}{T_i} + b_i + i_0 x) \tag{2.98}$$

where η_T is the equilibrium tidal potential, i refers to constituent number (note that the constituents here are numbered sequentially), e_i is a correction for earth tides based on Love numbers, H_i is the amplitude, f_i is a nodal factor, L_i is given below, t is time, T_i is the period of the constituent, b_i is the phase and x is the longitude of the actual position.

The phase b is based on the motion of the moon and the sun relative to the earth and can be given by

$$b_i = (i_1 - i_0)s + (i_2 + i_0)h + i_3 p + i_4 N + i_5 p_s + u_i \sin(N) \tag{2.99}$$

where i_0 is the species, i_1 to i_5 are Doodson numbers, u is a nodal modulation factor (see Table 2.3) and the astronomical arguments s, h, p, N and p_s are given in Table 2.2.

Table 2.2 Astronomical arguments (Pugh, 1987)

Mean longitude of the moon	s	277.02+481267.89T+0.0011T²
Mean longitude of the sun	h	280.19+36000.77T+0.0003T²
Longitude of lunar perigee	p	334.39+4069.04T-0.0103T²
Longitude of lunar ascending node	N	259.16-1934.14T+0.0021T²
Longitude of perihelion	p_s	281.22+1.72T+0.0005T²

In Table 2.2 the time, T, is in Julian century from January 1 1900 UTC, thus T = (365(y – 1900) + (d – 1) + i)/36525 and i = *int* (y-1901)/4), y is year and d is day number

L depends on species number i_0 and latitude y as

$i_0 = 0$ $\quad L = 3\sin^2(y) - 1$

$i_0 = 1$ $\quad L = \sin(2y)$

$i_0 = 2$ $\quad L = \cos^2(y)$

The nodal factor f_i represents modulations to the harmonic analysis and can for some constituents be given as shown in Table 2.3.

Table 2.3 Nodal modulation terms (Pugh, 1987)

	f_i	u_i
M_m	1.000 - 0.130 cos(N)	0
M_f	1.043 + 0.414 cos(N)	-23.7 sin(N)
Q_1, O_1	1.009 + 0.187 cos(N)	10.8 sin(N)
K_1	1.006 + 0.115 cos(N)	-8.9 sin(N)
$2N_2, \mu_2, \nu_2, N_2, M_2$	1.000 - 0.037 cos(N)	-2.1 sin(N)
K_2	1.024 + 0.286 cos(N)	-17.7 sin(N)

2.9 Wave Radiation

The second order stresses due to breaking of short period waves can be included in the simulation. The radiation stresses act as driving forces for the mean flow and can be used to calculate wave induced flow. For 3D simulations a simple approach is used. Here a uniform variation is used for the vertical variation in radiation stress.

2.10 Heat Exchange

The heat exchange with the atmosphere is calculated on basis of the four physical processes

- Latent heat flux (or the heat loss due to vaporisation)
- Sensible heat flux (or the heat flux due to convection)
- Net short wave radiation
- Net long wave radiation

Latent and sensible heat fluxes and long-wave radiation are assumed to occur at the surface. The absorption profile for the short-wave flux is approximated using Beer's law. The attenuation of the light intensity is described through the modified Beer's law as

$$I(d) = (1-\beta)I_0 e^{-\lambda d} \tag{2.100}$$

where $I(d)$ is the intensity at depth d below the surface; I_0 is the intensity just below the water surface; β is a quantity that takes into account that a fraction of light energy (the infrared) is absorbed near the surface; λ is the light extinction coefficient. Typical values for β and λ are 0.2-0.6 and 0.5-1.4 m^{-1}, respectively. β and λ are user-specified constants. The default values are $\beta = 0.3$ and $\lambda = 1.0\ m^{-1}$. The fraction of the light energy that is absorbed near the surface is βI_0. The net short-wave radiation, $q_{sr,net}$, is attenuated as described by the modified Beer's law. Hence the surface net heat flux is given by

$$Q_n = q_v + q_c + \beta q_{sr,net} + q_{lr,net} \tag{2.101}$$

For three-dimensional calculations the source term $\hat{H}$ is given by

$$\hat{H} = \frac{\partial}{\partial z}\left(\frac{q_{sr,net}(1-\beta)e^{-\lambda(\eta-z)}}{\rho_0 c_p}\right) = \frac{q_{sr,net}(1-\beta)\lambda e^{-\lambda(\eta-z)}}{\rho_0 c_p} \tag{2.102}$$

For two-dimensional calculations the source term $\hat{H}$ is given by

$$\hat{H} = \frac{q_v + q_c + q_{sr,net} + q_{lr,net}}{\rho_0 c_p} \tag{2.103}$$

The calculation of the latent heat flux, sensible heat flux, net short wave radiation, and net long wave radiation as described in the following sections.

In areas covered by ice the heat exchange is excluded.

2.10.1 Vaporisation

Dalton's law yields the following relationship for the vaporative heat loss (or latent flux), see Sahlberg, 1984

$$q_v = LC_e(a_1 + b_1 W_{2m})(Q_{water} - Q_{air}) \tag{2.104}$$

where $L = 2.5 \cdot 10^6\ J/kg$ is the latent heat vaporisation (in the literature $L = 2.5 \cdot 10^6 - 2300\ T_{water}$ is commonly used); $C_e = 1.32 \cdot 10^{-3}$ is the moisture transfer coefficient (or Dalton number); W_{2m} is the wind speed 2 m above the sea surface; Q_{water} is the water vapour density close to the surface; Q_{air} is the water vapour density in the atmosphere; a_1 and b_1 are user specified constants. The default values are $a_1 = 0.5$ and $b_1 = 0.9$.

Measurements of Q_{water} and Q_{air} are not directly available but the vapour density can be related to the vapour pressure as

$$Q_i = \frac{0.2167}{T_i + T_k} e_i \tag{2.105}$$

in which subscript *i* refers to both water and air. The vapour pressure close to the sea, e_{water}, can be expressed in terms of the water temperature assuming that the air close to the surface is saturated and has the same temperature as the water

$$e_{water} = 6.11 e^K \left(\frac{1}{T_k} - \frac{1}{T_{water} + T_k}\right) \tag{2.106}$$

where $K = 5418\ °K$ and $T_K = 273.15\ °K$ is the temperature at 0 C. Similarly the vapour pressure of the air, e_{air}, can be expressed in terms of the air temperature and the relative humidity, R

$$e_{air} = R \cdot 6.11 e^{K\left(\frac{1}{T_k} - \frac{1}{T_{air} + T_k}\right)} \tag{2.107}$$

Replacing Q_{water} and Q_{air} with these expressions the latent heat can be written as

$$q_v = -P_v (a_1 + b_1 W_{2m}) \cdot \left(\frac{\exp\left(K\left(\frac{1}{T_k} - \frac{1}{T_{water} + T_k}\right)\right)}{T_{water} + T_k} - \frac{R \cdot \exp\left(K\left(\frac{1}{T_k} - \frac{1}{T_{air} + T_k}\right)\right)}{T_{air} + T_k} \right) \tag{2.108}$$

where all constants have been included in a new latent constant $P_v = 4370\ J \cdot °K / m^3$. During cooling of the surface the latent heat loss has a major effect with typical values up to 100 W/m^2.

The wind speed, W_2, 2 m above the sea surface is calculated from the from the wind speed, W_{10}, 10 m above the sea surface using the following formula:

Assuming a logarithmic profile the wind speed, *u(z)*, at a distance *z* above the sea surface is given by

$$u(z) = \frac{u_*}{\kappa} \log\left(\frac{z}{z_o}\right) \tag{2.109}$$

where u_* is the wind friction velocity, z_0 is the sea roughness and κ =0.4 is von Karman's constant. u_* and z_0 are given by

$$z_0 = z_{Charnock}\, u_*^2 / g \tag{2.110}$$

$$u_* = \frac{\kappa u(z)}{\log\left(\frac{z}{z_0}\right)} \tag{2.111}$$

where $z_{Charnock}$ is the Charnock parameter. The default value is $z_{Charnock} = 0.01\,4$. The wind speed, W_2, 2 m above the sea surface is then calculated from the from the wind speed, W_{10}, 10m above the sea surface by first solving Eq. (2.114) and Eq. (2.115) iteratively for z_0 with $z=10m$ and $u(z)=W_{10}$. Then W_2 is given by

$$W_2 = W_{10}\frac{\log\left(\frac{2}{z_o}\right)}{\log\left(\frac{10}{z_0}\right)} \qquad W_{10} > 0.5m/s$$
$$W_2 = W_{10} \qquad W_{10} \le 0.5m/s \tag{2.112}$$

The heat loss due to vaporization occurs both by wind driven forced convection by and free convection. The effect of free convection is taken into account by the parameter a_1 in Eq. (2.104). The free convection is also taken into account by introducing a critical wind speed $W_{critical}$ so that the wind speed used in Eq. (2.112) is obtained as $W_{10}=max(W_{10},W_{critical})$. The default value for the critical wind speed is 2 m/s.

2.10.2 Convection

The sensible heat flux, $q_c\ (W/m^2)$, (or the heat flux due to convection) depends on the type of boundary layer between the sea surface and the atmosphere. Generally this boundary layer is turbulent implying the following relationship

$$q_c = \begin{cases} \rho_{air} c_{air} c_{heating} W_{10}(T_{air} - T_{water}) & T_{air} \ge T \\ \rho_{air} c_{air} c_{cooling} W_{10}(T_{air} - T_{water}) & T_{air} < T \end{cases} \tag{2.113}$$

where ρ_{air} is the air density 1.225 kg/m^3; $c_{air} = 1007\ J/(kg\cdot°K)$ is the specific heat of air; $c_{heating} = 0.0011$ and $c_{cooling} = 0.0011$, respectively, is the sensible transfer coefficient (or Stanton number) for heating and cooling (see Kantha and Clayson, 2000); W_{10} is the wind speed 10 m above the sea surface; T_{water} is the temperature at the sea surface; T_{air} is the temperature of the air.

The convective heat flux typically varies between 0 and 100 W/m^2.

The heat loss due to convection occurs both by wind driven forced convection by and free convection. The free convection is taken into account by introducing a critical wind speed $W_{critical}$ so that the wind speed used in Eq. (2.113) is obtained as $W_{10}=max(W_{10},W_{critical})$. The default value for the critical wind speed is 2 m/s.

2.10.3 Short wave radiation

Radiation from the sun consists of electromagnetic waves with wave lengths varying from 1,000 to 30,000 Å. Most of this is absorbed in the ozone layer, leaving only a fraction of the energy to reach the surface of the Earth. Furthermore, the spectrum changes when sunrays pass through the atmosphere. Most of the infrared and ultraviolet compound is absorbed such that the solar radiation on the Earth mainly consists of light with wave lengths between 4,000 and 9,000 Å. This radiation is normally termed short wave radiation. The intensity depends on the distance to the sun, declination angle and latitude, extraterrestrial radiation and the cloudiness and amount of water vapour in the atmosphere (see Iqbal, 1983)

The eccentricity in the solar orbit, E_0, is given by

$$E_0 = \left(\frac{r_0}{r}\right)^2 = 1.000110 + 0.034221\cos(\Gamma) + 0.001280\sin(\Gamma) + 0.000719\cos(2\Gamma) + 0.000077\sin(2\Gamma) \quad (2.114)$$

where r_0 is the mean distance to the sun, r is the actual distance and the day angle $\Gamma\ (rad)$ is defined by

$$\Gamma = \frac{2\pi(d_n - 1)}{365} \quad (2.115)$$

and d_n is the Julian day of the year.

The daily rotation of the Earth around the polar axes contributes to changes in the solar radiation. The seasonal radiation is governed by the declination angle, $\delta\ (rad)$, which can be expressed by

$$\delta = 0.006918 - 0.399912\cos(\Gamma) + 0.07257\sin(\Gamma) - 0.006758\cos(2\Gamma) + 0.000907\sin(2\Gamma) - 0.002697\cos(3\Gamma) + 0.00148\sin(3\Gamma) \quad (2.116)$$

The day length, n_d, varies with δ. For a given latitude, ϕ, (positive on the northern hemisphere) the day length is given by

$$n_d = \frac{24}{\pi}\arccos\left(-\tan(\phi)\tan(\delta)\right) \quad (2.117)$$

and the sunrise angle, $\omega_{sr}\ (rad)$, and the sunset angle $\omega_{ss}\ (rad)$ are

$$\omega_{sr} = \arccos\left(-\tan(\phi)\tan(\delta)\right) \quad and \quad \omega_{ss} = -\omega_{sr} \quad (2.118)$$

The intensity of short wave radiation on the surface parallel to the surface of the Earth changes with the angle of incidence. The highest intensity is in zenith and the lowest during sunrise and sunset. Integrated over one day the extraterrestrial intensity, $H_0\ (MJ/m^2/day)$, in short wave radiation on the surface can be derived as

$$H_0 = \frac{24}{\pi} q_{sc} E_0 \cos(\phi)\cos(\delta)\left(\sin(\omega_{sr}) - \omega_{sr}\cos(\omega_{sr})\right) \quad (2.119)$$

where $q_{sc} = 4.9212\ (MJ/m^2/h)$ is the solar constant.

For determination of daily radiation under cloudy skies, $H\ (MJ/m^2/day)$, the following relation is used

$$\frac{H}{H_0} = a_2 + b_2 \frac{n}{n_d} \tag{2.120}$$

in which n is the number of sunshine hours and n_d is the maximum number of sunshine hours. a_2 and b_2 are user specified constants. The default values are $a_2 = 0.295$ and $b_2 = 0.371$. The user-specified clearness coefficient corresponds to n / n_d. Thus the solar radiation, q_s (W/m^2), can be expressed as

$$q_s = \left(\frac{H}{H_0}\right) q_0 \left(a_3 + b_3 \cos(\omega_i)\right) \frac{10^6}{3600} \tag{2.121}$$

where

$$a_3 = 0.4090 + 0.5016 \sin\left(\omega_{sr} - \frac{\pi}{3}\right) \tag{2.122}$$

$$b_3 = 0.6609 + 0.4767 \sin\left(\omega_{sr} - \frac{\pi}{3}\right) \tag{2.123}$$

The extraterrestrial intensity, q_0 $(MJ/m^2/h)$ and the hour angle ω_i is given by

$$q_0 = q_{sc} E_0 \left(\sin(\phi)\sin(\delta) + \frac{24}{\pi}\cos(\phi)\cos(\delta)\cos(\omega_i)\right) \tag{2.124}$$

$$\omega_i = \frac{\pi}{12}\left(12 + \Delta t_{displacement} + \frac{4}{60}(L_S - L_E) - \frac{E_t}{60} - t_{local}\right) \tag{2.125}$$

$\Delta t_{displacement}$ is the displacement hours due to summer time and the time meridian L_S is the standard longitude for the time zone. $\Delta t_{displacement}$ and L_S are user specified constants. The default values are $\Delta t_{displacement} = 0$ (h) and $L_S = 0$ (deg). L_E is the local longitude in degrees. E_t (s) is the discrepancy in time due to solar orbit and is varying during the year. It is given by

$$E_t = \begin{pmatrix} 0.000075 + 0.001868\cos(\Gamma) - 0.032077\sin(\Gamma) \\ -0.014615\cos(2\Gamma) - 0.04089\sin(2\Gamma) \end{pmatrix} \cdot 229.18 \tag{2.126}$$

Finally, t_{local} is the local time in hours.

Solar radiation that impinges on the sea surface does not all penetrate the water surface. Parts are reflected back and are lost unless they are backscattered from the surrounding atmosphere. This reflection of solar energy is termed the albedo. The amount of energy, which is lost due to albedo, depends on the angle of incidence and angle of refraction. For a smooth sea the reflection can be expressed as

$$\alpha = \frac{1}{2}\left(\frac{\sin^2(i-r)}{\sin^2(i+r)} + \frac{\tan^2(i-r)}{\tan^2(i+r)}\right) \quad (2.127)$$

where i is the angle of incidence, r the refraction angle and α the reflection coefficient, which typically varies from 5 to 40 %. α can be approximated using

$$\alpha = \begin{cases} \frac{altitude}{5}\,0.48 & altitude < 5 \\ \frac{30 - altitude}{25}(0.48 - 0.05) & 5 \le altitude \le 30 \\ 0.05 & altitude > 30 \end{cases} \quad (2.128)$$

where the altitude in degrees is given by

$$altitude = 90 - \left(\frac{180}{\pi}\arccos(\sin(\delta)\sin(\phi) + \cos(\delta)\cos(\phi)\cos(\omega_i))\right) \quad (2.129)$$

Thus the net short wave radiation, $q_{s,net}\ (W/m^2)$, can possibly be expressed as

$$q_{sr,net} = (1-\alpha)q_s \quad (2.130)$$

The net short wave radiation, $q_{sr,net}$, can be calculated using empirical formulae as described above. Alternatively, the net short wave radiation can be calculated using Eq. (2.130) where the solar radiation, q_s, is specified by the user or the net short wave radiation, $q_{sr,net}$, can be given by the user.

2.10.4 Long wave radiation

A body or a surface emits electromagnetic energy at all wavelengths of the spectrum. The long wave radiation consists of waves with wavelengths between 9,000 and 25,000 Å. The radiation in this interval is termed infrared radiation and is emitted from the atmosphere and the sea surface. The long wave emittance from the surface to the atmosphere minus the long wave radiation from the atmosphere to the sea surface is called the net long wave radiation and is dependent on the cloudiness, the air temperature, the vapour pressure in the air and the relative humidity. The net outgoing long wave radiation, $q_{lr,net}\ (W/m^2)$, is given by Brunt's equation (See Lind and Falkenmark, 1972)

$$q_{lr,net} = -\sigma_{sb}(T_{air} + T_K)^4\left(a - b\sqrt{e_d}\right)\left(c + d\frac{n}{n_d}\right) \quad (2.131)$$

where e_d is the vapour pressure at dew point temperature measured in *mb*; n is the number of sunshine hours, n_d is the maximum number of sunshine hours; $\sigma_{sb} = 5.6697 \cdot 10^{-8}\ W/(m^2 \cdot {}^\circ K^4)$ is Stefan Boltzman's constant; $T_{air}\,(^\circ C)$ is the air temperature. The coefficients *a*, *b*, *c* and *d* are given as

$$a = 0.56; b = 0.077\, mb^{-1/4}; c = 0.10; d = .90 \tag{2.132}$$

The vapour pressure is determined as

$$e_d = 10 \cdot R\, e_{saturated} \tag{2.133}$$

where R is the relative humidity and the saturated vapour pressure, $e_{saturated}\ (kPa)$, with 100 % relative humidity in the interval from –51 to 52 °C can be estimated by

$$e_{saturated} = 3.38639 \cdot \left(\left(7.38 \cdot 10^{-3} \cdot T_{air} + 0.8072\right)^8 - 1.9 \cdot 10^{-5} \left|1.8 \cdot T_{air} + 48\right| + 1.316 \cdot 10^{-3}\right) \tag{2.134}$$

The net long wave radiation, $q_{lr,net}$, can be calculated using empirical formulae as described above. Alternatively, the net long wave radiation can be calculated as

$$q_{lr,net} = q_{ar,net} - q_{br} \tag{2.135}$$

where the net incident atmospheric radiation, $q_{ar,net}$, is specified by the user and the back radiation, q_{br}, is given by

$$q_{br} = (1 - r)\varepsilon\sigma_{sb} T_K^4 \tag{2.136}$$

where r=0.03 is the reflection coefficient and ε=0.985 is the emissivity factor of the atmosphere. The net long wave radiation can also be specified by the user.

3 Numerical Solution

3.1 Spatial Discretization

The discretization in solution domain is performed using a finite volume method. The spatial domain is discretized by subdivision of the continuum into non-overlapping cells/elements.

In the two-dimensional case the elements can be arbitrarily shaped polygons, however, here only triangles and quadrilateral elements are considered.

In the three-dimensional case a layered mesh is used: in the horizontal domain an unstructured mesh is used while in the vertical domain a structured mesh is used (see Figure 3.1). The vertical mesh is based on either sigma coordinates or combined sigma/z-level coordinates. For the hybrid sigma/z-level mesh sigma coordinates are used from the free surface to a specified depth and z-level coordinates are used below. The different types of vertical mesh are illustrated in Figure 3.2. The elements in the sigma domain and the z-level domain can be prisms with either a 3-sided or 4-sided polygonal base. Hence, the horizontal faces are either triangles or quadrilateral element. The elements are perfectly vertical and all layers have identical topology.

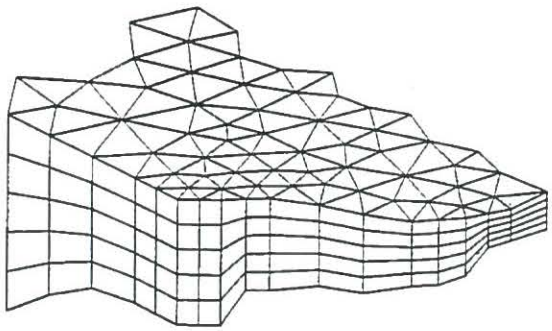

Figure 3.1 Principle of meshing for the three-dimensional case

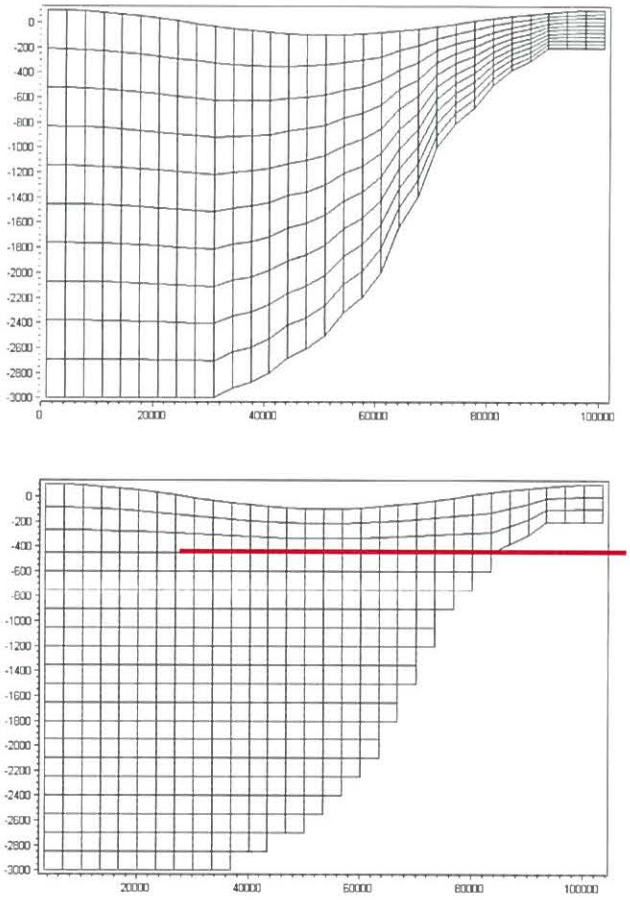

Figure 3.2 Illustrations of the different vertical grids. Upper: sigma mesh, Lower: combined sigma/z-level mesh with simple bathymetry adjustment. The red line shows the interface between the z-level domain and the sigma-level domain

The most important advantage using sigma coordinates is their ability to accurately represent the bathymetry and provide consistent resolution near the bed. However, sigma coordinates can suffer from significant errors in the horizontal pressure gradients, advection and mixing terms in areas with sharp topographic changes (steep slopes). These errors can give rise to unrealistic flows.

The use of z-level coordinates allows a simple calculation of the horizontal pressure gradients, advection and mixing terms, but the disadvantages are their inaccuracy in representing the bathymetry and that the stair-step representation of the bathymetry can result in unrealistic flow velocities near the bottom.

3.1.1 Vertical Mesh

For the vertical discretization both a standard sigma mesh and a combined sigma/z-level mesh can be used. For the hybrid sigma/z-level mesh sigma coordinates are used from the free surface to a specified depth, z_σ, and z-level coordinates are used below. At least one sigma layer is needed to allow changes in the surface elevation.

Sigma

In the sigma domain a constant number of layers, N_σ, are used and each sigma layer is a fixed fraction of the total depth of the sigma layer, h_σ, where $h_\sigma = \eta - \max(z_b, z_\sigma)$. The discretization in the sigma domain is given by a number of discrete σ-levels $\{\sigma_i,\ i = 1, (N_\sigma + 1)\}$. Here σ varies from $\sigma_1 = 0$ at the bottom interface of the lowest sigma layer to $\sigma_{N_\sigma+1} = 1$ at the free surface.

Variable sigma coordinates can be obtained using a discrete formulation of the general vertical coordinate (s-coordinate) system proposed by Song and Haidvogel (1994). First an equidistant discretization in a s-coordinate system *(-1≤ s ≤0)* is defined

$$s_i = -\frac{N_\sigma + 1 - i}{N_\sigma} \qquad i = 1, (N_\sigma + 1) \tag{3.1}$$

The discrete sigma coordinates can then be determined by

$$\sigma_i = 1 + \sigma_c s_i + (1 - \sigma_c) c(s_i) \quad i = 1, (N_\sigma + 1) \tag{3.2}$$

where

$$c(s) = (1 - b)\frac{\sinh(\theta s)}{\sinh(\theta)} + b\frac{\tanh\left(\theta\left(s + \frac{1}{2}\right)\right) - \tanh(\frac{\theta}{2})}{2\tanh(\frac{\theta}{2})} \tag{3.3}$$

Here σ_c is a weighting factor between the equidistant distribution and the stretch distribution, θ is the surface control parameter and b is the bottom control parameter. The range for the weighting factor is $0<\sigma_c\leq 1$ where the value 1 corresponds to equidistant distribution and 0 corresponds to stretched distribution. A small value of σ_c can result in linear instability. The range of the surface control parameter is $0<\theta\leq 20$ and the range of the bottom control parameter is $0\leq b\leq 1$. If $\theta<<1$ and $b=0$ an equidistant vertical resolution is obtained. By increasing the value of the θ, the highest resolution is achieved near the surface. If $\theta>0$ and $b=1$ a high resolution is obtained both near the surface and near the bottom.

Examples of a mesh using variable vertical discretization are shown in Figure 3.3 and Figure 3.4.

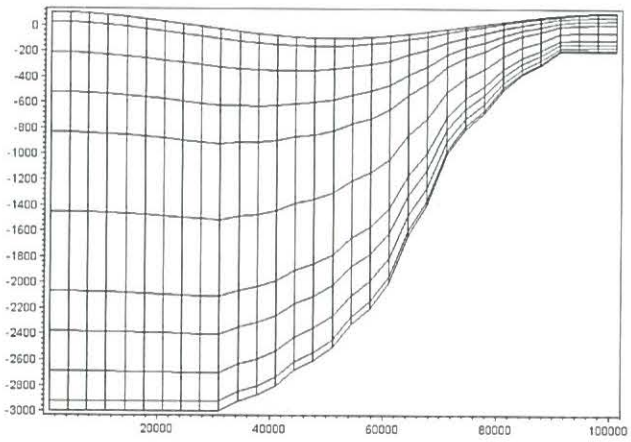

Figure 3.3 Example of vertical distribution using layer thickness distribution. Number of layers: 10, thickness of layers 1 to 10: .025, 0.075, 0.1, 0.01, 0.02, 0.02, 0.1, 0.1, 0.075, 0.025

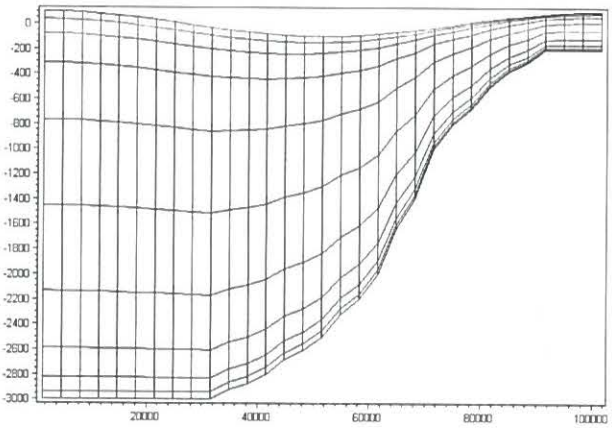

Figure 3.4 Example of vertical distribution using variable distribution. Number of layers: 10, σ_c = 0.1, θ = 5, b = 1

Combined sigma/z-level

In the z-level domain the discretization is given by a number of discrete z-levels $\{z_i,\ i = 1, (N_z + 1)\}$, where N_z is the number of layers in the z-level domain. z_1 is the minimum z-level and z_{N_z+1} is the maximum z-level, which is equal to the sigma depth, z_σ. The corresponding layer thickness is given by

$$\Delta z_i = z_{i+1} - z_i \qquad i = 1, N_z \tag{3.4}$$

The discretization is illustrated in Figure 3.5 and Figure 3.6.

Using standard z-level discretization the bottom depth is rounded to the nearest z-level. Hence, for a cell in the horizontal mesh with the cell-averaged depth, z_b, the cells in the corresponding column in the z-domain are included if the following criteria is satisfied

$$(z_{i+1} - z_i)/2 \geq z_b \quad i = 1, N_z \tag{3.5}$$

The cell-averaged depth, z_b, is calculated as the mean value of the depth at the vortices of each cell. For the standard z-level discretization the minimum depth is given by z_1. Too take into account the correct depth for the case where the bottom depth is below the minimum z-level ($z_1 > z_b$) a bottom fitted approach is used. Here, a correction factor, f_1, for the layer thickness in the bottom cell is introduced. The correction factor is used in the calculation of the volume and face integrals. The correction factor for the bottom cell is calculated by

$$f_1 = \frac{(z_2 - z_b)}{\Delta z_1} \tag{3.6}$$

The corrected layer thickness is given by $\Delta z_1^* = f_1 \Delta z_1$. The simple bathymetry adjustment approach is illustrated in Figure 3.5.

For a more accurate representation of the bottom depth an advanced bathymetry adjustment approach can be used. For a cell in the horizontal mesh with the cell-averaged depth, z_b, the cells in the corresponding column in the z-domain are included if the following criteria is satisfied

$$z_{i+1} > z_b \qquad i = 1, N_z \tag{3.7}$$

A correction factor, f_i, is introduced for the layer thickness

$$f_i = max\left(\frac{(z_{i+1} - z_b)}{\Delta z_i}, \frac{z_{min}}{\Delta z_i}\right) \qquad z_i < z_b < z_{i+1} \ or \ z_1 > z_b$$
$$f_i = 1 \qquad z_1 \geq z_b \tag{3.8}$$

A minimum layer thickness, Δz_{min}, is introduced to avoid very small values of the correction factor. The correction factor is used in the calculation of the volume and face integrals. The corrected layer thicknesses are given by $\{\Delta z_i^* = f_i \Delta z_i, \ i = 1, N_z\}$. The advanced bathymetry adjustment approach is illustrated in Figure 3.6.

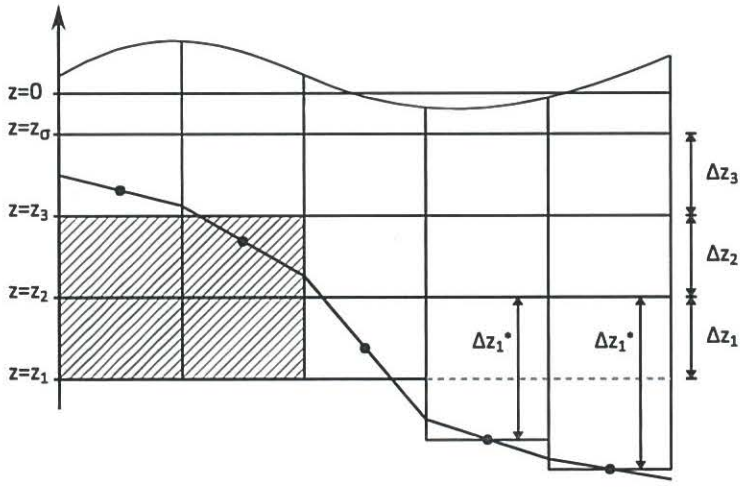

Figure 3.5 Simple bathymetry adjustment approach

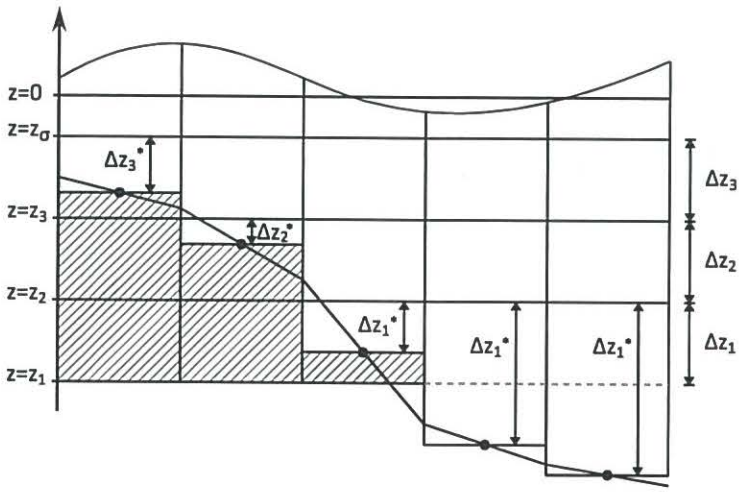

Figure 3.6 Advanced bathymetry adjustment approach

3.1.2 Shallow water equations

The integral form of the system of shallow water equations can in general form be written

$$\frac{\partial \boldsymbol{U}}{\partial t} + \nabla \cdot \boldsymbol{F}(\boldsymbol{U}) = \boldsymbol{S}(\boldsymbol{U}) \tag{3.9}$$

where $\boldsymbol{U}$ is the vector of conserved variables, $\boldsymbol{F}$ is the flux vector function and $\boldsymbol{S}$ is the vector of source terms.

In Cartesian coordinates the system of 2D shallow water equations can be written

$$\frac{\partial \boldsymbol{U}}{\partial t} + \frac{\partial \left(\boldsymbol{F}_x^I - \boldsymbol{F}_x^V\right)}{\partial x} + \frac{\partial \left(\boldsymbol{F}_y^I - \boldsymbol{F}_y^V\right)}{\partial y} = \boldsymbol{S} \tag{3.10}$$

where the superscripts *I* and *V* denote the inviscid (convective) and viscous fluxes, respectively and where

$$\boldsymbol{U} = \begin{bmatrix} h \\ h\overline{u} \\ h\overline{v} \end{bmatrix},$$

$$\boldsymbol{F}_x^{\,I} = \begin{bmatrix} h\overline{u} \\ h\overline{u}^2 + \frac{1}{2}g(h^2 - d^2) \\ h\overline{u}\overline{v} \end{bmatrix}, \quad \mathrm{F}_x^{\,V} = \begin{bmatrix} 0 \\ hA\left(2\frac{\partial \overline{u}}{\partial x}\right) \\ hA\left(\frac{\partial \overline{u}}{\partial y} + \frac{\partial \overline{v}}{\partial x}\right) \end{bmatrix}$$

$$\boldsymbol{F}_y^{\,I} = \begin{bmatrix} h\overline{v} \\ h\overline{v}\overline{u} \\ h\overline{v}^2 + \frac{1}{2}g(h^2 - d^2) \end{bmatrix}_a, \quad \mathrm{F}_y^{\,V} = \begin{bmatrix} 0 \\ hA\left(\frac{\partial \overline{u}}{\partial y} + \frac{\partial \overline{v}}{\partial x}\right) \\ hA\left(2\frac{\partial \overline{v}}{\partial x}\right) \end{bmatrix} \tag{3.11}$$

$$\boldsymbol{S} = \begin{bmatrix} 0 \\ g\eta\frac{\partial d}{\partial x} + f\overline{v}h - \frac{h}{\rho_0}\frac{\partial p_a}{\partial x} - \frac{gh^2}{2\rho_0}\frac{\partial \rho}{\partial x} - \frac{1}{\rho_0}\left(\frac{\partial s_{xx}}{\partial x} + \frac{\partial s_{xy}}{\partial y}\right) \\ \qquad + \frac{\tau_{sx}}{\rho_0} - \frac{\tau_{bx}}{\rho_0} + hu_s \\ g\eta\frac{\partial d}{\partial y} - f\overline{u}h - \frac{h}{\rho_0}\frac{\partial p_a}{\partial y} - \frac{gh^2}{2\rho_0}\frac{\partial \rho}{\partial y} - \frac{1}{\rho_0}\left(\frac{\partial s_{yx}}{\partial x} + \frac{\partial s_{yy}}{\partial y}\right) \\ \qquad + \frac{\tau_{sy}}{\rho_0} - \frac{\tau_{by}}{\rho_0} + hv_s \end{bmatrix}$$

In Cartesian coordinates the system of 3D shallow water equations can be written

$$\frac{\partial \boldsymbol{U}}{\partial t} + \frac{\partial \boldsymbol{F}_x^I}{\partial x'} + \frac{\partial \boldsymbol{F}_y^I}{\partial y'} + \frac{\partial \boldsymbol{F}_\sigma^I}{\partial \sigma} + \frac{\partial \boldsymbol{F}_x^V}{\partial x} + \frac{\partial \boldsymbol{F}_y^V}{\partial y} + \frac{\partial \boldsymbol{F}_\sigma^V}{\partial \sigma} = \boldsymbol{S} \tag{3.12}$$

where the superscripts *I* and *V* denote the inviscid (convective) and viscous fluxes, respectively and where

$$\boldsymbol{U}=\begin{bmatrix} h \\ hu \\ hv \end{bmatrix},$$

$$\boldsymbol{F}_x^I=\begin{bmatrix} h\overline{u} \\ hu^2+\frac{1}{2}g(h^2-d^2) \\ huv \end{bmatrix},\quad \boldsymbol{F}_x^V=\begin{bmatrix} 0 \\ hA\left(2\frac{\partial u}{\partial x}\right) \\ hA\left(\frac{\partial u}{\partial y}+\frac{\partial v}{\partial x}\right) \end{bmatrix}$$

$$\boldsymbol{F}_y^I=\begin{bmatrix} h\overline{v} \\ hvu \\ hv^2+\frac{1}{2}g(h^2-d^2) \end{bmatrix},\quad \boldsymbol{F}_y^V=\begin{bmatrix} 0 \\ hA\left(\frac{\partial u}{\partial y}+\frac{\partial v}{\partial x}\right) \\ hA\left(2\frac{\partial v}{\partial x}\right) \end{bmatrix} \tag{3.13}$$

$$\boldsymbol{F}_\sigma^I=\begin{bmatrix} h\omega \\ h\omega u \\ h\omega v \end{bmatrix},\quad \boldsymbol{F}_\sigma^V=\begin{bmatrix} 0 \\ \frac{\upsilon_t}{h}\frac{\partial u}{\partial \sigma} \\ \frac{\upsilon_t}{h}\frac{\partial v}{\partial \sigma} \end{bmatrix}$$

$$\boldsymbol{S}=\begin{bmatrix} 0 \\ g\eta\frac{\partial d}{\partial x}+fvh-\frac{h}{\rho_0}\frac{\partial p_a}{\partial x'}-\frac{hg}{\rho_0}\int_z^\eta\frac{\partial \rho}{\partial x}dz-\frac{1}{\rho_0}\left(\frac{\partial s_{xx}}{\partial x}+\frac{\partial s_{xy}}{\partial y}\right)+hu_s \\ g\eta\frac{\partial d}{\partial y}-fuh-\frac{h}{\rho_0}\frac{\partial p_a}{\partial y'}-\frac{hg}{\rho_0}\int_z^\eta\frac{\partial \rho}{\partial y}dz-\frac{1}{\rho_0}\left(\frac{\partial s_{yx}}{\partial x}+\frac{\partial s_{yy}}{\partial y}\right)+hv_s \end{bmatrix}$$

Integrating Eq. (3.9) over the *i*th cell and using Gauss's theorem to rewrite the flux integral gives

$$\int_{A_i}\frac{\partial \boldsymbol{U}}{\partial t}d\Omega+\int_{\Gamma_i}(\boldsymbol{F}\cdot\boldsymbol{n})\,ds=\int_{A_i}\boldsymbol{S}(\boldsymbol{U})d\Omega \tag{3.14}$$

where A_i is the area/volume of the cell Ω is the integration variable defined on A_i, Γ_i is the boundary of the *i*th cell and *ds* is the integration variable along the boundary. ***n*** is the unit outward normal vector along the boundary. Evaluating the area/volume integrals by a one-point quadrature rule, the quadrature point being the centroid of the cell, and evaluating the boundary intergral using a mid-point quadrature rule, Eq. (3.14) can be written

$$\frac{\partial U_i}{\partial t} + \frac{1}{A_i}\sum_j^{NS} \boldsymbol{F}\cdot\boldsymbol{n}\,\Delta\Gamma_j = S_i \tag{3.15}$$

Here U_i and S_i, respectively, are average values of U and S over the *i*th cell and stored at the cell centre, NS is the number of sides of the cell, n_j is the unit outward normal vector at the *j*th side and $\Delta\Gamma_j$ the length/area of the *j*th interface.

Both a first order and a second order scheme can be applied for the spatial discretization.

For the 2D case an approximate Riemann solver (Roe's scheme, see Roe, 1981) is used to calculate the convective fluxes at the interface of the cells. Using the Roe's scheme the dependent variables to the left and to the right of an interface have to be estimated. Second-order spatial accuracy is achieved by employing a linear gradient-reconstruction technique. The average gradients are estimated using the approach by Jawahar and Kamath, 2000. To avoid numerical oscillations a second order TVD slope limiter (Van Leer limiter, see Hirch, 1990 and Darwish, 2003) is used.

For the 3D case an approximate Riemann solver (Roe's scheme, see Roe, 1981) is used to calculate the convective fluxes at the vertical interface of the cells (x'y'-plane). Using the Roe's scheme the dependent variables to the left and to the right of an interface have to be estimated. Second-order spatial accuracy is achieved by employing a linear gradient-reconstruction technique. The average gradients are estimated using the approach by Jawahar and Kamath, 2000. To avoid numerical oscillations a second order TVD slope limiter (Van Leer limiter, see Hirch, 1990 and Darwish, 2003) is used. The convective fluxes at the horizontal interfaces (vertical line) are derived using first order upwinding for the low order scheme. For the higher order scheme the fluxes are approximated by the mean value of the fluxes calculated based on the cell values above and below the interface for the higher order scheme.

3.1.3 Transport equations

The transport equations arise in the salt and temperature model, the turbulence model and the generic transport model. They all share the form of Equation Eq. (2.20) in Cartesian coordinates. For the 2D case the integral form of the transport equation can be given by Eq. (3.9) where

$$\boldsymbol{U} = h\overline{C}$$

$$\begin{aligned}\boldsymbol{F}^I &= \left[h\overline{u}\overline{C},\quad h\overline{v}\overline{C}\right]\\ \boldsymbol{F}^V &= \left[hD_h\frac{\partial\overline{C}}{\partial x},\quad hD_h\frac{\partial\overline{C}}{\partial y}\right]\end{aligned} \tag{3.16}$$

$$\boldsymbol{S} = -hk_p\overline{C} + hC_sS.$$

For the 3D case the integral form of the transport equation can be given by Eq. (3.9) where

$$\boldsymbol{U} = hC$$

$$\boldsymbol{F}^I = \left[huC, \quad hvC, \quad h\omega C\right]$$
$$\boldsymbol{F}^V = \left[hD_h\partial\frac{\partial C}{\partial x}, \quad hD_h\partial\frac{\partial C}{\partial y}, \quad h\frac{D_h}{h}\partial\frac{\partial C}{\partial \sigma}\right] \tag{3.17}$$

$$\boldsymbol{S} = -hk_pC + hC_sS.$$

The discrete finite volume form of the transport equation is given by Eq. (3.15). As for the shallow water equations both a first order and a second order scheme can be applied for the spatial discretization.

In 2D the low order approximation uses simple first order upwinding, i.e., element average values in the upwinding direction are used as values at the boundaries. The higher order version approximates gradients to obtain second order accurate values at the boundaries. Values in the upwinding direction are used. To provide stability and minimize oscillatory effects, a TVD-MUSCL limiter is applied (see Hirch, 1990, and Darwish, 2003).

In 3D the low order version uses simple first order upwinding. The higher order version approximates horizontal gradients to obtain second order accurate values at the horizontal boundaries. Values in the upwinding direction are used. To provide stability and minimize oscillatory effects, an ENO (Essentially Non-Oscillatory) type procedure is applied to limit the horizontal gradients. In the vertical direction a 3rd order ENO procedure is used to obtain the vertical face values (Shu, 1997).

3.2 Time Integration

Consider the general form of the equations

$$\frac{\partial \boldsymbol{U}}{\partial t} = \boldsymbol{G}(\boldsymbol{U}) \tag{3.18}$$

For 2D simulations, there are two methods of time integration for both the shallow water equations and the transport equations: A low order method and a higher order method. The low order method is a first order explicit Euler method

$$\boldsymbol{U}_{n+1} = \boldsymbol{U}_n + \Delta t\ \boldsymbol{G}(\boldsymbol{U}_n) \tag{3.19}$$

where Δt is the time step interval. The higher order method uses a second order Runge Kutta method on the form:

$$\begin{aligned}\boldsymbol{U}_{n+\frac{1}{2}} &= \boldsymbol{U}_n + \tfrac{1}{2}\Delta t\ \boldsymbol{G}(\boldsymbol{U}_n)\\ \boldsymbol{U}_{n+1} &= \boldsymbol{U}_n + \Delta t\ \boldsymbol{G}(\boldsymbol{U}_{n+\frac{1}{2}})\end{aligned} \tag{3.20}$$

For 3D simulations the time integration is semi-implicit. The horizontal terms are treated implicitly and the vertical terms are treated implicitly or partly explicitly and partly implicitly. Consider the equations in the general semi-implicit form.

$$\frac{\partial \boldsymbol{U}}{\partial t} = \boldsymbol{G}_h(\boldsymbol{U}) + \boldsymbol{G}_v(B\boldsymbol{U}) = \boldsymbol{G}_h(\boldsymbol{U}) + \boldsymbol{G}_v^I(\boldsymbol{U}) + \boldsymbol{G}_v^V(\boldsymbol{U}) \tag{3.21}$$

where the h and v subscripts refer to horizontal and vertical terms, respectively, and the superscripts refer to invicid and viscous terms, respectively. As for 2D simulations, there is a lower order and a higher order time integration method.

The low order method used for the 3D shallow water equations can written as

$$\boldsymbol{U}_{n+1} - \tfrac{1}{2}\Delta t\left(\boldsymbol{G}_v(\boldsymbol{U}_{n+1}) + \boldsymbol{G}_v(\boldsymbol{U}_n)\right) = \boldsymbol{U}_n + \Delta t\ \boldsymbol{G}_h(\boldsymbol{U}_n) \tag{3.22}$$

The horizontal terms are integrated using a first order explicit Euler method and the vertical terms using a second order implicit trapezoidal rule. The higher order method can be written

$$\begin{aligned} \boldsymbol{U}_{n+1/2} - \tfrac{1}{4}\Delta t\ \left(\boldsymbol{G}_v(\boldsymbol{U}_{n+1/2}) + \boldsymbol{G}_v(\boldsymbol{U}_n)\right) &= \boldsymbol{U}_n + \tfrac{1}{2}\Delta t\ \boldsymbol{G}_h(\boldsymbol{U}_n) \\ \boldsymbol{U}_{n+1} - \tfrac{1}{2}\Delta t\ \left(\boldsymbol{G}_v(\boldsymbol{U}_{n+1}) + \boldsymbol{G}_v(\boldsymbol{U}_n)\right) &= \boldsymbol{U}_n + \Delta t\ \boldsymbol{G}_h(\boldsymbol{U}_{n+1/2}) \end{aligned} \tag{3.23}$$

The horizontal terms are integrated using a second order Runge Kutta method and the vertical terms using a second order implicit trapezoidal rule.

The low order method used for the 3D transport equation can written as

$$\boldsymbol{U}_{n+1} - \tfrac{1}{2}\Delta t\left(\ \boldsymbol{G}_v^V(\boldsymbol{U}_{n+1}) + \boldsymbol{G}_v^V(\boldsymbol{U}_n)\right) = \boldsymbol{U}_n + \Delta t\ \boldsymbol{G}_h(\boldsymbol{U}_n) + \Delta t\ \boldsymbol{G}_v^I(\boldsymbol{U}_n) \tag{3.24}$$

The horizontal terms and the vertical convective terms are integrated using a first order explicit Euler method and the vertical viscous terms are integrated using a second order implicit trapezoidal rule. The higher order method can be written

$$\begin{aligned} \boldsymbol{U}_{n+1/2} - \tfrac{1}{4}\Delta t\ \left(\boldsymbol{G}_v^V(\boldsymbol{U}_{n+1/2}) + \boldsymbol{G}_v^V(\boldsymbol{U}_n)\right) = \\ \boldsymbol{U}_n + \tfrac{1}{2}\Delta t\ \boldsymbol{G}_h(\boldsymbol{U}_n) + \tfrac{1}{2}\Delta t\ \boldsymbol{G}_v^I(\boldsymbol{U}_n) \\ \boldsymbol{U}_{n+1} - \tfrac{1}{2}\Delta t\ \left(\boldsymbol{G}_v^V(\boldsymbol{U}_{n+1}) + \boldsymbol{G}_v^V(\boldsymbol{U}_n)\right) = \\ \boldsymbol{U}_n + \Delta t\ \boldsymbol{G}_h(\boldsymbol{U}_{n+1/2}) + \Delta t\ \boldsymbol{G}_v^I(\boldsymbol{U}_{n+1/2}) \end{aligned} \tag{3.25}$$

The horizontal terms and the vertical convective terms are integrated using a second order Runge Kutta method and the vertical terms are integrated using a second order implicit trapezoidal rule for the vertical terms.

3.3 Boundary Conditions

3.3.1 Closed boundaries

Along closed boundaries (land boundaries), normal fluxes are forced to zero for all variables. For the momentum equations, this leads to full-slip along land boundaries. For the shallow water equations, the no slip condition can also be applied where both the normal and tangential velocity components are zero.

3.3.2 Open boundaries

For the shallow water equations a number of different boundary conditions can be applied

The flux, velocity and Flather boundary conditions are all imposed using a weak approach. A ghost cell technique is applied where the primitive variables in the ghost cell are specified. The water level is evaluated based on the value of the adjacent interior cell, and the velocities are evaluated based on the boundary information. For a discharge boundary, the transverse velocity is set to zero for inflow and passively advected for outflow. The boundary flux is then calculated using an approximate Riemann solver.

The Flather (1976) condition is one of the most efficient open boundary conditions. It is very efficient in connection with downscaling coarse model simulations to local areas (see Oddo and Pinardi (2007)). The instabilities, which are often observed when imposing stratified density at a water level boundary, can be avoided using Flather conditions

The level boundary is imposed using a strong approach based on the characteristic theory (see e.g. Sleigh et al., 1998).

The discharge boundary condition is imposed using both a weak formulation using ghost cell technique described above and a strong approach based on the characteristic theory (see e.g. Sleigh et al., 1998).

Note that using the weak formulation for a discharge boundary the effective discharge over the boundary may deviate from the specified discharge.

For transport equations, either a specified value or a zero gradient can be given. For specified values, the boundary conditions are imposed by applying the specified concentrations for calculation of the boundary flux. For a zero gradient condition, the concentration at the boundary is assumed to be identical to the concentration at the adjacent interior cell.

3.3.3 Flooding and drying

The approach for treatment of the moving boundaries problem (flooding and drying fronts) is based on the work by Zhao et al. (1994) and Sleigh et al. (1998). When the depths are small the problem is reformulated and only when the depths are very small the elements/cells are removed from the calculation. The reformulation is made by setting the momentum fluxes to zero and only taking the mass fluxes into consideration.

The depth in each element/cell is monitored and the elements are classified as dry, partially dry or wet. Also the element faces are monitored to identify flooded boundaries.

- An element face is defined as flooded if the following two criteria are satisfied: Firstly, the water depth at one side of face must be less than a tolerance depth, h_{dry} , and the water depth at the other side of the face larger than a tolerance depth, h_{flood} . Secondly, the sum of the still water depth at the side for which the water depth is less than h_{dry} and the surface elevation at the other side must be larger than zero.

- An element is dry if the water depth is less than a tolerance depth, h_{dry}, and no of the element faces are flooded boundaries. The element is removed from the calculation.
- An element is partially dry if the water depth is larger than h_{dry} and less than a tolerance depth, h_{wet}, or when the depth is less than the h_{dry} and one of the element faces is a flooded boundary. The momentum fluxes are set to zero and only the mass fluxes are calculated.
- An element is wet if the water depth is greater than h_{wet}. Both the mass fluxes and the momentum fluxes are calculated.

The wetting depth, h_{wet}, must be larger than the drying depth, h_{dry}, and flooding depth, h_{flood}, must satisfy

$$h_{dry} < h_{flood} < h_{wet} \tag{3.26}$$

The default values are $h_{dry} = 0.005\,m$, $h_{flood} = 0.05\,m$ and $h_{wet} = 0.1\,m$.

Note, that for very small values of the tolerance depth, h_{wet}, unrealistically high flow velocities can occur in the simulation and give cause to stability problems.

4 Infiltration and Leakage

The effect of infiltration and leakage at the surface zone may be important in cases of flooding scenarios on otherwise dry land. It is possible to account for this in one of two ways: by Net infiltration rates or by constant infiltration with capacity.

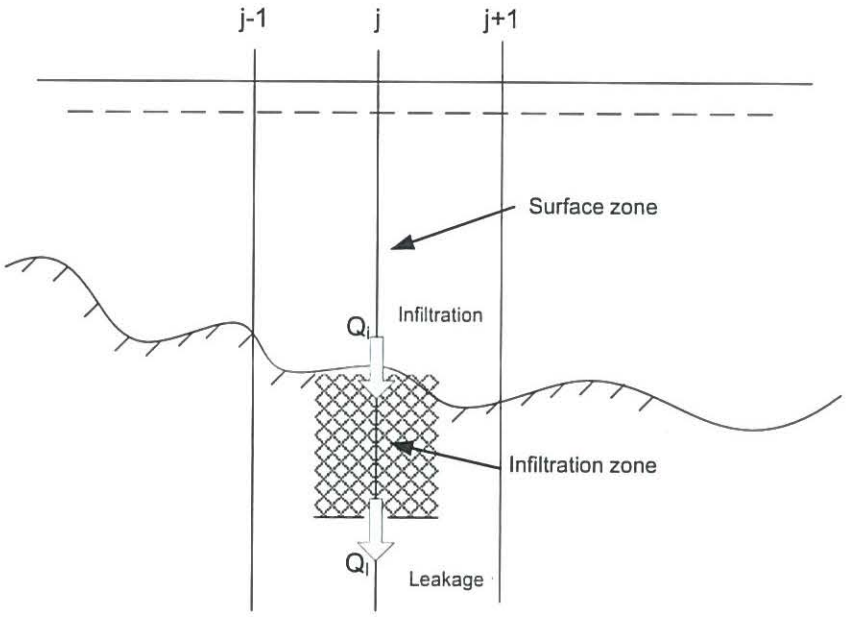

Figure 4.1 Illustration of infiltration process

4.1 Net Infiltration Rates

The net infiltration rate is defined directly. This will act as a simple sink in each element in the overall domain area.

The one-dimensional vertical continuity equation is solved at each hydrodynamic time step after the two-dimensional horizontal flow equations have been solved. The calculation of the new water depth in the free surface zone for each horizontal element is found by

$$H(j) = H(j) - V_{infiltration}(j) \,/A(j) \tag{4.1}$$

Where $V_{infiltration}(j)$ is the infiltrated volume in element (j) and A(j) the area of the element.

If $H(j)$ becomes marked as *dry* then element (j) will be taken out of the two-dimensional horizontal flow calculations and no infiltration can occur until the element is flooded again.

In summary: when using Net infiltration rate an unsaturated zone is never specified and thus has no capacity limits, so the specified infiltration rates will always be fully effectuated as long as there is enough water available in the element.

4.2 Constant Infiltration with Capacity

Constant infiltration with capacity describes the infiltration from the free surface zone to the unsaturated zone and from the unsaturated zone to the saturated zone by a simplified model. The model assumes the following:

- The unsaturated zone is modelled as an infiltration zone with constant porosity over the full depth of the zone.
- The flow between the free surface zone and the infiltration zone is based on a constant flow rate, i.e. $V_{infiltration} = Q_i \cdot \Delta t$ where Q_i is the prescribed flow rate.
- The flow between the saturated and unsaturated zone is modelled as a leakage Q_l having a constant flow rate, i.e. $V_{leakage} = Q_l \cdot \Delta t$.

The simplified model described above is solved through a one-dimensional continuity equation. Feedback from the infiltration and leakage to the two-dimensional horizontal hydrodynamic calculations is based solely on changes to the depth of the free surface zone – the water depth.

Note that the infiltration flow cannot exceed the amount of water available in the free surface water zone nor the difference between the water capacity of the infiltration zone and the actual amount of water stored there. It is possible that the infiltration flow completely drains the free surface zone from water and thus creates a dried-out point in the two-dimensional horizontal flow calculations.

The one-dimensional vertical continuity equation is solved at each hydrodynamic time step after the two-dimensional horizontal flow equations have been solved. The solution proceeds in the following way:

1. Calculation of the volume from leakage flow in each horizontal element – $V_{leakage}(j)$

$$V_{leakage}(j) = Q_l(j) \cdot \Delta t \cdot A(j) \tag{4.2}$$

$$V_{leakage}(j) = \min(V_{leakage}(j), V_i(j)) \tag{4.3}$$

$$V_i(j) := V_i(j) - V_{leakage}(j) \tag{4.4}$$

Where $V_i(j)$ is the total amount of water in the infiltration zone and $Q_l(j)$ is the leakage flow rate.

2. Calculation of the volume from infiltration flow in each horizontal element – $V_{infiltration}(j)$

$$V_{infiltration}(j) = Q_i(j) \cdot \Delta t \cdot A(j) \tag{4.5}$$

$$V_{infiltration}(j) = \min\left(V_{infiltration}(j), SC_i(j) - V_i(j), H(j) \cdot A(j)\right) \tag{4.6}$$

$$V_i(j) := V_i(j) + V_{infiltration}(j) \tag{4.7}$$

Where $Q_i(j)$ is the infiltration rate, $SC_i(j)$ is the water storage capacity and $H(j)$ the depth of the free surface.

3. Calculation of the new water depth in the free surface zone for each horizontal element

$$H(j) = H(j) - V_{infiltration}(j)/A(j) \quad (4.8)$$

If $H(j)$ becomes marked as *dry* then element *(j)* will be taken out of the two-dimensional horizontal flow calculations. The element can still *leak* but no infiltration can occur until the element is flooded again.

The water storage capacity of the infiltration zone is calculated as

$$SC_i(j) = Z_i(j) \cdot A(j) \cdot \gamma(j) \quad (4.9)$$

Where $Z_i(j)$ is the depth of the infiltration zone and $\gamma(j)$ is the porosity of the same zone.

In summary, when using Constant infiltration with capacity there can be situations where the picture is altered and the rates are either only partially effectuated or not at all:

- If $= H(j) < H_{dry}$ on the surface (dry surface) => infiltration rate is not effectuated
- If: the water volume in the infiltration zone reaches the full capacity => infiltration rate is not effectuated
- If: the water volume is zero in the infiltration zone (the case in many initial conditions) => leakage rate is not effectuated
- Leakage volume must never eclipse the available water volume in the infiltration zone, if so we utilise the available water volume in infiltration zone as leakage volume
- Infiltration volume must never eclipse the available water volume on the surface, if so we utilise the available water on the surface as infiltration volume

5 Validation

The new finite-volume model has been successfully tested in a number of basic, idealised situations for which computed results can be compared with analytical solutions or information from the literature. The model has also been applied and tested in more natural geophysical conditions; ocean scale, inner shelves, estuaries, lakes and overland, which are more realistic and complicated than academic and laboratory tests. A detailed validation report is under preparation.

This chapter presents a comparison between numerical model results and laboratory measurements for a dam-break flow in an L-shaped channel.

Additional information on model validation and applications can be found here

http://www.mikepoweredbydhi.com/download/product-documentation

5.1 Dam-break Flow through Sharp Bend

The physical model to be studied combines a square-shaped upstream reservoir and an L-shaped channel. The flow will be essentially two-dimensional in the reservoir and at the angle between the two reaches of the L-shaped channel. However, there are numerical and experimental evidences that the flow will be mostly unidimensional in both rectilinear reaches. Two characteristics or the dam-break flow are of special interest, namely

- The "damping effect" of the corner
- The upstream-moving hydraulic jump which forms at the corner

The multiple reflections of the expansion wave in the reservoir will also offer an opportunity to test the 2D capabilities of the numerical models. As the flow in the reservoir will remain subcritical with relatively small-amplitude waves, computations could be checked for excessive numerical dissipation.

5.1.1 Physical experiments

A comprehensive experimental study of a dam-break flow in a channel with a 90 bend has been reported by Frazão and Zech (2002, 1999a, 1999b). The channel is made of a 3.92 and a 2.92 metre long and 0.495 metre wide rectilinear reaches connected at right angle by a 0.495 x 0.495 m square element. The channel slope is equal to zero. A guillotine-type gate connects this L-shaped channel to a 2.44 x 2.39 m (nearly) square reservoir. The reservoir bottom level is 33 cm lower that the channel bed level. At the downstream boundary a chute is placed. See the enclosed figure for details.

Frazão and Zech performed measurements for both dry bed and wet bed condition. Here comparisons are made for the case where the water in the reservoir is initially at rest, with the free surface 20 cm above the channel bed level, i.e. the water depth in the reservoir is 53 cm. The channel bed is initially dry. The Manning coefficients evaluated through steady-state flow experimentation are 0.0095 and 0.0195 $s/m^{1/3}$, respectively, for the bed and the walls of the channel.

The water level was measured at six gauging points. The locations of the gauges are shown in Figure 5.1 and the coordinates are listed in Table 5.1.

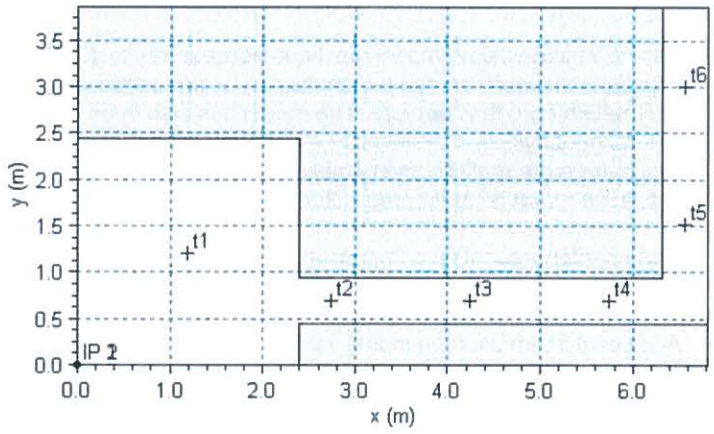

Figure 5.1 Set-up of the experiment by Frazão and Zech (2002)

Table 5.1 Location of the gauging points

Location	x (m)	y (m)
T1	1.19	1.20
T2	2.74	0.69
T3	4.24	0.69
T4	5.74	0.69
T5	6.56	1.51
T6	6.56	3.01

5.1.2 Numerical experiments

Simulations are performed using both the two-dimensional and the three-dimensional shallow water equations.

An unstructured mesh is used containing 18311 triangular elements and 9537 nodes. The minimum edge length is 0.01906 m and the maximum edge length is 0.06125 m. In the 3D simulation 10 layers is used for the vertical discretization. The time step is 0.002 s. At the downstream boundary, a free outfall (absorbing) boundary condition is applied. The wetting depth, flooding depth and drying depth are 0.002 m, 0.001 m and 0.0001 m, respectively.

A constant Manning coefficient of 105.26 $m^{1/3}/s$ is applied in the 2D simulations, while a constant roughness height of $5 \cdot 10^{-5}$ m is applied in the 3D simulation.

5.1.3 Results

In Figure 5.2 time series of calculated surface elevations at the six gauges locations are compared to the measurements. In Figure 5.3 contour plots of the surface elevations are shown at T = 1.6, 3.2 and 4.8 s (two-dimensional simulation).

In Figure 5.4 a vector plot and contour plots of the current speed at a vertical profile along the centre line (from (x,y)=(5.7, 0.69) to (x,y)=(6.4, 0.69)) at T = 6.4 s is shown.

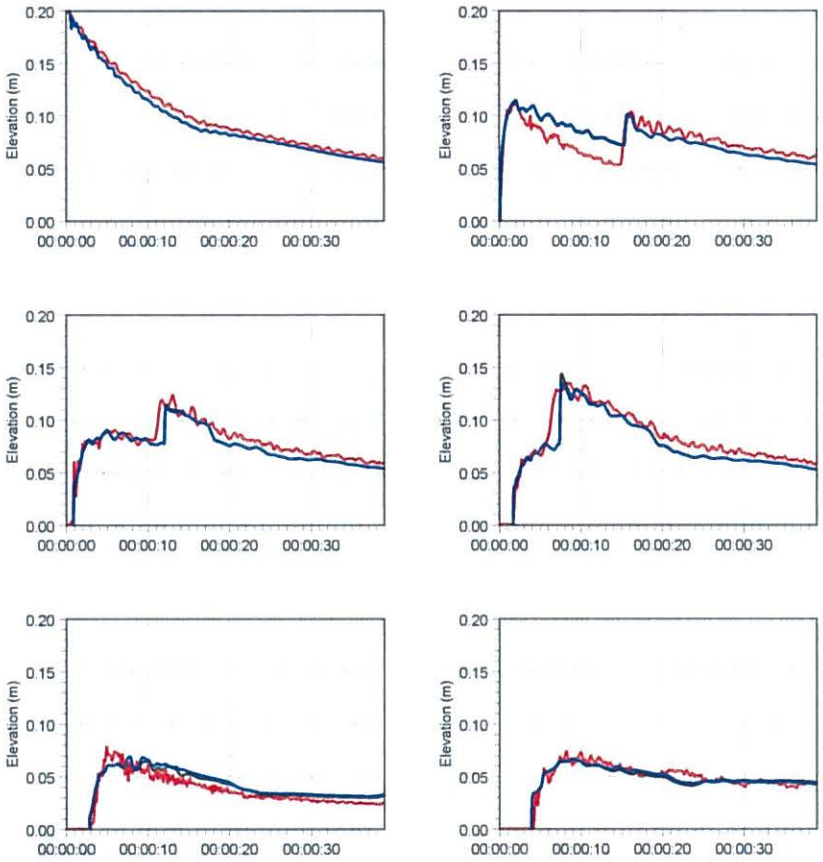

Figure 5.2 Time evolution of the water level at the six gauge locations. (blue) 3D calculation, (black) 2D calculation and (red) Measurements by Frazão and Zech (1999a,b)

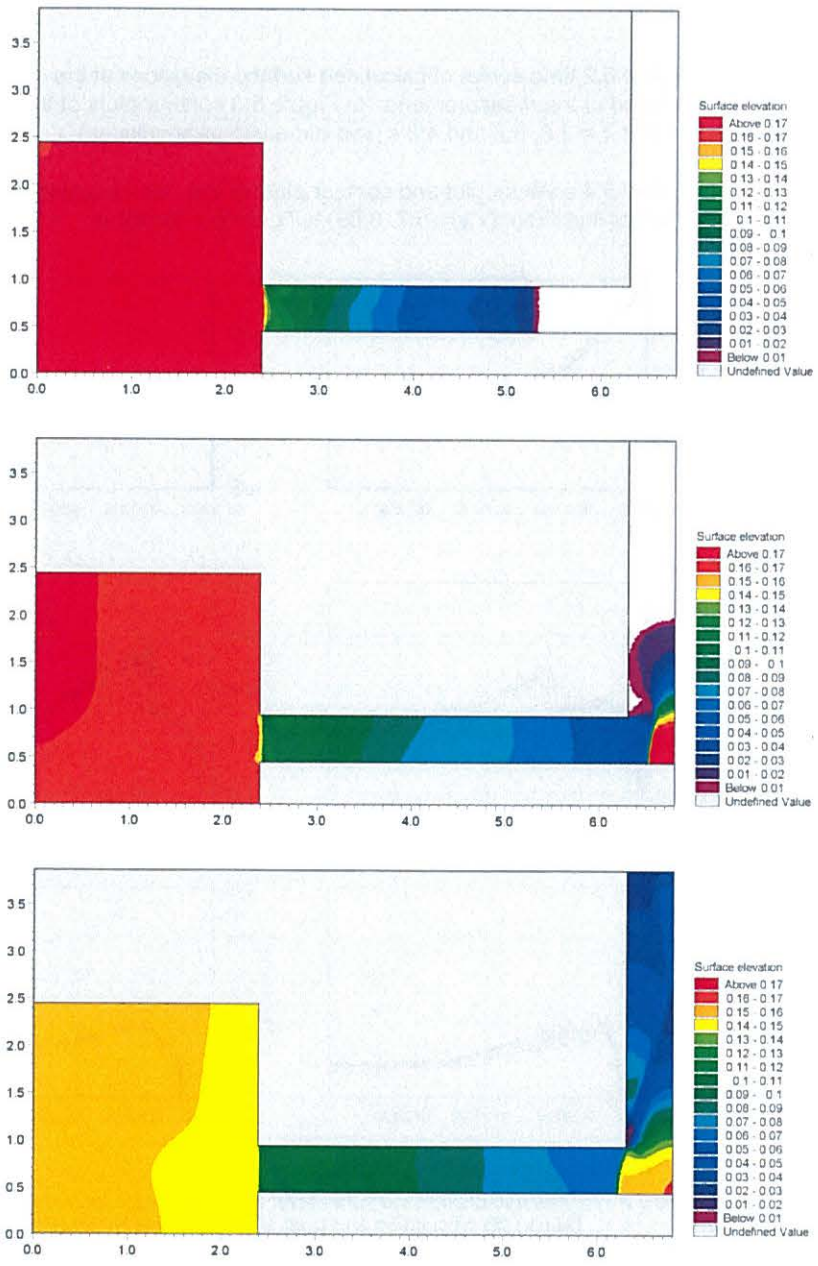

Figure 5.3 Contour plots of the surface elevation at T = 1.6 s (top), T = 3.2 s (middle) and T = 4.8 s (bottom).

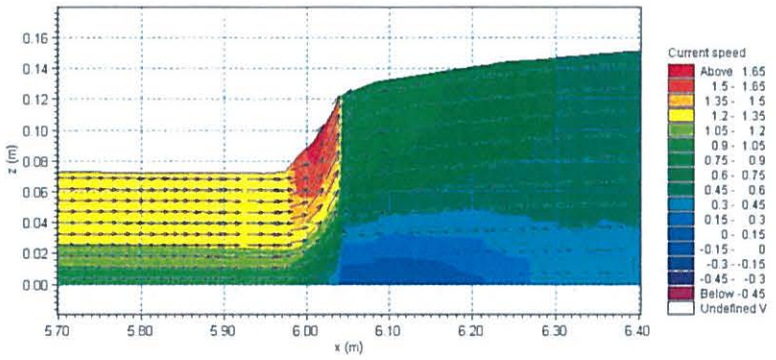

Figure 5.4 Vector plot and contour plots of the current speed at a vertical profile along the centre line at T = 6.4 s

6 References

/1/ Darwish M.S. and Moukalled F. (2003), TVD schemes for unstructured grids, Int. J. of Heat and Mass Transfor, 46, 599-611)

/2/ Fredsøe, J. (1984), Turbulent boundary layers in Combined Wave Current Motion. J. Hydraulic Engineering, ASCE, Vol 110, No. HY8, pp. 1103-1120.

/3/ Geernaert G.L. and Plant W.L (1990), Surface Waves and fluxes, Volume 1 – Current theory, Kluwer Academic Publishers, The Netherlands.

/4/ Hirsch, C. (1990). Numerical Computation of Internal and External Flows, Volume 2: Computational Methods for Inviscid and Viscous Flows, Wiley.

/5/ Iqbal M. (1983). An Introduction to solar Radiation, Academic Press.

/6/ Jawahar P. and H. Kamath. (2000). A high-resolution procedure for Euler and Navier-Stokes computations on unstructured grids, Journal Comp. Physics, 164, 165-203.

/7/ Jones, O., Zyserman, J.A. and Wu, Yushi (2014), Influence of Apparent Roughness on Pipeline Design Conditions under Combined Waves and Current, *Proceedings of the ASME 2014 33rd International Conference on Ocean, Offshore and Arctic Engineering*.

/8/ Kantha and Clayson (2000). Small Scale Processes in Geophysical Fluid flows, International Geophysics Series, Volume 67.

/9/ Lind & Falkenmark (1972), Hydrology: en inledning till vattenressursläran, Studentlitteratur (in Swedish).

/10/ Munk, W., Anderson, E. (1948), Notes on the theory of the thermocline, Journal of Marine Research, 7, 276-295.

/11/ Oddo P. and N. Pinardi (2007), Lateral open boundary conditions for nested limited area models: A scale selective approach, Ocean Modelling 20 (2008) 134-156.

/12/ Pugh, D.T. (1987), Tides, surges and mean sea-level: a handbook for engineers and scientists. Wiley, Chichester, 472pp

/13/ Rodi, W. (1984), Turbulence models and their applications in hydraulics, IAHR, Delft, the Netherlands.

/14/ Rodi, W. (1980), Turbulence Models and Their Application in Hydraulics - A State of the Art Review, Special IAHR Publication.

/15/ Roe, P. L. (1981), Approximate Riemann solvers, parameter vectors, and difference-schemes, Journal of Computational Physics, 43, 357-372.

/16/ Sahlberg J. (1984). A hydrodynamic model for heat contents calculations on lakes at the ice formation date, Document D4: 1984, Swedish council for Building Research.

/17/ Shu C.W. (1997), Essentially Non-Oscillatory and Weighted Essenetially Non-Oscillatory Schemes for Hyperbolic Conservation Laws, NASA/CR-97-206253, ICASE Report No. 97-65, NASA Langley Research Center, pp. 83.

/18/ Sleigh, P.A., Gaskell, P.H., Bersins, M. and Wright, N.G. (1998), An unstructured finite-volume algorithm for predicting flow in rivers and estuaries, Computers & Fluids, Vol. 27, No. 4, 479-508.

/19/ Smagorinsky (1963), J. General Circulation Experiment with the Primitive Equations, Monthly Weather Review, 91, No. 3, pp 99-164.

/20/ Soares Frazão, S. and Zech, Y. (2002), Dam-break in channel with 90° bend, Journal of Hydraulic Engineering, ASCE, 2002, 128, No. 11, 956-968.

/21/ Soares Frazão, S. and Zech, Y. (1999a), Effects of a sharp bend on dam-break flow, Proc., 28th IAHR Congress, Graz, Austria, Technical Univ. Graz, Graz, Austria (CD-Rom).

/22/ Soares Frazão, S. and Zech, Y. (1999b), Dam-break flow through sharp bends – Physical model and 2D Boltzmann model validation, Proc., CADAM Meeting Wallingford, U.K., 2-3 March 1998, European Commission, Brussels, Belgium, 151-169.

/23/ UNESCO (1981), The practical salinity scale 1978 and the international equation of state of seawater 1980, UNESCO technical papers in marine science, 36, 1981.

/24/ Wu, Jin (1994), The sea surface is aerodynamically rough even under light winds, Boundary layer Meteorology, 69, 149-158.

/25/ Wu, Jin (1980), Wind-stress Coefficients over sea surface and near neutral conditions – A revisit, Journal of Physical. Oceanography, 10, 727-740.

/26/ Zhao, D.H., Shen, H.W., Tabios, G.Q., Tan, W.Y. and Lai, J.S. (1994), Finite-volume two-dimensional unsteady-flow model for river basins, Journal of Hydraulic Engineering, ASCE, 1994, 120, No. 7, 863-833.

STUDY REPORT W&AR-03
RESERVOIR TEMPERATURE MODEL

ATTACHMENT B

MIKE3 FM SCIENTIFIC REFERENCE MANUAL 2011

This Page Intentionally Left Blank.

MIKE BY DHI

MIKE 21 & MIKE 3 FLOW MODEL FM

Hydrodynamic and Transport Module

Scientific Documentation

Agern Allé 5
DK-2970 Hørsholm
Denmark

Tel: +45 4516 9200
Support: +45 4516 9333
Fax: +45 4516 9292

mikebydhi@dhigroup.com
www.mikebydhi.com

PLEASE NOTE

COPYRIGHT

LIMITED LIABILITY

The liability of DHI is limited as specified in Section III of your 'DHI Software Licence Agreement':

'IN NO EVENT SHALL DHI OR ITS REPRESENTATIVES (AGENTS AND SUPPLIERS) BE LIABLE FOR ANY DAMAGES WHATSOEVER INCLUDING, WITHOUT LIMITATION, SPECIAL, INDIRECT, INCIDENTAL OR CONSEQUENTIAL DAMAGES OR DAMAGES FOR LOSS OF BUSINESS PROFITS OR SAVINGS, BUSINESS INTERRUPTION, LOSS OF BUSINESS INFORMATION OR OTHER PECUNIARY LOSS ARISING OUT OF THE USE OF OR THE INABILITY TO USE THIS DHI SOFTWARE PRODUCT, EVEN IF DHI HAS BEEN ADVISED OF THE POSSIBILITY OF SUCH DAMAGES. THIS LIMITATION SHALL APPLY TO CLAIMS OF PERSONAL INJURY TO THE EXTENT PERMITTED BY LAW. SOME COUNTRIES OR STATES DO NOT ALLOW THE EXCLUSION OR LIMITATION OF LIABILITY FOR CONSEQUENTIAL, SPECIAL, INDIRECT, INCIDENTAL DAMAGES AND, ACCORDINGLY, SOME PORTIONS OF THESE LIMITATIONS MAY NOT APPLY TO YOU. BY YOUR OPENING OF THIS SEALED PACKAGE OR INSTALLING OR USING THE SOFTWARE, YOU HAVE ACCEPTED THAT THE ABOVE LIMITATIONS OR THE MAXIMUM LEGALLY APPLICABLE SUBSET OF THESE LIMITATIONS APPLY TO YOUR PURCHASE OF THIS SOFTWARE.'

PRINTING HISTORY

June 2004 ..... Edition 2004
August 2005 ..... Edition 2005
April 2006 ..... Edition 2007
December 2006 ..... Edition 2007
October 2007 ..... Edition 2008
January 2009 ..... Edition 2009
February 2010 ..... Edition 2009
July 2010 ..... Edition 2011

CONTENTS

MIKE 21 & MIKE 3 FLOW MODEL FM
Hydrodynamic and Transport Module
Scientific Documentation

1 INTRODUCTION 1

2 GOVERNING EQUATIONS 3
2.1 3D Governing Equations in Cartesian Co-ordinates 3
2.1.1 Shallow water equations 3
2.1.2 Transport equations for salt and temperature 5
2.1.3 Transport equation for a scalar quantity 6
2.1.4 Turbulence model 7
2.1.5 Governing equations in Cartesian and sigma-co-ordinates 10
2.2 3D Governing Equations in Spherical and Sigma Co-ordinates 12
2.3 2D Governing Equations in Cartesian Co-ordinates 13
2.3.1 Shallow water equations 13
2.3.2 Transport equations for salt and temperature 14
2.3.3 Transport equations for a scalar quantity 15
2.4 2D Governing Equations in Spherical Co-ordinates 15
2.5 Bottom Stress 16
2.6 Wind Stress 17
2.7 Ice Coverage 18
2.8 Tidal Potential 19
2.9 Wave Radiation 20
2.10 Heat Exchange 21
2.10.1 Vaporisation 22
2.10.2 Convection 23
2.10.3 Short wave radiation 23
2.10.4 Long wave radiation 26

3 NUMERICAL SOLUTION 29
3.1 Spatial Discretization 29
3.1.1 Vertical Mesh 31
3.1.2 Shallow water equations 34
3.1.3 Transport equations 38
3.2 Time Integration 39
3.3 Boundary Conditions 40
3.3.1 Closed boundaries 40
3.3.2 Open boundaries 40
3.3.3 Flooding and drying 41

4 VALIDATION 43
4.1 Dam-break Flow through Sharp Bend 43
4.1.1 Physical experiments 43
4.1.2 Numerical experiments 45
4.1.3 Results 45

5 REFERENCES 49

1 INTRODUCTION

This document presents the scientific background for the new MIKE 21 & MIKE 3 Flow Model FM[1] modelling system developed by DHI Water & Environment. The objective is to provide the user with a detailed description of the flow and transport model equations, numerical discretization and solution methods. Also model validation is discussed in this document.

MIKE 21 & MIKE 3 Flow Model FM is based on a flexible mesh approach and it has been developed for applications within oceanographic, coastal and estuarine environments. The modelling system may also be applied for studies of overland flooding.

The system is based on the numerical solution of the two/three-dimensional incompressible Reynolds averaged Navier-Stokes equations invoking the assumptions of Boussinesq and of hydrostatic pressure. Thus, the model consists of continuity, momentum, temperature, salinity and density equations and it is closed by a turbulent closure scheme. For the 3D model the free surface is taken into account using a sigma-coordinate transformation approach.

The spatial discretization of the primitive equations is performed using a cell-centred finite volume method. The spatial domain is discretized by subdivision of the continuum into non-overlapping elements/cells. In the horizontal plane an unstructured grid is used while in the vertical domain in the 3D model a structured mesh is used. In the 2D model the elements can be triangles or quadrilateral elements. In the 3D model the elements can be prisms or bricks whose horizontal faces are triangles and quadrilateral elements, respectively.

[1] Including the MIKE 21 Flow Model FM (two-dimensional flow) and MIKE 3 Flow Model FM (three-dimensional flow)

2 GOVERNING EQUATIONS

2.1 3D Governing Equations in Cartesian Co-ordinates

2.1.1 Shallow water equations

The model is based on the solution of the three-dimensional incompressible Reynolds averaged Navier-Stokes equations, subject to the assumptions of Boussinesq and of hydrostatic pressure.

The local continuity equation is written as

$$\frac{\partial u}{\partial x}+\frac{\partial v}{\partial y}+\frac{\partial w}{\partial z}=S \tag{2.1}$$

and the two horizontal momentum equations for the x- and y-component, respectively

$$\frac{\partial u}{\partial t}+\frac{\partial u^2}{\partial x}+\frac{\partial vu}{\partial y}+\frac{\partial wu}{\partial z}=fv-g\frac{\partial \eta}{\partial x}-\frac{1}{\rho_0}\frac{\partial p_a}{\partial x}- \frac{g}{\rho_0}\int_z^{\eta}\frac{\partial \rho}{\partial x}dz-\frac{1}{\rho_0 h}\left(\frac{\partial s_{xx}}{\partial x}+\frac{\partial s_{xy}}{\partial y}\right)+F_u+\frac{\partial}{\partial z}\left(\nu_t\frac{\partial u}{\partial z}\right)+u_sS \tag{2.2}$$

$$\frac{\partial v}{\partial t}+\frac{\partial v^2}{\partial y}+\frac{\partial uv}{\partial x}+\frac{\partial wv}{\partial z}=-fu-g\frac{\partial \eta}{\partial y}-\frac{1}{\rho_0}\frac{\partial p_a}{\partial y}- \frac{g}{\rho_0}\int_z^{\eta}\frac{\partial \rho}{\partial y}dz-\frac{1}{\rho_0 h}\left(\frac{\partial s_{yx}}{\partial x}+\frac{\partial s_{yy}}{\partial y}\right)+F_v+\frac{\partial}{\partial z}\left(\nu_t\frac{\partial v}{\partial z}\right)+v_sS \tag{2.3}$$

where t is the time; x, y and z are the Cartesian co-ordinates; η is the surface elevation; d is the still water depth; $h=\eta+d$ is the total water depth; u, v and w are the velocity components in the x, y and z direction; $f=2\Omega\sin\phi$ is the Coriolis parameter (Ω is the angular rate of revolution and ϕ the geographic latitude); g is the gravitational acceleration; ρ is the density of water; s_{xx}, s_{xy}, s_{yx} and s_{yy} are components of the radiation stress tensor; ν_t is the vertical turbulent (or eddy) viscosity; p_a is the atmospheric pressure; ρ_o is the reference density of water. S is the magnitude of the discharge due to point sources and (u_s, v_s) is the velocity by which the water is discharged into the ambient water. The horizontal stress terms are described using a gradient-stress relation, which is simplified to

$$F_u = \frac{\partial}{\partial x}\left(2A\frac{\partial u}{\partial x}\right) + \frac{\partial}{\partial y}\left(A\left(\frac{\partial u}{\partial y} + \frac{\partial v}{\partial x}\right)\right) \tag{2.4}$$

$$F_v = \frac{\partial}{\partial x}\left(A\left(\frac{\partial u}{\partial y} + \frac{\partial v}{\partial x}\right)\right) + \frac{\partial}{\partial y}\left(2A\frac{\partial v}{\partial y}\right) \tag{2.5}$$

where A is the horizontal eddy viscosity.

The surface and bottom boundary condition for u, v and w are

At $z = \eta$:

$$\frac{\partial \eta}{\partial t} + u\frac{\partial \eta}{\partial x} + v\frac{\partial \eta}{\partial y} - w = 0, \quad \left(\frac{\partial u}{\partial z}, \frac{\partial v}{\partial z}\right) = \frac{1}{\rho_0 \nu_t}\left(\tau_{sx}, \tau_{sy}\right) \tag{2.6}$$

At $z = -d$:

$$u\frac{\partial d}{\partial x} + v\frac{\partial d}{\partial y} + w = 0, \quad \left(\frac{\partial u}{\partial z}, \frac{\partial v}{\partial z}\right) = \frac{1}{\rho_0 \nu_t}\left(\tau_{bx}, \tau_{by}\right) \tag{2.7}$$

where $\left(\tau_{sx}, \tau_{sy}\right)$ and $\left(\tau_{bx}, \tau_{by}\right)$ are the x and y components of the surface wind and bottom stresses.

The total water depth, h, can be obtained from the kinematic boundary condition at the surface, once the velocity field is known from the momentum and continuity equations. However, a more robust equation is obtained by vertical integration of the local continuity equation

$$\frac{\partial h}{\partial t} + \frac{\partial h\bar{u}}{\partial x} + \frac{\partial h\bar{v}}{\partial y} = hS + \hat{P} - \hat{E} \tag{2.8}$$

where $\hat{P}$ and $\hat{E}$ are precipitation and evaporation rates, respectively, and $\bar{u}$ and $\bar{v}$ are the depth-averaged velocities

$$h\bar{u} = \int_{-d}^{\eta} u dz, \quad h\bar{v} = \int_{-d}^{\eta} v dz \tag{2.9}$$

The fluid is assumed to be incompressible. Hence, the density, ρ, does not depend on the pressure, but only on the temperature, T, and the salinity, s, via the equation of state

$$\rho = \rho(T, s) \tag{2.10}$$

Here the UNESCO equation of state is used (see UNESCO, 1981).

2.1.2 Transport equations for salt and temperature

The transports of temperature, T, and salinity, s, follow the general transport-diffusion equations as

$$\frac{\partial T}{\partial t}+\frac{\partial uT}{\partial x}+\frac{\partial vT}{\partial y}+\frac{\partial wT}{\partial z}=F_T+\frac{\partial}{\partial z}\left(D_v\frac{\partial T}{\partial z}\right)+\hat{H}+T_sS \tag{2.11}$$

$$\frac{\partial s}{\partial t}+\frac{\partial us}{\partial x}+\frac{\partial vs}{\partial y}+\frac{\partial ws}{\partial z}=F_s+\frac{\partial}{\partial z}\left(D_v\frac{\partial s}{\partial z}\right)+s_sS \tag{2.12}$$

where D_v is the vertical turbulent (eddy) diffusion coefficient. $\hat{H}$ is a source term due to heat exchange with the atmosphere. T_s and s_s are the temperature and the salinity of the source. F are the horizontal diffusion terms defined by

$$(F_T,F_s)=\left[\frac{\partial}{\partial x}\left(D_h\frac{\partial}{\partial x}\right)+\frac{\partial}{\partial y}\left(D_h\frac{\partial}{\partial y}\right)\right](T,s) \tag{2.13}$$

where D_h is the horizontal diffusion coefficient. The diffusion coefficients can be related to the eddy viscosity

$$D_h=\frac{A}{\sigma_T}\quad\text{and}\quad D_v=\frac{\nu_t}{\sigma_T} \tag{2.14}$$

where σ_T is the Prandtl number. In many applications a constant Prandtl number can be used (see Rodi (1984)).

The surface and bottom boundary conditions for the temperature are

At $z=\eta$:

$$D_h\frac{\partial T}{\partial z}=\frac{Q_n}{\rho_0c_p}+T_p\hat{P}-T_e\hat{E} \tag{2.15}$$

At $z=-d$:

$$\frac{\partial T}{\partial z}=0 \tag{2.16}$$

where Q_n is the surface net heat flux and $c_p = 4217\ J/(kg \cdot °K)$ is the specific heat of the water. A detailed description for determination of $\tilde{H}$ and Q_n is given in Section 2.7.

The surface and bottom boundary conditions for the salinity are

At $z = \eta$:

$$\frac{\partial s}{\partial z} = 0 \tag{2.17}$$

At $z = -d$:

$$\frac{\partial s}{\partial z} = 0 \tag{2.18}$$

When heat exchange from the atmosphere is included, the evaporation is defined as

$$\tilde{E} = \begin{cases} \dfrac{q_v}{\rho_0 l_v} & q_v > 0 \\ 0 & q_v \le 0 \end{cases} \tag{2.19}$$

where q_v is the latent heat flux and $l_v = 2.5 \cdot 10^6$ is the latent heat of vaporisation of water.

2.1.3 Transport equation for a scalar quantity

The conservation equation for a scalar quantity is given by

$$\frac{\partial C}{\partial t} + \frac{\partial uC}{\partial x} + \frac{\partial vC}{\partial y} + \frac{\partial wC}{\partial z} = F_C + \frac{\partial}{\partial z}\left(D_v \frac{\partial C}{\partial z}\right) - k_p C + C_s S \tag{2.20}$$

where C is the concentration of the scalar quantity, k_p is the linear decay rate of the scalar quantity, C_s is the concentration of the scalar quantity at the source and D_v is the vertical diffusion coefficient. F_C is the horizontal diffusion term defined by

$$F_C = \left[\frac{\partial}{\partial x}\left(D_h \frac{\partial}{\partial x}\right) + \frac{\partial}{\partial y}\left(D_h \frac{\partial}{\partial y}\right)\right] C \tag{2.21}$$

where D_h is the horizontal diffusion coefficient.

2.1.4 Turbulence model

The turbulence is modelled using an eddy viscosity concept. The eddy viscosity is often described separately for the vertical and the horizontal transport. Here several turbulence models can be applied: a constant viscosity, a vertically parabolic viscosity and a standard k-ε model (Rodi, 1984). In many numerical simulations the small-scale turbulence can not be resolved with the chosen spatial resolution. This kind of turbulence can be approximated using sub-grid scale models.

Vertical eddy viscosity

The eddy viscosity derived from the log-law is calculated by

$$\nu_t = U_\tau h\left(c_1\frac{z+d}{h}+c_2\left(\frac{z+d}{h}\right)^2\right) \qquad (2.22)$$

where $U_\tau = \max(U_{\tau s}, U_{\tau b})$ and c_1 and c_2 are two constants. $U_{\tau s}$ and $U_{\tau b}$ are the friction velocities associated with the surface and bottom stresses, $c_1 = 0.41$ and $c_2 = -0.41$ give the standard parabolic profile.

In applications with stratification the effects of buoyancy can be included explicitly. This is done through the introduction of a Richardson number dependent damping of the eddy viscosity coefficient, when a stable stratification occurs. The damping is a generalisation of the Munk-Anderson formulation (Munk and Anderson, 1948)

$$\nu_t = \nu_t^*(1+aRi)^{-b} \qquad (2.23)$$

where ν_t^* is the undamped eddy viscosity and Ri is the local gradient Richardson number

$$Ri = -\frac{g}{\rho_0}\frac{\partial\rho}{\partial z}\left(\left(\frac{\partial u}{\partial z}\right)^2+\left(\frac{\partial v}{\partial z}\right)^2\right)^{-1} \qquad (2.24)$$

$a = 10$ and $b = 0.5$ are empirical constants.

In the k-ε model the eddy-viscosity is derived from turbulence parameters k and ε as

$$\nu_t = c_\mu\frac{k^2}{\varepsilon} \qquad (2.25)$$

where k is the turbulent kinetic energy per unit mass (TKE), ε is the dissipation of TKE and c_μ is an empirical constant.

The turbulent kinetic energy, k, and the dissipation of TKE, ε, are obtained from the following transport equations

$$\frac{\partial k}{\partial t}+\frac{\partial uk}{\partial x}+\frac{\partial vk}{\partial y}+\frac{\partial wk}{\partial z}=F_k+\frac{\partial}{\partial z}\left(\frac{\nu_t}{\sigma_k}\frac{\partial k}{\partial z}\right)+P+B-\varepsilon \tag{2.26}$$

$$\frac{\partial \varepsilon}{\partial t}+\frac{\partial u\varepsilon}{\partial x}+\frac{\partial v\varepsilon}{\partial y}+\frac{\partial w\varepsilon}{\partial z}= F_\varepsilon+\frac{\partial}{\partial z}\left(\frac{\nu_t}{\sigma_\varepsilon}\frac{\partial \varepsilon}{\partial z}\right)+\frac{\varepsilon}{k}\left(c_{1\varepsilon}P+c_{3\varepsilon}B-c_{2\varepsilon}\varepsilon\right) \tag{2.27}$$

where the shear production, P, and the buoyancy production, B, are given as

$$P=\frac{\tau_{xz}}{\rho_0}\frac{\partial u}{\partial z}+\frac{\tau_{yz}}{\rho_0}\frac{\partial v}{\partial z}\approx \nu_t\left(\left(\frac{\partial u}{\partial z}\right)^2+\left(\frac{\partial v}{\partial z}\right)^2\right) \tag{2.28}$$

$$B=-\frac{\nu_t}{\sigma_t}N^2 \tag{2.29}$$

with the Brunt-Väisälä frequency, N, defined by

$$N^2=-\frac{g}{\rho_0}\frac{\partial \rho}{\partial z} \tag{2.30}$$

σ_t is the turbulent Prandtl number and σ_k, σ_ε, $c_{1\varepsilon}$, $c_{2\varepsilon}$ and $c_{3\varepsilon}$ are empirical constants. F are the horizontal diffusion terms defined by

$$(F_k,F_\varepsilon)=\left[\frac{\partial}{\partial x}\left(D_h\frac{\partial}{\partial x}\right)+\frac{\partial}{\partial y}\left(D_h\frac{\partial}{\partial y}\right)\right](k,\varepsilon) \tag{2.31}$$

The horizontal diffusion coefficients are given by $D_h=A/\sigma_k$ and $D_h=A/\sigma_\varepsilon$, respectively.

Several carefully calibrated empirical coefficients enter the k-e turbulence model. The empirical constants are listed in (2.47) (see Rodi, 1984).

Table 2.1 Empirical constants in the k-ε model.

c_μ	$c_{1\varepsilon}$	$c_{2\varepsilon}$	$c_{3\varepsilon}$	σ_t	σ_k	σ_ε
0.09	1.44	1.92	0	0.9	1.0	1.3

At the surface the boundary conditions for the turbulent kinetic energy and its rate of dissipation depend on the wind shear, U_s

At $z = \eta$:

$$k = \frac{1}{\sqrt{c_\mu}} U_{\tau s}^2 \tag{2.32}$$

$$\varepsilon = \frac{U_{\tau s}^3}{\kappa \Delta z_b} \qquad \text{for} \quad U_s > 0$$

$$\frac{\partial k}{\partial z} = 0 \qquad \varepsilon = \frac{\left(k\sqrt{c_\mu}\right)^{3/2}}{a\kappa h} \qquad \text{for} \quad U_s = 0 \tag{2.33}$$

where κ=0.4 is the von Kármán constant, $a = 0.07$ is and empirical constant and Δz_s is the distance from the surface where the boundary condition is imposed. At the seabed the boundary conditions are

At $z = -d$:

$$k = \frac{1}{\sqrt{c_\mu}} U_{\tau b}^2 \qquad \varepsilon = \frac{U_{\tau b}^3}{\kappa \Delta z_b} \tag{2.34}$$

where Δz_b is the distance from the bottom where the boundary condition is imposed.

Horizontal eddy viscosity

In many applications a constant eddy viscosity can be used for the horizontal eddy viscosity. Alternatively, Smagorinsky (1963) proposed to express sub-grid scale transports by an effective eddy viscosity related to a characteristic length scale. The subgrid scale eddy viscosity is given by

$$A = c_s^2 l^2 \sqrt{2 S_{ij} S_{ij}} \tag{2.35}$$

where c_s is a constant, l is a characteristic length and the deformation rate is given by

$$S_{ij} = \frac{1}{2}\left(\frac{\partial u_i}{\partial x_j} + \frac{\partial u_j}{\partial x_i}\right) \quad (i,j = 1,2) \tag{2.36}$$

2.1.5 Governing equations in Cartesian and sigma-co-ordinates

The equations are solved using a vertical σ-transformation

$$\sigma = \frac{z - z_b}{h}, \quad x' = x, \quad y' = y \tag{2.37}$$

where σ varies between 0 at the bottom and 1 at the surface. The co-ordinate transformation implies relations such as

$$\frac{\partial}{\partial z} = \frac{1}{h}\frac{\partial}{\partial \sigma} \tag{2.38}$$

$$\left(\frac{\partial}{\partial x}, \frac{\partial}{\partial y}\right) = \left(\frac{\partial}{\partial x'} - \frac{1}{h}\left(-\frac{\partial d}{\partial x} + \sigma\frac{\partial h}{\partial x}\right)\frac{\partial}{\partial \sigma}, \frac{\partial}{\partial y'} - \frac{1}{h}\left(-\frac{\partial d}{\partial y} + \sigma\frac{\partial h}{\partial y}\right)\frac{\partial}{\partial \sigma}\right) \tag{2.39}$$

In this new co-ordinate system the governing equations are given as

$$\frac{\partial h}{\partial t} + \frac{\partial hu}{\partial x'} + \frac{\partial hv}{\partial y'} + \frac{\partial h\omega}{\partial \sigma} = hS \tag{2.40}$$

$$\begin{aligned}\frac{\partial hu}{\partial t} + \frac{\partial hu^2}{\partial x'} + \frac{\partial hvu}{\partial y'} + \frac{\partial h\omega u}{\partial \sigma} = fvh - gh\frac{\partial \eta}{\partial x'} - \frac{h}{\rho_0}\frac{\partial p_a}{\partial x'} - \\ \frac{hg}{\rho_0}\int_z^\eta \frac{\partial \rho}{\partial x}dz - \frac{1}{\rho_0}\left(\frac{\partial s_{xx}}{\partial x} + \frac{\partial s_{xy}}{\partial y}\right) + hF_u + \frac{\partial}{\partial \sigma}\left(\frac{\nu_v}{h}\frac{\partial u}{\partial \sigma}\right) + hu_s S\end{aligned} \tag{2.41}$$

$$\begin{aligned}\frac{\partial hv}{\partial t} + \frac{\partial huv}{\partial x'} + \frac{\partial hv^2}{\partial y'} + \frac{\partial h\omega v}{\partial \sigma} = -fuh - gh\frac{\partial \eta}{\partial y'} - \frac{h}{\rho_0}\frac{\partial p_a}{\partial y'} - \\ \frac{hg}{\rho_0}\int_z^\eta \frac{\partial \rho}{\partial y}dz - \frac{1}{\rho_0}\left(\frac{\partial s_{yx}}{\partial x} + \frac{\partial s_{yy}}{\partial y}\right) + hF_v + \frac{\partial}{\partial \sigma}\left(\frac{\nu_v}{h}\frac{\partial v}{\partial \sigma}\right) + hv_s S\end{aligned} \tag{2.42}$$

$$\begin{aligned}\frac{\partial hT}{\partial t} + \frac{\partial huT}{\partial x'} + \frac{\partial hvT}{\partial y'} + \frac{\partial h\omega T}{\partial \sigma} = \\ hF_T + \frac{\partial}{\partial \sigma}\left(\frac{D_v}{h}\frac{\partial T}{\partial \sigma}\right) + h\tilde{H} + hT_s S\end{aligned} \tag{2.43}$$

$$\frac{\partial hs}{\partial t} + \frac{\partial hus}{\partial x'} + \frac{\partial hvs}{\partial y'} + \frac{\partial h\omega s}{\partial \sigma} = hF_s + \frac{\partial}{\partial \sigma}\left(\frac{D_v}{h}\frac{\partial s}{\partial \sigma}\right) + hs_s S \tag{2.44}$$

$$\frac{\partial hk}{\partial t}+\frac{\partial huk}{\partial x'}+\frac{\partial hvk}{\partial y'}+\frac{\partial h\omega k}{\partial \sigma}= hF_k+\frac{1}{h}\frac{\partial}{\partial \sigma}\left(\frac{\nu_t}{\sigma_k}\frac{\partial k}{\partial \sigma}\right)+h(P+B-\varepsilon) \tag{2.45}$$

$$\frac{\partial h\varepsilon}{\partial t}+\frac{\partial hu\varepsilon}{\partial x'}+\frac{\partial hv\varepsilon}{\partial y'}+\frac{\partial h\omega\varepsilon}{\partial \sigma}= hF_\varepsilon+\frac{1}{h}\frac{\partial}{\partial \sigma}\left(\frac{\nu_t}{\sigma_\varepsilon}\frac{\partial \varepsilon}{\partial \sigma}\right)+h\frac{\varepsilon}{k}\left(c_{1\varepsilon}P+c_{3\varepsilon}B-c_{2\varepsilon}\varepsilon\right) \tag{2.46}$$

$$\frac{\partial hC}{\partial t}+\frac{\partial huC}{\partial x'}+\frac{\partial hvC}{\partial y'}+\frac{\partial h\omega C}{\partial \sigma}=hF_C+\frac{\partial}{\partial \sigma}\left(\frac{D_v}{h}\frac{\partial C}{\partial \sigma}\right)-hk_pC+hC_s \tag{2.47}$$

The modified vertical velocity is defined by

$$\omega=\frac{1}{h}\left[w+u\frac{\partial d}{\partial x'}+v\frac{\partial d}{\partial y'}-\sigma\left(\frac{\partial h}{\partial t}+u\frac{\partial h}{\partial x'}+v\frac{\partial h}{\partial y'}\right)\right] \tag{2.48}$$

The modified vertical velocity is the velocity across a level of constant σ. The horizontal diffusion terms are defined as

$$hF_u\approx\frac{\partial}{\partial x}\left(2hA\frac{\partial u}{\partial x}\right)+\frac{\partial}{\partial y}\left(hA\left(\frac{\partial u}{\partial y}+\frac{\partial v}{\partial x}\right)\right) \tag{2.49}$$

$$hF_v\approx\frac{\partial}{\partial x}\left(hA\left(\frac{\partial u}{\partial y}+\frac{\partial v}{\partial x}\right)\right)+\frac{\partial}{\partial y}\left(2hA\frac{\partial v}{\partial y}\right) \tag{2.50}$$

$$h(F_T,F_s,F_k,F_\varepsilon,F_c)\approx\left[\frac{\partial}{\partial x}\left(hD_h\frac{\partial}{\partial x}\right)+\frac{\partial}{\partial y}\left(hD_h\frac{\partial}{\partial y}\right)\right](T,s,k,\varepsilon,C) \tag{2.51}$$

The boundary condition at the free surface and at the bottom are given as follows

At σ=1:

$$\omega=0,\quad\left(\frac{\partial u}{\partial \sigma},\frac{\partial v}{\partial \sigma}\right)=\frac{h}{\rho_0\nu_t}\left(\tau_{sx},\tau_{sy}\right) \tag{2.52}$$

At σ=0:

(2.53)

$$\omega = 0, \quad \left(\frac{\partial u}{\partial \sigma}, \frac{\partial v}{\partial \sigma}\right) = \frac{h}{\rho_0 \nu_t}\left(\tau_{bx}, \tau_{by}\right)$$

The equation for determination of the water depth is not changed by the co-ordinate transformation. Hence, it is identical to Eq. (2.6).

2.2 3D Governing Equations in Spherical and Sigma Co-ordinates

In spherical co-ordinates the independent variables are the longitude, λ, and the latitude, ϕ. The horizontal velocity field (u,v) is defined by

$$u = R\cos\phi\frac{d\lambda}{dt} \qquad v = R\frac{d\phi}{dt} \tag{2.54}$$

where R is the radius of the earth.

In this co-ordinate system the governing equations are given as (all superscripts indicating the horizontal co-ordinate in the new co-ordinate system are dropped in the following for notational convenience)

$$\frac{\partial h}{\partial t} + \frac{1}{R\cos\phi}\left(\frac{\partial hu}{\partial \lambda} + \frac{\partial hv\cos\phi}{\partial \phi}\right) + \frac{\partial h\omega}{\partial \sigma} = hS \tag{2.55}$$

$$\begin{aligned}\frac{\partial hu}{\partial t} + \frac{1}{R\cos\phi}\left(\frac{\partial hu^2}{\partial \lambda} + \frac{\partial hvu\cos\phi}{\partial \phi}\right) + \frac{\partial h\omega u}{\partial \sigma} = \left(f + \frac{u}{R}\tan\phi\right)vh - \\ \frac{1}{R\cos\phi}\left(gh\frac{\partial \eta}{\partial \lambda} + \frac{1}{\rho_0}\frac{\partial p_a}{\partial \lambda} + \frac{g}{\rho_0}\int_z^\eta \frac{\partial \rho}{\partial \lambda}dz + \frac{1}{\rho_0}\left(\frac{\partial s_{xx}}{\partial \lambda} + \cos\phi\frac{\partial s_{xy}}{\partial \phi}\right)\right) + \\ hF_u + \frac{\partial}{\partial \sigma}\left(\frac{\nu_v}{h}\frac{\partial u}{\partial \sigma}\right) + hu_s S\end{aligned} \tag{2.56}$$

$$\begin{aligned}\frac{\partial hv}{\partial t} + \frac{1}{R\cos\phi}\left(\frac{\partial huv}{\partial \lambda} + \frac{\partial hv^2\cos\phi}{\partial \phi}\right) + \frac{\partial h\omega v}{\partial \sigma} = -\left(f + \frac{u}{R}\tan\phi\right)uh - \\ \frac{1}{R}\left(gh\frac{\partial \eta}{\partial \phi} + \frac{1}{\rho_0}\frac{\partial p_a}{\partial \phi} + \frac{g}{\rho_0}\int_z^\eta \frac{\partial \rho}{\partial \phi}dz + \frac{1}{\rho_0}\left(\frac{1}{\cos\phi}\frac{\partial s_{yx}}{\partial \lambda} + \frac{\partial s_{yy}}{\partial \phi}\right)\right) + \\ hF_v + \frac{\partial}{\partial \sigma}\left(\frac{\nu_v}{h}\frac{\partial v}{\partial \sigma}\right) + hv_s S\end{aligned} \tag{2.57}$$

$$\begin{aligned}\frac{\partial hT}{\partial t} + \frac{1}{R\cos\phi}\left(\frac{\partial huT}{\partial \lambda} + \frac{\partial hvT\cos\phi}{\partial \phi}\right) + \frac{\partial h\omega T}{\partial \sigma} = \\ hF_T + \frac{\partial}{\partial \sigma}\left(\frac{D_v}{h}\frac{\partial T}{\partial \sigma}\right) + h\bar{H} + hT_s S\end{aligned} \tag{2.58}$$

$$\frac{\partial hs}{\partial t}+\frac{1}{R\cos\phi}\left(\frac{\partial hus}{\partial \lambda}+\frac{\partial hvs\cos\phi}{\partial \phi}\right)+\frac{\partial h\omega s}{\partial \sigma}= hF_s+\frac{\partial}{\partial \sigma}\left(\frac{D_v}{h}\frac{\partial s}{\partial \sigma}\right)+hs_sS \tag{2.59}$$

$$\frac{\partial hk}{\partial t}+\frac{1}{R\cos\phi}\left(\frac{\partial huk}{\partial \lambda}+\frac{\partial hvk\cos\phi}{\partial \phi}\right)+\frac{\partial h\omega k}{\partial \sigma}= hF_k+\frac{1}{h}\frac{\partial}{\partial \sigma}\left(\frac{\nu_t}{\sigma_k}\frac{\partial k}{\partial \sigma}\right)+h(P+B-\varepsilon) \tag{2.60}$$

$$\frac{\partial h\varepsilon}{\partial t}+\frac{1}{R\cos\phi}\left(\frac{\partial hu\varepsilon}{\partial \lambda}+\frac{\partial hv\varepsilon\cos\phi}{\partial \phi}\right)+\frac{\partial h\omega\varepsilon}{\partial \sigma}= hF_\varepsilon+\frac{1}{h}\frac{\partial}{\partial \sigma}\left(\frac{\nu_t}{\sigma_\varepsilon}\frac{\partial \varepsilon}{\partial \sigma}\right)+h\frac{\varepsilon}{k}\left(c_{1\varepsilon}P+c_{3\varepsilon}B-c_{2\varepsilon}\varepsilon\right) \tag{2.61}$$

$$\frac{\partial hC}{\partial t}+\frac{1}{R\cos\phi}\left(\frac{\partial huC}{\partial \lambda}+\frac{\partial hvC\cos\phi}{\partial \phi}\right)+\frac{\partial h\omega C}{\partial \sigma}= hF_C+\frac{\partial}{\partial \sigma}\left(\frac{D_v}{h}\frac{\partial C}{\partial \sigma}\right)-hk_pC+hC_sS \tag{2.62}$$

The modified vertical velocity in spherical co-ordinates is defined by

$$\omega=\frac{1}{h}\left[w+\frac{u}{R\cos\phi}\frac{\partial d}{\partial \lambda}+\frac{v}{R}\frac{\partial d}{\partial y}-\sigma\left(\frac{\partial h}{\partial t}+\frac{u}{R\cos\phi}\frac{\partial h}{\partial \lambda}+\frac{v}{R}\frac{\partial h}{\partial \phi}\right)\right] \tag{2.63}$$

The equation determining the water depth in spherical co-ordinates is given as

$$\frac{\partial h}{\partial t}+\frac{1}{R\cos\phi}\left(\frac{\partial h\bar{u}}{\partial \lambda}+\frac{\partial h\bar{v}\cos\phi}{\partial \phi}\right)=hS \tag{2.64}$$

2.3 2D Governing Equations in Cartesian Co-ordinates

2.3.1 Shallow water equations

Integration of the horizontal momentum equations and the continuity equation over depth $h=\eta+d$ the following two-dimensional shallow water equations are obtained

$$\frac{\partial h}{\partial t}+\frac{\partial h\bar{u}}{\partial x}+\frac{\partial h\bar{v}}{\partial y}=hS \tag{2.65}$$

$$\frac{\partial h\bar{u}}{\partial t}+\frac{\partial h\bar{u}^2}{\partial x}+\frac{\partial h\bar{v}\bar{u}}{\partial y}=f\bar{v}h-gh\frac{\partial \eta}{\partial x}-\frac{h}{\rho_0}\frac{\partial p_a}{\partial x}-\frac{gh^2}{2\rho_0}\frac{\partial \rho}{\partial x}+\frac{\tau_{sx}}{\rho_0}-\frac{\tau_{bx}}{\rho_0}-\frac{1}{\rho_0}\left(\frac{\partial s_{xx}}{\partial x}+\frac{\partial s_{xy}}{\partial y}\right)+\frac{\partial}{\partial x}\left(hT_{xx}\right)+\frac{\partial}{\partial y}\left(hT_{xy}\right)+hu_sS \tag{2.66}$$

$$\frac{\partial h\bar{v}}{\partial t}+\frac{\partial h\bar{u}\bar{v}}{\partial x}+\frac{\partial h\bar{v}^2}{\partial y}=-f\bar{u}h-gh\frac{\partial \eta}{\partial y}-\frac{h}{\rho_0}\frac{\partial p_a}{\partial y}-\frac{gh^2}{2\rho_0}\frac{\partial \rho}{\partial y}+\frac{\tau_{sy}}{\rho_0}-\frac{\tau_{by}}{\rho_0}-\frac{1}{\rho_0}\left(\frac{\partial s_{yx}}{\partial x}+\frac{\partial s_{yy}}{\partial y}\right)+\frac{\partial}{\partial x}\left(hT_{xy}\right)+\frac{\partial}{\partial y}\left(hT_{yy}\right)+hv_sS \tag{2.67}$$

The overbar indicates a depth average value. For example, $\bar{u}$ and $\bar{v}$ are the depth-averaged velocities defined by

$$h\bar{u}=\int_{-d}^{\eta}u\,dz\,,\quad h\bar{v}=\int_{-d}^{\eta}v\,dz \tag{2.68}$$

The lateral stresses T_{ij} include viscous friction, turbulent friction and differential advection. They are estimated using an eddy viscosity formulation based on of the depth average velocity gradients

$$T_{xx}=2A\frac{\partial \bar{u}}{\partial x},\quad T_{xy}=A\left(\frac{\partial \bar{u}}{\partial y}+\frac{\partial \bar{v}}{\partial x}\right),\quad T_{yy}=2A\frac{\partial \bar{v}}{\partial y} \tag{2.69}$$

2.3.2 Transport equations for salt and temperature

Integrating the transport equations for salt and temperature over depth the following two-dimensional transport equations are obtained

$$\frac{\partial h\bar{T}}{\partial t}+\frac{\partial h\bar{u}\bar{T}}{\partial x}+\frac{\partial h\bar{v}\bar{T}}{\partial y}=hF_T+h\hat{H}+hT_sS \tag{2.70}$$

$$\frac{\partial h\bar{s}}{\partial t}+\frac{\partial h\bar{u}\bar{s}}{\partial x}+\frac{\partial h\bar{v}\bar{s}}{\partial y}=hF_s+hs_sS \tag{2.71}$$

where $\bar{T}$ and $\bar{s}$ is the depth average temperature and salinity.

2.3.3 Transport equations for a scalar quantity

Integrating the transport equations for a scalar quantity over depth the following two-dimensional transport equations are obtained

$$\frac{\partial h\overline{C}}{\partial t}+\frac{\partial h\overline{u}\,\overline{C}}{\partial x}+\frac{\partial h\overline{v}\,\overline{C}}{\partial y}=hF_C-hk_p\overline{C}+hC_sS \tag{2.72}$$

where $\overline{C}$ is the depth average scalar quantity.

2.4 2D Governing Equations in Spherical Co-ordinates

In spherical co-ordinates the independent variables are the longitude, λ ,and the latitude, ϕ. The horizontal velocity field (u,v) is defined by

$$\overline{u}=R\cos\phi\frac{d\lambda}{dt} \qquad \overline{v}=R\frac{d\phi}{dt} \tag{2.73}$$

where R is the radius of the earth.

In spherical co-ordinates the governing equation can be written

$$\frac{\partial h}{\partial t}+\frac{1}{R\cos\phi}\left(\frac{\partial h\overline{u}}{\partial\lambda}+\frac{\partial h\overline{v}\cos\phi}{\partial\phi}\right)=0 \tag{2.74}$$

$$\begin{aligned}&\frac{\partial h\overline{u}}{\partial t}+\frac{1}{R\cos\phi}\left(\frac{\partial h\overline{u}^2}{\partial\lambda}+\frac{\partial h\overline{v}\overline{u}\cos\phi}{\partial\phi}\right)=\left(f+\frac{\overline{u}}{R}\tan\phi\right)\overline{v}h\\&-\frac{1}{R\cos\phi}\left(gh\frac{\partial\eta}{\partial\lambda}-\frac{h}{\rho_0}\frac{\partial p_a}{\partial\lambda}+\frac{gh^2}{2\rho_0}\frac{\partial\rho}{\partial\lambda}+\frac{1}{\rho_0}\left(\frac{\partial s_{xx}}{\partial\lambda}+\cos\phi\frac{\partial s_{xy}}{\partial\phi}\right)\right)+\\&\frac{\tau_{sx}}{\rho_0}-\frac{\tau_{bx}}{\rho_0}+\frac{\partial}{\partial x}\left(hT_{xx}\right)+\frac{\partial}{\partial y}\left(hT_{xy}\right)+hu_sS\end{aligned} \tag{2.75}$$

$$\begin{aligned}&\frac{\partial h\overline{v}}{\partial t}+\frac{1}{R\cos\phi}\left(\frac{\partial h\overline{u}\overline{v}}{\partial\lambda}+\frac{\partial h\overline{v}^2\cos\varphi}{\partial t}\right)=-\left(f+\frac{\overline{u}}{R}\tan\phi\right)\overline{u}h\\&-\frac{1}{R}\left(gh\frac{\partial\eta}{\partial\phi}-\frac{h}{\rho_0}\frac{\partial p_a}{\partial\phi}+\frac{gh^2}{2\rho_0}\frac{\partial\rho}{\partial\phi}+\frac{1}{\rho_0}\left(\frac{1}{\cos\phi}\frac{\partial s_{yx}}{\partial\lambda}+\frac{\partial s_{yy}}{\partial\phi}\right)\right)+\\&\frac{\tau_{sy}}{\rho_0}-\frac{\tau_{by}}{\rho_0}+\frac{\partial}{\partial x}\left(hT_{xy}\right)+\frac{\partial}{\partial y}\left(hT_{yy}\right)+hv_sS\end{aligned} \tag{2.76}$$

$$\frac{\partial h\overline{T}}{\partial t}+\frac{1}{R\cos\phi}\left(\frac{\partial h\overline{u}\,\overline{T}}{\partial\lambda}+\frac{\partial h\overline{v}\,\overline{T}\cos\phi}{\partial\phi}\right)=hF_T+h\hat{H}+hT_sS \tag{2.77}$$

$$\frac{\partial h\overline{s}}{\partial t}+\frac{1}{R\cos\phi}\left(\frac{\partial h\overline{us}}{\partial\lambda}+\frac{\partial h\overline{vs}\cos\phi}{\partial\phi}\right)=hF_s+hs_sS \tag{2.78}$$

$$\frac{\partial h\overline{C}}{\partial t}+\frac{1}{R\cos\phi}\left(\frac{\partial h\overline{u}\overline{C}}{\partial\lambda}+\frac{\partial h\overline{v}\overline{C}\cos\phi}{\partial\phi}\right)=hF_C-hk_p\overline{C}+hC_sS \tag{2.79}$$

2.5 Bottom Stress

The bottom stress, $\vec{\tau}_b=(\tau_{bx},\tau_{by})$, is determined by a quadratic friction law

$$\frac{\vec{\tau}_b}{\rho_0}=c_f\vec{u}_b|\vec{u}_b| \tag{2.80}$$

where c_f is the drag coefficient and $\vec{u}_b=(u_b,v_b)$ is the flow velocity above the bottom. The friction velocity associated with the bottom stress is given by

$$U_{\tau b}=\sqrt{c_f|u_b|^2} \tag{2.81}$$

For two-dimensional calculations $\vec{u}_b$ is the depth-average velocity and the drag coefficient can be determined from the Chezy number, C, or the Manning number, M

$$c_f=\frac{g}{C^2} \tag{2.82}$$

$$c_f=\frac{g}{\left(Mh^{1/6}\right)^2} \tag{2.83}$$

For three-dimensional calculations $\vec{u}_b$ is the velocity at a distance Δz_b above the sea bed and the drag coefficient is determined by assuming a logarithmic profile between the seabed and a point Δz_b above the seabed

$$c_f=\frac{1}{\left(\frac{1}{\kappa}\ln\left(\frac{\Delta z_b}{z_0}\right)\right)^2} \tag{2.84}$$

where κ=0.4 is the von Kármán constant and z_0 is the bed roughness length scale. When the boundary surface is rough, z_0, depends on the roughness height, k_s

$$z_0 = mk_s \tag{2.85}$$

where m is approximately 1/30.

Note, that the Manning number can be estimated from the bed roughness length using the following

$$M = \frac{25.4}{k_s^{1/6}} \tag{2.86}$$

2.6 Wind Stress

In areas not covered by ice the surface stress, $\vec{\tau}_s = (\tau_{sx}, \tau_{sy})$, is determined by the winds above the surface. The stress is given by the following empirical relation

$$\vec{\tau}_s = \rho_a c_d |u_w| \vec{u}_w \tag{2.87}$$

where ρ_a is the density of air, c_d is the drag coefficient of air, and $\vec{u}_w = (u_w, v_w)$ is the wind speed 10 m above the sea surface. The friction velocity associated with the surface stress is given by

$$U_{\tau} = \sqrt{\frac{\rho_a c_f |\vec{u}_w|^2}{\rho_0}} \tag{2.88}$$

The drag coefficient can either be a constant value or depend on the wind speed. The empirical formula proposed by Wu (1980, 1994) is used for the parameterisation of the drag coefficient.

$$c_f = \begin{cases} c_a & w_{10} < w_a \\ c_a + \dfrac{c_b - c_a}{w_b - w_a}(w_{10} - w_a) & w_a \le w_{10} < w_b \\ c_b & w_{10} \ge w_b \end{cases} \tag{2.89}$$

where c_a, c_b, w_a and w_b are empirical factors and w_{10} is the wind velocity 10 m above the sea surface. The default values for the empirical factors are $c_a = 1.255 \cdot 10^{-3}$, $c_b = 2.425 \cdot 10^{-3}$, $w_a = 7$ m/s and $w_b = 25$ m/s. These give generally good results for open sea applications. Field measurements of the drag coefficient collected over

lakes indicate that the drag coefficient is larger than open ocean data. For a detailed description of the drag coefficient see Geernaert and Plant (1990).

2.7 Ice Coverage

It is possible to take into account the effects of ice coverage on the flow field.

In areas where the sea is covered by ice the wind stress is excluded. Instead, the surface stress is caused by the ice roughness. The surface stress, $\vec{\tau}_s = (\tau_{sx}, \tau_{sy})$, is determined by a quadratic friction law

$$\frac{\vec{\tau}_s}{\rho_0} = c_f \vec{u}_s |\vec{u}_s| \tag{2.90}$$

where c_f is the drag coefficient and $\vec{u}_s = (u_s, v_s)$ is the flow velocity below the surface. The friction velocity associated with the surface stress is given by

$$U_{\tau s} = \sqrt{c_f |u_s|^2} \tag{2.91}$$

For two-dimensional calculations $\vec{u}_s$ is the depth-average velocity and the drag coefficient can be determined from the Manning number, M

$$c_f = \frac{g}{\left(Mh^{1/6}\right)^2} \tag{2.92}$$

The Manning number is estimated from the bed roughness length using the following

$$M = \frac{25.4}{k_s^{1/6}} \tag{2.93}$$

For three-dimensional calculations $\vec{u}_s$ is the velocity at a distance Δz_s below the surface and the drag coefficient is determined by assuming a logarithmic profile between the surface and a point Δz_b below the surface

$$c_f = \frac{1}{\left(\frac{1}{\kappa}\ln\left(\frac{\Delta z_s}{z_0}\right)\right)^2} \tag{2.94}$$

where κ=0.4 is the von Kármán constant and z_0 is the bed roughness length scale. When the boundary surface is rough, z_0, depends on the roughness height, k_s

$$z_0 = mk_s \tag{2.95}$$

where m is approximately 1/30.

2.8 Tidal Potential

The tidal potential is a force, generated by the variations in gravity due to the relative motion of the earth, the moon and the sun that act throughout the computational domain. The forcing is expanded in frequency space and the potential considered as the sum of a number of terms each representing different tidal constituents. The forcing is implemented as a so-called equilibrium tide, which can be seen as the elevation that theoretically would occur, provided the earth was covered with water. The forcing enters the momentum equations (e.g. (2.66) or (2.75)) as an additional term representing the gradient of the equilibrium tidal elevations, such that the elevation η can be seen as the sum of the actual elevation and the equilibrium tidal potential.

$$\eta = \eta_{ACTUAL} + \eta_T \tag{2.96}$$

The equilibrium tidal potential η_T is given as

$$\eta_T = \sum_i e_i H_i f_i L_i \cos(2\pi \frac{t}{T_i} + b_i + i_0 x) \tag{2.97}$$

where η_T is the equilibrium tidal potential, i refers to constituent number (note that the constituents here are numbered sequentially), e_i is a correction for earth tides based on Love numbers, H_i is the amplitude, f_i is a nodal factor, L_i is given below, t is time, T_i is the period of the constituent, b_i is the phase and x is the longitude of the actual position.

The phase b is based on the motion of the moon and the sun relative to the earth and can be given by

$$b_i = (i_1 - i_0)s + (i_2 + i_0)h + i_3 p + i_4 N + i_5 p_s + u_i \sin(N) \tag{2.98}$$

where i_0 is the species, i_1 to i_5 are Doodson numbers, u is a nodal modulation factor (see Table 2.3) and the astronomical arguments s, h, p, N and p_s are given in Table 2.2.

Table 2.2 Astronomical arguments (Pugh, 1987)

Mean longitude of the moon	s	$277.02+481267.89T+0.0011T^2$
Mean longitude of the sun	h	$280.19+36000.77T+0.0003T^2$
Longitude of lunar perigee	p	$334.39+4069.04T+0.0103T^2$
Longitude of lunar ascending node	N	$259.16+1934.14T+0.0021T^2$
Longitude of perihelion	p_s	$281.22+1.72T+0.0005T^2$

In Table 2.2 the time, T, is in Julian century from January 1 1900 UTC, thus $T = (365(y-1900)+(d-1)+i)/36525$ and $i = int\ (y-1901)/4)$, y is year and d is day number

L depends on species number i_0 and latitude y as

$$i_0 = 0 \qquad L = 3\sin^2(y) - 1$$
$$i_0 = 1 \qquad L = \sin(2y)$$
$$i_0 = 2 \qquad L = \cos^2(y)$$

The nodal factor f_i represents modulations to the harmonic analysis and can for some constituents be given as shown in Table 2.3.

Table 2.3 Nodal modulation terms (Pugh, 1987)

	f_i	u_i
M_m	1.000 - 0.130 cos(N)	0
M_f	1.043 + 0.414 cos(N)	-23.7 sin(N)
Q_1, O_1	1.009 + 0.187 cos(N)	10.8 sin(N)
K_1	1.006 + 0.115 cos(N)	-8.9 sin(N)
$2N_2, \mu_2, \nu_2, N_2, M_2$	1.000 + 0.037 cos(N)	-2.1 sin(N)
K_2	1.024 + 0.286 cos(N)	-17.7 sin(N)

2.9 Wave Radiation

The second order stresses due to breaking of short period waves can be included in the simulation. The radiation stresses act as driving forces for the mean flow and can be used to calculate wave induced flow. For 3D simulations a simple approach is used. Here a uniform variation is used for the vertical variation in radiation stress.